"ANALYSIS OF LINEAR AND NONLINEAR CIVIL ENGINEERING PROBLEMS USING FINITE ELEMENT TECHNIQUES"

JOHN STAFFORD CRAIG

A THESIS SUBMITTED FOR THE DEGREE OF

DOCTOR OF PHILOSOPHY

DEPARTMENT OF CIVIL ENGINEERING, UNIVERSITY OF ASTON IN BIRMINGHAM

MAY 1971

SUMMARY

The finite element method is now well established among engineers as being an extremely useful tool in the analysis of problems with complicated boundary conditions. One aim of this thesis is to investigate the suitability of this method in the analysis of complete complex structures. The method becomes particularly powerful when it is used in conjunction with prismatic members to analyse such structures. A further aim is to extend the method to cover the nonlinear range in order to analyse continua subjected to general conditions of nonlinearity. Examples of these are creep, plasticity and discontinuity.

In the elastic region, the accuracy of previous analyses has been assessed in relation to simple structures which can be checked against the more conventional calculations. In this thesis, the method which is proposed is used to analyse different geometrical configurations. The effect of subdivision and interaction of element types on accuracy as well as the computation involved is established.

Two methods are proposed for the analysis of nonlinear problems. The first, which is iterative, considers the secant modulus of the stress-strain relationship to represent the material stiffness. The second, on the other hand, uses the instantaneous tangent modulus of the stress-strain relationship to trace, in an incremental manner, the load-deflection history up to and including failure. These are used to investigate the deformation of a Perspex shear wall when loaded under general conditions of creep and the nonlinear settlement of a footing which is loaded on a sand foundation. Soil mechanics problems of this sort are usually attempted using 'Boussinesq' type calculations. With the proposed method it is possible to represent the interaction of structure and foundation as well as the nonlinear stress-strain relationship of the soil.

ACKNOWLEDGEMENTS

The author would like to thank his tutor, Professor K. I. Majid, for his help and encouragement during the last three years. His sincere thanks are also given to Mr. D. H. Bennett and Dr. K. Starzewski of the Soil Mechanics department for their great consideration and availability for discussion on the work which the author did in this field. He is especially indebted to Nawaz M.Sc., who worked with him in the laboratory and gave useful assistance during this work. Thanks are also owing to the chief technician, Mr. Walter Parsons and his team of technicians for their helpfulness and efforts in all the experimental work which was completed.

In the preparation of this thesis, the author would like to thank Miss Pat Sage for tracing the diagrams and the office staff of Freeman, Fox and Partners for their assistance and consideration. Among others, these include notably, Miss C. Lawson and Mr. W.T. Palmer. Above all, the author owes his greatest thanks to Miss Lynne Gajdzik for her efficient and patient typing of the script.

Finally, the author would like to thank the Atlas computer staff at Chilton for their prompt service and the Science Research Council for their financial support.

CONTENTS

NOTATION

A_{o-12}	Constants of displacement function
A^l	Area of plate element
$A^l_{1,2,3}$	Areas within triangular plate element
B	Angle of orthotropy in element
C_{ri}	Column number of rectangular element i in displacement transformation matrix
C_{ti}	Column number of triangular element i in displacement transformation matrix
D	Flexural rigidity of plate
E	Young's Modulus
E_o	Modulus of elasticity under initial conditions
E_i	Modulus of elasticity at ith iteration
$E_{1,2}$	Modulus of elasticity in principal directions
$E_{p,q}$	Modulus of elasticity in P and Q directions
E_s	Secant modulus of elasticity
E_{si}	Secant modulus of elasticity at ith iteration.
E_t	Tangent modulus of elasticity
E_{ti}	Tangent modulus of elasticity at ith increment
G	Shear Modulus
$G_{1,2}$	Shear modulus in principal directions
I	Unit identity matrix
$I_{R,Q,RQ}$	Second moment of area about R, Q axes and product moment of area
J	Torsional constant
K	Bulk modulus
$L_{1,2,3}$	Area Coordinates

M_i	Function of reduced stiffness matrix at ith cycle
$M_{pi,qi}$	Nodal moments on elements at node i
M_{xi}, M_{yi}, M_{zi}	Applied moments on joint i about X,Y,Z axes
N_i	Function of reduced stiffness matrix at ith cycle
P,Q,R	Local element axes
P_i, Q_i, R_i	Nodal element forces at node i in P,Q,R directions
P_{ij}, Q_{ij}	Representative forces at node i along side i to j
R_s	Secant modulus
R_{si}	Secant modulus at ith iteration
R_t	Tangent modulus
R_{ti}	Tangent modulus at ith increment
S_i	Reduced stiffness matrix at ith cycle
Tol	Tolerance level for convergence of moduli in plates
Tol^1	Tolerance for convergence of moduli in plates
U	Strain energy
X,Y,Z	Overall or global axes of structure
X_i, Y_i, Z_i	Applied forces on joint i of a structure in X,Y,Z directions
a	Dimension of rectangular plate in P direction
$a_{1,2,3}$	Function of plate dimensions
b	Dimension of rectangular plate in Q direction
$b_{1,2,3}$	Function of plate dimensions
e_o	Nonlinear strain
$c_{1,2,3}$	Function of plate dimensions
$e_{1,2}$	Principal strains

e_c	Creep strain
e_i	Strain in ith increment of load
e_{max}	Maximum shear strain
$e_{p,q}$	Strain in P and Q directions
e_{pq}	Shear strain
e_p	Plastic strain
e_θ	Temperature strain
$\bar{e}$	Representative strain
l_{ij}, m_{ij}, n_{ij}	Direction cosines in three dimensional space
$l_{p,q}, m_{p,q}$	Direction cosines in two dimensional space
$m_{p,q,pq}$	Moments per unit run at centroid of element
p,q,r	Coordinates in P,Q,R directions
p_c, q_c	Offsets of member connection at joint
p_i, q_i, r_i	Coordinates of element at node i
p_s, q_s	Offsets of shear centre from centroid in P and Q directions
$s_{1,2}$	Principal stresses
s_i	Stress change in ith increment
$s_{p,q}$	Stress in P and Q directions
s_{pq}	Shear stress
s_s	Component of stress causing change in shape
s_v	Component of stress causing change in volume
$s_{x,y,z}$	Stress in x,y,z directions
$\bar{s}$	Representative stress

t	Plate thickness
u,v,w	Plate deflections in P,Q,R directions
u_i,v_i,w_i	Plate deflections at node i in P,Q,R directions
w^*	Displacement in R direction of simply supported element
w^R	Rigid body displacement in R direction
x,y	Force per unit run
x_i,y_i,z_i	Displacement at joint i in the X,Y,Z directions
$\underline{A}$	Displacement transformation matrix
$\underline{A}_1$	Displacement transformation matrix for unknown displacement at joints
$\underline{A}_2$	Displacement transformation matrix for known displacement at joints
$\underline{A}_i$	Displacement transformation matrix for joint group i
$\underline{A}_{m,r,t}$	Displacement transformation matrix for members, rectangular and triangular plates
$\underline{A}_{ir,or,it,ot}$	Displacement transformation matrix for 'in plane', 'out of plane', rectangular and triangular plates
$(\underline{A}_e)_i$	Displacement transformation matrix for joint group i where suffix e stands for element type:- m,r,t,ir,or,it,ot
$\underline{B}$	Strain matrix
$\underline{B}^*$	Strain matrix of simply supported element
$\underline{C}$	Matrix relating element displacement to constants in displacement function
$\underline{D}$	Elasticity matrix
$\underline{D}_{1,2}$	Elasticity matrix in principal planes
$\underline{D}_i$	Elasticity matrix for increment i
$\underline{H}$	Elasticity transformation matrix

$\underline{J}$	Vector of constants of displacement function
$\underline{K}$	Overall stiffness matrix
$\underline{K}_{ii}$	Stiffness matrix of joint group i
$\underline{K}_{ij}$	Stiffness of elements joining groups i to j
$\underline{K}_{ll}$	Stiffness matrix of elements at joints with unknown displacements
$\underline{K}_{22}$	Stiffness matrix of elements at joints with known displacements
$\underline{K}_{llmrt}$	Stiffness matrix of members, rectangular and triangular plates
$\underline{K}_i$	Stiffness matrix for increment i
$\underline{L}$	Load vector of structure
$\underline{L}_1$	Load vector corresponding to unknown deflections
$\underline{L}_2$	Load vector corresponding to known deflections
$\underline{L}_i$	Load vector for joint group i
$\underline{N}$	Displacement function matrix
$\underline{N}_{pi,qi}$	Elements of displacement function corresponding to P,Q directions at node i
$\underline{P}$	Element force vector of structure
$\underline{P}_o$	Initial load vector
$\underline{P}_1$	Element force vector corresponding to unknown deflections
$\underline{P}_2$	Element force vector corresponding to known deflections
$\underline{P}_i$	Force vector of element i
$\underline{S}$	Stress matrix
$\underline{S}_i$	Stress matrix for increment i
$\underline{S}_{m,r,t}$	Stress matrix for members, rectangular and triangular plates

$\underline{S}_{ir,or,it,ot}$	Stress matrix for 'in plane', 'out of plane', rectangular and triangular plates
$(\underline{S}_e)_i$	Stress matrix for joint group i where suffix e stands for element type:- m,r,t,ir,or,it,ot
$\underline{T}$	Element stiffness transformation matrix
$\underline{U}$	Transformation matrix relating element displacements to 'misaligned' joint displacements
$\underline{V}$	Transformation matrix relating 'misaligned' displacements to joint displacements
$\underline{X}$	Joint displacement vector of structure
$\underline{X}_1$	Joint displacement vector of unknown displacements
$\underline{X}_2$	Joint displacement vector of known displacements
$\underline{X}_i$	Displacement vector of joint group i
$\underline{Y}$	Displacement vector of 'misaligned' joints
$\underline{Z}$	Element displacement vector of structure
$\underline{Z}_1$	Element displacement vector for unknown displacements
$\underline{Z}_2$	Element displacement vector for known displacements
$\underline{Z}_i$	Nodal displacement vector for element i
$\underline{Z}_{m,r,t}$	Nodal displacement vector for members, rectangular and triangular plates
$\underline{Z}_{or,ir,ot,it}$	Nodal displacement vector for 'in plane', 'out of plane', rectangular and triangular plates
$(\underline{Z}_e)_i$	Nodal displacement vector for joint group i where suffix e stands for element type:- m,r,t,or,ir,ot,it
$\underline{Z}^*$	Nodal displacement vector for simply supported element
$\underline{a}$	Submatrix of displacement transformation matrix
$\underline{e}$	Vector of strains in element

$\underline{f}$	Displacement vector within element
$\underline{k}$	Unassembled element stiffness matrix of structure
$\underline{k}_i$	Element stiffness matrix of joint group i
$\underline{k}_{m,r,t}$	Unassembled stiffness matrix for members, rectangular and triangular plates
$\underline{k}_{or,ir,it,ot}$	Unassembled stiffness matrix for 'out of plane', 'in plane' rectangular and triangular plates
$\underline{k}^*$	Unassembled stiffness matrix for simply supported element
$\underline{ke}$	Elastic unassembled element stiffness matrix
$\underline{kp}$	Plastic unassembled element stiffness matrix
$\underline{kep}$	Elasto-plastic unassembled element stiffness matrix
$\underline{kg}$	Geometrical stiffness matrix
$\underline{keg}$	Tangential geometrical stiffness matrix
$\underline{s}$	Vector of stresses
$\Delta\underline{L}$	Finite increment of loads
$\Delta\underline{L}_i$	ith increment of loads
$\Delta\underline{e}$	Finite increment of strains
$\Delta\underline{e}_i$	ith increment of strains
$\Delta\underline{s}$	Finite increment of stresses
$\Delta\underline{s}_i$	ith increment of stresses
$\Delta\underline{X}$	Finite increment of displacements
$\Delta\underline{X}_i$	ith increment of displacements
$\Delta\gamma_{oct}$	Finite increment of octahedral shear strain
$(\Delta\gamma_{oct})_i$	ith increment of octahedral shear strain

$\Delta\sigma_{oct}$	Finite increment of octahedral mean stress
$(\Delta\sigma_{oct})_i$	ith increment of octahedral mean stress
$\Delta\tau_{oct}$	Finite increment of octahedral shear stress
η_i	ith coordinate of strain on piecewize representative stress strain curve
Σ_i	ith coordinate of stress on piecewize representative stress strain curve
α	Angle of rotation of principal stresses
α_{ij}	Constants of elasticity matrix in local axes
α^1_{ij}	Constants of elasticity matrix in principal axes
$\alpha_{p,q,r}$	Angular rotation of triangular plate element about P,Q,R axes
$\alpha_{pi,qi,ri}$	Angular rotation of triangular plate element at node i about P,Q,R axes
$\alpha^*_{pi,qi,ri}$	Nodal rotation of simply supported triangular element
γ_{oct}	Octahedral shear strain
ϵ_{oct}	Octahedral normal strain
$\theta_{xi,yi,zi}$	Rotations at joint i about X,Y,Z, axes
ν	Poisson's ratio
$\nu_{1,2}$	Poisson's ratio in principal directions
$\nu_{p,q}$	Poisson's ratio in P,Q directions
ν_i	Poisson's ratio at ith increment/ iteration
ρ	Density
σ_{oct}	Octahedral mean stress
τ_{oct}	Octahedral shear stress

* The symbols σ and $\dot{e}$ are used in the figures and tables instead of s and e where appropriate to avoid ambiguity.

$\phi_{pi,qi,ri}$	Angular rotation of rectangular plate element about P,Q,R axes at node i
$\psi_{pi,qi,ri}$	Angular rotation of prismatic member element about P,Q,R axes at node i
ψ_{Rij}	Angular rotation about R axis of member element i in plane frame at node j

CHAPTER 1

INTRODUCTION

1.1. Matrix Displacement Method

The basic elasticity equations which must be satisfied in structural analysis are:-

(i) Strain-displacement equations.

(ii) Stress-strain equations.

(iii) Equilibrium equations.

(iv) Compatibility equations.

These equations form the basis of any structural problem. Since the beginning of the last century the first three have been used to solve statically determinate structures and, with the inclusion of the fourth, statically indeterminate structures. An advancement was made when Castigliano introduced his strain energy theorems towards the end of the last century. These lead on to the concepts of virtual work and complementary virtual work which now form the basis for modern matrix analysis.

Numerical analyses nowadays are divided into two main fields, either the solution of the governing differential equations defining the displacements or stresses, or the matrix methods. The former, called the finite difference method, is limited in application as it considers the whole structure as one unit and can only be used for certain configurations. The latter was evolved on the assumption that any structure is made up of a combination of structural elements, each possessing a particular stiffness or flexibility, which, when assembled in the manner of the structure, behaved in an identical way to the actual case. For a framework of prismatic members it can be seen that this assumption is true and has been used in practically all other methods of analysis.

The elements of a structure can be broadly subdivided into member

and plate types. These are defined by nodes at either of their ends, or in the case of the plates, at each of their corners. The nodes of the elements are joined together to make up the structure at joints. Thus, returning to the example of a framework, this is idealized into beam elements joined together at a discrete number of joints where the forces on the nodes of each element are in equilibrium with themselves or an imposed load at that position.

Two types of analysis stem from this idealization, the matrix force method and the matrix displacement method. The force method considers the forces in the structure as unknowns whereas the displacement method solves for displacements. The force method was formerly more attractive to the engineer as less work was involved with its solution, but, special redundant forces have to be selected before the analysis and hence the process is not as fully automatic as the displacement method. Its application to the finite element method, which will be described later, is also more limited and hence this method will only be mentioned in passing.

Consider, for example, a member element. A set of forces can be found at either node which equilibrates the stresses throughout the beam and is related to the nodal displacements by the equation in matrix notation,

$$\underline{P} = \underline{k}\,\underline{Z} \qquad (1.1)$$

where $\underline{P}$, the element forces acting at the nodes, is a column vector. For an assembly of n number of elements this will take the form:-

$$\underline{P} = \{\underline{P}_1, \underline{P}_2, \underline{P}_3 \ldots \underline{P}_n\}$$

$\underline{Z}$ is the nodal displacement vector corresponding to the force vector. Thus:-

$$\underline{Z} = \{\underline{Z}_1, \underline{Z}_2, \underline{Z}_3 \cdots\cdots \underline{Z}_n\}$$

The matrix $\underline{k}$ is defined as the element stiffness matrix. That a unique stiffness matrix exists is shown by the presence of slope deflection equations. The matrix will be square and symmetrical due to the theorems of Maxwell and Betti.

These individual stiffnesses are assembled in the following manner:-

For convenience the displacement matrix of the total structure is defined relative to some arbitrary reference axes X, Y, Z and given by the column vector:-

$$\underline{X} = \{\underline{X}_1, \underline{X}_2 \cdots\cdots \underline{X}_j \cdots\cdots \underline{X}_n\}$$

for a structure containing n joints, where X_j is a submatrix of the form:-

$$\underline{X}_j = \{x_j, y_j, z_j, \theta_{xj}, \theta_{yj}, \theta_{zj}\}$$

The six elements of $\underline{X}_j$ correspond to the possible degrees of freedom, both translational and rotational, at joint j. It is now possible to relate the element displacements to the joint displacements by the equation:-

$$\underline{Z} = \underline{A}\,\underline{X} \qquad (1.2)$$

The matrix $\underline{A}$ is called the displacement transformation matrix and is rectangular. Its elements are constants referring to the cosine of the angle between the various member and reference axes. A load vector, equivalent to the joint displacement vector, is defined as:-

$$\underline{L} = \{\underline{L}_1, \underline{L}_2, \underline{L}_3, \cdots\cdots \underline{L}_j \cdots \underline{L}_n\}$$

where, at a joint for instance, the submatrix L_j is a vector of forces and moments taking the form:-

$$\underline{L}_j = \{X_j, Y_j, Z_j, Mx_j, My_j, Mz_j\}$$

The principle of virtual work states that, for a structure in

equilibrium, the applied virtual work is equal to the internal virtual work, hence:-

$$\underline{X}^1\underline{L} = \underline{Z}^1\underline{P} \qquad (1.3)$$

From equations (1.2) and (1.3) it is clear that,

$$\underline{L} = \underline{A}^1\underline{P} \qquad (1.4)$$

but from equations (1.1) and (1.2),

$$\underline{P} = \underline{k}\,\underline{A}\,\underline{X} \qquad (1.5)$$

hence, from equations (1.4) and (1.5),

$$\underline{L} = \underline{A}^1\,\underline{k}\,\underline{A}\,\underline{X} \qquad (1.6)$$

Equation (1.6) relates the applied forces of the structure to its displacements and can be rewritten as:-

$$\underline{L} = \underline{K}\,\underline{X} \qquad (1.7)$$

Hence $\underline{K}$ is the overall stiffness matrix of the structure and,

$$\underline{K} = \underline{A}^1\,\underline{k}\,\underline{A} \qquad (1.8)$$

This method was derived using the concept of virtual work and it is evident that the basic equations of elasticity are not violated. Strain-displacement, stress-strain, and equilibrium equations within each element are represented by equation (1.1). Although this equation also includes continuity of diaplacement (and hence strain) for this element, overall compatibility is achieved by the "uniqueness" of the displacement vector $\underline{X}$. Equation (1.4) is, in fact, the overall equilibrium equation for the structure at each joint.

The matrix $\underline{K}$ is the overall stiffness matrix of a structure as a free body, hence $\underline{L}$, the load matrix, constitutes a system of forces, both imposed and reactive, in equilibrium acting on all the joints of the structure. Even if all these forces were known, which would not be true of the reactive forces in the general case, six of the equations (in a

three dimensional structure), in equation (1.7) would be linearly dependant. This is overcome by specifying the displacements at the reactions to be zero. Hence the corresponding rows and columns in the $\underline{K}$ and $\underline{L}$ matrices disappear and the overall stiffness matrix becomes nonsingular, thus allowing inversion.

It is now possible, if the stiffnesses of the individual elements and the geometry of the structure are known, to solve the equation:-

$$\underline{X} = \underline{K}^{-1} \underline{L} \qquad (1.9)$$

and proceed to find the forces throughout the structure using equation (1.5)

1.2 The Finite Element Method

As previously mentioned, the displacement method can be extended to include the analysis of two, or three dimensional, continua. The method depends on the splitting up of the structure into elements and a similar technique is again used with the continuum. Consider a structure as shown in fig. 1.1. This can be idealized into two prismatic elements, AB and EF and one plate element BCDE. It is evident that, to find the distribution of stress and displacement throughout the plate using the displacement method, it will have to be further divided up in a manner, say, shown by the dotted lines. Hence nine plate elements, numbered 1-9, are produced along with the fictitious joints G-R. If, for each element, a relationship in the form of equation (1.1) can be found then the analysis can be carried out as before. This procedure broadly defines the finite element method.

Unlike a framework, it is now apparent that the nodal points are

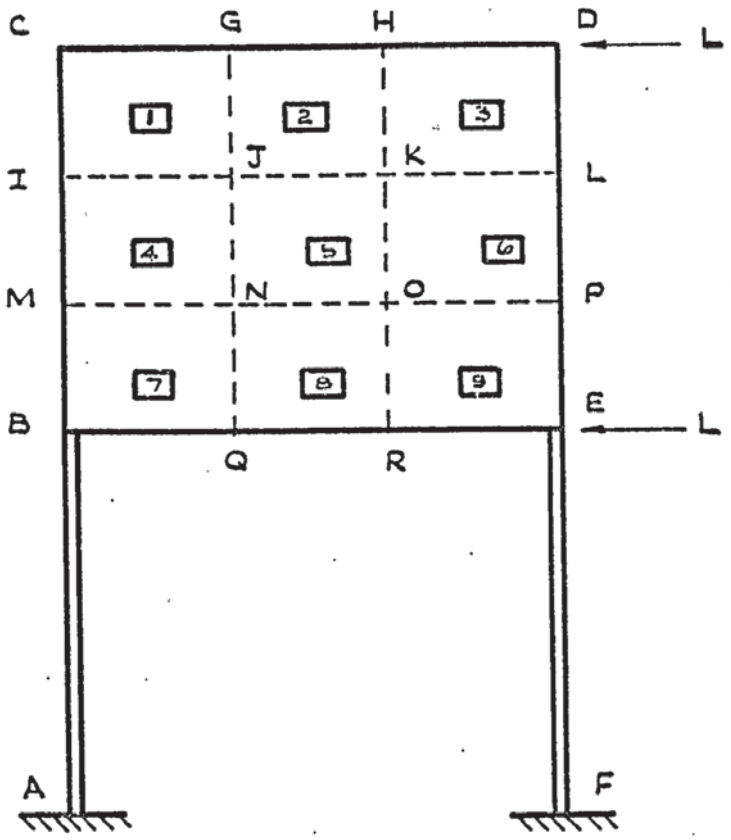

FIGURE 1.1

no longer physically structural and the plate elements are continuously attached between their nodes. The plate forces, $\underline{P}$, which are considered to act on the nodes also have no physical significance but, obviously, are necessary in the displacement method of analysis.

As before, equation (1.1) still has to satisfy and represent the displacement-strain, stress-strain and equilibrium equations. In addition to this, as the plates are continuous in a medium, displacement and stress continuity should prevail across their interfaces.

In practice, all these conditions cannot be satisfied and so certain assumptions are made so that, in the limit as the subdivision of elements across a continuum becomes infinite, the answer obtained from the approximate plate element stiffness matrices converges to the exact one. Generally speaking, plate stiffness matrices are evaluated using one of two basic assumptions:-

(i) Assume that the displacements within the boundaries of an element can be expressed as a function of the nodal displacements. Hence a 'displacement function' is assigned to the element. This satisfies the stress-strain and displacement-strain equations. If this function leads to the fact that the displacements along an element's interface (or edge), follows a curve which can be defined by values at either of its ends, then continuity of displacements between elements will exist. For example, in fig. 1.1., for instance, plate numbers 1 and 2 have a common interface between joints G and J. When the loads L are applied, each element will deform between its nodes which are connected to these joints. Hence the deflections at either node of the plates which are connected to the joint will be the same. These deflections can be made to specify the deflected form along the interface uniquely. If this condition is satisfied then

continuity of displacements within the element and compatibility of deformation throughout the structure are satisfied. Such elements are called conforming. Although this assumption ensures overall equilibrium of structure and element, local equilibrium of the element within and on its boundaries will generally be violated and this will lead to stress discontinuities across element interfaces.

(ii) Assume that the stress at any point within an element can be expressed as a function of the nodal forces. This assumption usually leads to the formation of a flexibility matrix which is used in the matrix force method. However it can be used in the calculation of stiffness matrices and hence it will suffice here to say that total and elemental equilibrium is satisfied throughout but local discontinuities of displacement exist. Obviously stress will be continuous between element interfaces if the so called 'stress function' can be expressed uniquely by its nodal values at these positions.

1.3 Formation of Plate Element Stiffness Matrix

Although there exist a number of methods of formulating a stiffness matrix, the two just described are the most attractive to the engineer as the extent of their accuracy can be justified theoretically.

Of these two, the displacement 'model' is the most commonly used as it has been found easier to arrive at a satisfactory displacement function. This function will relate the internal displacements in the element to the nodal displacements in equation form as:-

$$\underline{f} = \underline{N}\,\underline{Z} \qquad (1.10)$$

where f is the displacement of a point within the element and N, the function, is such that strains will vary continuously across the element.

For a flat plate there are two types of stiffness matrix, one relating 'in plane' forces to their corresponding displacements which are shown in fig. 1.2 (a) for a rectangular plate, the other relating 'out of plane' forces to the displacements, given in fig. 1.2 (b). For 'in plane' action,

$$f = \begin{Bmatrix} u\ (p,q) \\ v\ (p,q) \end{Bmatrix}$$

where u and v are internal displacements in the P and Q directions at any position (p,q).

For 'out of plane' action the deformation can be expressed as functions of the vertical deflection. Its derivatives will define the rotation. It is now possible to relate the strains to the displacements in the manner:-

$$\underline{e} = \underline{B}\ \underline{Z} \qquad (1.11)$$

The matrix $\underline{e}$ is a column vector of strains at any point in an element defined in the P-Q plane where:-

$$\underline{e} = \{e_p,\ e_q,\ e_{pq}\}$$

These can be expressed in terms of $\underline{f}$ by basic equations of elasticity (1) For example, for plane strain:-

$$e_p = \partial u/\partial p;\ eq = \partial v/\partial q;\ e_{pq} = \partial u/\partial q + \partial v/\partial p$$

Also, using basic equations of elasticity (2), the stresses can be related to the strains in the form:-

$$\underline{s} = \underline{D}\ \underline{e} \qquad (1.12)$$

where $\underline{D}$ is the elasticity matrix, consisting of material properties and $\underline{s}$ is the stress matrix as given by:-

$$\underline{s} = \{s_p,\ s_q,\ s_{pq}\}$$

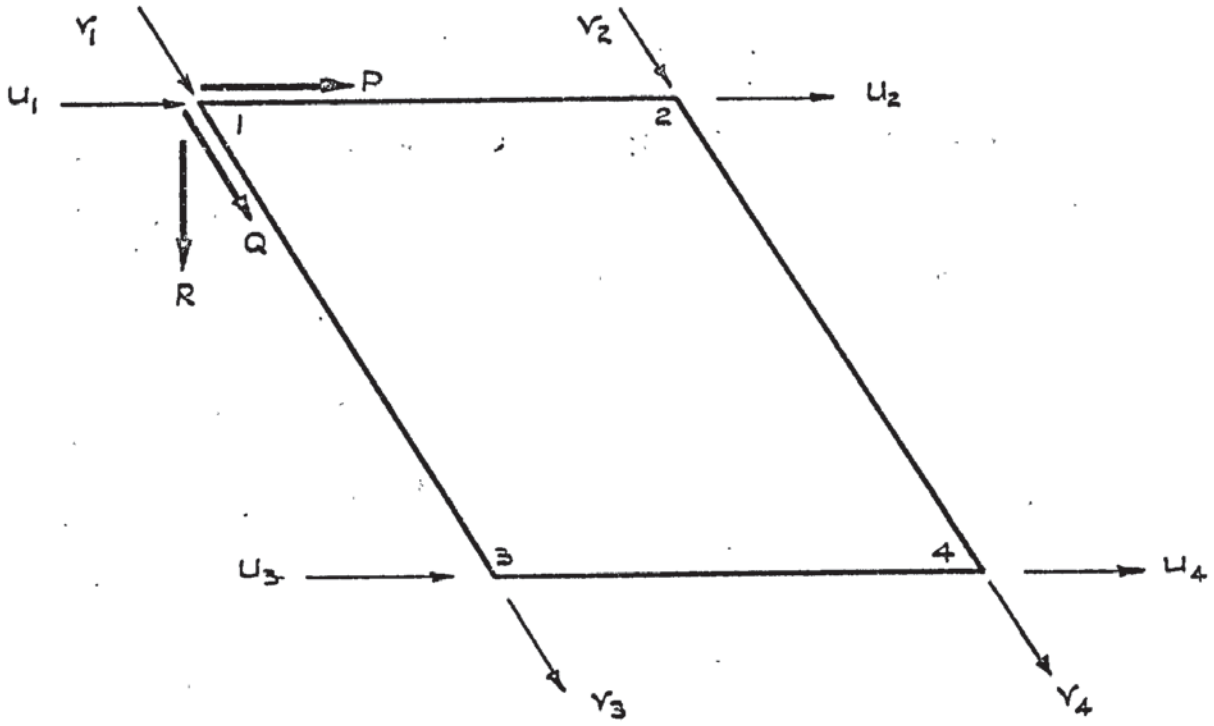

(a) IN PLANE DISPLACEMENTS

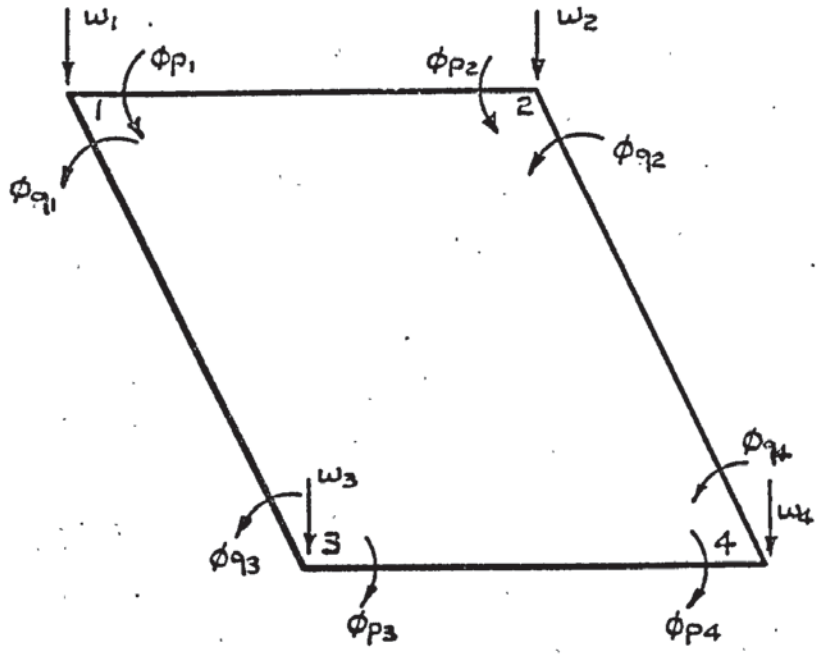

(B) OUT OF PLANE DISPLACEMENTS.

FIGURE 1.2. DISPLACEMENTS FOR A RECTANGULAR ELEMENT

The nodal forces are defined as being statically equivalent to the boundary stresses. The principle of virtual work can be used to equate the external work done by the forces to the work done internally by the stresses. When an arbitrary virtual displacement is applied:-

$$\delta \underline{Z}^{1} \underline{P} = \int_{v} \delta \underline{e}^{1} \underline{s} \qquad (1.13)$$

using equations (1.11) and (1.12):-

$$\delta \underline{Z}^{1} \underline{P} = \delta \underline{Z}^{1} \left(\int_{v} \underline{B}^{1} \underline{D} \underline{B} \, d\,(\mathrm{Vol}) \right) \underline{Z}$$

Hence:-

$$\underline{P} = \int_{v} \underline{B}^{1} \underline{D} \underline{B} \, d\,(\mathrm{Vol}) \, \underline{Z} \qquad (1.14)$$

The element stiffness matrix, by comparison with equation (1.1), is defined as:-

$$\underline{k} = \int_{v} \underline{B}^{1} \underline{D} \underline{B} \, d\,(\mathrm{Vol}) \qquad (1.15)$$

This method of derivation is covered by numerous authors (2,3).

Although it is possible to obtain a stiffness matrix in this fashion, its accuracy in solving a given problem will hinge on the choice of displacement function. Even if the element does conform, certain approximations are still present and would only disappear if the function expressed the real situation within a plate. The satisfaction of the stress-equilibrium equations would then be inherent. It is therefore desirable, when dealing with problems whose exact solutions are unknown, to find some limits or bounds within which the accuracy of the finite element model will fall.

The principle of minimum potential energy states that -'for a prescribed set of displacements and strains the equilibrium conditions are satisfied when the total potential energy assumes a stationary value'. For a stable structure this would be a minimum. It can be

shown (3,4) that an expression for an element stiffness matrix, identical to the one just described, can be derived using this principle. The method is, in fact, equating the strain and kinetic energy of the model to that of the actual continuum. It follows that the strain energy in the model due to a displacement function will always be below that of the actual case.

Theoretically a continuum has an infinite number of degrees of freedom, whereas the displacement method considers the number to be finite. It may therefore be considered as giving a release to the structure at each joint. An exact answer will only be reached on infinite subdivision of the elements. Therefore elements obtained from a displacement function will form a lower bound solution. This is usually accepted of conforming elements as discontinuities of displacements across their interfaces will cause infinite strains and will store energy. In the physical sense the structure would be further 'relaxed' along these interfaces and hence might ever tend to overestimate solution. The speed and even presence of monotonic convergence of solution are usually demonstrated by practical application.

Stress functions which lead to flexibility matrices have been proved to form upper bounds (4). Hence, for a rather limited range of applications, an exact solution could be bracketed between the two solutions.

1.4. Historical Review of the Finite Element Method

In the last fifteen years since its formulation, the finite element method, in conjunction with the matrix displacement method, has emerged as probably the most powerful tool available to the engineer in the analysis of complex problems.

Navier, as long ago as 1872, had suggested a method of analysis

based on taking the deflections as unknowns but it received little attention due to the Volume of mathematics involved. Indeed, had it not been for a parallel growth of computer technology within the last few years the finite element method would probably have suffered the same fate.

Livesley (5,6) was one of the first to adapt the matrix displacement method for the computational analysis of bare frameworks. Around the same time, in 1954, Argyris (7) formulated comprehensively the matrix force and displacement method. He showed that each one stemmed from the concepts of complementary virtual work and virtual work respectively. He also derived a stiffness matrix for a rectangular plate element for 'in plane' action. This was done by assuming linear distribution of displacements in the plate and imposing unit displacements at each corner. The unit displacement theorem states that:-

$$P_L = \int e_L^1 \, sdv$$

where 'P_L' is the appropriate force corresponding to the displacement. Thus by adding the stiffnesses for each imposed deflection, it was possible to build up an (8x8) stiffness matrix for the plate. This method is analogous to that of using a displacement function.

Two years later, Turner et al (8) first laid the foundations of the finite element technique by deriving stiffness matrices for various spar, rib and cover plate elements. An 'in plane' stiffness matrix was derived for a triangular element by assuming a constant strain pattern over the element. They showed that this assumption lead to a linear distribution of displacement in the element. To equilibrate the nodal forces to the stresses, the basic stress patterns that could be expected were considered and the forces were obtained by direct

equilibrium. They did point out though that the same result could have been obtained using Castigliano's energy theorems. A method for finding the stiffness of a quadrilateral was shown by splitting the area up into triangles and summing the contributing stiffnesses.

Clough (9) extended the idea of assumed stress and corresponding 'node displacement' patterns to derive stiffness matrices for both rectangular and triangular elements. A valuable contribution was made though on introducing the principle of virtual work to obtain overall equilibrium of the element.

The finite element method was next extended into the 'out of plane' or bending action. Previously, for 'in plane' stiffnesses, two translational degrees of freedom were considered for each node. Melosh (10) derived a stiffness matrix for the bending of a rectangular plate having vertical and two rotational degrees of freedom. The expression for bending strain energy in a plate with uniform flexural rigidity D is,

$$U = \frac{D}{2}\iint\left[\frac{\partial^2 w}{\partial p^2} + \frac{\partial^2 w}{\partial q^2} + 2\nu\frac{\partial^2 w}{\partial p^2}\frac{\partial^2 w}{\partial q^2} + 2(1-\nu)\frac{\partial^2 w}{\partial p \partial q}\right]dA$$

The vertical displacement w was taken to vary as a cubic polynomial over the length. For the P direction, i.e.

$$w = A_3 p^3 + A_2 p^2 + A_1 p + A_o$$

The constants A_o - A_3 can be evaluated by making this function equal the nodal deflections and rotations at each corner. Thus the strain energy for the plate can be evaluated by differentiation of the polynomial and integration of the resulting terms over the appropriate area. Castigliano's theorem was again used in evaluation of the final stiffness.

By this time definite methods of derivation of the stiffness matrix were being formulated and these were reviewed by Gallagher (11) to be:-

1) Inversion of a flexibility matrix (12).

2) Direct formulation (8).

3) From virtual work or, unit displacement theorem (7).

He might well have included formulation by Castigliano's theorem as a fourth. Although the interrelation of some derivations was noticed and, in fact, would give the same results of stiffness for particular elements, the actual implications of the basic assumptions were not yet realised.

The majority of elements thus formed were known to converge to a good value for solution as their subdivision was refined but the extent of accuracy that could be expected was not yet defined. It was Melosh (13) who, in 1963, first tackled this problem. Errors could be classified as those involved in the structural idealization, the computation, or the finite element method itself. In the investigation of the latter he showed that solutions obtained using extremum variational theorems of elasticity could be bounded between upper and lower limits. Using a displacement function he showed the approximation to be 'minimizing' the potential energy of the system and hence forming a lower bound. He concluded that, as long as the structural idealization was not redefined on subdivision, monotonic convergence would exist but not necessarily to the correct solution. He stated that for this to be the function must satisfy the following requirements:-

1) Strains must be continuous over the elements.

2) Inter-element displacement continuity must exist i.e. conform.

3) Functions must be expressible in the form of equation (1.10) in order to satisfy linear elasticity.

Optional requirements were:-

4) They should exhibit monotonic convergence as previously described.

5) Rigid body movements should not cause straining.

The last option, in fact, should not be violated, as extra energy not existing in a structure, would be introduced into the idealization.

Fraeijs de Veubeke (12,4) proved upper and lower limits to exist for 'equilibrium and displacement models' but, while agreeing with Melosh's requirements, thought that different element patterns might cause convergence to an erroneous answer. He also pointed out the difficulty in forming a stiffness matrix for an equilibrium model (i.e. by inverting a flexibility matrix) which will include all possible rigid body deformations.

Zienkiewicz (14) formulated a stiffness matrix for 'out of plane' bending in a rectangular element. He assumed the vertical displacement w to vary throughout the element as a polynomial:-

$$w = A_1 + A_2p + A_3q + A_4p^2 + A_5pq + A_6q^2 + A_7p^3 + A_8p^2q + A_9pq^2 + A_{10}q^3 + A_{11}p^3q + A_{12}pq^3$$

The twelve constants A_{1-12} which correspond to the rigid body movements can evaluated in a similar manner to that employed by Melosh. Hence at any node i :-

$$\bar{p} = p_i, \quad q = q_i \text{ and } \theta_{Fi} = (\partial w/\partial q)i$$

Thus the function can be reformulated as:-

$$\underline{Z} = \underline{C}\,\underline{J} \qquad (1.16)$$

where the matrix $\underline{C}$ relates the nodal displacements to the unknown constants. Also, the strains can be related in the form,

$$\underline{e} = \underline{a}\,\underline{J} \qquad (1.17)$$

Hence, from equations (1.16) and (1.17) and by analogy with (1.11)

$$\underline{B} = \underline{a}\,\underline{C}^{-1} \qquad (1.18)$$

Along the edge where p or q is a constant the deflection will vary as a cubic. The slopes will vary as a quadratic. It can be seen that both matrices of Melosh (10) and Zienkiewicz will conform for vertical displacements but not slope along their interfaces. Even so, remarkably good results were shown for each.

When specifying a displacement function in the form of a polynomial the number of unknown constants must be equal to the number of nodal displacements so that they might be evaluated. Pian (15,16) proposed a way of overcoming this and suggested that a fully 'displacement-equilibrium' satisfying function could be found. Gallagher was quick to point out the impracticability of this but the principle could be used to obtain conforming functions. Various authors have made attempts at this (17, 18,19, 20) but success has been limited due to subsequent approximations (21).

Irons (22) relaxes Melosh's requirements for convergence and accuracy by proposing that, for elements in bending,

1) They must be able to exhibit all rigid body movements.

2) They must have a continuous displacement within and across interfaces in deflection and slope.

These reiterate Melosh's proposals but, in addition,

3) They must be able to represent constant stress.

This last proposal can be substantiated by the fact that an infinite

subdivision implies constant stresses in the limit.

He also shows that proposals '2' and '3' are incompatible by proving for such elements that a fully conforming element cannot display a constant twist which is equivalent to '$\frac{\partial^2 w}{\partial p \partial q}$' in the displacement function. This explains the limited success previously mentioned.

The triangular element would appear to have the best shape for an analysis as it could be used to approximate any irregular linear boundary. Attempts at forming a bending stiffness matrix had been largely unsuccessful. This was due to the fact that the polynomial displacement function had to be restricted to nine terms corresponding to the degrees of freedom. A full third order polynomial consists of ten terms.

Clough and Tocher (21) proposed and compared three alternative functions:-

1) $w = A_1 + A_2p + A_3q + A_4p^2 + A_5q^2 + A_6p^3 + A_7p^2q + A_8pq^2 + A_9q^3$

For symmetry, the pq term was omitted. This corresponds to the uniform twist term and hence produced an over stiff matrix.

2) $w = A_1 + A_2p + A_3q + A_4p^2 + A_5pq + A_6q^2 + A_7p^3 + A_8(p^2q + pq^2) + A_9q^3$

By grouping two polynomial terms under one constant, the results gained were reasonable but for some configurations of the triangle, the matrix $\underline{C}$ became singular.

3) Condense the full ten terms into nine using a Ritz procedure. This generally caused the matrix to be too flexible.

A fully conforming matrix was constructed by splitting the element into three subelements and writing a displacement function for each such that the slope across the external interface varied linearly.

This was achieved by omitting the p^2q term. The subelements were then reassembled and the unknown constants were evaluated from the compatibility requirements of the total element. This gave good results but the speed of convergence was low. When comparing conforming and nonconforming rectangular and triangular elements, Clough showed the non-conforming rectangular and the triangular element just described to give the best results.

Melosh (23) produced a triangular plate element for bending with a linear displacement distribution. The results obtained were poor except in cases where the shear rigidities were high or low. This was a consequence of the method used in its formulation.

Bazeley et al (19) proposed that only the conditions concerning constant stress and rigid body representation need be satisfied for accurate convergence as conformity would be satisfied in the limit of subdivision. This explained the good results obtained using the non conforming rectangular element. On this assumption they produced a bending stiffness matrix for a triangular element which gave very good results. An adapted derivation of this element appears in the next chapter.

It was not unnatural that most of the research in this field was prompted by its needs in the so called "Aerospace Industry". Here the structural idealization was well defined and, with a few notable exceptions such as Zienkiewicz and Clough, the analysis of Civil engineering structures by the finite element Method was still in its infancy. Since about 1965 various authors (24, 25, 26, 27, 28) have realised this deficiency and made valuable contributions.

Up until this time attention was mainly focused on the

generation of accurate elements of different shapes and their applicability in analysing complex structures was little mentioned. Jennings and Majid (29) presented a method of analysing general three dimensional space frames by computers. The member elements were formed such that effects of end irregularities such as gusset plates and the misalignment of members at joints could be taken into account. Unsymmetrical members could also be accommodated. Each member was defined by its joints at each end and an 'in plane' joint to define its local axes. The element stiffness matrices were aligned along the leading diagonal so as to retain the basic equation (1.1) for the whole structure.

The displacement transformation matrix was constructed using an intermediate set of displacements $\underline{Y}$, which related the joint displacements to the member reference axes in the form:-

$$\underline{Y} = \underline{V}\underline{X} \qquad (1.19)$$

By then relating this set of displacements, effects of misalignment of members could be accounted for:-

$$\underline{Z} = \underline{U}\,\underline{Y} \qquad (1.20)$$

From equations (1.19), (1.20) and analogy with (1.2):-

$$\underline{A} = \underline{U}\,\underline{V} \qquad (1.21)$$

Each joint was assumed to have six degrees of freedom and, where reactions were specified, the corresponding rows of the $\underline{V}$ matrix were eliminated. The analysis was completed in a manner already described.

The storage required to accommodate these matrices even for a small structure would be prohibitive. To overcome this a set of sparse matrix routines were used. These were developed by Jennings and reduced the storage requirement by only storing the non zero elements in a matrix.

The matrices were stored in a vector array in sequence by rows. Each row was preceded by minus the row number followed by the various column numbers and associated non zero elements in that row. The matrix was terminated by a zero.

For example, the matrix:-

$$\begin{bmatrix} 2 & 0 & 0 & 4 \\ 0 & 7 & 2 & 1 \\ 0 & 0 & 0 & 0 \\ 0 & 0 & 4 & 2 \end{bmatrix}$$

was stored as:-

-1,1,2,4,4, -2,2,7,3,2,4,1, -4,3,4,4,2,0

Another array was used to store the starting location of each matrix and also the total number of matrices in the array. Routines were written to manipulate the matrices for such operations as:- Addition, transformation, multiplication or inversion.

Later Majid and Williamson (30,31) included into this program the facility for rectangular plates for 'in plane' and 'out of plane' analysis and were thus able to analyse such three dimensional structures as tables and portal sheds. Thus the finite element method was becoming a more practical proposition in the analysis of Civil Engineering structures.

1.5 Causes of Nonlinearity in Materials

The finite element method described so far has been limited to various conditions. Some of these are that the structure remains in the linear elastic range, the deflections are small and the plates in bending are thin, with the stress (varying linearly throughout the thickness.) It was therefore a logical step to extend these analyses into the nonlinear range. The need for this was even more pronounced

when considering continua in two or three dimensions where such elements as the plane strain, axi-symmetrical, or solid element are employed.

Generally, the main influences on nonlinearity in a continuum will be:-

(i) Temperature changes.

(ii) Plasticity.

(iii) Creep.

(iv) Large deflections or change of geometry.

(v) Nonlinear material properties.

These could act independently or concurrently during the loading or unloading of the structure. The effects of temperature change, plasticity and creep can be predetermined and are known to depend on such factors as stress level, stress history and time. Nonlinearity due to large deflections or change of geometry could be caused by the buckling of thin plates or slender stanchions as well as the great deformation which will develop in very elastic continua.

In general the nonlinear properties of such materials as Aluminium are not as serious as the above effects and are usually considered to be of secondary importance. Nonlinear deformation can also be expected when a so-called 'continuum' acts discontinuously. Examples of this are the cracking which occurs in concrete and the deformation characteristics of a sand or clay mass.

In order to analyse such problems the nonlinear behaviour of materials can be represented as a series of linear steps. It will be shown in the next section that it is possible to proceed iteratively or incrementally through each step. This necessitates the suitable adjustment of the elastic properties to determine the pseudo-elastic

representation of the structure for each increment. A summary of the methods used by various authors is given in the next section.

1.6 Methods of Nonlinear Analysis

Clough and Zienkiewicz (32,2) have both used a direct iterative procedure which may be summarised as follows:-

(i) A load is applied to the structure and the state of stress and strain is evaluated throughout using a value of Young's Modulus equivalent to a state of zero stress. Fig. 13(a) shows a stress-strain relationship for a nonlinear material. The initial value of Young's Modulus, E_0, which is used is given by the slope of the line OA which is tangential to the curve at O.

(ii) Depending on the stress or strain level, the modulus of elasticity is changed throughout for each element. In the figure, point B can be established and the slope of OB gives the first alteration of the modulus to E_1.

(iii) The analysis is performed again using the new values to find the state of stress and strain.

(iv) Procedures (ii) and (iii) are repeated using values E_2, E_3 etc until the new values of the moduli have converged on the ones used in the previous iteration i.e. when points B and D have converged on one another.

A stress-strain relationship must be found which is representative of the material properties. For uniaxial stress this would be straight forward. For triaxial systems, a direct stress-strain graph is usually inadequate as it ignores the influence of the stresses in the two other directions to that which is being considered. It is more common therefore to find a function of the principal stresses to express the nonlinear relationship. Convergence of results cannot be

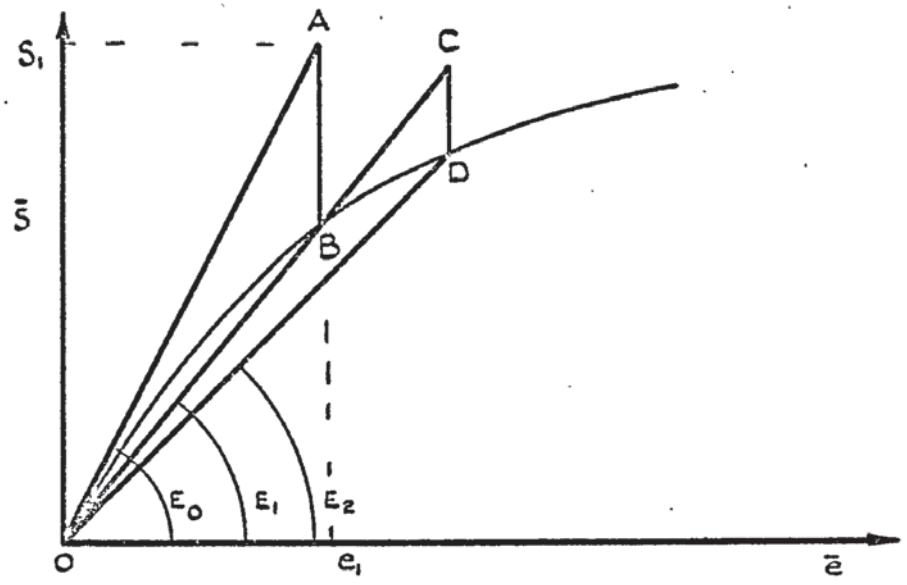

FIGURE. 1.3. (a) NONLINEAR. ITERATIVE PROCEDURE

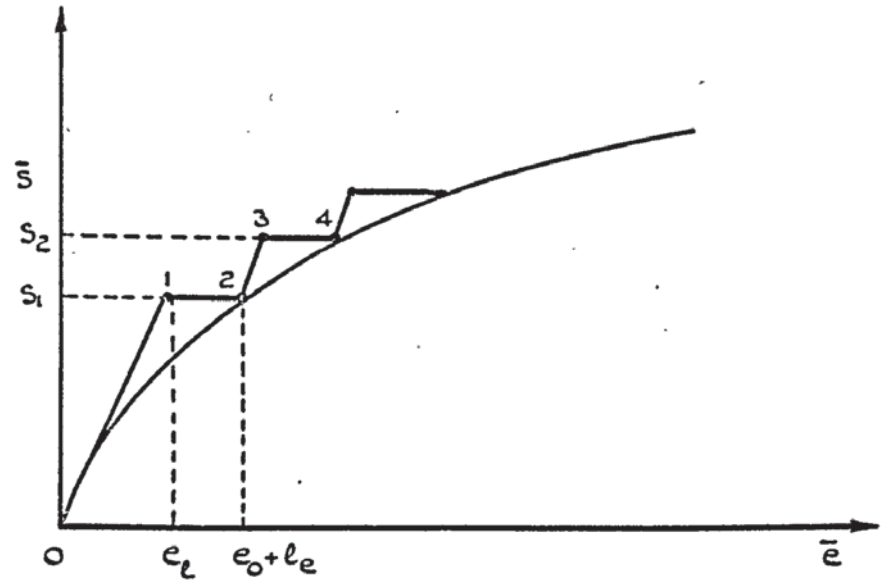

FIGURE 1. 3. (b) NONLINEAR INCREMENTAL - INITIAL LOAD PROCEDURE

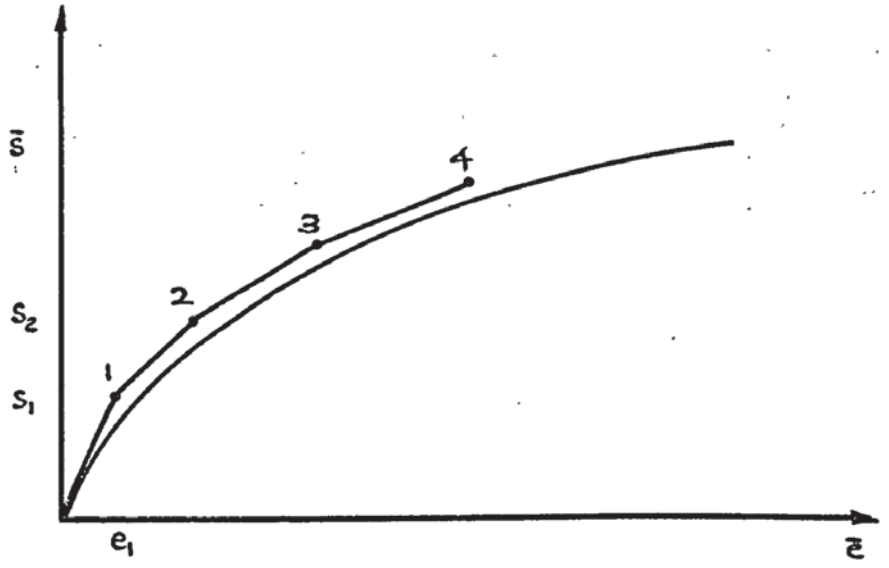

FIGURE. 1.3. (c) NONLINEAR INCREMENTAL TANGENTIAL PROCEDURE.

proved but is known to be present for most practical cases. Both Clough and Zienkiewicz used this method with isotropic material of constant Poisson's ratio. An extension of this method, to include orthotropy and variable Poissons' ratios, is given later in this thesis.

In 1965 Argyris (33,34,35) proposed an incremental approach to the analysis of plasticity, creep and problems concerning large deflections. It was now possible to use a more mathematical model for the system. The laws concerning these phenomena split up the total strain into its various components thus:-

$$e = e_e + e_p + e_\theta + e_c \qquad (1.22)$$

where e is the total strain and suffixes e, p, θ, c refer to the strain due to elasticity, plasticity, temperature change and creep respectively. Equation (1.22) can be rewritten as,

$$\underline{e} = \underline{D}^{-1}\underline{s} + \underline{e}_o \qquad (1.23)$$

where e_o is the additional inelastic strain. The analysis proceeds by adding the loads in an incremental way. The first increment occurs in the purely elastic range hence,

$$\Delta \underline{L} = \underline{K}\,\Delta \underline{X} \qquad (1.24)$$

where Δ represents a finite increment. The stress increment, deflection increment and time and temperature increments are all known. From these the nonlinear strains e_o if any, can be calculated independently. These are converted into initial loads which represent the element forces needed to suppress this additional strain, and are denoted by $\underline{P}_o$. Subsequent solutions for the following load increments are solved from the equation,

$$\Delta \underline{L} = \underline{K}\Delta \underline{X} + \underline{A}^{1}\Delta \underline{P}_o \qquad (1.25)$$

The total deflection and stress in the medium is obtained by simply adding the increments. This method is shown diagrammatically in fig. 1.3(b) where the initial elastic strain e_e, due to s_1, is added to the inelastic strain e_o before the stress is increased from s_1 to s_2.

Argyris suggested that provided the increments are small, it can be assumed that the additional strains calculated from one increment act in the following increment. An alternative approach would be to use these strains as the first iteration in an increment to find the additional strains in the next. When these two quantities are equal the iteration is stopped. This would allow the use of larger increments. This method has the drawback that, as strains become infinite, so will $\underline{P}o$ and hence convergence will not occur. To overcome this Pope (36) and later, Marcal and King et Al.(37,38), formed an approach which used the elastic tangent moduli. They were able to proceed incrementally in a manner given by fig. 1.3(c).

It can be seen that in proceeding between point 1 and 2 and 2 to 3 etc. on the curve the tangent modulus could be used to follow the actual deformation closely. This was done by the matrix addition of the stiffness matrices due to elasticity $\underline{k}e$ and those due to plasticity $\underline{k}p$ in such a manner that:-

$$\underline{k}ep = \underline{k}e + \underline{k}p \qquad (1.26)$$

where $\underline{k}ep$ is the tangent modulus and is represented by the slope of the line joining points 1 and 2. This will tend to zero at failure.

Argyris (35) used a similar method to analyse structures where the movement of elements is relatively large but their individual strains small. By redefining their local axes after each increment he was able to construct a geometry matrix $\underline{k}g$ which could be combined with the elastic

stiffness matrix thus,

$$\underline{k}_{eg} = \underline{k}e + \underline{k}g \qquad (1.27)$$

Of the three basic methods described above each has advantages and disadvantages. The iterative technique can be applied to all problems of nonlinearity but can suffer from drawbacks occuring when strains become infinite at failure. It can also suffer when a reduction of load under increasing strain takes place. Furthermore it is found more difficult to represent the unloading of various elements where, say, a purely elastic change would occur. When dealing with problems of creep and plasticity the second and third methods would appear preferable. In these cases the strains can be subdivided as shown by equation (1.22) and more realistic mathematical models exist. The incremental method will also give a general developement of the analysis up to failure whereas the iterative technique has to be solved for each loading case. More computation is therefore involved in the iterative method. For the analysis of large deflections, whether of the post-buckling type or due to the deformable nature of the material, either method is theoretically applicable. Again the incremental procedure would provide a more convenient solution. In this thesis an incremental method of analysis is presented, whereby the stress-strain diagram is first converted to a tangent modulus-strain diagram which is then used to carry the incremental analysis. In the proposed method, matrix additions, of the type suggested by either Argyris, Pope, Marcal or King, are not preformed. Instead the actual stress-strain diagram is used to represent the total state of strain at a given instant. It should be pointed out that in the case of materials such as sand, the total strain cannot be separated into its various elastic and inelastic components and therefore the incremental methods suggested by the other authors cannot be used with such material.

The next section gives a review of the attempts at nonlinear analysis in relation to problems in soil mechanics. The concentration in this particular area stems from the advantage the finite element method has in the solution of such problems. This will be investigated later on in the thesis. The work in this field has been limited but not without success. Firstly, however, an outline of the more well known work on creep is given, a study of which is also investigated.

1.7 Review of Nonlinear Analyses

It was mentioned in the previous section how the effects of temperature change and plasticity could be accounted for. Other authors including Argyris have used this incremental - initial load approach and this was a development from the method of taking initial stresses or strains into account. Again creep presents, in theory, no additional difficulties and an incremental analysis will depend on the laws which are to be used to calculate the creep strain. Zienkiewicz (2) has outlined ways of obtaining this and, with Watson and King (37,38) developed an incremental - tangential approach to analyse the visco-elastic creep in materials. For this type of creep the analyses are more simplified. It is acceptable to assume that the creep strain is linearly related to the stress level and a function can be found to convert the elastic stiffness of an element into its tangential stiffness. Visco-elastic materials also show a marked dependence on stress history which makes more complicated loading systems difficult to take into account. Examples of materials which exhibit visco-elasticity are plastics, Perspex and concrete.

It will suffice here to say therefore that creep presents little difficulty in nonlinear analysis as long as suitable theory is available for its computation. The problems which occur in soil

mechanics are many and varied. These will include slope stability, settlement of foundations and the numerous problems concerned with permanent earthworks. Soil, whether of a sand or clay nature, is known to be a nonlinear material. It is conceivable therefore that a finite element nonlinear analysis, similar to that just described can be applied to certain problems. Three major advantages of this method are:-

(i) First of all complicated boundary conditions can be represented easily. This is a well known advantage of the method. When such conditions appear in the field simplifications have to be introduced for laboratory analysis. It has also been found extremely difficult to scale up results of test models which simulate the actual conditions. This is mainly due to the fixed grain size of both model and proposed work. Many problems in soil mechanics can be classed under a condition of plane strain. Examples would be long retaining walls or strip footings acting on the ground. These can be analysed by considering a unit width of the cross-section under a condition where the strain across the width is zero. For such problems, a plane strain two-dimensional element can be used. An axi-symmetric element, which was formulated by Clough (32), could be used for such cases as point loads on round footings being loaded on a three dimensional continuum. Other problems could be tackled using a 'brick-shaped' three dimensional element. It is thus possible to use a more accurate structural model than the more classical techniques of analysis.

(ii) The second advantage is the fact that nonlinearity can be taken into account in the soil. This leads on to the representation of its stress-strain characteristics which is a more complex problem. The main difficulty is that of assigning pseudo -elastic constants to a

material which can act discontinuously. The difficulty in the case of sand is more pronounced than that of clay due to its granular nature and will be discussed in more detail in chapter 7.

(iii) Furthermore, another advantage is that inhomogeneity and anisotropy can be catered for with little difficulty. This merely entails giving the elements different properties and, as long as each individual element is considered homogeneous, the overall continuum can be unhomogeneous. Orthotropy, at any angle to the local axes of an element, can be accomodated by suitable arrangement of the elasticity matrix. Thus differing layers or strata can be accounted for.

At present, the most common method of calculating pressure under footings is by the well known Boussinesq equations. This assumes a homogeneous, isotropic, elastic half space or 'semi-infinite' continuum acting with a predetermined Young's Modulus. The deflection of the footing is calculated using parameters obtained from the results of laboratory tests which can take differing strata properties into account. While being reasonably reliable, the basic assumptions are obviously in error and an accurate prediction of the contact pressure which will act between the underside of the footing and the ground will be hard to make. This will depend on the flexibility of the footing. Cheung and Zienkiewicz (39) combined the action of flexible plate elements acting on foundations which were either of the Winkler type (a series of independant isolated springs) or the Boussinesq type in the case of the half-space. They were able to obtain a more accurate value of the contact pressure in the latter case and it was notable that at the edge of a rigid footing this pressure tended to infinity as suggested by the theory. Cheung and Nag (40) developed this theory to include the separation of foundation and plates by using a nonlinear iterative

procedure. This work was more of a development of the Boussinesq theory and did not take into account the nonlinearity of the soil or change of contact pressure with deflection.

Clough and Woodward (41) used a plane strain technique to estimate the change of stress that would occur in an embankment as it was constructed in successive layers. The self weight of the layer was represented by nodal loads and the properties of the preceding layers were altered according to the consolidating pressures. The stress-strain relationship of the element was represented by the elasticity matrix. It was assumed that this was comprised of two constants K and G to represent the bulk and shear moduli respectively. Hence this matrix became:-

$$\begin{bmatrix} K+G & K-G & 0 \\ K-G & K+G & 0 \\ 0 & 0 & G \end{bmatrix}$$

With respect to principal stresses and strains. By altering these moduli for successive layers they produced a stress history for the embankment.

Girijavallabdan and Reese (42) used the finite element method to investigate the load-deflection characteristics of a footing on clay and, also, the movement of a retaining wall into a sand mass. For this a nonlinear iterative procedure was used. For the stress-strain relationship a graph of Octahedral shear stress against shear strain was prepared. Hence the shear modulus was used to govern the deformation. Better results were obtained in the case of clay as this can be considered as an incompressible continuum whereas the granular nature of sands causes dilation on shear and hence discontinuity. Even so, the results which were obtained were encouraging.

For incompressible materials Poisson's ratio equals a half. This introduces a zero onto the loading diagonal of the plane strain elasticity matrix and the overall stiffness matrix becomes singular. Values for Poisson's ratio can be used reliably up to .47. Christian (43) suggested a method of overcoming this for clays. This was similar in nature to that proposed by Herrmann (44) whereby the ratio was considered to have an effective and total value similar to the concept of effective stress which occurs in soil under the influence of pore pressure. For a uniform sand mass the dissipation of pore pressure is rapid and hence this approach is not practical. The increased interest into a stress-strain relationship for soils is however apparent and is brought about by the more obvious assumptions used up till recently in the more classical methods.

1.8 Scope of Work.

In this thesis an attempt is made to investigate the suitability of the finite element method, in both its linear and nonlinear contexts, to solve practical civil engineering problems. These refer to the analysis of large three dimensional structures and, in the nonlinear range, the prediction of the settlement of footings on a sand foundation and the analysis of a shear wall which is loaded subject to creep.

For two dimensional problems, complex shapes have been analysed for stress and deflection and good results have been obtained when compared with photoelastic solutions. The 'in plane' elements used for such analyses are fully conforming and have changed little since their original formulation. The 'out of plane' element has been mainly investigated in relation to problems with known numerical solutions. These are necessarily simple cases, and the extent of its accuracy in analysing the more complex shapes with differing refinements and configurations of element subdivision have therefore to be investigated.

The triangular element is perhaps the most versatile shape for the representation of continua and hence chapter 2 describes a formulation of an 'out of plane' stiffness matrix for this element. As already mentioned, local equilibrium is usually violated in such elements and hence the values of stress are generally not as accurate as displacement. This chapter also gives two methods of its evaluation, either from the nodal forces or 'so called' stress matrices.

The following two chapters describe methods and the computer programs used in the elastic and nonlinear problems. In the former case the program of Majid and Williamson is extended to include the triangular element as well as to compute the stresses in plates. This program could now analyse generally shaped three dimensional structures, consisting of member, rectangular and triangular plate elements.

The various methods of nonlinear analysis have been described and it is apparent that its application must be considered before the form of program can be decided. The two methods which are used have been given previously along with their reasons. It is therefore possible to judge the relative merits of an incremental or iterative technique. As is more often the case in the study of soil mechanics problems, it is of more interest to investigate the effects of an imposed deflection on the soil than a load. A method of doing this is therefore developed and written into the program in this chapter.

Before using the triangular element in complex structures it was first necessary to assess its accuracy in straightforward problems. This was done in chapter 5 by comparing its results to those of the rectangular elements.

The following chapter describes the use of the elastic program to analyse a folded plate roof structure. Different element subdivisions are attempted as well as a 'mixture' of elements. Their influence on

results and the accuracy involved is compared against experimental values. By this means the suitability of the method is judged in the analyses of such buildings and there follows a description of this method in analysing two large engineering stuctures; those of a road bridge and an electro-filter precipitator casing.

The following two chapters investigate the nonlinear problems of the settlement of a footing on a sand mass and the deformation of a shear wall under the influence of creep.

Up till recently the study of the behaviour of soil has been more concerned with limit analyses and the variation of strain distribution up to failure is only now being investigated. Before accurate predictions of failure can be derived it would appear that these distributions must be known. The advantages of a finite element technique for such problems have already been given but, in addition to comparing the load settlement characteristics of this with experimental values, a comparison of the strain distribution throughout the mass can also be made. Both types of nonlinear program are used in this chapter.

In the analysis of a shear wall which takes place in chapter 8, a method of solution is evolved so as not to rely heavily on available theory or empirical formulae. In fact two different analyses are compared using the iterative procedure.

CHAPTER 2

FORMATION OF ELEMENT STIFFNESS AND STRESS MATRICES

2.1 Introduction

In order to analyse general structures by the finite element method it is desirable to include the triangular element in the 'library' of element shapes. Its basic shape makes it the most versatile of plate elements.

As mentioned in the previous chapter, a number of methods have been proposed for finding an 'out of plane' stiffness matrix. In this chapter a method is used so that it is applicable in analysing large structures and its final expression is suitable for inclusion into an elastic analysis program.

It is apparent that to find an element stiffness which is fully conforming in displacement and curvature, without suffering from any subsequent defects, is hard. Where this has been achieved (21) it has been shown that the speed of convergence of the element is slow. Hence for practical subdivision, it was overstiff. For the analysis of large structures conformity could be sacrificed for economy of computing time and storage.

The method used was based on that of Bazeley et Al (19) but adapted in such a way as to be orientated into an acceptable form for the elastic analysis program of Majid and Williamson (30).

The triangular 'in plane' stiffness matrix is well documented (2,3,8,9) and hence only brief mention will be made of it in the next section.

Two methods of evaluating plate stresses are given. Either from plate forces or their stress matrices.

2.2 'In Plane' Triangular Element Stiffness Matrix

Fig. 2.1 shows a triangular element situated in the plane PQ of its local axes P, Q, R, as defined by the right hand rule, such that the origin is at corner 1, the P axis runs from corner 1 to 2 and the Q axis is at right angles to side 1-2 in the direction of corner 3.

The displacements within the element at any point P^1 (p,q) in the P and Q directions can be written as linear polynomials respectively,

$$u = A_1 + A_2 p + A_3 q$$

$$v = A_4 + A_5 p + A_6 q$$

From this basic assumption a stiffness matrix can be formulated using the method given in the previous chapter. The final expression is given in fig. 2.2. This relates the applied forces P_i, Q_i at any node i to the corresponding displacements u_i, v_i in the P and Q directions respectively. No 'in plane' rotational term α_{ri} which is about the R axis at node i, is included in its formulation and, since the $\underline{B}$ matrix is independent of p and q terms, the stress is constant throughout an element. Therefore microscopic equilibrium is not violated but stress discontinuities will exist between elements.

2.3 'Out of plane' Stiffness Matrix

The impracticability of describing a displacement function as a polynomial in terms of axial coordinates has led to the use of area coordinates.

Fig. 2.3 shows a triangle situated between axes P and Q. Any point P^1 (p,q) in the triangle can divide its area into three A_1^1, A_2^1 and A_3^1 as shown. This point can be defined uniquely by the ratio of such areas to the total area of the triangle which is denoted by A^1.

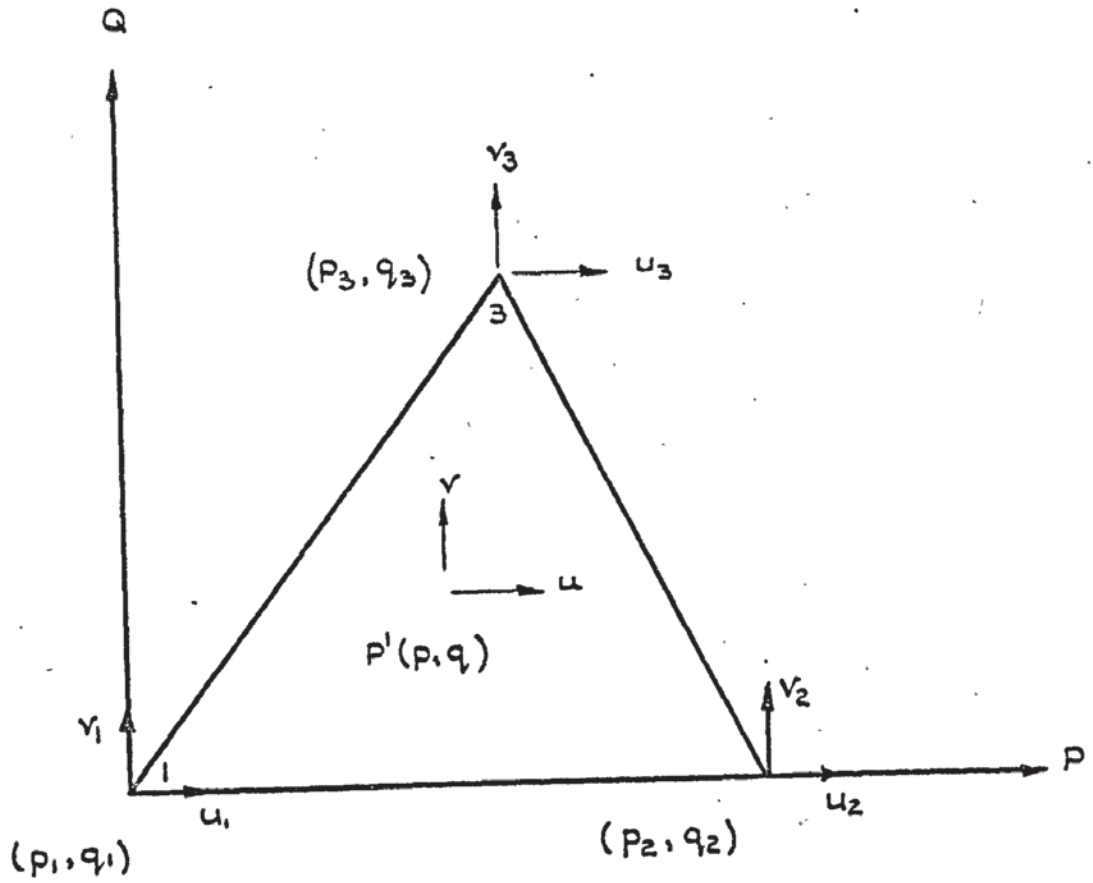

FIGURE 2.1.

$$\begin{bmatrix} P_1 \\ Q_1 \\ P_2 \\ Q_2 \\ Q_3 \\ Q_3 \end{bmatrix} = \frac{E t}{2 p_2 q_3 (1-\nu^2)} \left[\begin{array}{c|c|c|c|c|c} q_3 + \lambda_2 \lambda_3^2 & & & & & \\ -q_3 \lambda_3 (\lambda_2 + \nu) & \lambda_2 q_3^2 + \lambda_3^2 & & & & \\ -q_3^2 - \lambda_2 \lambda_3 p_3 & q_3 (\lambda_2 p_3 + \nu \lambda_3) & q_3^2 + \lambda_2 p_3^2 & & & \\ q_3 (\lambda_2 \lambda_3 + \nu p_3) & -\lambda_2 q_3^2 - p_3 \lambda_3 & -p_3 q_3 (\nu + \lambda_2) & \lambda_2 q_3^2 + p_3^2 & & \\ \lambda_2 \lambda_3 p_2 & -\lambda_2 p_2 q_3 & -\lambda_2 p_2 p_3 & \lambda_2 p_2 q_3 & \lambda_2 p_2^2 & \\ -\nu p_2 q_3 & p_2 \lambda_3 & \nu p_2 q_3 & -p_2 p_3 & 0 & p_2^2 \end{array}\right] \begin{bmatrix} u_1 \\ v_1 \\ u_2 \\ v_2 \\ u_3 \\ v_3 \end{bmatrix}$$

Symmetrical

$$\lambda_2 = \frac{1-\nu}{2} \qquad \lambda_3 = p_3 - p_2$$

FIGURE 2.2. IN PLANE TRIANGULAR STIFFNESS MATRIX

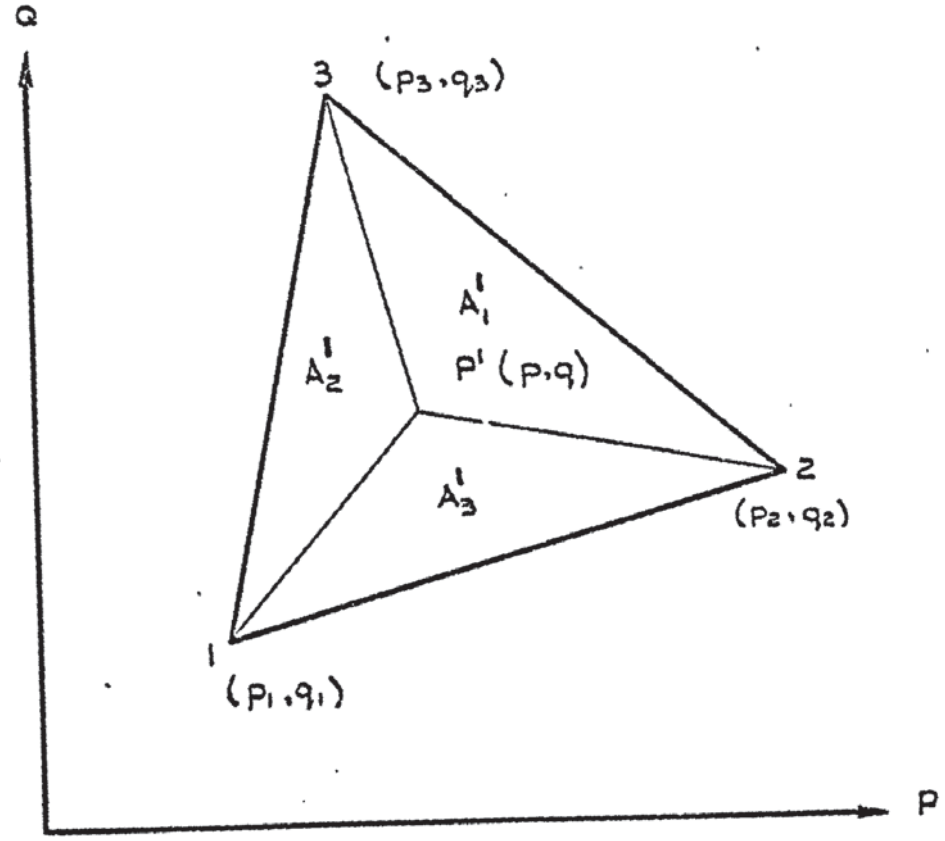

FIGURE 2.3

The Area coordinates become,

$$L_1 = A_1^1/A^1; \quad L_2 = A_2^1/A^1; \quad L_3 = A_3^1/A^1 \qquad (2.1)$$

For instance, at side 1-2, $L_3 = o$ and at corner 3, $L_3 = 1$. Let,

$$\begin{aligned} a_1 &= p_2 q_3 - p_3 q_2 \\ b_1 &= q_2 - q_3 \\ c_1 &= p_3 - p_2 \end{aligned} \qquad (2.2)$$

Similarly expressions for a_2 etc. are obtained by cycling the subscript in order 1, 2, 3.

From equations (2.1) and (2.2) it can be shown that:-

$$\begin{aligned} L_1 &= (a_1 + b_1 p + c_1 q)/2A^1 \\ L_2 &= (a_2 + b_2 p + c_2 q)/2A^1 \\ L_3 &= (a_3 + b_3 p + c_3 q)/2A^1 \end{aligned} \qquad (2.3)$$

Rearranging equations (2.3), p and q are shown to be,

$$\begin{aligned} p &= L_1 p_1 + L_2 p_2 + L_3 p_3 \\ q &= L_1 q_1 + L_2 q_2 + L_3 p_3 \end{aligned} \qquad (2.4)$$

The existence of this linear relationship will be made use of in the next section.

2.4 Displacement Function

The displacement function chosen must be able to represent a rigid body movement and a condition of constant strain. In satisfying the former condition, the vertical displacement, w at any point within the element can be divided into two components. The first is the displacement of the element without any straining and the second is the additional displacement due to its 'out of plane' action. Hence,

$$w = w^R + w^* \qquad (2.5)$$

w^R is therefore the rigid body movement of the element vertically downwards. w^* is the displacement of the element as if it were simply

supported and had angular rotations imposed at its nodes.

The displacement function relating w^R to the nodal displacements must vary linearly between the nodes so as not to cause bending. By analogy with equation (2.4) this can be written as:-

$$w^R = w_1 L_1 + w_2 L_2 + w_3 L_3 \qquad (2.6)$$

At any node i, the displacement vector of a simply supported element $\underline{Z}_i^*$ is reduced to:-

$$\underline{Z}_i^* = \begin{Bmatrix} \alpha^*_{pi} \\ \alpha^*_{qi} \end{Bmatrix}$$

where α^*_p and α^*_q are the angular slopes of this element, as defined by the right hand screw rule. The nodal slopes are given by the terms α_{pi} and α_{qi} as shown in fig. 2.4, where,

$$\alpha_p = \partial w/\partial q; \quad \alpha_q = -\partial w/\partial p \qquad (2.7)$$

The two rotations can be related by the equation (2.5) thus,

$$\alpha^*_p = \partial w^*/\partial q = -\alpha_p - \partial w^R/\partial q$$
$$\alpha^*_q = -\partial w^*/\partial p = \alpha_q + \partial w^R/\partial p \qquad (2.8)$$

The last terms in these equations can be evaluated from equation (2.6) and hence the nodal element displacements can be related to the simply supported ones by the equation,

$$\underline{Z}^* = \underline{T}\,\underline{Z} \qquad (2.9)$$

An expression for the transformation matrix $\underline{T}$ is given in fig. 2.5. From the principles of virtual work it can be shown that:-

$$\underline{k} = \underline{T}^1\,\underline{k}^*\,\underline{T}$$

where $\underline{k}^*$ is the stiffness matrix of a simply supported element in bending.

In order to determine $\underline{k}^*$, a displacement function must be found in the form,

$$\underline{w}^* = \underline{N}\,\underline{z}^* \qquad (2.11)$$

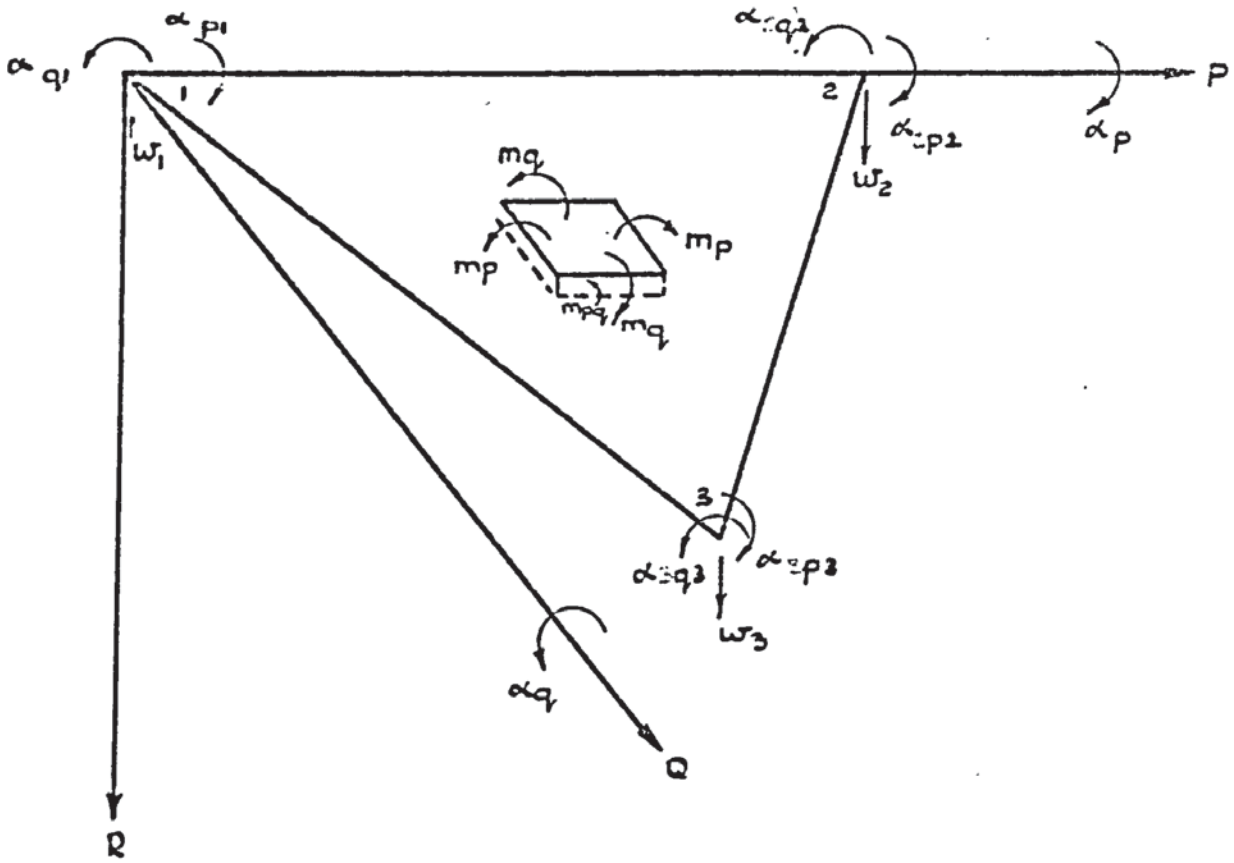

FIGURE 2.4.

$$\frac{1}{2\Delta}\begin{bmatrix} -c_1 & 2\Delta & 0 & -c_2 & 0 & 0 & -c_3 & 0 & 0 \\ b_1 & 0 & 2\Delta & b_2 & 0 & 0 & b_3 & 0 & 0 \\ -c_1 & 0 & 0 & -c_2 & 2\Delta & 0 & -c_3 & 0 & 0 \\ b_1 & 0 & 0 & b_2 & 0 & 2\Delta & b_3 & 0 & 0 \\ -c_1 & 0 & 0 & -c_2 & 0 & 0 & -c_3 & 2\Delta & 0 \\ b_1 & 0 & 0 & b_2 & 0 & 0 & b_3 & 0 & 2\Delta \end{bmatrix}$$

FIGURE 2.5. MATRIX 'T'

or, more fully,

$$w^* = N_{p1} \alpha^*_{p1} + N_{q1}\alpha^*_{q1} + N_{p2}\alpha^*_{p2} + N_{q2}\alpha^*_{q2} + N_{p3}\alpha^*_{q3} + N_{q3}\alpha^*_{q3} \qquad (2.12)$$

In choosing such a function, it is apparent that w^* must be zero at all nodes and equations (2.8) and (2.12) be satisfied. Thus at node 1 for instance:-

$$\partial N_{p1}/\partial q = 1 \text{ and } \partial N_{q1}/\partial p = -1$$

at the other nodes 2 and 3,

$$\partial N_{p1}/\partial q = \partial N_{q1}/\partial p = 0$$

while at nodes 1, 2 and 3,

$$\partial N_{p1}/\partial p = \partial N_{q1}/\partial q = 0$$

with similar conditions for the other functions. Suitable functions which satisfy these conditions are:-

$$N_{p1} = (b_2L_3 - b_3L_2)\, L_1^2$$
$$N_{q1} = (C_2L_3 - C_3L_2)\, L_1^2 \qquad (2.13)$$

The other functions are obtained by cycling the subscripts as before.

The displacement function takes the form of a cubic expression. As this curve can be defined by four constants, a slope and displacement at each node or corner, it will conform for displacement. However, for slope across the boundaries, the expression will vary as a quadratic, as given by its first derivative. As only two constants are defined, these being the slopes at either nodes, it will not conform in this case and the phenomenon known as 'Kinking' will occur when adjacent elements deform.

This displacement function will not be able to represent a constant strain condition. To do this w^* must be expressible as a general quadratic of the form,

$$w^* = G_1L_2L_3 + G_2L_3L_1 + G_3L_1L_2 \qquad (2.14)$$

where $C_{1,2,3}$ are arbitrary constants.

The function $L_1L_2L_3$ is cubic and gives zero values of itself and its slopes at all nodes. Thus it can be added to the function in any proportion denoted by B. Hence,

$$N_{pl} = b_2(L_1^2L_3 + BL_1L_2L_3) - b_3\ (L_1^2L_2 + BL_1L_2L_3) \qquad (2.15)$$

From equation (2.14) an expression for B can be found and substituted into equation (2.12) along with equation (2.15). By analogy with equation (2.14) it is found that the function can take up this quadratic form when $B = \frac{1}{2}$. Hence the final expression for the displacement function is,

$$N_{pl} = b_2(L_1^2L_3 + \tfrac{1}{2}L_1L_2L_3) - b_3\ (L_1^2L + \tfrac{1}{2}L_1L_2L_3) \qquad (2.16)$$

The other terms follow on similarly.

2.5 Elasticity and Strain Matrix

By basic assumption the strains vary linearly through the thickness of the plate. The stresses can be determined from the internal moments per unit run at any point denoted by m_p, m_q, m_{pq} using a sign convention as defined in fig. 2.4. The corresponding curvatures will be $\partial^2w/\partial p^2$, $\partial^2w/\partial q^2$, $\partial^2w/\partial p\partial q$. Hence a moment curvature relationship can be used instead of the stress-strain, where,

$$\underline{s} \equiv \underline{m} = \{m_p,\ m_q,\ m_{pq}\}$$

$$\underline{e} \equiv \{-\partial^2w/\partial p^2,\ -\partial^2w/\partial q^2,\ 2\partial^2w/\partial p\partial q\}$$

The elasticity matrix D can be shown (1) to be:-

$$Et^3/12(1-\nu^2) \begin{bmatrix} 1 & \nu & 0 \\ \nu & 1 & 0 \\ 0 & 0 & (1-\nu)/2 \end{bmatrix}$$

Where E is the Young's modulus, ν the Poisson's ratio and t the thickness of the plate.

The strain matrix $\underline{B}^*$ will differ for the simply supported case and is defined as:-

$$\underline{e} = \underline{B}^*\ \underline{Z}^*$$

Hence $\underline{B}^*$ will take the form:-

$$\underline{B}^* = \left[\underline{B}_1^*, \underline{B}_2^*, \underline{B}_3^*\right]$$

where, for instance, $\underline{B}_1^*$ is a submatrix of the form:-

$$\begin{bmatrix} -\partial^2 N_{p1}/\partial p^2, & -\partial^2 N_{q1}/\partial p^2 \\ -\partial^2 N_{p1}/\partial q^2, & -\partial^2 N_{q1}/\partial q^2 \\ -2\partial^2 N_{p1}/\partial p \partial q, & 2\partial^2 N_{q1}/\partial p \partial q \end{bmatrix}$$

A final expression for $\underline{B}^*$ is given in appendix 2.

2.6 Formulation of the final Stiffness Matrix

By analogy with equation (1.15), it can be seen that:-

$$\underline{k}^* = \iint \underline{B}^{*1} \; \underline{D} \; \underline{B}^* \, dpdq \qquad (2.18)$$

It is apparent from appendix 2 that $\underline{B}^*$ takes the form,

$$B^*(i,j) = X(i,j)L_1 + Y(i,j)L_2 + Z(i,j)L_3 \qquad (2.19)$$

where X,Y,Z(i,j) are dimensional constants of the triangle.

An expression for the product $\underline{KP} = \underline{B}^{*1} \; \underline{D} \; \underline{B}^*$ can now be obtained in the form:-

$$KP(i,j) = L_1^2 \; (X) + L_2^2 \; (Y) + L_3^2 \; (Z) + L_1L_2 \; (X,Y) + L_1L_3 \; (X,Z) + L_2L_3 \; (Y,Z) \qquad (2.20)$$

where the functions X,Y,Z include the known constants of the various elements in the $\underline{B}^*$ matrix, X(i,j), Y(i,j) Z(i,j), and constants from the elasticity matrix. It follows that:-

$$\underline{k}^*(i,j) = \iint KP \; (i,j) \; dpdq \qquad (2.21)$$

The only terms involving p and q which have therefore to be integrated in equation (2.20) are L_1^2, L_2^2, L_3^2, L_1L_2, L_2L_3, L_1L_3.

For a triangle orientated as in fig. 2.3,

$\iint dpdq$ = area of the triangle

$\iint pdpdq$ = first moment of area

$\iint p^2 dpdq$ = second moment of area

$\iint pq \; dpdq$ = product moment of area.

Hence it is possible to obtain expressions for the integrations. Thus:-

$$\iint L_1 L_2 dpdq = \frac{1}{144} \{36a_1a_2 + 12((a_1b_2 + a_2b_1)(p_1 + p_2 + p_3) + (a_1c_2 + a_2c_1)(q_1 + q_2 + q_3)) + 6(b_1b_2x + c_1c_2y) + 3(b_1c_2 + b_2c_1)z\} \quad (2.22)$$

where,

$$x = p_1^2 + p_2^2 + p_3^2 + p_1p_2 + p_2p_3 + p_1p_3$$

$$y = q_1^2 + q_2^2 + q_3^2 + q_1q_2 + q_2q_3 + q_1q_3$$

$$z = 2p_1q_1 + 2p_2q_2 + 2p_3q_3 + p_1q_2 + p_1q_3 + p_2q_1 + p_2q_3 + p_3q_1 + p_3q_2$$

The other integrals are obtained by cycling the subscripts in the usual manner.

2.7 Evaluation of the Stiffness Matrix

A computer program was written in Atlas Autocode to construct the 'out of plane' stiffness matrix $\underline{k}$ for the triangular matrix. The coordinates and properties of the matrix are fed in and the integrals L_{ij} of equation (2.22) are evaluated and stored in a vector array. The constants of the $\underline{B}^*$ matrix, X(i,j), Y(i,j), Z(i,j), which appear in equation (2.19) are determined for this element and similarly stored in an array. These can then be simply multiplied together in the form of equation (2.20) to form the matrix $\underline{k}^*$. Matrix $\underline{T}$, which is given in fig. 2.5, is constructed and the final stiffness matrix obtained from equation (2.10). This program appears in appendix 1.

For use in the elastic analysis program, which will be described in the next chapter, it is advantageous to evaluate the final expressions of the stiffness matrix. This will also save a large amount of computing time.

The use of forming a stiffness matrix for an element situated anywhere in the P-Q plane is limited. The advantage being that, for two

dimensional problems, the direction cosines, which form the elements of the displacement transformation matrix $\underline{A}$, are all unity. The elastic analysis program analyses generally shaped, three dimensional problems and hence the triangle was orientated as shown in fig. 2.4. Therefore,

$$p_1 = q_1 = q_2 = 0.$$

Hence the copius algebra involved in evaluating the final stiffness terms is reduced and it was possible to proceed manually to obtain this expression for the stiffness. The computer program of appendix 1 was used as a check for the large amount of algebra. The expressions for the terms of $\underline{k}^*$ are given in appendix 2. These consist of the material properties E, ν, t and its principal dimensions p_2, p_3, q_2. The former values are fed in as data to the elastic analysis program and the latter can be calculated from the joint coordinates at the nodes of the element. It is now straightforward to program this stiffness matrix. Its addition into the elastic analysis program is described in the next chapter. Chapter 5 investigates the performance of the element and, in chapter 6, its applicability in analysing large structures is determined.

2.8 Calculation of Stress from Forces

Fig. 2.6 shows the nodal forces which act at any node i of a plate element. These consist of the 'in plane' forces P_i and Q_i in the direction of the local axes P,Q,R and the 'out of plane' forces R_i, M_{pi} and M_{qi} acting as shown as determined by the right hand screw rule.

These forces on the elements will be in equilibrium with each other along its sides thus satisfying macroscopic equilibrium and will represent the stress distribution around the sides of the element.

Fig. 2.7 shows the side 1-2 of an element, of length a , with forces P_1, Q_1 acting at node 1 and P_2, Q_2 at node 2. If a linear stress distribution is assumed between the nodes and has a value of y force per

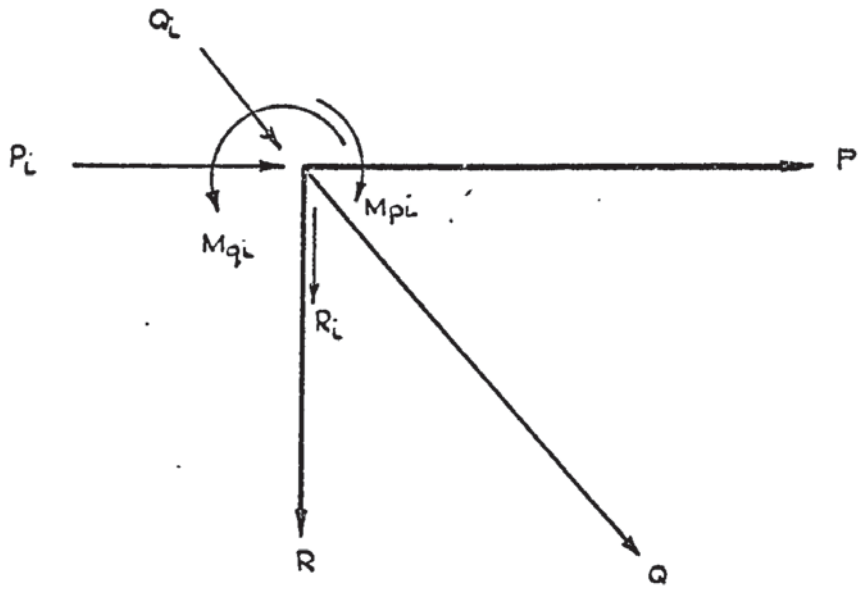

FIGURE 2.6 EQUIVALENT FORCES ACTING ON A PLATE AT NODE 'L'

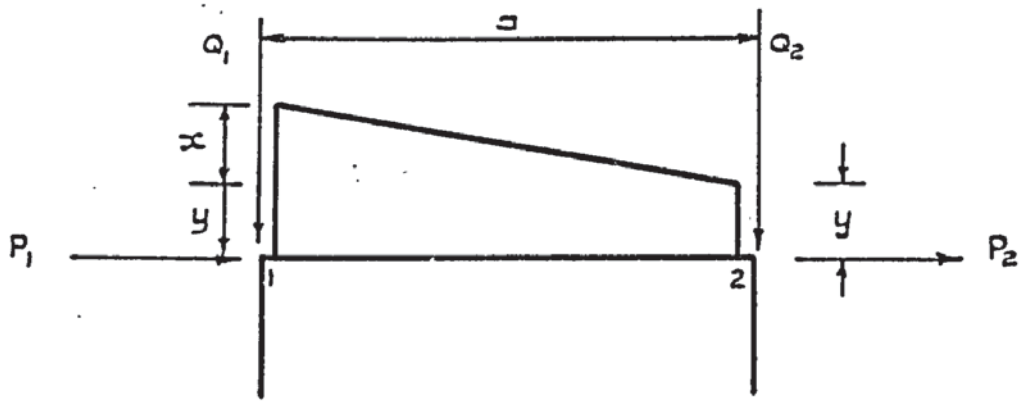

FIGURE 2.7 ASSUMED STRESS DISTRIBUTION BETWEEN TWO CONCENTRATED FORCES.

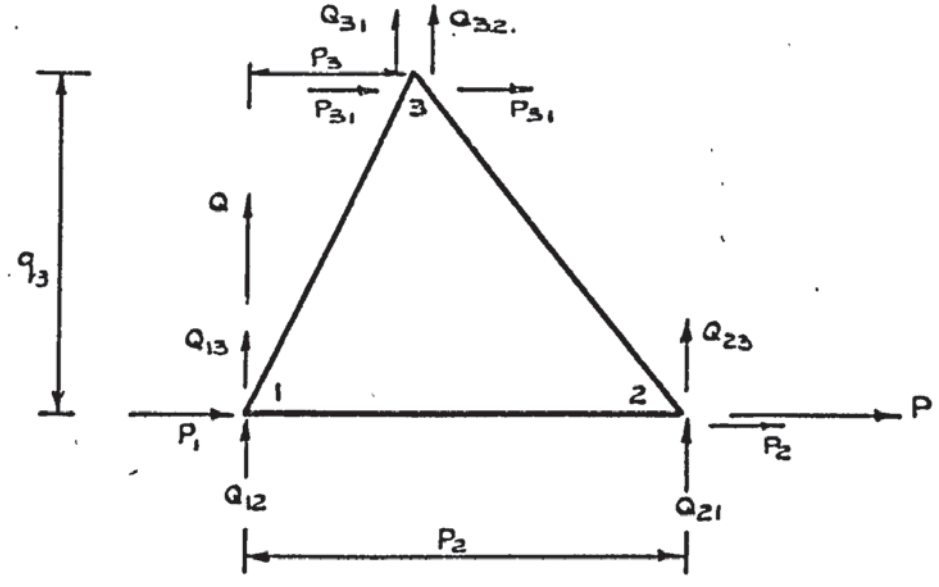

FIGURE 2.8. FORCES ACTING ON TRIANGULAR ELEMENT.

unit run at node 2 and x + y force per unit run at node 1 then it can be shown from consideration of equilibrium that:-

$$x = 6(Q_1 - Q_2)/a$$

$$\text{and } y = 2(2Q_2 - Q_1)/a \qquad (2.23)$$

From equations (2.23) the stresses are calculated as:-

$$s_{q1} = (x + y)/t;\ s_{q2} = y/t \qquad (2.24)$$

For a rectangular element the stress distribution is assumed linear for both 'in plane' and 'out of plane' elements. Equations (2.23) would equally apply for moment forces, say M_{p1} and M_{p2}. In this case the stresses depend on the section modulus thus,

$$s_{q1} = \pm 6(x + y)/t^2;\quad s_{q2} = \pm 6y/t^2 \qquad (2.25)$$

Similarly the shear along side 1-2 can be calculated using the forces P_1 and P_2. Therefore along any element side the shear and bending stresses for 'in plane' and 'out of plane' cases can be found at either node.

If the plate is defined so that the positive R axis runs from its top surface to bottom, the top and bottom stresses can be evaluated by simply adding or subtracting the bending stress from the 'in plane' stress.

Fig. 2.8 shows a triangular element whose principal dimensions are p_2, p_3, q_3. When considering stress in the P direction on side 1-3, this will act on the projection of this side. If an equation similar to (2.23) is used, it can be seen that, as the triangle becomes right angular, the stresses become infinite. For this reason the nodal forces are divided into two as shown. These are:-

$$Q_3 = Q_{31} + Q_{32}$$

$$Q_2 = Q_{21} + Q_{23}$$

$$Q_1 = Q_{12} + Q_{13} \qquad (2.26)$$

Where Q_{12} is the force at node 1 representing stress on face 1-2 and Q_{13} on face 1-3, and similarly at the other nodes.

Using forces Q_{12} and Q_{21} in equations similar to those of (2.23) and (2.24) stresses $\tilde{s}_{12}$ and $\tilde{s}_{21}$ at nodes 1 and 2 respectively can be found for side 1 -2. Similar stresses for the two other projections of sides 1-3 and 3-2 can also be found. For equilibrium at the nodes

$$\tilde{s}_{12} = \tilde{s}_{13};\ \tilde{s}_{21} = \tilde{s}_{23};\ \tilde{s}_{31} = \tilde{s}_{32} \qquad (2.27)$$

Using the expressions for the stress in equations (2.26) and (2.27) values of the forces are found to be:-

$$Q_{13} = (Q_1(3a - 5b) + Q_2(2b - a) + Q_3(2a - 3b))/(4(a - c - b))$$

$$Q_{23} = (Q_1(c - a) + Q_2(3a - 2c - b) + Q_3(2a - c - b))/4(a - c - b))$$

$$Q_{32} = (2Q_1P_3 - Q_2P_3 + Q_3P_2 + P_3Q_{23} - 2Q_{13}(P_3 + P_2))/P_2 \qquad (2.28)$$

where, for these equations,

$$a = P_2\,P_3^2$$

$$b = P_3\,P_2^2$$

$$c = P_2^3$$

It can be seen from the above equations that,

if $P_3 = 0$ then $Q_{13} = 0$

if $P_2 = P_3$ then $Q_{23} = 0$

Therefore, if the triangle is right angular no infinite stresses will occur. Similarly it can be shown in the P direction that:-

$$P_{31} = (2P_3 + P_1 - P_2)/4 \qquad (2.29)$$

Therefore the stresses round the triangle at each node can be found by determining the equivalent forces from equation (2.28) and (2.29) and using these to evaluate the stresses. As before, the moment per unit run can be found in a similar manner and the top and bottom surface stresses evaluated.

2.9 Calculation of Stress using Stress Matrices

Considering equations (1.11) and (1.12) it is apparent that:-

$$\underline{s} = \underline{B}\ \underline{D}\ \underline{Z} \qquad (2.30)$$

Equation (2.30) can be rewritten as:-

$$\underline{s} = \underline{S}\ \underline{Z} \qquad (2.31)$$

where $\underline{S}$, the stress matrix, is the product $\underline{D}\ \underline{B}$. The elasticity matrix $\underline{D}$ can be written as:-

$$\alpha_o \begin{bmatrix} \alpha_{11} & \alpha_{12} & \alpha_{13} \\ \alpha_{21} & \alpha_{22} & \alpha_{23} \\ \alpha_{31} & \alpha_{32} & \alpha_{33} \end{bmatrix}$$

where its elements α_{ij} are constants of the material and depend on whether the problem considered is of plane stress, plane strain, isotropic or orthotropic.

For the rectangular plates the stress is assumed to vary linearly throughout its boundaries. The $\underline{B}$ matrix was evaluated for 'in plane' and 'out of plane' action at the centre of gravity. Figs. 2.9 and 2.10 give the final expressions for the stress matrices of a rectangular plate to evaluate 'in plane' and 'out of plane' stresses respectively. Theses are for a plate of dimensions a in the P direction and b in the Q direction. The values of α_{ij} are given for the state of plane stress. For the 'in plane' stresses, the values s_p, s_q, s_{pq} can be obtained at its centre of gravity by multiplying this matrix by the 'in plane' nodal displacement vector.

As previously mentioned, the 'out of plane' elasticity matrix relates the moments per unit run, m_p, m_q, m_{pq}, to the curvatures. These are converted to stresses by dividing by the section modulus. Therefore, by multiplying the constant α_o by the section modulus $6/t^2$, a new constant is found as shown in fig. 2.10. Hence this matrix now gives the bending stresses directly.

$$\frac{\alpha_0}{2ab}\begin{bmatrix} -\alpha_{11}b & -\alpha_{21}b & \alpha_{11}b & -\alpha_{21}a & -\alpha_{11}b & \alpha_{21}a & \alpha_{11}b & \alpha_{21}a \\ -\alpha_{21}b & -\alpha_{22}a & \alpha_{21}b & -\alpha_{22}a & -\alpha_{21}b & \alpha_{22}a & \alpha_{21}b & \alpha_{22}a \\ -\alpha_{33}a & -\alpha_{33}b & -\alpha_{33}a & \alpha_{33}b & \alpha_{33}a & -\alpha_{33}b & \alpha_{33}a & \alpha_{33}b \end{bmatrix}$$

$$\alpha_0 = \frac{\text{thickness} \times E}{(1-\nu^2)} \qquad \alpha_{11} = 1 \qquad \alpha_{12} = \nu \qquad \alpha_{22} = 1 \qquad \alpha_{33} = \frac{1-\nu}{2}$$

FIGURE 2.9 THE 'IN PLANE' STRESS MATRIX FOR A RECTANGULAR PLATE.

$$\frac{Et}{4ab(1-\nu^2)}\begin{bmatrix} 0 & -\nu a & b & 0 & -\nu a & -b & 0 & \nu a & b & 0 & \nu a & -b \\ 0 & -a & \nu b & 0 & -a & -\nu b & 0 & a & \nu b & 0 & a & -\nu b \\ 8\alpha_{33} & b\alpha_{33} & -a\alpha_{33} & -8\alpha_{33} & -b\alpha_{33} & -a\alpha_{33} & -8\alpha_{33} & b\alpha_{33} & a\alpha_{33} & 8\alpha_{33} & -b\alpha_{33} & a\alpha_{33} \end{bmatrix}$$

$$\alpha_{33} = \frac{1-\nu}{2}$$

FIGURE 2.10 THE 'OUT OF PLANE' STRESS MATRIX FOR A RECTANGULAR ELEMENT.

The 'in plane' stresses are positive when tensile and the moments per unit run are shown by fig. 2.4 to be positive when 'hogging'. Thus, by adding the two types, the top surface stresses are found and, by subtraction, the bottom stresses.

The 'in plane' stress matrix for the triangular plate is given in fig. 2.11. This is a constant stress element and the values of stress are assumed to act at the centre of gravity. Weighting procedures have been attempted (47). to find a more meaningful value of stress at the nodes by without much success.

It can be shown from equations (2.9) and (2.17) that, for the 'out of plane' triangular plate element:-

$$\underline{S} = \underline{D}\ \underline{B}^{*}\ \underline{T} \qquad (2.32)$$

The elasticity matrix $\underline{D}$ is the same as for the rectangular element. Matrix $\underline{T}$ is given in fig. 2.5. Matrix $\underline{B}^{*}$ is that which appears in appendix 2 only simplified for a position at the centre of gravity where:-

$$L_1 = L_2 = L_3 = 1/3$$

The final expression was not needed to be evaluated. The product $\underline{D}\ \underline{B}^{*}$ appears in appendix 2. In the program which will be described in the next chapter the elements of the above product could be calculated and the stress matrix consisted of simple functions of the elements of the $\underline{T}$ matrix.

In general, stress discontinuities at nodal points can be expected for most practical subdivisions. Only when the mesh of elements is greatly refined will these disappear. It is proposed that by averaging the stress throughout the element, which is tantamount to evaluating stress at its centre of gravity, a better representation is found than by averaging nodal values round a joint. Another difficulty which is overcome by this method is that of theoretically infinite stresses which will occur under a point load at a joint.

$$\frac{\alpha_0}{p_2 q_3}\begin{bmatrix} -\alpha_{11} q_3 & \alpha_{12}(p_3-p_2) & \alpha_{11} q_3 & -\alpha_{21} p_3 & 0 & \alpha_{21} p_2 \\ -\alpha_{21} q_3 & \alpha_{22}(p_3-p_2) & \alpha_{12} q_3 & -\alpha_{22} p_3 & 0 & \alpha_{22} p_2 \\ \alpha_{33}(p_3-p_2) & -q_3 \alpha_{33} & -\alpha_{33} p_3 & \alpha_{33} q_3 & \alpha_{33} p_2 & 0 \end{bmatrix}$$

$$\alpha_0 = \frac{E}{1-\nu^2} \qquad \alpha_{11} = 1 \qquad \alpha_{12} = \nu \qquad \alpha_{22} = 1 \qquad \alpha_{33} = \frac{1-\nu}{2}$$

FIGURE 2.11. THE 'IN PLANE' STRESS MATRIX FOR A TRIANGULAR PLATE.

These two methods of calculating stress are included into the elastic analysis program in the next chapter and compared for reliability of results in chapter 5.

CHAPTER 3

ELASTIC ANALYSIS PROGRAMS

3.1 Introduction

This chapter describes the development of the analysis program written by Majid and Williamson. The facility to analyse structures which contain flat triangular plate elements for both 'in plane' and 'out of plane' actions is included. The triangular plate stiffness matrix which was derived in the previous chapter is used in these analyses. The programming language used throughout was Atlas Autocode.

In order to evaluate plate stresses, programs were written based on the methods given in the last chapter. These were formed so as to be run after the analysis program which calculates deflections and element forces.

Even when using sparse matrix routines, the storage capacity of the largest computers is quickly filled for the analysis of relatively medium sized structures. To overcome this a tridiagonalisation scheme was used. Although this is now a well known technique among engineers the next section gives a description of how it was included into the elastic analysis program.

3.2 Tridiagonalisation of the Stiffness Matrix

If the joints in a structure can be divided into groups numbered 1 to n such that those in any intermediate group i are only connected to groups i-1 and i+1 then the overall stiffness matrix will take the form of:-

$$\begin{bmatrix} \underline{L}_1 \\ \underline{L}_2 \\ \underline{L}_3 \\ \vdots \end{bmatrix} \quad \begin{bmatrix} \underline{K}_{11}\underline{K}_{12} & & \\ \underline{K}_{21}\underline{K}_{22}\underline{K}_{23} & & \\ \underline{K}_{32}\underline{K}_{33}\underline{K}_{34} & & \\ & \ddots & \end{bmatrix} \quad \begin{bmatrix} \underline{X}_1 \\ \underline{X}_2 \\ \underline{X}_3 \\ \vdots \end{bmatrix}$$

(cont'd overpage)

$$\begin{bmatrix} \vdots \\ \underline{L}_{i-1} \\ \underline{L}_i \\ \underline{L}_{i+1} \\ \vdots \\ \underline{L}_n \end{bmatrix} = \begin{bmatrix} \ddots & & & & \\ & \underline{K}_{i-1,i-2}\underline{K}_{i-1,-1}\underline{K}_{i-1,i} & & & \\ & & \underline{K}_{i,i-1}\underline{K}_{i,i}\underline{K}_{i,i+1} & & \\ & & & \underline{K}_{i+1,i}\underline{K}_{i+1,i+1}\underline{K}_{i+1,i+2} & \\ & & & & \ddots \\ & & & & \underline{K}_{n,n-1}\underline{K}_{nn} \end{bmatrix} \begin{bmatrix} \vdots \\ \underline{X}_{i-1} \\ \underline{X}_i \\ \underline{X}_{i+1} \\ \vdots \\ \underline{X}_n \end{bmatrix} \quad (3.1)$$

The overall stiffness matrix is reformed to have three submatrices grouped around its leading diagonal with zero elsewhere.

In equation (3.1) $\underline{X}_i$ is the displacement vector of joint group i corresponding to loads $\underline{L}_i$. The matrix $\underline{K}_{ii}$ represents the stiffness of joint group i and the offdiagonal submatrices represent the stiffness of the elements joining the groups.

In a similar manner, the overall displacement transformation of the structure can be expressed in terms of submatrices for each group:-

$$\underline{A} = \left\{ \underline{A}_1, \underline{A}_2, \underline{A}_3 \cdots \underline{A}_{i-1}, \underline{A}_i, \underline{A}_{i+1} \cdots \underline{A}_n \right\} \qquad (3.2)$$

where $\underline{A}_i$ is the displacement transformation matrix of group i. From equation (3.1) and (3.2) it follows that:-

$$\underline{K}_{ii} = \underline{A}_i \underline{k}_i \underline{A}_i \qquad (3.3)$$

$$\underline{K}_{ij} = \underline{A}_i \underline{k}_{ij} \underline{A}_j \qquad (3.4)$$

where $\underline{k}_{ij}$ is the unassembled stiffness matrix of elements connecting joint groups i to j. Therefore j can take the values of i-1, i or i+1. If it is specified that all elements connecting groups i to i+1 are included in group i then equation (3.4) can be written as:-

$$\underline{K}_{ij} = \underline{A}_i \underline{k}_i \underline{A}_j \qquad (3.5)$$

The rows of the displacement transformation matrices correspond to the overall $\underline{Z}$ matrix of the structure and equation (3.5) is automatically partitioned to the form of equation (3.4). This saves the computation which would be involved in establishing $\underline{k}_{ij}$. The only information required to form equations (3.3) and (3.5) is that concerning joint groups i and j.

By solving the equations of (3.1) of each group, this matrix will reduce to:-

$$\begin{bmatrix} \bar{L}_1 \\ \bar{L}_2 \\ \vdots \\ \bar{L}_i \\ \vdots \\ \bar{L}_{n-1} \\ \bar{L}_n \end{bmatrix} = \begin{bmatrix} I & \bar{K}_{12} & & & & & \\ & I & \bar{K}_{23} & & & & \\ & & \ddots & \ddots & & & \\ & & & I & \bar{K}_{i,i+1} & & \\ & & & & \ddots & \ddots & \\ & & & & & I & \bar{K}_{n-1,n} \\ & & & & & & I \end{bmatrix} \begin{bmatrix} \underline{X}_1 \\ \underline{X}_2 \\ \vdots \\ \underline{X}_i \\ \vdots \\ \underline{X}_{n-1} \\ \underline{X}_n \end{bmatrix} \quad (3.6)$$

where $\bar{K}_{i,i+1} = \underline{K}^{*-1}_{i,i}\, \underline{K}_{i,i+1}$

$$\bar{L}_i = \underline{K}^{*-1}_{i,i}\, \underline{L}^{*}_{i} \quad (3.7)$$

and $$\underline{K}^{*}_{i,i} = \underline{K}_{ii} - \underline{K}_{i,i-1}\, K^{*-1}_{i-1,i-1}\, \underline{K}_{i-1,i} \quad (3.8)$$

$$\underline{L}^{*}_{i} = \underline{L}_i - \underline{K}_{i,i-1}\, K^{*-1}_{i-1,i-1}\, \underline{L}^{*}_{i-1}$$

The matrix I is a unity identity matrix. It can be shown that:-

$$\underline{K}^{*}_{11} = \underline{K}_{11} \text{ and } \underline{L}^{*}_{1} = \underline{L}_1 \quad (3.9)$$

From equation (3.6)

$$\underline{X}_n = \bar{L}_n \quad (3.10)$$

Back substituting:-

$$\underline{X}_{n-1} = \bar{L}_{n-1} - \bar{K}_{n-1,n} \underline{X}_n \quad (3.11)$$

Generally the joint displacements $\underline{X}_i$ can be computed from:-

$$\underline{X}_i = \bar{L}_i - \bar{K}_{i,i+1}\, \underline{X}_{i+1} \quad (3.12)$$

Rearranging equation (3.12),

$$\underline{X}_i = \begin{bmatrix} \bar{K}_{i,i+1} & \bar{L}_i \end{bmatrix} \begin{bmatrix} -\underline{X}_{i+1} \\ I \end{bmatrix} \quad (3.13)$$

where I is again a unit identity matrix. Denoting the compounded matrix $\begin{bmatrix} \bar{K}_{i,i+1} & \bar{L}_i \end{bmatrix}$ by S_i, equation (3.13) becomes:-

$$\underline{X}_i = S_i \begin{bmatrix} \underline{X}_{i+1} \\ \underline{I} \end{bmatrix} \qquad (3.14)$$

It can be seen that the matrix S_i only involves matrices concerning groups i-1, i, i+1. It is therefore possible to proceed through the joint groups of a structure determining the matrices S_1 to S_n. From equation (3.10) the displacements of the last joint group can be calculated. Backsubstituting, $\underline{X}_{n-1}$ can be calculated from equation (3.11) and the remaining displacements are similarly calculated from equation (3.14).

Before proceeding to the method involved in setting up the individual stiffness and transformation matrices, the next section gives a general description of the matrix operations involved in the program.

It will be shown that the data concerning only two of the joint groups need be stored in the computer at any one time. At the same time a magnetic tape can be used as a backing store to retain the matrices S_i and $\underline{k}\,\underline{A}_i$. Therefore the process of tridiagonalisation will save on computer storage.

3.3 Description of Analysis Program

The program can be divided into two main parts. The first is the calculation and storage on magnetic tape of S_i and $\underline{k}\underline{A}_i$ for all the joint groups. This is called the reduction process. The second is the recalling of these matrices from the magnetic tape to determine the joint displacements in a manner just described and, at the same time, to evaluate the member and plate forces from the equation,

$$\underline{P} = \underline{k}\underline{A}_1\underline{X}_1 + \underline{k}\underline{A}_2\underline{X}_2 + \ldots + \underline{k}\underline{A}_n\underline{X}_n \qquad (3.14a)$$

This is called the backsubstitution process.

The data required for each joint group during the reduction process is as follows:-

1. Joint data. This consists of the coordinates and degrees of freedom of each joint.

2. Member data. This defines the members running between joints and gives their properties.
3. Rectangular and triangular plate data. This gives the joints at each corner of the plates and their properties.
4. Load data. This is presented in the form of a sparse matrix vectorially equivalent to the displacement matrix.

All elements spanning from group i to i+1 are considered to be in group i. In addition to this a set of general data gives information concerning the type of problem and the storage requirements. A complete explanation of the data required for this program is given in appendix 3.

A flow diagram which is given in fig. 3.1 represents the reduction process. Each block of this is labelled 1 to 16 for ease in future reference. A table of the matrix operations which are involved are given in table 3.1 and this is divided into stages 1-23 for a similar reason.

Initially, the general data and joint data for groups 1 and 2 are read in by the program (blocks 1, 2 and 3, fig. 3.1). From this, the matrices $\underline{k}_1$ and $\underline{A}_1^1$ can be constructed for the first group (block 5). The matrices $\underline{kA}_1$ and $\underline{K}_{11}$ can now be formed by matrix multiplication (block 6) and the former matrix is also written onto magnetic tape (block 13) before considering the next joint group.

The third joint group data is read (block 3) and this replaces the first in main store. In a similar manner to the above, $\underline{k}_2$ and $\underline{A}_2^1$ are constructed for the second group. It is perhaps worth pointing out here that joint data for group i+1 must be available before $\underline{A}_i$ or $\underline{k}_i$ is constructed as every element joining group i+1 and i is considered to be in group i.

From equations (3.13), (3.7) and (3.9) it is apparent that matrix

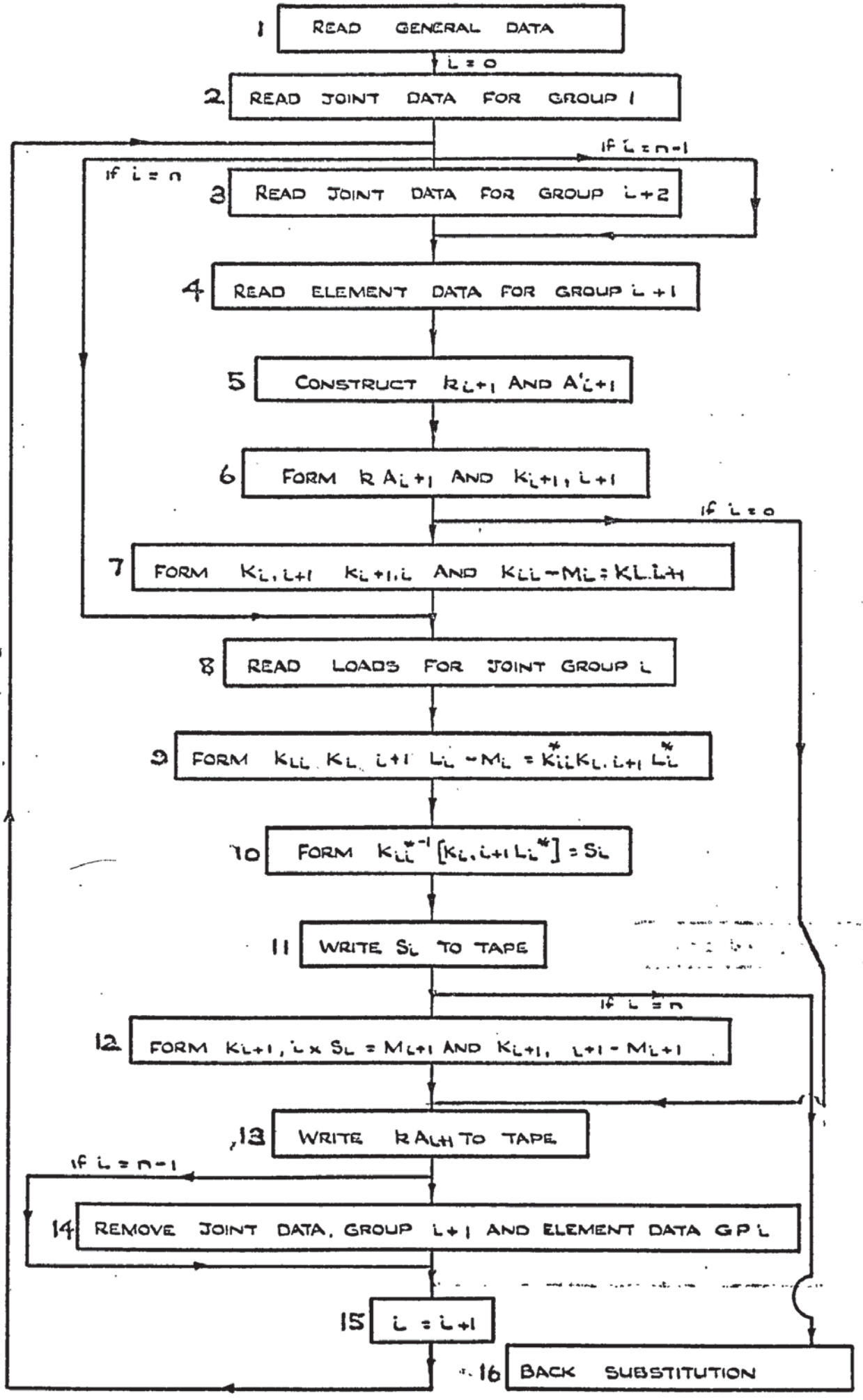

FIGURE 3.1. FLOW DIAGRAM FOR REDUCTION LOOP FOR 'n' JOINT GROUPS

	Operation	MATRICES IN STORE. 1	2	3	4	5	6	Remarks.
1	START	KA_L	K_{LL}-M_L					MATRICES IN STORE FROM PREVIOUS REDUCTION LOOP
2	FORM R_{L+1}	KA_L	K_{LL} M_L	R_{L+1}				K_{L+1} INCLUDES MEMBERS CONNECTED TO L AND L+2
3	FORM A'_{L+1}	KA_L	K_{LL}-M_L	K_{L+1}	A'_{L+1}			FORM A' FOR L+1 JOINT GROUP
4	MULT. 4 x 1 = 5	KA_L	K_{LL}-M_L	K_{L+1}	A'_{L+1}	$K_{L+1,L}$		$K_{L+1,L} = A'_{L+1} KA_L$
5	REMOVE 1	K_{LL}-M_L	K_{L+1}	A'_{L+1}	$K_{L+1,L}$			
6	TRANSPOSE 3 INTO 5	K_{LL}-M_L	K_{L+1}	A'_{L+1}	$K_{L+1,L}$	A_{L+1}		
7	MULT 2 x 5 = 6	K_{LL}-M_L	K_{L+1}	A'_{L+1}	$K_{L+1,L}$	A_{L+1}	KA_{L+1}	KA_{L+1} WRITTEN TO MAG. TAPE
8	REMOVE 2 AND 5	K_{LL}-M_L	A'_{L+1}	$K_{L+1,L}$	KA_{L+1}			
9	MULT. 2 x 4 = 5	K_{LL}-M_L	A'_{L+1}	$K_{L+1,L}$	KA_{L+1}	$K_{L+1,L+1}$		
10	REMOVE 2	K_{LL}-M_L	K_{L+1}	KA_{L+1}	$K_{L+1,L+1}$			
11	TRANSPOSE 2 INTO 5	K_{LL}-M_L	$K_{L+1,L}$	KA_{L+1}	$K_{L+1,L+1}$	$K_{L,L+1}$		
12	ADD 1 + 5 = 6	K_{LL}-M_L	$K_{L+1,L}$	KA_{L+1}	$K_{L+1,L+1}$	$K_{L,L+1}$	N'_L	COMPOUND $(K_{LL}-m_L)$; $K_{L,L+1}$ TO FORM N_L
13	REMOVE 5 AND 1	$K_{L+1,L}$	KA_{L+1}	$K_{L+1,L+1}$	N_L			
14	READ 5	K_{L+1L}	KA'_{L+1}	$K_{L+1,L+1}$	N_L	L'		READ TRANSPOSED LOAD MATRIX FOR GROUP L
15	TRANS. 5 INTO 6	$K_{L+1,L}$	KA'_{L+1}	$K_{L+1,L+1}$	N_L	L'	L	
16	REMOVE 5	K_{L+1L}	KA_{L+1}	$K_{L+1,L+1}$	N_L	L		
17	ADD 4 + 5 = 6	$K_{L+1,L}$	KA_{L+1}	$K_{L+1,L+1}$	N_L	L	N_L L	COMPOUND TO FORM $(K_{LL} - m_L)$ $K_{LL+1,L}$
18	REMOVE 4 AND 5	$K_{L+1,L}$	KA_{L+1}	$K_{L+1,L+1}$	N_L L			
19	DIV. (4)	$K_{L+1,L}$	KA_{L+1}	$K_{L+1,L+1}$	S_L			SOLVE 4 TO FORM $(K_{LL}-m_L)^{-1}$ K_{LL+1} L = S_L
20	MULT. 1 x 4 = 5	$K_{L+1,L}$	KA_{L+1}	$K_{L+1,L+1}$	S_L	M_{L+1}		$K_{L+1,L} \times S_L = m_{L+1}$
21	REMOVE 1 AND 4	KA_{L+1}	$K_{L+1,L+1}$	M_{L+1}				S_L WRITTEN TO MAG. TAPE
22	ADD 2 + 3 = 4	KA_{L+1}	$K_{L+1,L+1}$	M_{L+1}	$K_{L+1,L+1}$ - M_{L+1}			
23	REMOVE 2 AND 3	KA_{L+1}	$K_{L+1,L+1}$ - M_{L+1}					MATRICES IN STORE AT END OF REDUCTION LOOP

TABLE 3.1. MATRIX OPERATIONS IN REDUCTION LOOP.

S_1 becomes simply:-

$$S_1 = \underline{K}_{11}^{-1} \left[\underline{K}_{12} \; \underline{L}_1 \right] \qquad (3.15)$$

The matrix $\underline{K}_{12}$ can be formed using equation (3.5) and the load vector $\underline{L}_1$ is read in (block 8). Therefore no difficulty is encountered in the construction of S_1 (block 10). A sparse matrix inversion routine is used to evaluate K_{11}^{-1}. The matrix S_1 is written to the magnetic tape along with $\underline{kA}_2$ (blocks 10 and 14). Subsequent loops of the reduction process can therefore be summed up as follows:-

(i) Replacing unwanted joint data for group i, say, with data for group i+2.

(ii) Replacing unwanted element data for group i, with data for group i+1.

(iii) Forming and storing on magnetic tape, the matrices S_i and $\underline{kA}_{i+1}$.

For the general case, in any loop of the reduction cycle, it can be shown from equations (3.7), (3.8) and (3.13) that:-

$$S_i = (\underline{K}_{ii} - \underline{K}_{i,i-1} \; S_{i-1})^{-1} \; \underline{K}_{i,i+1} \; \underline{L}_i \qquad (3.15a)$$

The matrices $\underline{K}_{ii}$, $\underline{K}_{i,i-1}$ and S_{i-1} are all formed in the previous reduction loop. Therefore the expression $(\underline{K}_{ii} - \underline{K}_{i,i-1} \; S_{i-1})$ is kept in store from this loop along with $\underline{kA}_i$ which is used in the calculation of $\underline{K}_{i,i+1}$ At the start of any loop which calculates S_i and $\underline{kA}_{i+1}$ therefore, the first two matrices in the sparse matrix array will be those given at stage 1, table 3.1, where $M_i = \underline{K}_{i,i-1} \; S_{i-1}$. The new data is read in, as already described, and this enables the construction of matrices $\underline{A}_{i+1}$, $\underline{k}_{i+1}$ (stages 2 and 3, block 5). The matrices $\underline{K}_{i+1,i+1}$ $\underline{kA}_{i+1}$ and $\underline{K}_{i,i+1}$ are all formed by straightforward multiplication (stages 4-11, block 6). The expression $\underline{K}_{ii} - M_i$ can now be compounded with $\underline{K}_{i,i+1}$ to form the matrix N_i (stage 12, block 7). The load matrix $\underline{L}_i$ is next read in its

transposed form and is compounded with N_i (stage 17, block 9). The inversion of this expression (stage 18) gives the matrix S_i which is then sent to the magnetic tape. Before starting the next loop the expression $\underline{K}_{i+1,i+1} - M_{i+1}$ must first be formed before S_{i+1} can be calculated. The remaining matrix operations given in the table are therefore self explanatory. It is apparent throughout that, once a matrix is finished with, it is removed from the store and at the end of the reduction cycle all matrices are eliminated.

A flow diagram showing the backsubstitution process is given in fig. 3.2 and the matrix operations involved, in table 3.2. The matrices S_i and $\underline{kA}_i$ are read back from the magnetic tape alternately starting at the last group. Care is taken that when $\underline{X}_{i+1}$ is compounded with I, the first row number of I is the same as that of $K_{ii}^{*-1}\ \underline{L}_i^*$ in S_i as shown by equations (3.13) and (3.7). The member and plate forces are constructed for each group and added together to evaluate the forces of those spanning the groups, as shown in equation (3.14a).

Before the termination of the program the reactions for the last joint group can be calculated, if required, from equation (1.4). The load vector $\underline{L}$ includes both the implied and reactive forces. Equation (1.4) becomes,

$$\underline{L}_n = \underline{A}^1{}_n \underline{P} \qquad (3.16)$$

Previously, the rows and columns in the displacement transformation matrices were omitted for the reactions. Therefore $\underline{A}_n$ has to be recomputed with all the joints having complete freedom of movement. To do this a reaction parameter is specified giving the degrees of freedom of the joints depending on the type of structure. For example this would be six for a space frame and three for a plane frame. The transformation matrix so formed can be multiplied by the force matrix to give the reactions for the last joint group. These can also act as a check on the accuracy of

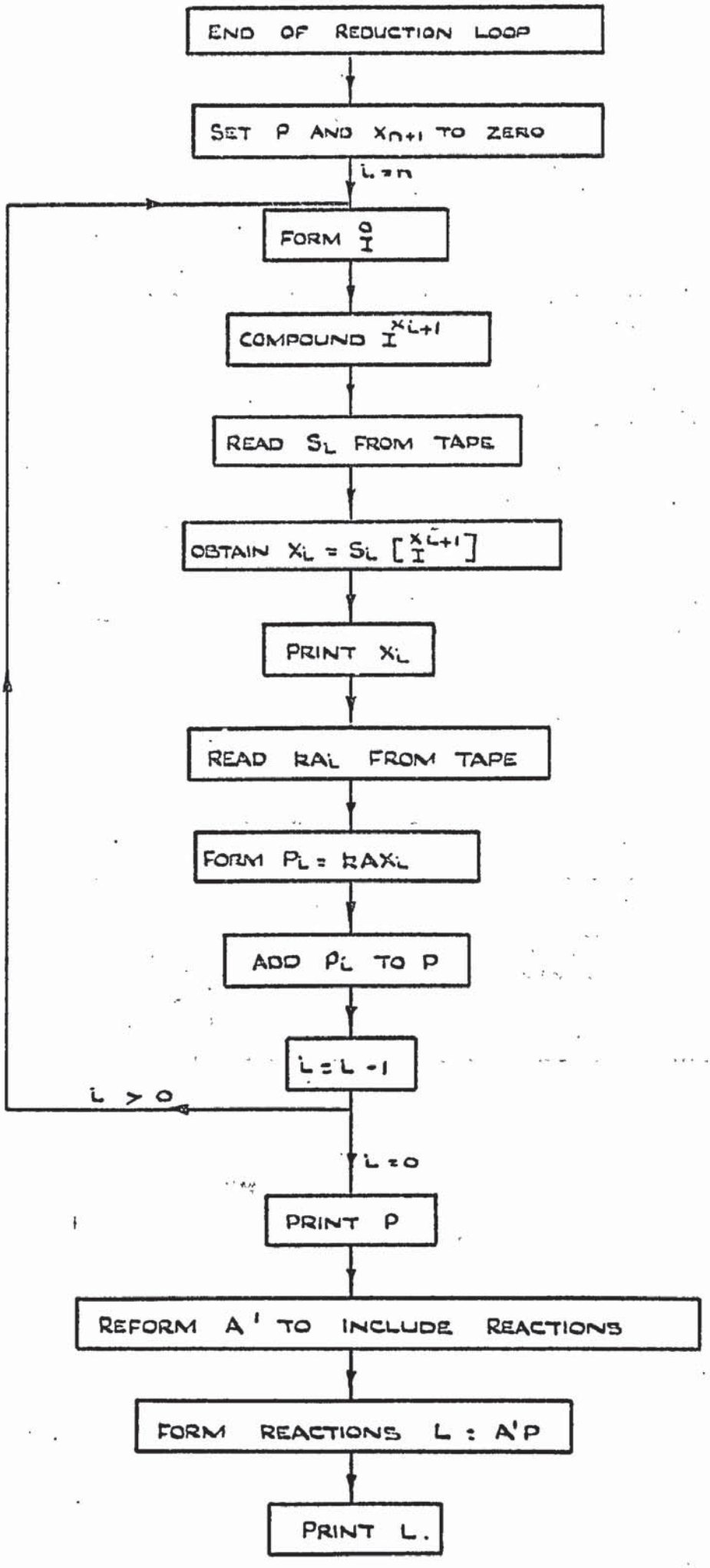

FIGURE 3.2. FLOW DIAGRAM FOR BACK SUBSTITUTION LOOP FOR 'n' JOINT GROUPS.

OPERATION	MATRICES IN STORE 1	2	3	4	REMARKS
START	X_{i+1}	P			X_{i+1} & P OBTAINED IN PREVIOUS LOOP
FORM $\begin{matrix}0\\I\end{matrix}$	X_{i+1}	P	$\begin{matrix}0\\I\end{matrix}$		THE IDENTITY MATRIX MUST BE COMPATIBLE WITH I IN S_i
ADD 3+1 = 4	X_{i+1}	P	$\begin{matrix}0\\I\end{matrix}$	$\begin{matrix}-X_{i+1}\\I\end{matrix}$	COMPOUND $-X_{i+1}$ WITH IDENTITY MATRIX
REMOVE 1 & 3	P	$\begin{matrix}-X_{i+1}\\I\end{matrix}$			
READ S_i OFF TAPE	P	$\begin{matrix}-X_{i+1}\\I\end{matrix}$	S_i		S_i SENT TO TAPE DURING REDUCTION LOOP
MULT. 3x2 = 4	P	$\begin{matrix}-X_{i+1}\\I\end{matrix}$	S_i	x_i	$x_i = S_i \times \begin{matrix}-X_{i+1}\\I\end{matrix}$
REMOVE 2 & 3	P	x_i			PRINT DISPLACEMENTS FOR GROUP i
READ KA OFF TAPE	P	x_i	KA_i		KA SENT TO TAPE DURING REDUCTION LOOP
MULT 3x2 = 4	P	x_i	KA_i	P_i	$P_i = KA_i \times x_i$
REMOVE 3	P	x_i	P_i		
ADD 1+3 = 4	P	x_i	P_i	P	$P = P+P_i$ NEW TOTAL MEMBER FORCES
REMOVE 1 & 3	x_i	P			MATRICES IN STORE AT END OF REDUCTION LOOP.

TABLE 3.2. MATRIX OPERATIONS IN BACK-SUBSTITUTION LOOP.

the inversion procedure as the implied loads specified in the data should agree closely with those given in the reactions.

The magnetic tape is also used in another capacity during the reduction cycle. At the end of each loop a test is made to ensure that there is enough computing time left to complete the next loop. If not, the working store is written onto the magnetic tape and the computation stopped. On the subsequent run of the program this information is read back into the working store and the analysis continued from its last position. Data requirements for a restart are also given in appendix 3.

This describes the method of computing the displacements and forces. The next section explains the construction of the unassembled stiffness matrices and the displacement transformation matrices.

3.4 Construction of Matrices

In order to construct the unassembled element stiffness matrices for the relationship $\underline{P} = \underline{k}\ \underline{Z}$, the different element types are grouped along the leading diagonal of the matrix in the form:-

$$\begin{bmatrix} P_m \\ P_{or} \\ P_{ir} \\ P_{ot} \\ P_{it} \end{bmatrix} = \begin{bmatrix} \underline{k}_m & o & o & o & o \\ o & \underline{k}_{or} & o & o & o \\ o & o & \underline{k}_{ir} & o & o \\ o & o & o & \underline{k}_{ot} & o \\ o & o & o & o & \underline{k}_{it} \end{bmatrix} \begin{bmatrix} \underline{Z}_m \\ \underline{Z}_{or} \\ \underline{Z}_{ir} \\ \underline{Z}_{ot} \\ \underline{Z}_{it} \end{bmatrix} \qquad (3.17)$$

where the suffixes m, r, t, o, i refer to members, rectangular plates, triangular plates, 'out of plane' action and 'in plane' actions respectively.

The individual element stiffnesses can be computed directly and fed into the sparse matrix array in the form of equation (3.17). As previously mentioned, this is done a group at a time and only two

groups are present at any one time. In order to keep the general form of equation (3.17), a gap was allowed between the beginning of each submatrix so that all the element stiffnesses of the structure could be progressively fed in up to the last group. Thus this kept the element displacement matrix compatible with the whole structure and the transformation matrix. This also ensured the automatic partitioning required in equations (3.3) and (3.5).

The displacement transformation matrix is similarly constructed from:-

$$\begin{bmatrix} \underline{Z}_m \\ \underline{Z}_{or} \\ \underline{Z}_{ir} \\ \underline{Z}_{ot} \\ \underline{Z}_{it} \end{bmatrix} = \begin{bmatrix} \underline{A}_m \\ \underline{A}_{or} \\ \underline{A}_{ir} \\ \underline{A}_{ot} \\ \underline{A}_{it} \end{bmatrix} \begin{bmatrix} \underline{X} \end{bmatrix} \qquad (3.18)$$

From equations (3.17) and (3.18) it follows that the overall stiffness matrix $\underline{K}$ can be obtained from:-

$$\underline{K} = \underline{A}^1 \underline{k} \underline{A} = \begin{bmatrix} \underline{A}_m \underline{A}_{or} \underline{A}_{ir} \underline{A}_{ot} \underline{A}_{it} \end{bmatrix} \begin{bmatrix} \underline{k}_m & o & o & o & o \\ o & \underline{k}_{or} & o & o & o \\ o & o & \underline{k}_{ir} & o & o \\ o & o & o & \underline{k}_{ot} & o \\ o & o & o & o & \underline{k}_{it} \end{bmatrix} \begin{bmatrix} \underline{A}_m \\ \underline{A}_{or} \\ \underline{A}_{ir} \\ \underline{A}_{ot} \\ \underline{A}_{it} \end{bmatrix} \qquad (3.19)$$

Hence,

$$\underline{K} = \underline{A}_m^1 \underline{k}_m \underline{A}_m + \underline{A}_{or}^1 \underline{k}_{or} \underline{A}_{or} + \underline{A}_{ir}^1 \underline{k}_{ir} \underline{A}_{ir} + \underline{A}_{ot}^1 \underline{k}_{ot} \underline{A}_{ot} + \underline{A}_{it}^1 \underline{k}_{it} \underline{A}_{it}$$

In practice, it was found more convenient to construct the individual element type displacement transformation matrices in their transposed form. These could then be compounded in the form of equation

(3.18) before multiplication with the unassembled stiffness matrix. Care was taken to make all the matrices compatible in size and position to each other. These matrices consist of direction cosines which are defined as follows. Fig. 3.3 shows two sets of orthogonal axes randomly orientated where X,Y,Z represents the global reference axes and P,Q,R the individual element local axes. Any movement within these axes can be related to the global axes by nine direction cosines. In matrix form,

$$\begin{bmatrix} u \\ v \\ w \end{bmatrix} = \begin{bmatrix} l_1 & m_1 & n_1 \\ l_2 & m_2 & n_2 \\ l_3 & m_3 & n_3 \end{bmatrix} \begin{bmatrix} x \\ y \\ z \end{bmatrix} \qquad (3.20)$$

where u, v, w are the displacements in the P,Q,R directions and x, y, z are those in the X,Y,Z directions. The elements l_1, m_1, n_1 etc. are the cosines of the angles shown in fig. 3.3. The remaining elements are found in a similar manner.

The transformation matrices are constructed in a similar manner for each element and are shown here for the triangular element. For 'in plane' action the two local translational movements at each node will be related to the global joint movements. For a plate whose corners 1, 2, 3 are connected to joints i, j, k respectively, the displacement transformation is given by:-

$$\begin{bmatrix} \underline{Z}_1 \\ \underline{Z}_2 \\ \underline{Z}_3 \end{bmatrix} = \begin{bmatrix} \underline{a} & o & o \\ o & \underline{a} & o \\ o & o & \underline{a} \end{bmatrix} \begin{bmatrix} \underline{X}_i \\ \underline{X}_j \\ \underline{X}_k \end{bmatrix} \qquad (3.21)$$

where, as before,

$$\underline{Z}_1 = \{u_1, v_1\}$$

and, $\underline{X}_i = \{x_i, y_i, z_i, \theta_{xi}, \theta_{yi}, \theta_{zi}\}$

As the 'in plane' rotation is not considered, $\underline{a}$ is a submatrix of the form,

$$\underline{a} = \begin{bmatrix} l_1 & m_1 & n_1 & o & o & o \\ l_2 & m_2 & n_2 & o & o & o \end{bmatrix} \qquad (3.22)$$

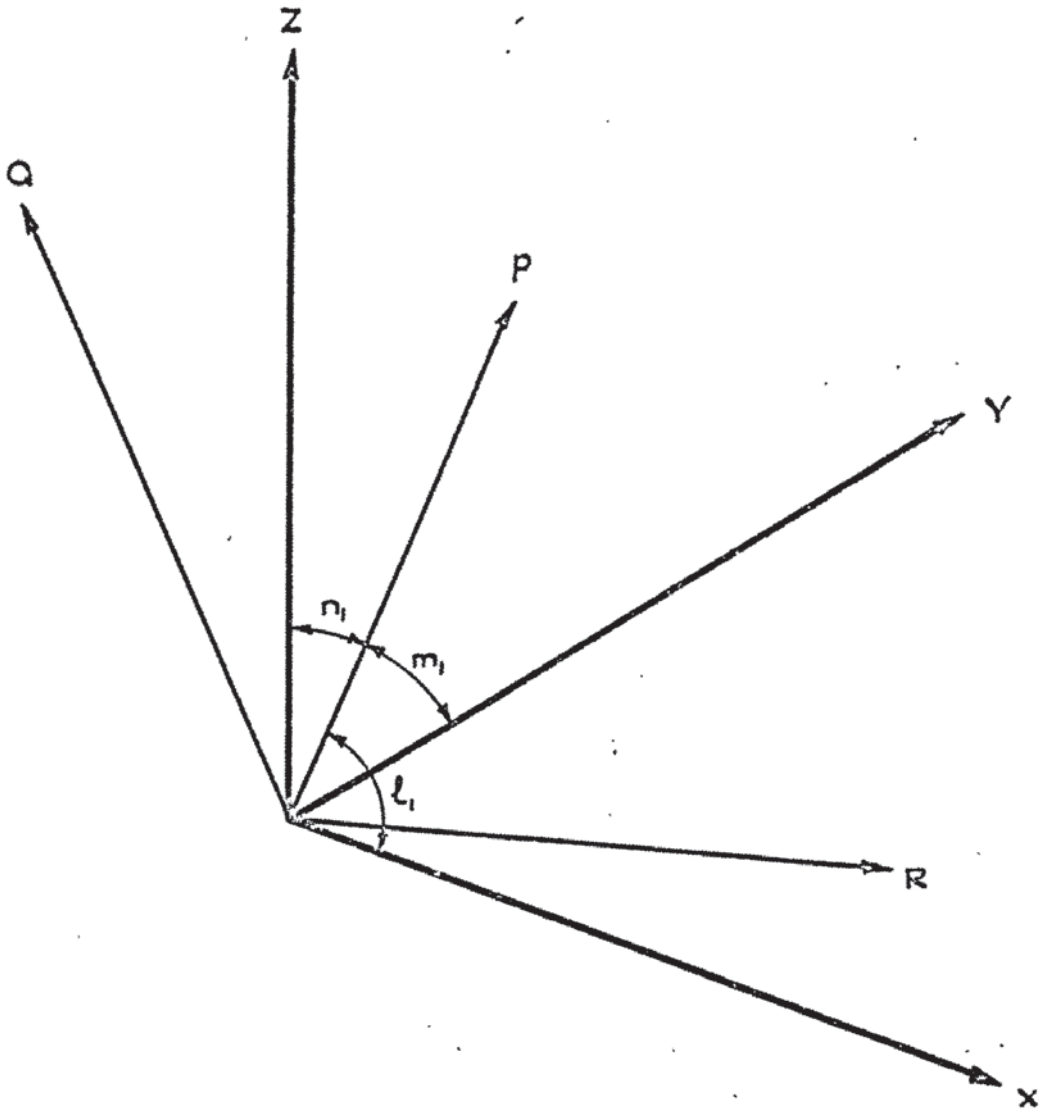

FIGURE 3.3

The direction cosines are calculated as soon as the joint and plate data are available. The transformed matrix $\underline{A}^1$ was formed by determining its elements a joint at a time. Fig. 3.4 shows the contributions of the cosines at any joint J connecting two plates. Fig. 3.5 gives a flow diagram showing how the matrix is constructed. Each joint in a group is inspected in turn and the plate and corner number which are attached to it are stored. If no plates are attached then the number of rows corresponding to the degrees of freedom of the joint are left blank. A routine was written to insert the direction cosines of the attached plates into the matrix. As it was constructed in sparse form, the row number was first fed in corresponding to the degree of freedom being considered at the joint. This was followed by the column number which corresponded to the row number of the $\underline{Z}$ matrix of the attached plate and was determined by the element's position in the unassembled stiffness matrix. The value of the direction cosine was then inserted. When all the cosines concerning one joint had been inserted, the three rows corresponding to the rotations were left blank. If any of the degrees of freedom at a joint were found to be restrained then that row was not included. When the cosines of all the elements connected to that joint had been fed in, the next joint was considered and so on until all the joints in that group had been examined and $\underline{A}^1_{it}$ constructed.

For the 'out of plane' transformation matrix, '$\underline{a}$' in equation (3.21) now takes the form:-

$$\underline{a} = \begin{bmatrix} l_3 & m_3 & n_3 & o & o & o \\ o & o & o & l_1 & m_1 & n_1 \\ o & o & o & l_2 & m_2 & n_2 \end{bmatrix} \qquad (3.23)$$

where, for 'out of plane' action:-

$$\underline{z}_1 = \{w_1, \alpha_{p1}, \alpha_{q1}\}$$

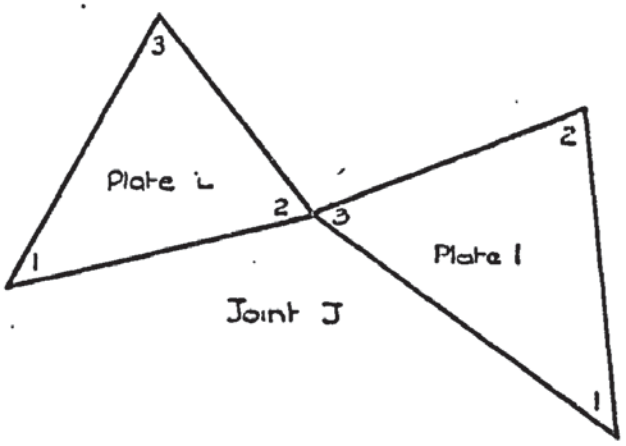

System of two plate elements connected to a joint 'J'

	Plate 1						Contribution to 'A' of plates 1-i	Plate i					
	Corner 1		Corner 2		Corner 3			Corner 1		Corner 2		Corner3	
	u	v	u	v	u	v		u	v	u	v	u	v
X_j					ℓ_{11}	ℓ_{21}				ℓ_{1i}	ℓ_{2i}		
Y_j					m_{11}	m_{21}				n_{1i}	m_{2i}		
Z_j					n_{11}	n_{21}				n_{1i}	n_{2i}		
Q_{xy}					δ	0				δ	0		
Q_{yj}					δ	0				δ	0		
Q_{zj}					δ	0				δ	0		

Part of the 'A' matrix for 'in plane' plates for the above system of plates jointed to joint J

FIGURE 3.4

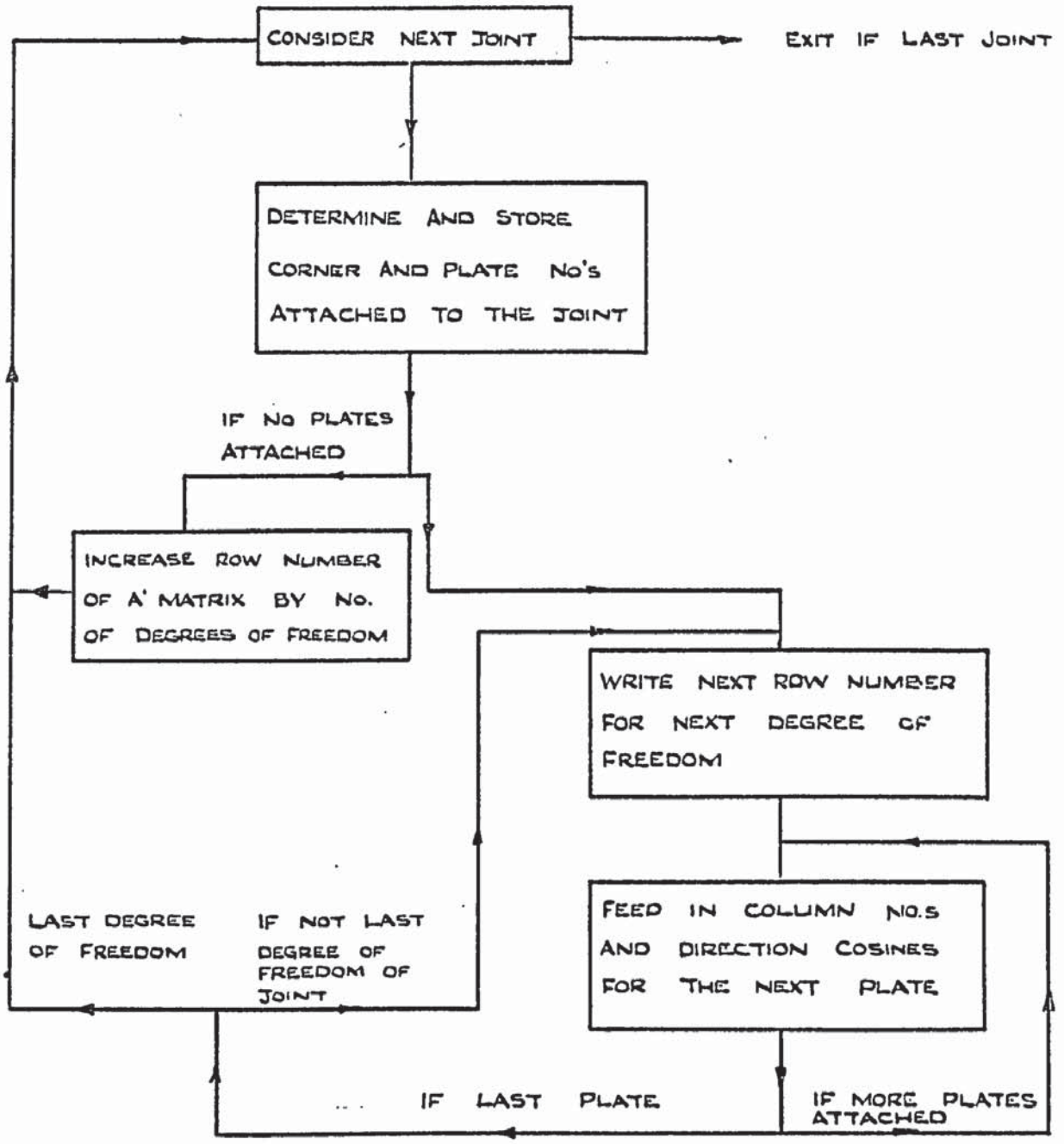

FIGURE 3.5 FLOW DIAGRAM OF FORMATION OF TRANSPOSED DISPLACEMENT TRANSFORMATION MATRIX FOR PLATE ELEMENTS

The direction cosines l_3, m_3, n_3 relate the local movement of the plate w in the vertical R direction to the global displacement. The cosines l_1, m_1, n_1 and l_2, m_2, n_2 relate the rotations about the P and Q axes respectively to those of the global axes. Again these can be calculated from the geometrical positioning of the plane of the plate. Fig. 3.6 shows the contributions of direction cosines in the $\underline{A}^1_{ot}$ matrix of two plates which are connected at any joint J. The 'out of plane' transformation matrix is constructed similarly to that of the 'in plane' and the same flow diagram, as shown in fig. 3.5, was used. Again, each joint is inspected in turn and plate and corner numbers which are attached are stored. The method of the positioning of the cosines is changed to suit the fig. 3.6. If no plates were connected to a joint then those rows in the matrix were left blank and if any degree of freedom of the joint was supressed then the appropriate row was omitted.

All the transformation matrices for the different elements are formed in a similar manner and are of the same size. For any group i therefore, the overall displacement transformation matrix is formed by adding the individual matrices in such a manner:-

$$\underline{A}^1_i = (\underline{A}^1_m)_i + (\underline{A}^1_{or})_i + (\underline{A}^1_{ir})_i + (\underline{A}^1_{ot})_i + (\underline{A}^1_{it})_i \qquad (3.24)$$

The elastic analysis program just described calculates the displacements at the joints and the members and plate forces. The remaining two sections describe programs to calculate the plate stresses, either using the stress matrices or the plate forces.

3.5 Description of Stress Program

This program was written so that it should be run after the elastic analysis program and make use of the information which had been stored on the magnetic tape during this run. In using the stress matrices it is apparent from equation (2.30) that the element displacement vector

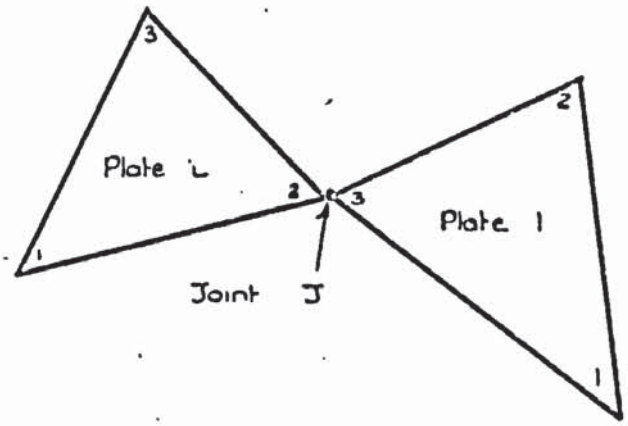

System of two plate elements connected to a joint 'J'

	Plate 1									−1	Plate i								
	Corner 1			Corner 2			Corner 3				Corner 1			Corner 2			Corner 3		
	w	α_p	α_q	w	α_p	α_q	w	α_p	α_q		w	α_p	α_q	w	α_p	α_q	w	α_p	α_q
X_j							ℓ_{31}							ℓ_{3i}					
Y_j							m_{31}							m_{3i}					
Z_j							n_{31}							n_{3i}					
θ_{xj}								ℓ_{11}	ℓ_{21}						ℓ_{1i}	ℓ_{2i}			
θ_{yj}								m_{11}	m_{21}						m_{1i}	m_{2i}			
θ_{zj}								n_{11}	n_{21}						n_{1i}	n_{2i}			

Contribution to 'A' of plates

Part of the 'A' matrix for 'out of plane' plates for the above system of plates joined to joint J.

FIGURE 3.6.

will first have to be formed. In order to achieve this, the displacement transformation matrix and displacement matrix must be known. Therefore for each group the following matrices were stored on tape as soon as they were formed:-

$$(\underline{\Lambda}^1_{or})_i,\ (\underline{\Lambda}^1_{ir})_i,\ (\underline{\Lambda}^1_{ot})_i,\ (\underline{\Lambda}^1_{it})_i.$$

The displacement matrices '$\underline{X}_i$' were put onto magnetic tape as they were evaluated in the backsubstitution loop. The individual plate dimensions and properties were stored in an array in the analysis program and were also sent to the magnetic tape at the end of the analysis. These were needed for the construction of the stress matrices. Along with this, general information as to the type and number of elements present, the number of groups and the greatest number of elements in a group were also sent to the tape. The positions of all these matrices on the tape were also stored and the position of this general information was printed out.

A flow diagram of the stress program is shown in fig. 3.7. The general data, a description of which is given in appendix 3, is read in and allows all the information concerning the plates to be read from the magnetic tape to the main store. The displacement and transformation matrices are read down from the tape group by group and multiplied together to form the element displacement matrices:-

$$(\underline{Z}_{or})_i,\ (\underline{Z}_{ir})_i,\ (\underline{Z}_{ot})_i,\ (\underline{Z}_{it})_i.$$

These are added as they are formed so that, at the last group, the total displacement vector for each type of element was in the store. A specification of the matrix operations involved is given in table 3.3. These matrices are compatible with the $\underline{Z}$ matrix of the structure and, before being multiplied by the stress matrices, are first compounded by rows so that the first element of each matrix is at row 1. The stress matrices $\underline{S}_{or}$, $\underline{S}_{ir}$, $\underline{S}_{ot}$, $\underline{S}_{it}$ are next constructed for each element along

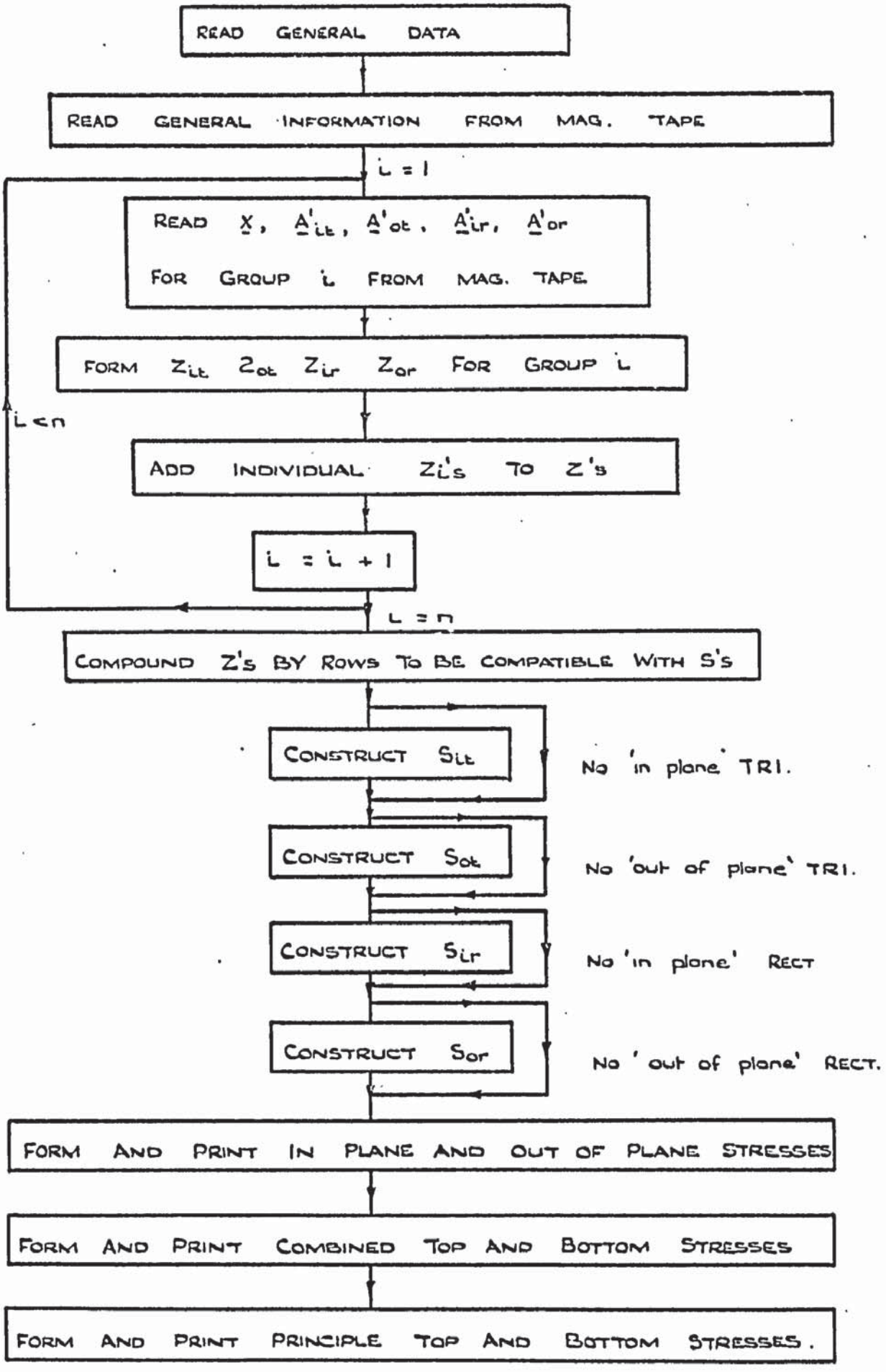

FIGURE 3.7. FLOW DIAGRAM FOR STRESS PROGRAM.

OPERATION	1	2	3	4	5	6	7	8	9	10	11	12	13	REMARKS.
START	Z_{lt}	Z_{ot}	Z_{lr}	Z_{or}										MATRICE IN STORE FROM PREVIOUS LOOP
READ FROM MAG. TAPE	Z_{lt}	Z_{ot}	Z_{lr}	Z_{or}	X_i	$(A'_{lt})_i$	$(A'_{ot})_i$	$(A'_{lr})_i$	$(A'_{or})_i$					READ A'S AND X FOR GROUP i FROM MAG TAPE
TRANSPOSE (6-9)	Z_{lt}	Z_{ot}	Z_{lr}	Z_{or}	X_i	$(A'_{lt})_i$	$(A'_{ot})_i$	$(A'_{lr})_i$	$(A'_{or})_i$	$(A_{lt})_i$	$(A_{ot})_i$	$(A_{lr})_i$	$(A_{or})_i$	
REMOVE (6-9)	Z_{lt}	Z_{ot}	Z_{lr}	Z_{or}	X_i	$(A_{lt})_i$	$(A_{ot})_i$	$(A_{lr})_i$	$(A_{or})_i$					
MULT (6-9) x15 (10-13)	Z_{lt}	Z_{ot}	Z_{lr}	Z_{or}	X_i	$(A_{lt})_i$	$(A_{ot})_i$	$(A_{lr})_i$	$(A_{or})_i$	(Z_{lt})	$(Z_{ot})_i$	$(Z_{lr})_i$	$(Z_{or})_i$	FORM $(Z)_i = A_{ki}$ FOR ELEMENT TYPES
REMOVE (5-9)	Z_{lt}	Z_{ot}	Z_{lr}	Z_{or}	$(Z_{lt})_i$	$(Z_{ot})_i$	$(Z_{lr})_i$	$(Z_{or})_i$						
ADD 5+1 = 9 etc	Z_{lt}	Z_{ot}	Z_{lr}	Z_{or}	$(Z_{lt})_i$	$(Z_{ot})_i$	$(Z_{lr})_i$	$(Z_{or})_i$	Z_{lt}.	Z_{ot}	Z_{lr}	Z_{or}		ACCUMULATE $Z = Z + (Z)_i$ NEW TOTAL OF DISPLACEMENTS
REMOVE 1-8	Z_{lt}	Z_{ot}	Z_{lr}	Z_{or}										
	LAST GROUP, TOTAL PLATE DISPLACEMENTS IN STORE													
	Z_{lt}	Z_{ot}	Z_{lr}	Z_{or}										Z'S COMPOUNDED BY ROWS
CONSTRUCT STRESS MATRICES	Z_{lt}	Z_{ot}	Z_{lr}	Z_{or}	S_{lt}	S_{ot}	S_{lr}	S_{or}						CONSTRUCT STRESS MATRICES
MULT 5 x 1 = 9 etc.	Z_{lt}.	Z_{ot}	Z_{lr}	Z_{or}	S_{lt}.	S_{ot}	S_{lr}	S_{or}	σ_{lt}	σ_{ot}	σ_{lr}	σ_{or}		$\sigma = Sz$
REMOVE 1-8	σ_{lt}	σ_{ot}	σ_{lr}	σ_{or}										
TRANSPOSE (1-4)	σ_{lt}	σ_{ot}	σ_{lr}	σ_{or}	σ'_{lt}	σ'_{ot}	σ'_{lt}	σ_{or}'						PRINT MATRICES 5-8
REMOVE 1-4	σ_{lt}'	σ_{ot}'	σ_{lr}'	σ_{or}'										
ADD 1+2 = 5, 1-2 = 6 etc.	σ_{lt}'	σ_{ot}'	σ_{lr}'	σ_{or}'	σ_t' TOP	σ_t' BOTTOM	σ_r' TOP	σ_r' BOTTOM						$\sigma' = \sigma_l' \pm \sigma_o'$
USE PRINCIPLE STRESS ROUTINE	σ_{lt}'	σ_{ot}'	σ_{lr}'	σ_{or}'	σ_t'	σ_t'	σ_r'	σ_r'						PRINT MATRICES 5-8 PRINT PRINCIPLE STRESSES

TABLE 3.3. MATRIX OPERATIONS FOR STRESS PROGRAMS.

the leading diagonal and multiplied in the form:-

$$(s)_e = (\S)_e (Z)_e \qquad (3.25)$$

where 'e' stands for the type and action of element. The stresses $(s_p)_e$, $(s_q)_e$, $(s_{pq})_e$ are found for each element. The 'in' and 'out of plane' stresses are added and subtracted to find the top and bottom stresses on the plates and a routine written to calculate the principal stresses and the angle of inclination from the local axes from consideration of Mohr's circle.

3.6 Description of Force Program

The elastic analysis program was altered so that it printed out on punched tape at the end of the run the following data:-

(i) The number of rectangular and triangular plates.

(ii) A parameter to specify the type of plates and whether 'in plane' and 'out of plane' actions were present.

(iii) The plate dimensions and properties.

(iv) The 'out of plane' forces for the rectangular plates.

(v) The 'in plane' forces for the rectangular plates.

(vi) The 'out of plane' forces for the triangular plates.

(vii) The 'in plane'forces for the triangular plates.

This information could be used as data for the force program to calculate the stresses. A flow diagram of this program is given in fig. 3.8.

The rectangular plates are considered first and the 'out of plane' forces read in. From equation (2.25) the bending stresses and vertical shear stresses are found. The 'in plane' forces are converted to stresses from equation (2.24) and hence the top and bottom plate stresses can be evaluated at each node and printed out as before.

The plate forces for the triangular plates are read in and converted into the equivalent forces on each side by equations (2.28).

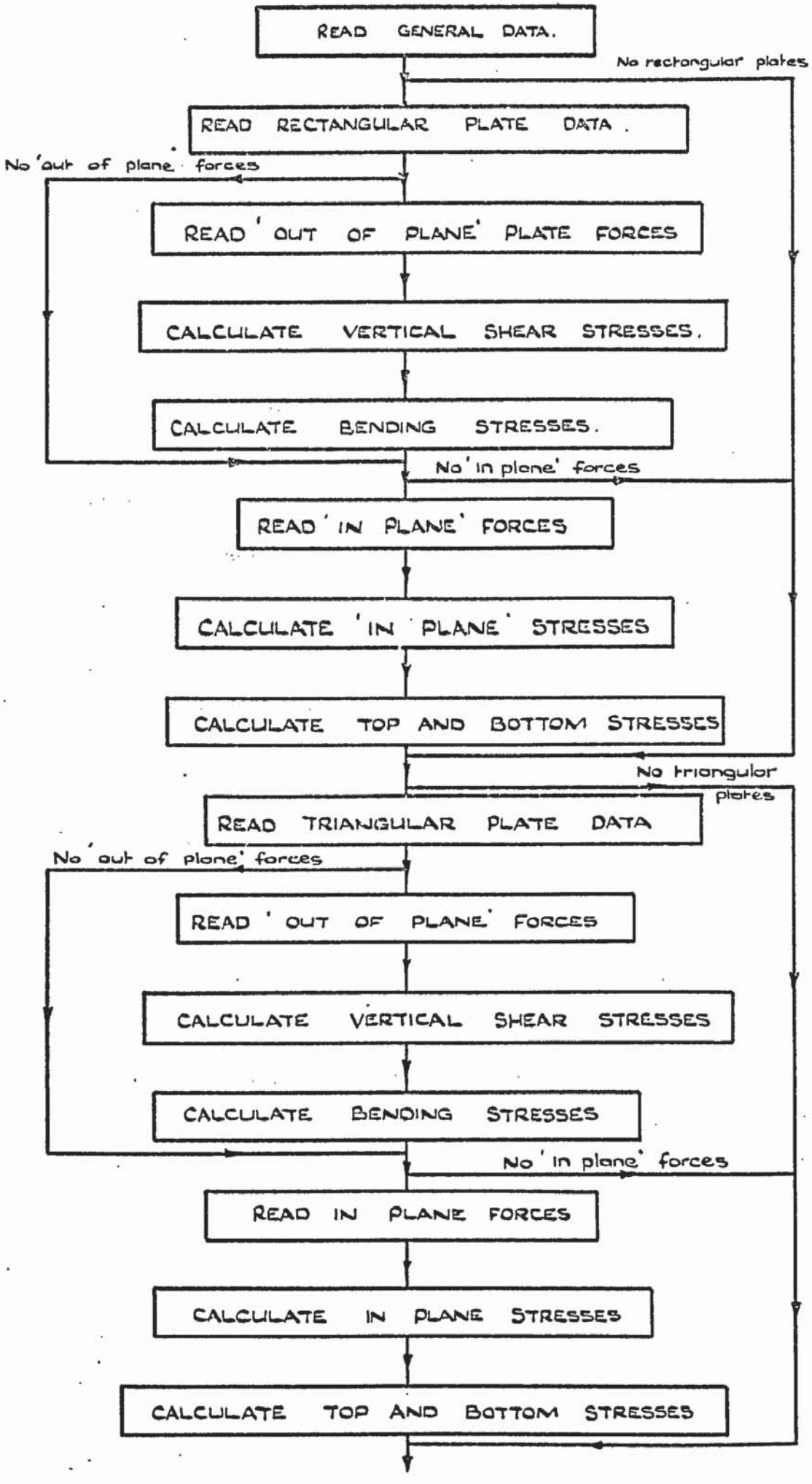

FIGURE 3.8. FLOW DIAGRAM FOR STRESS (FROM FORCES) PROGRAM.

These are used to evaluate the nodal stresses in a manner just described for the rectangular plates.

The two methods of evaluating stress are compared in chapter 5. It would first appear that the latter method, from the plate forces, would be more attractive as less computation is involved but this does suffer from drawbacks. As sparse matrix techniques are not used in this method the force matrices could not be stored on magnetic tape for later use without serious programming complications. Hence this data was printed out on punched tape and for large problems the bulk of data involved is rather cumbersome. The plate dimensions are printed out group by group and the rectangular and triangular data has to be separated manually before the force program is run. The elastic analysis program is used in chapters 5 and 6 to assess the triangular element and for the analysis of a folded plate roof and other large structures.

CHAPTER 4

NONLINEAR ANALYSIS PROGRAMS

4.1 Introduction

It would be possible to carry out a nonlinear analysis for a structure by running a linear analysis program repeatedly and altering the elastic constants manually between each run. This will, no doubt, involve a great deal of tedious work. In this chapter two types of nonlinear analyses are presented together with their programming procedures. These are the nonlinear iterative and nonlinear incremental methods of analysis. The first method has facilities to include imposed known deflections as well as loads on the structure. These facilities are particularly used in problems such as soil mechanics, where the results of settlements or movements of retaining walls are sometimes of more interest in studying the behaviour of soil. The program procedures for each method is explained with the aid of flow diagrams and tables to show the manner in which various matrices are constructed, stored or manipulated within the core store of the computer or during their storage on magnetic tapes.

4.2 Method of imposing deflections

In general, when analysing a structure, a set of equations of the form $\underline{L} = \underline{K}\ \underline{X}$ are solved. For such an analysis the degrees of freedom corresponding to the support reactions are suppressed and therefore excluded from the above set of equations. In fact this process of supressing the known, zero deflections can be extended so that all the other non-zero known deflections are grouped together and used to solve the remaining equations for the unknown deflections.

In many cases these known deflections are mixed in a random

manner with the rest of the unknown deflections. For this reason, before the analysis takes place, the stiffness equations are rearranged and then partitioned so that the two sets of the known and unknown deflections are separated into two distinct submatrices. In a given problem with n degrees of freedom, if $\underline{X}$ is the displacement vector corresponding to all the degrees of freedom, in which $\underline{X}_1$ corresponds to the unknown displacements and $\underline{X}_2$ to those that are known, then matrix $\underline{X}$ can be partitioned so that:-

$$\underline{X} = \begin{bmatrix} \underline{X}_1 \\ \underline{X}_2 \end{bmatrix} \qquad (4.1)$$

Corresponding to each submatrix in $\underline{X}$, the load matrix $\underline{L}$ is also partitioned. In this matrix $\underline{L}_1$ is vectorially equivalent to the unknown displacements $\underline{X}_1$ while $\underline{L}_2$ corresponds to $\underline{X}_2$. The overall stiffness equations thus become:-

$$\begin{bmatrix} \underline{L}_1 \\ \underline{L}_2 \end{bmatrix} = \begin{bmatrix} \underline{K}_{11} & \underline{K}_{12} \\ \underline{K}_{21} & \underline{K}_{22} \end{bmatrix} \begin{bmatrix} \underline{X}_1 \\ \underline{X}_2 \end{bmatrix} \qquad (4.2)$$

In these equations the submatrices $\underline{K}_{11}$ and $\underline{K}_{22}$ are square and define the stiffness of the structure corresponding to the set of unknown and known deflections respectively. Expanding equations (4.2) gives:-

$$\begin{bmatrix} \underline{L}_1 \\ \underline{L}_2 \end{bmatrix} = \begin{bmatrix} \underline{A}_1^1 \, \underline{k} \, \underline{A}_1 & \underline{A}_1^1 \, \underline{k} \, \underline{A}_2 \\ \underline{A}_2^1 \, \underline{k} \, \underline{A}_1 & \underline{A}_2^1 \, \underline{k} \, \underline{A}_2 \end{bmatrix} \begin{bmatrix} \underline{X}_1 \\ \underline{X}_2 \end{bmatrix} \qquad (4.3)$$

It is noticed that the stiffness matrix $\underline{k}$, in equation (4.3) is that for all the elements in the structure. In reality, of course, only some of the elements contribute to the stiffnesses $\underline{A}_1^1 \, \underline{k} \, \underline{A}_1$, $\underline{A}^1 \, \underline{k} \, \underline{A}_2$ etc. at a given joint. On the other hand each displacement transformation $\underline{A}_1$ and $\underline{A}_2$ are defined as:-

$$\begin{aligned} \underline{Z}_1 &= \underline{A}_1 \, \underline{X}_1 \\ \underline{Z}_2 &= \underline{A}_2 \, \underline{X}_2 \end{aligned} \qquad (4.4)$$

In these equations $\underline{A}_1$ has the same number of rows, as $\underline{Z}_1$ while it has the same number of columns as in a single column of $\underline{X}_1$. Similarly for $\underline{A}_2$. The matrix $\underline{Z}_1'$ gives the components of $\underline{X}_1$ resolved along the local element coordinates. Because sparse matrix techniques of storage are being employed, it is possible to include all the elements in $\underline{Z}_1$ and $\underline{Z}_2$. This gives rise to a large number of zeros in both $\underline{A}_1$ and $\underline{A}_2$ which does not create over population in these matrices since all zeros are excluded during the construction of these matrices.

Equations (4.2) can now be solved for the unknown displacements, thus:-

$$\underline{X}_1 = \underline{K}_{11}^{-1} \left[\underline{L}_1 - \underline{K}_{12} \underline{X}_2 \right] \qquad (4.5)$$

It is interesting to note that the loads $\underline{L}_2$ will have no influence on the analysis. The element displacements $\underline{Z}$ are obtainable from:-

$$\underline{Z} = \begin{bmatrix} \underline{A}_1 & \underline{A}_2 \end{bmatrix} \begin{bmatrix} \underline{X}_1 \\ \underline{X}_2 \end{bmatrix}$$

i.e. $\underline{Z} = \underline{A}_1 \underline{X}_1 + \underline{A}_2 \underline{X}_2 = \underline{Z}_1 + \underline{Z}_2 \qquad (4.6)$

Similarly, the element forces are:

$$\underline{P} = \underline{k}\, \underline{A}_1 \underline{X}_1 + \underline{k}\, \underline{A}_2 \underline{X}_2 = \underline{P}_1 + \underline{P}_2 \qquad (4.7)$$

As an example, consider a simple portal frame with two joints in which the vertical displacement y_1 at joint 1 and the horizontal displacement x_2 at joint 2 are known. The equations $\underline{L} = \underline{K}\,\underline{X}$ will be changed from:-

$$\begin{bmatrix} X_1 \\ Y_1 \\ M_{z1} \\ X_2 \\ Y_2 \\ M_{z2} \end{bmatrix} = \begin{bmatrix} K_{11} & & & & & \\ K_{21} & K_{22} & & \text{symmetrical} & & \\ K_{31} & K_{32} & K_{33} & & & \\ K_{41} & K_{42} & K_{43} & K_{44} & & \\ K_{51} & K_{52} & K_{53} & K_{54} & K_{55} & \\ K_{61} & K_{62} & K_{63} & K_{64} & K_{65} & K_{66} \end{bmatrix} \begin{bmatrix} x_1 \\ y_1 \\ \theta_{z1} \\ x_2 \\ y_2 \\ \theta_{z2} \end{bmatrix} \qquad (4.8a)$$

into:-

$$\begin{bmatrix} X_1 \\ M_{z1} \\ Y_2 \\ M_{z2} \\ \hline Y_1 \\ X_2 \end{bmatrix} = \left[\begin{array}{cccc|c} K_{11} & & & & \\ K_{31} & K_{33} & & & \text{symmetrical} \\ K_{51} & K_{53} & K_{55} & & \\ K_{61} & K_{63} & K_{65} & K_{66} & \\ \hline K_{21} & K_{23} & K_{25} & K_{26} & K_{22} \\ K_{41} & K_{43} & K_{45} & K_{46} & K_{42} \quad K_{44} \end{array}\right] \begin{bmatrix} x_1 \\ \theta_{z1} \\ y_1 \\ \theta_{z2} \\ \hline y_1 \\ x_2 \end{bmatrix} \qquad (4.8b)$$

i.e.

$$\begin{bmatrix} \underline{L}_1 \\ \underline{L}_2 \end{bmatrix} = \begin{bmatrix} \underline{K}_{11} & \underline{K}_{12} \\ \underline{K}_{27} & \underline{K}_{22} \end{bmatrix} \begin{bmatrix} \underline{X}_1 \\ \underline{X}_2 \end{bmatrix} \qquad (4.8c)$$

In the actual computer program, the matrices in equation (4.8b) are not derived by rearrangement of the rows and columns of those in equation (4.8a). Instead these matrices are constructed directly. This is achieved by feeding, in the joint data, first of all the degrees of freedom of the unknown displacements in each joint followed by the known degrees of freedom throughout the structure. Thus in the case of the above portal, unknown degrees of freedom corresponding to joint 1 will be represented as:-

$$\{x_1\ y_1\ z_1\ \theta_{x1}\ \theta_{y1}\ \theta_{z1}\} = \{1\ 0\ 0\ 0\ 0\ 1\} \qquad (4.9a)$$

where unity represents an unknown degree of freedom while a zero may be representing a known or a suppressed degree of freedom. Similarly the unknown degrees of freedom for joint 2 will be:-

$$\{x_2\ y_2\ z_2\ \theta_{x2}\ \theta_{y2}\ \theta_{z2}\} = \{0\ 1\ 0\ 0\ 0\ 1\} \qquad (4.9b)$$

On the other hand the known degrees of freedom for these joints are fed into the computer as:-

$$\{x_1\ y_1\ z_1\ \theta_{x1}\ \theta_{y}\ \theta_{z1}\} = \{0\ 1\ 0\ 0\ 0\ 0\} \qquad (4.10a)$$

and

$$\{x_2\ y_2\ z_2\ \theta_{x1}\ \theta_{y1}\ \theta_{z1}\} = \{1\ 0\ 0\ 0\ 0\ 0\} \qquad (4.10b)$$

respectively.

These figures show that a totally suppressed degree of freedom in joint 1 is represented by a zero in both equation (4.9) and (4.10). Thus for the two dimensional portal z, θ_x and θ_y are suppressed for both joints. From equation (4.5) it is noticed that $\underline{K}_{11}$ corresponding to the unknown displacements and $\underline{K}_{12}$ corresponding to $\underline{X}_2$ are the only two stiffness submatrices required to be constructed. The zeros in equations (4.9) and (4.10) will indicate which of the rows and columns in $\underline{K}_{11}$ and $\underline{K}_{12}$ should be excluded. Here again the advantage of sparse matrix operations play their part by preventing the storage of a large number of zero rows and columns in these matrices.

4.3 Nonlinear Iterative analysis

It was stated earlier that two different methods of non-linear analysis were developed. The non-linear iterative analysis was used for two dimensional structures consisting of members, rectangular and triangular plates under 'in-plane' forces. Facilities were available in the actual program so that plane stress as well as plane strain problems can be dealt with. In the non-linear iterative analysis, two stress-strain relationships were included to calculate both instantaneous secant modulus E_p and E_q along the P and Q axes of the elements. Two further relationships between E_p and ν_p as well as E_q and ν_q were also included so that, for orthotropic material, the instantaneous secant Poisson ratios ν_p and ν_q are also calculated.

Consider a typical piecewize linear stress strain curve in which the nodes are specified by $\Sigma_1, \eta_1, \Sigma_2, \eta_2 \ldots \Sigma_i, \eta_i$ where Σ_i is the value of the stress at a node on this curve, while η_i is the corresponding value of the strain as shown in fig. 4.1(a).

Let s_1 be the stress in a given direction, such as the P direction, obtained by the first analysis of the structure in a linear

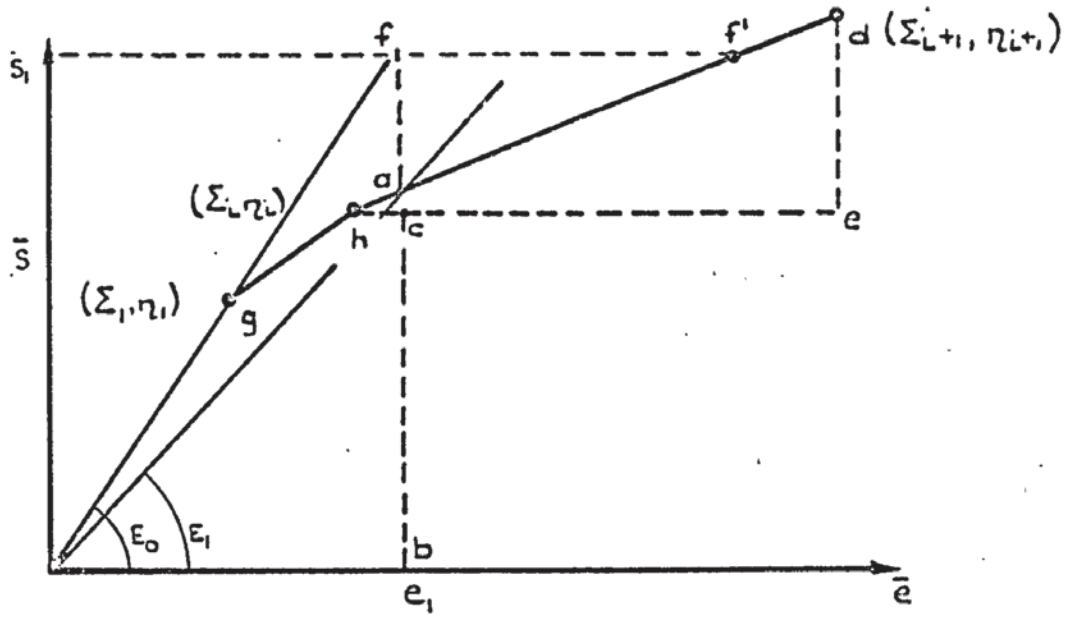

FIGURE 4.1 (a) DETERMINATION OF SECANT MODULUS

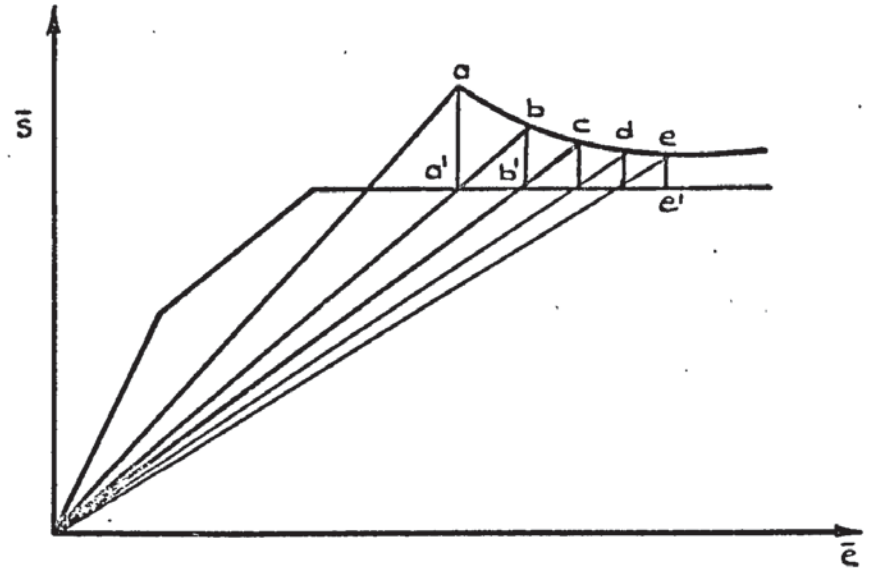

FIGURE 4.1 (b) CONVERGENCE TOWARDS FAILURE STRESS.

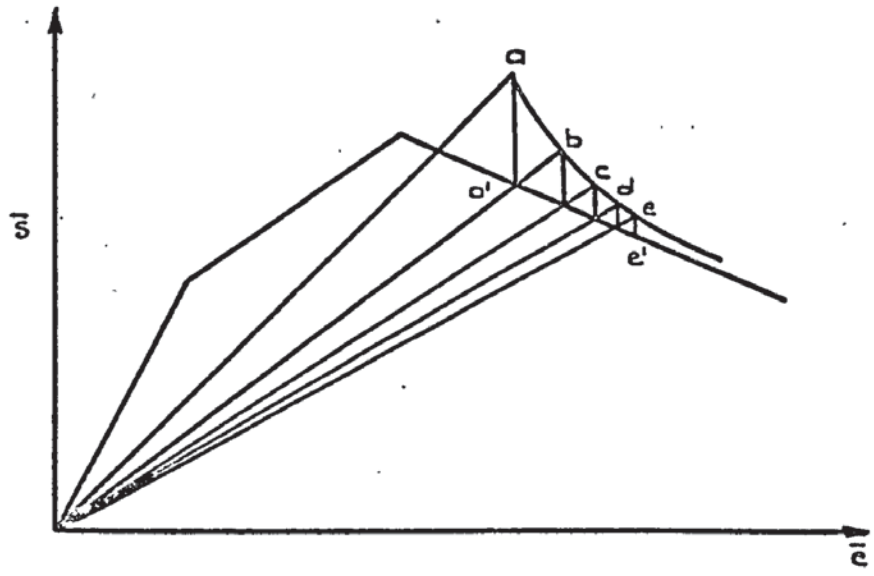

FIGURE 4.1. (c) CONVERGENCE ALONG DROOPING STRESS-STRAIN SECTION

manner with the modulus of elasticity being equal to E_o. Let the corresponding strain be e_1. These are shown in the figure. It is noticed from the figure that the value of E_o, used in the linear analysis is not representative of this element, since the actual strain is past the value of strain η_i at the ith node on the curve. An improved value E_1 can be calculated as follows:-

Considering points f and g in the figure, it is noticed that

$$E_o = s_1/e_1 = \Sigma_1/\eta_1$$

i.e. $e_1 = s_1 \eta_1/\Sigma_1$

Since e_1 lies between η_i and η_{i+1}, it follows, from the similar triangles ach and deh, that

$$ac = (\Sigma_{i+1} - \Sigma_i)\ (\Sigma_1 - \eta_i) \ /\ (\eta_{i+1} - \eta_i)$$

Hence the ordinate ab, on the i to i+1 position of the curve, is:-

$$ab = ac + \Sigma_i = \Sigma_i + (\Sigma_{i+1} - \Sigma_i)\ (e_1 - \eta_i) \ /\ (\eta_{i+1} - \eta_i)$$

It follows that the improved secant modulus E_1 is given by:-

$$E_1 = ab/e_1 = \frac{\Sigma_1}{s_1\eta_1}\left[\Sigma_i + (\Sigma_{i+1} - \Sigma_i)\ (e_1 - \eta_i) \ /\ (\eta_{i+1} - \eta_i)\right] \qquad (4.11)$$

This value of E_1 may now be used for the element under consideration, in a revised analysis of the structure, which in turn involves inaccuracies due to the fact that E_1 has not sufficiently converged to the previous value. The process can be repeatedly improved and a final acceptable jth value E_jth can be shown to be given by:-

$$E_j = \frac{E_{j-1}}{s_j}\left[\Sigma_k + (\Sigma_{k+1} - \Sigma_k)\ \left(\frac{s_j}{E_{j-1}} - \eta_k\right) \ /\ (\eta_{k+1} - \eta_k)\right] \qquad (4.12)$$

A comparison of equations (4.11) and (4.12) indicates that after the i th iteration the current value of e_j may have moved from the range of (i to i+1) to that of (k to k+1).

Similar calculations are carried out for the improved value of E in the orthogonal direction and for each and every element in the structure.

These values of E_t for each element can be used to calculate, using simple trigonometry, the corresponding values of σ in both directions. In this manner one final analysis of the structure under the applied loads gives the accurate stresses in each element. These may be different from one element to another, not only because they are subject to different loads but also due to the fact that their E values are different. It is to be pointed out that for isotropic structures the only alteration required to the above orthotropic analysis, is to feed the same values of Σ and η at the nodes for both curves.

It is significant to state that when using fig. 4.1(a), point f was used to fix the value of the strain e_1 which was subsequently employed in the calculation of the new value of E. Instead, point f' could have also been established and used for predicting another new value for E. At first sight f' may appear to speed up the process of convergence. However, at high values of s, and particularly when some of the elements reach failure, both points f and f' may happen to lie above Σ_{max}, corresponding the the highest node of the stress-strain curve. This indeed would aggravate the problem of convergence.

The nonlinear iterative method is particularly useful when a structure is analysed under a fixed set of loads, which happen to give rise to stresses below the failure stresses of any of the elements. This method gives good convergence even up to the pre-failure load. However, when the final position of the stress-strain curve is flat or drooping, as shown in figs. 4.1(b) and 4.1(c), it is possible to experience difficulties of convergence. In both figures, repeated analyses may diminish the distance aa^1, bb^1, --- ee^1, but the true state of affairs may never be attained before other factors play their part and cause divergence of results. This indeed may have been the cause in the inability to detect the failure of the sand foundation for a footing which is described

in more detail at a later chapter.

It should also be pointed out that during the process of iteration, while, at a given cycle, the value of E for some elements are increased, those of other elements may remain constant or even be decreased. Such a development may also contribute to delay the convergence towards the actual solution.

4.4 Nonlinear Incremental Analysis

The nonlinear incremental analysis can be carried out with all the facilities stated earlier, regarding stress-strain relationship and E-ν relationships for orthotropic or isotropic material. In this analysis a history of load-deflection or load factor-stress relationship of the structure is traced from that at the unloaded state, up to and including the state of failure. In order to do this, the instantaneous tangent modulus of each element is employed for the analysis under a given set of loads.

Consider the stress-strain relationship of fig. 4.1(d) which is smooth and nonlinear. Under a given stress s_i the tangent modulus E_{ti} is given by the slope of the stress-strain curve at point (a) corresponding to the stress s_i. In fig. 4.1(e) this value of E_{ti} is shown as a point on a curve relating various values of E_t against the strain . This curve can be produced by measuring various values of the slope of the stress-strain curve of fig. 4.1(d). Instead of using the curve of fig. 4.1(d) in an analysis, that of fig. 4.1(e) directly gives the tangent modulus in an element under any state of strain, which appears to be more convenient to use instead of calculating the slope of the stress-strain diagram. At the unloaded state of the structure, the value of E_t for an element is given by the ordinate Ob, in fig. 4.1(e).

Consider the application of a small increment of loads $\Delta \underline{L}_1$ to the structure and solve for the resulting displacements $\Delta \underline{X}_1$ by the inverse transformation $\Delta \underline{X} = \underline{K}^{-1} \Delta \underline{L}$. If $\Delta \underline{L}$ is sufficiently small, then in the $\underline{K}$ matrix, the value of Ob, can be used to represent the initial

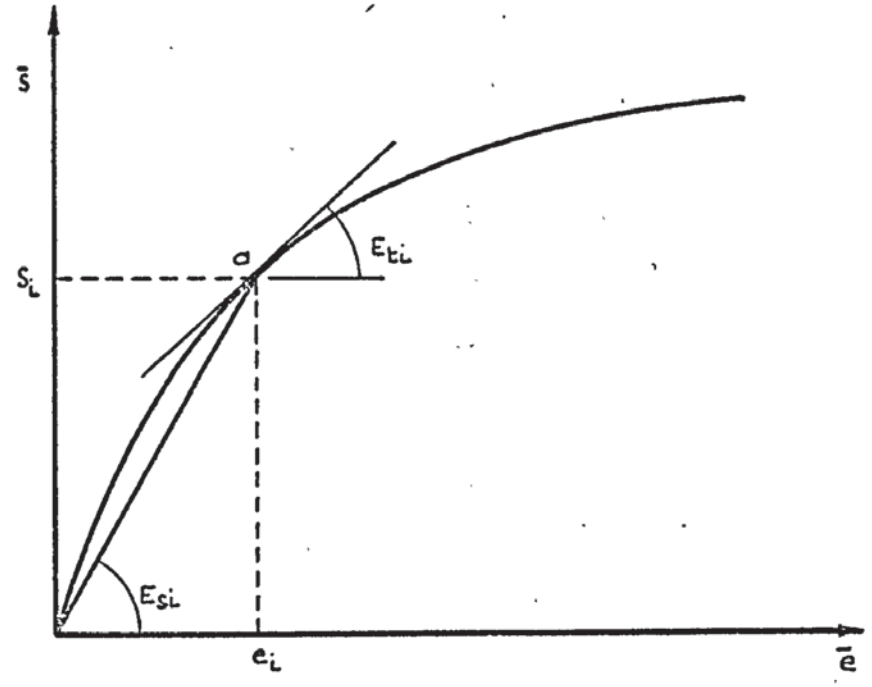

FIGURE 4.1. (d) EVALUATION OF TANGENT MODULUS ON STRESS - STRAIN CURVE.

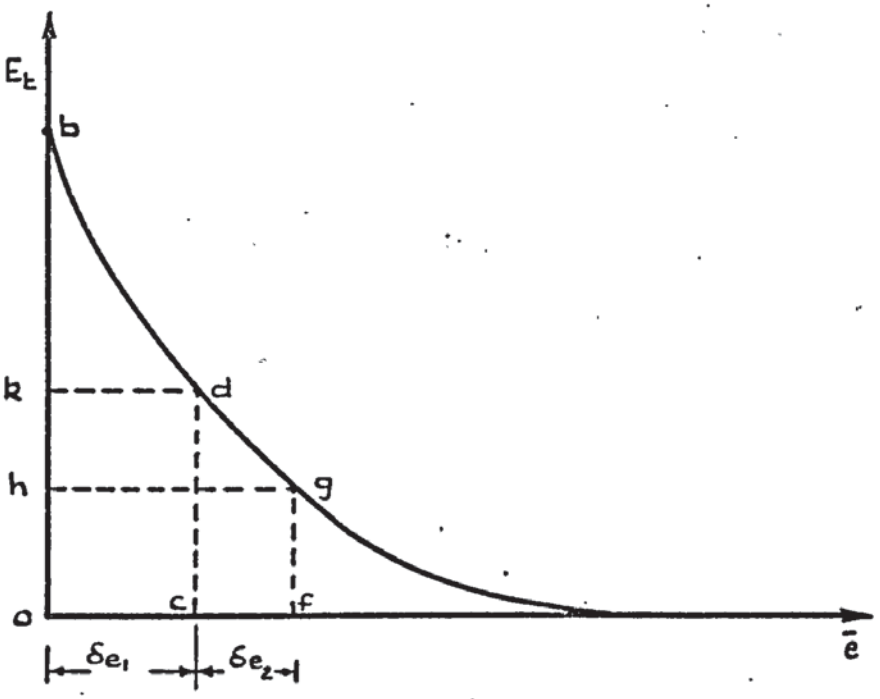

FIGURE 4.1. (e) GRAPH OF TANGENT MODULUS AGAINST STRAIN.

tangent modulus for all the elements. Once the vector $\Delta \underline{X}_1$ is found, the stresses $\Delta \underline{s}_1$ throughout the structure can be evaluated as usual from $\Delta s = \underline{S}\,\underline{A}\,\Delta \underline{X}$. The corresponding strains $\Delta \underline{e}_1$ are also calculated from $\Delta \underline{e} = \underline{D}^{-1} \Delta \underline{s}$. For an element the value of a strain δe_1 calculated in this manner is shown in fig. 4.1(e) as the absissa oc. The corresponding tangent modulus for this element can be read off as ok in this figure. Consider now the application of a further increment of loads $\Delta \underline{L}_2$. During the analysis of the structure subject only to the set of loads $\Delta \underline{L}_2$, the instantaneous value of E_t inst = ok can be used to represent the tangent modulus for the element and the corresponding stiffness equations can be constructed and solved for $\Delta \underline{X}_2$, where $\Delta \underline{X}_2$ is an increment of deflections resulting from the application of the load $\Delta \underline{L}_2$ alone. The corresponding increments of stresses and strains are $\Delta \underline{s}_2$ and $\Delta \underline{e}_2$ respectively. For the single element considered earlier the increment of its strain is δe_2. Thus under the loads $\Delta \underline{L}_1 + \Delta \underline{L}_2$ acting together, the total strain in the element is $\Delta \underline{e}_1 + \Delta \underline{e}_2$, which is given by of in fig 4.1(e). Once again a new instantaneous E_t for this element is obtained from this figure, which is now given by the ordinate oh.

This process of using the current instantaneous E_t to solve the structure for a new increment $\Delta \underline{X}_i$ under the loads $\Delta \underline{L}_i$ can be continued until failure. At the end of each solution j, the total loads, deflections, stresses and strains are given by:-

1. The total load vector $\underline{L}_j$ is:-

$$\underline{L}_j = \sum_{i=1}^{j} \Delta \underline{L}_i \qquad (4.13)$$

2. The total deflections are:-

$$\underline{X}_j = \sum_{i=1}^{j} \Delta \underline{X}_i = \sum_{i=1}^{j} \underline{K}_i^{-1} \Delta \underline{L}_i \qquad (4.14)$$

3. The total stresses are:-

$$\underline{s}_j = \sum_{i=1}^{j} \Delta \underline{s}_i = \sum_{i=1}^{j} \underline{S}_i\,\underline{A}\,\Delta \underline{X}_i \qquad (4.15)$$

4. Finally the total strains are:-

$$\underline{e}_j = \sum_{i=1}^{j} \Delta \underline{e}_i = \sum_{i=1}^{j} \underline{D}_i^{-1} \Delta \underline{s}_i \qquad (4.16)$$

These final values of strain $\underline{e}_j$ are used in conjunction with fig. 4.1(e) to evaluate the instantaneous tangent modulus E_{tj}.

In this manner the loads can be increased up to failure which is identified by the fact that at failure the determinant of the most recent stiffness matrix $|\underline{K}_i|$ is equal to zero. At this stage the process is terminated.

It is clear that provided the increments $\Delta \underline{L}_i$ are small, the method converges rapidly with the accuracy of the analysis being improved by taking small $\Delta \underline{L}_i$ steps.

The advantage of the above method becomes apparent when it is realised that for most materials the elastic and the inelastic strains can not be separated easily. This method does suffer from this drawback.

4.5 Nonlinear Iterative Program

A was decided to write a nonlinear program to analyse two dimensional continua consisting of member, rectangular and triangular plate elements. The plate elements could be of plane stress or plane strain depending on the type of problem. As only two dimensional continua are considered, the degrees of freedom at each joint are reduced to three. These are two translational and one 'in plane' rotation which will not be present where plates only are considered. The stiffness matrix will be considerably reduced in size from that of the three dimensional case and therefore it was decided to consider all joints to be in one group and dispense with tridiagonalisation. This was found to simplify the program while still enabling adequate storage for the largest analyses which were considered. This is due to the fact that sparse matrix routines are used for the manipulation of the matrices. At the same time the program was

written to analyse structures under either imposed loads, imposed deflections or both acting simultaneously. The form of the program is to evaluate the stresses in a structure whose elastic constants correspond to those at zero stress level. Using these stresses, new values for the constants are evaluated so that they may be used in a analysis of the structure. This is repeated until the constants on two successive iterations are practically equal. In order to evaluate the elastic constants, two stress-strain curves were fed in, one for the 'P' and one for the Q direction. Corresponding to these, two other curves relating Young's Modulus and Poisson's Ratio were also fed into the computer. Fig. 4.2 gives a flow diagram for the iterative program and table 4.2 gives the matrix manipulations which are involved. These are marked off in blocks and stages as before. The complete element and general data is first read in for the structure. A specification of this is given in appendix 4. For individual problems the data form has had to be slightly changed and where this occurs it is mentioned in the text.

The known deflection and load vectors are next read in (block 2) and the initial values of the modulus of elasticity and Poisson's Ratio are determined for the first iteration. As shown by equation (4.5) the matrices $\underline{K}_{11}$ and $\underline{K}_{12}$ have first to be established for the structure. A flow diagram showing how this is done is given in fig. 4.3 (as referenced in block 4, fig. 4.2) and the matrix operations involved are shown in table 4.1. To form the overall stiffness matrices it was found more convenient to form the stiffness matrices of each individual element type first. The stiffness of the structure could then be found by the straightforward addition of the individual stiffnesses in the form:-

$$\underline{K}_{11m} + \underline{K}_{11r} + \underline{K}_{11t} + \underline{K}_{11mrt} = \underline{K}_{11\ \text{overall}} \qquad (4.17a)$$

and,

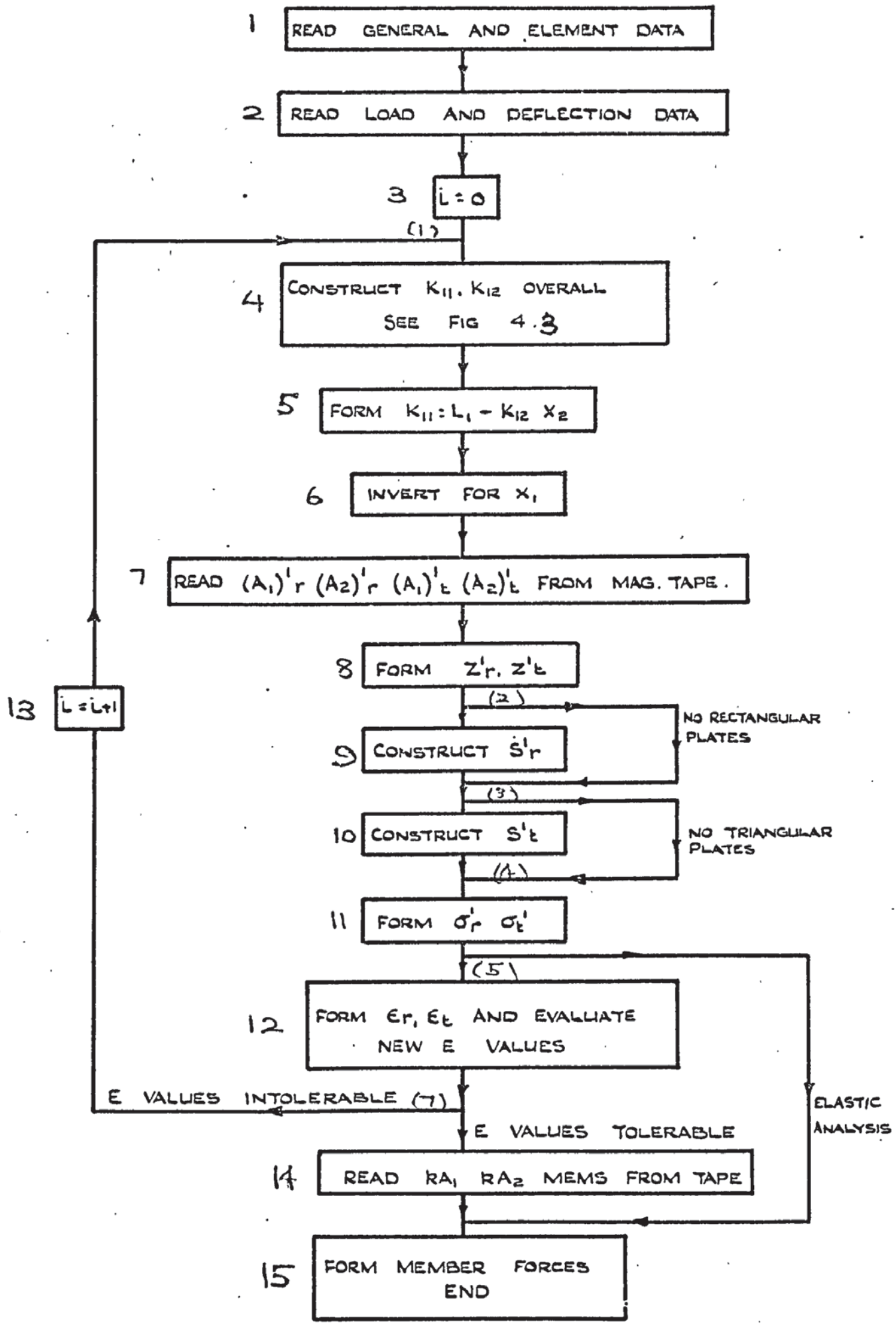

FIGURE 4.2. FLOW DIAGRAM FOR ITERATIVE PROGRAM.

	OPERATION	1	2	3	4	5	6	7	8	9	10	11	12	13	REMARKS
1	START	L_1'	X_2'												START OF PROGRAM
2		L_1'	X_2'	A_{1rn}'	A_{2rn}'	R_{rn}									IF $L>0$ READ 3 & 4 FROM TAPE ELSE CONSTRUCT 3, 4, 5
3	TRANS 3 & 4 MULT. 5 x 4, 3	L_1'	X_2'	A_{1rn}'	A_{2rn}'	R_{rn}	A_{1rn}	A_{2rn}	RA_{m1}	RA_{m2}					
4	REMOVE 5, 6, 7. MULT 3 x 5, 6	L_1'	X_2'	A_{1rn}'	A_{2rn}'	RA_{1rn}	RA_{2rn}	K_{11rn}	K_{12rn}						$K_{11} = A_1' RA_1$; $K_{12} = A_1' RA_2$
5	REMOVE 3, 4	L_1'	X_2'	RA_{1m}	RA_{2m}	K_{11m}	K_{12m}								RETURN HERE SECOND ITERATION (5, 6 OFF TAPE) $L>0$
6		L_1'	X_2'	RA_{1m}	RA_{2m}	K_{11m}	K_{12m}	$A_1'r$	$A_2'r$	R_r					IF L ?0 READ 7 & 8 FROM TAPE ELSE CONSTRUCT 7, 8, 9
7	TRANS 7 & 8 MULT 7, 9, 10	L_1'	X_2'	RA_{1m}	RA_{2m}	K_{11m}	K_{12m}	$A_1'r$	$A_2'r$	R_r	A_{1r}	A_{2r}	$A_1'R_r$	K_{11r}	
8	REMOVE 9, 10 MULT 10 x 9	L_1'	X_2'	RA_{1m}	RA_{2m}	K_{11m}	K_{12m}	$A_1'r$	$A_2'r$	A_{2r}	$A_1'R$	K_{11r}	K_{12r}		
9	REMOVE 9, 10 ADD 5 + 9	L_1'	X_2'	RA_{1m}	RA_{2m}	K_{11m}	K_{12m}	$A_1'r$	$A_2'r$	K_{11r}	K_{12r}	K_{11mr}			RA_1 RA_2 K_{11m} K_{12m} WRITTEN TO TAPE
10	REMOVE 3, 4, 5 ADD 3 + 7	L_1'	X_2'	K_{12m}	$A_1'r$	$A_2'r$	K_{11r}	K_{12r}	K_{11mr}	K_{12mr}					A_{1r}' A_{2r}' WRITTEN TO TAPE $K_{11m} + K_{11r} = K_{11mr}$
11	REMOVE 3 - 7	L_1'	X_2'	K_{11mr}	K_{12mr}										$K_{12m} + K_{12r} = K_{12mr}$
12		L_1'	X_2'	K_{11mr}	K_{12mr}	A_{1t}'	A_{2t}'	R_t							IF $L>0$ READ 5, 6 FROM TAPE ELSE CONSTRUCT 5, 6, 7.
13	TRANS 5, 6 MULT 5, 7, 8	L_1'	X_2'	K_{11mr}	K_{12mr}	$A_1't$	A_{2r}'	Rt	A_{rt}	A_{2t}	$A_1'R$	K_{11t}			
14	REMOVE 7, 8 MULT 8 x 7	L_1'	X_2'	K_{11mr}	K_{12mr}	$A_1't$	$A_2't$	A_{2t}	$A_1'R_t$	K_{11t}	K_{12t}				5, 6 WRITTEN TO TAPE
15	REMOVE 5 - 8 ADD 3+5, 4+6	L_1'	X_2'	K_{11mr}	K_{12mr}	K_{11t}	K_{12t}	K_{11mrt}	K_{12mrt}						$K_{11mr} + K_{11t} = K_{11mrt} = K_{11}$ OVERALL
16	REMOVE 3 - 6	L_1'	X_2'	K_{11mrt}	K_{12mrt}										$K_{12mr} + K_{12t} = K_{12mrt} = K_{12}$ OVERALL

TABLE 4.1. MATRIX OPERATIONS TO FORM K OVERALL.

	OPERATION	1	2	3	4	5	6	7	8	9	10	11	REMARKS
1		L_1'	X_2'	K_{11}	K_{12}								K_{11}, K_{12} OVERALL FORMED.
2	TRANS 1, 2 MULT 4 x 6	L_1'	X_2'	K_{11}	K_{12}	L_1	X_2	$K_{12} X_2$					
3	SUBTRACT 5-7 COMPOUND 3 & 8	L_1'	X_2'	K_{11}	K_{12}	L_1	X_2	$K_{12} X_2$	$L_1 - K_{12} X_2$	K_{11} : $L_1 K_{12} X_2$			K_{11} COMPOUNDED WITH $L_1 - K_{12} X_2$ FOR INVERSION
4	REMOVE 3-9	L_1'	X_2'	K_1 : $L_1 - K_{12} X_2$									
5	DIV. 3 & TRANS	L_1'	X_2'	X_1	X_1'								INVERT TO FORM X_1
6	REMOVE 3	L_1'	X_2'	X_1'	A_{1t}'	A_{2t}'	A_{1r}'	A_{2r}'					4-7 READ BACK FROM MAG TAPE.
7	MULT 4,6 x 3 5,7 x 2	L_1'	X_2'	X_1'	A_{1t}'	A_{2t}'	A_{1r}'	A_{2r}'	Z_{1t}'	Z_{2t}'	Z_{1r}'	Z_{2r}'	$Z' = x' A'$
8	REMOVE 4 - 8 ADD 4+5, 6+7	L_1'	X_2'	X_1'	Z_{1t}'	Z_{2t}'	Z_{1r}'	Z_{2r}'	Z_t'	Z_r'			$Z' = Z_1' + Z_2'$
9	REMOVE 4 - 8	L_1'	X_2'	X_1'	Z_t'	Z_r'	S_r'	S_t'					CONSTRUCT STRESS MATRICES
10	MULT 6 x 5 7 x 4	L_1'	X_2'	X_1'	Z_t'	Z_r'	S_r'	S_t'	σ_r'	σ_t'			EVALUATE STRESSES
11	REMOVE 4 - 8	L_1'	X_2'	X_1'	σ_r'	σ_t'							TEST L VALUES RETURN TO TABLE 4.1. IF NOT OK.
12	REMOVE 4 & 5	L_1'	X_2'	X_1'	RA_{1m}	RA_{2m}							4,5 READ BACK FROM TAPE
13	TRANS 2, 3 MULT 4x6 5x7	L_1'	X_2'	X_1'	RA_{1m}	RA_{2m}	X_1	X_2	P_{1m}	P_{2m}			$P = RAX$
14	REMOVE 4-8 ADD 4 + 5	L_1'	X_2'	X_1'	P_{1m}	P_{2m}	P_m						$P = P_1 + P_2$
15	TRANS 6	L_2'	X_2'	X_1'	P_{1m}	P_{2m}	P_m	P_m'					PRINT P

TABLE 4.2 MATRIX OPERATIONS FOR ITERATIVE PROGRAM.

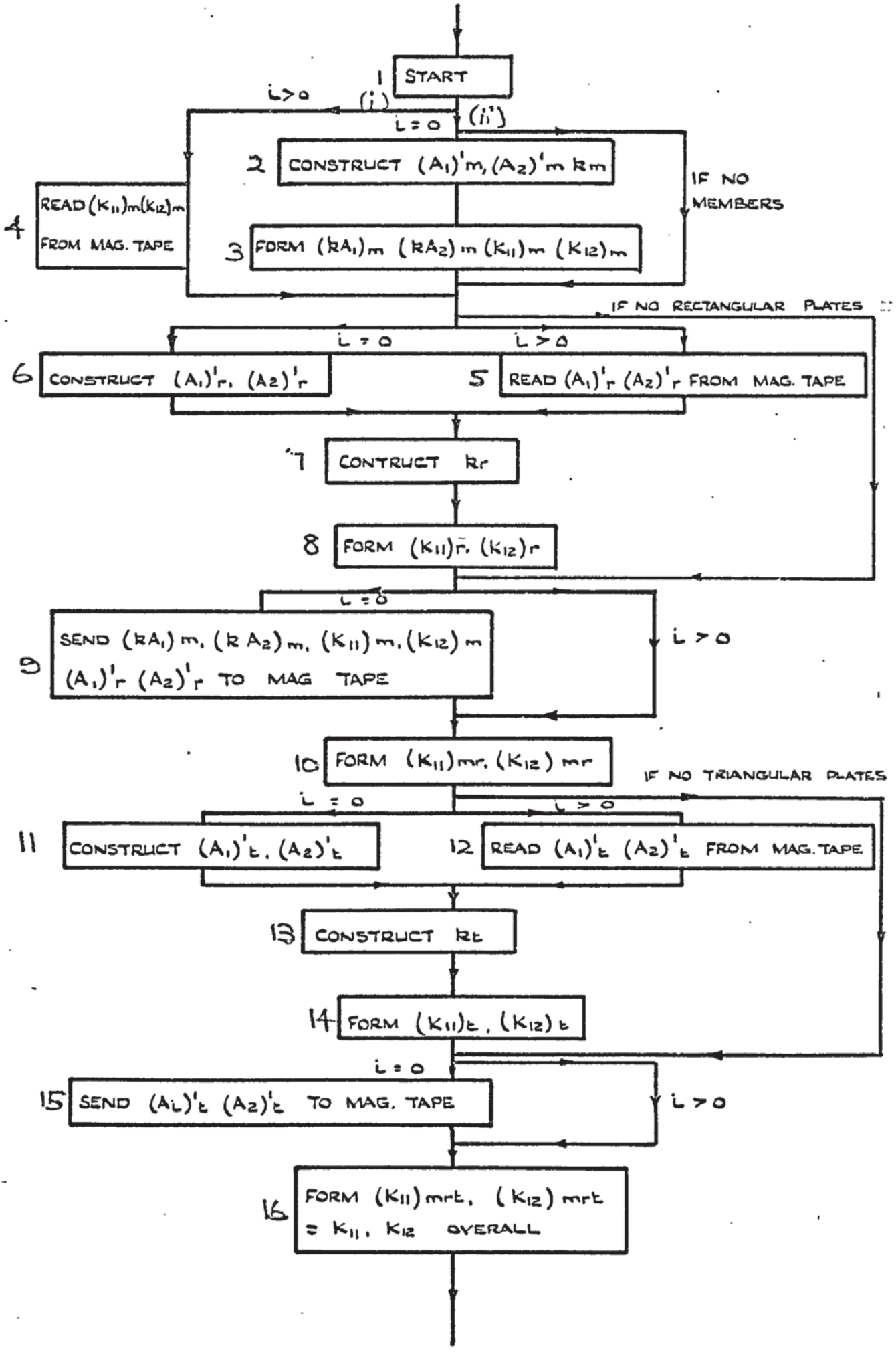

FIGURE 4.3. FLOW DIAGRAM FOR CONSTRUCTION OF K_{11} AND K_{12} OVERALL.

$$\underline{K}_{12m} + \underline{K}_{12r} + \underline{K}_{12t} = \underline{K}_{12mrt} = \underline{K}_{12 \text{ overall}} \qquad (4.17b)$$

where the suffices m, r, t refer to members, rectangular and triangular plates respectively. When using one joint group this method is at least as fast computationally as that used in the elastic analysis program. Expanding equations (4.17)

$$\underline{K}_{11 \text{ overall}} = \underline{A}^{1}_{1m}\underline{k}_{m}\underline{A}_{1m} + \underline{A}^{1}_{1r}\underline{k}_{r}\underline{A}_{r} + \underline{A}^{1}_{1t}\underline{k}_{t}\underline{A}_{1t} \qquad (4.18a)$$

and

$$\underline{K}_{12 \text{ overall}} = \underline{A}^{1}_{1m}\underline{k}_{m}\underline{A}_{21} + \underline{A}^{1}_{1r}\underline{k}_{r}\underline{A}_{2r} + \underline{A}^{1}_{1t}\underline{k}_{t}\underline{A}_{2t} \qquad (4.18b)$$

In equations (4.18) care was taken to ensure that all the matrices are compatible and of the same size before their addition. An explanation of their construction will be given in the next section.

The displacement transformation matrices $\underline{A}^{1}_{1m}$ and $\underline{A}^{1}_{2m}$ are constructed first (stage 2, table 4.1 and block 2 fig. 4.3). This is followed by the unassembled element stiffness matrix $\underline{k}_{m}$. The matrices $\underline{K}_{11}$, $\underline{K}_{12}$, $\underline{kA}_{1}$ and $\underline{kA}_{2}$ are formed from straightforward multiplication (stages 3 and 4). The latter two matrices are needed to calculate the member forces at the end of the analysis. If no members are present this section of the program is by-passed (branch (2) fig. 4.3) and four null matrices are inserted in the sparse array. When the stiffnesses are added these will have no influence on the final matrix. This technique is repeated for the rectangular and triangular plates if neither of these elements are present. It is also worth pointing out at this stage that if there is no imposed deflection, the matrix $\underline{A}_{2}$ as well as $\underline{X}_{2}$ is automatically nulled and therefore $\underline{K}_{12}$ is not constructed. Equation (4.5) then reduces to the case of imposed loading only.

The transformation and stiffness matrices are next formed for the rectangular plates (stage 6, blocks 6 and 7) and multiplied together to form $\underline{K}_{11r}$ and $\underline{K}_{12r}$ (stage 8 in table 4.1 and block 8 in fig. 4.3).

At this point, the matrices which are of no further use in this iteration, but will be needed for the later computation are written up onto the magnetic tape (stage 9 and block 9). These are $\underline{k}_m\underline{A}_{1m}$, $\underline{k}_m\underline{A}_{2m}$, $\underline{K}_{11m}$, $\underline{K}_{12m}$, $\underline{A}^1_{1r}$, $\underline{A}^1_{2r}$ and can now be cleared out of the main working store (stage 10). The stiffnesses of the members and rectangular plates are added to form $\underline{K}_{11mr}$ and $\underline{K}_{12mr}$ (stages 10, 11, block 10). The matrices $A_{1t}{}^1$, A^1_{2t}, k_t are constructed for the triangular plates and hence $\underline{K}_{11t}$ and $\underline{K}_{12t}$ are evalutated. (stage 12, 13 and 14 and blocks 11, 13, 14). The matrices A^1_{1t} and A^1_{2t} are also sent to the magnetic tape (stage 14 block 15) and the stiffnesses added to form the overall stiffness matrices (stage 15, block 16). Thus:-

$$\underline{K}_{11mr} + \underline{K}_{11t} = \underline{K}_{11mrt} = \underline{K}_{11} \text{ overall}$$
$$\underline{K}_{12mr} + \underline{K}_{12t} = \underline{K}_{12}{}^{mrt} = \underline{K}_{12} \text{ overall} \qquad (4.19)$$

Equation (4.5) is formed and solved for the unknown displacement $\underline{X}_1$ (stages 3, 4, 5 in table 4.2, and blocks 5 and 6 in fig. 4.2). It is next necessary to evaluate the plate stresses. The transformation matrices are recalled from the magnetic tape (stage 6 and block 7) and the element displacement vectors $\underline{z}^1_t$ and $\underline{z}^1_r$ are formed from equations 4.6 (stage 7 and 8 and block 8). Their formation in transposed form was purely to save the computing time. The transposed stress matrices were next constructed and the transposed stresses found from,

$$\underline{s}^1 = \underline{z}^1\,\underline{S}^1 \qquad (4.20)$$

These are given in stages 9, 10 and 11 in table 4.2 and blocks 9 and 10 and 11 in fig. 4.2. The stresses have now been determined throughout the continuum and the elastic constants are next checked and adjusted if necessary (block 12) before proceding to the next iteration.

The above calculations are applicable to a case of orthotropy where the material's principal directions lie along the P and Q axes. Obviously, with small alteration to the program, other causes of non-linearity can be accomodated.

The new values E which have just been calculated are compared with the original values E_o for each element to determine whether another iteration is necessary (branch (7) fig. 4.2). For each element a tolerance test is carried out to find whether $(E_1 - E_o)/E_o$ is less than a specified tolerance to decide whether the iteration has converged sufficiently. If 80% of the plates are below this tolerance and the remaining 20% also lie below a more lenient tolerance which is also given in the general data, then no more iterations are carried out. The choice of 80% is arbitrary but saves computing time for the minimal advantage in accuracy which would be gained by iteration until all the plates have correct values of the modulus of elasticity. This also prevents any oscillations around final values which might occur among a group of plates and prevent completion of the analysis. The values E_1 are then used to determine the values of Poisson's Ratio for the plates which are found from the Young's Modulus - Poisson's Ratio relationship. If all the elastic constants are tolerable then the matrices $\underline{kA}_1$ and $\underline{kA}_2$ for the members are read back from the magnetic tape and the member forces calculated (stages 12 to 15, table 4.2 and blocks 14 and 15 in fig. 4.2). The program is then terminated. However, if a further iteration is necessary then the overall stiffnesses need to be recalculated using the new values of Young's Modulus and Poisson's ratio. This is shown in fig. 4.3 where the counter i is now greater than zero.

For the type of problem investigated in this thesis it was unnecessary to introduce nonlinearity into the member element as only continuous materials are investigated. Therefore the stiffnesses of the members could be read back from the tape and null matrices inserted in the place of $\underline{kA}_1$ and $\underline{kA}_2$ for the members to ensure compatibility with the first iteration (block 4 in fig. 4.3). When reconstructing the stiffnesses of the plates, both rectangular and triangular, it was only necessary to

form the unassembled stiffness matrix. The transformation matrices are read back from the magnetic tape (blocks 5 and 12, fig. 4.3). There was no need in this iteration to write anything onto the tape.

The magnetic tape was used in two capacities. The first has already been mentioned and is that of a backing store for temporarily unwanted matrices. Therefore, when the main store was becoming full at the end of the rectangular plate analysis, the matrices for these plates and members were sent to the tape. This was not done sooner as the matrices concerning the members were anticipated to be small. Two routines were used to write matrices onto the magnetic tape and read backwards from tape. This prevented excess rewinding of the tape to the new starting position. The matrices need to be positioned in the best order so as to cause as little rewinding of the tape as possible. This order was of the form:

$$\underline{kA}_{1m},\ \underline{kA}_{2m},\ \underline{K}_{11m},\underline{K}_{12m},\underline{A}^{1}_{1r},\underline{A}^{1}_{2r},\underline{A}^{1}_{1t},\underline{A}^{1}_{2t}$$

As in the elastic analysis program, the computing time was tested at the end of every iteration to ensure that there was enough time for the next. If not, the general information and plate properties were written onto the tape. None of the element data was required. The program could then be restarted from this position at a later date.

The next section explains how the displacement transformation matrices $\underline{A}^{1}_{1}$ and $\underline{A}^{1}_{2}$ were set up as well as the unassembled stiffness matrices.

4.6 Construction of the matrices.

For each type of element it is required to construct the displacement transformation matrices $\underline{A}^{1}_{1}$ and $\underline{A}^{1}_{2}$ as well as the element stiffness matrix $\underline{k}$. To construct $\underline{A}^{1}_{1}$ and $\underline{A}^{1}_{2}$ two separate blocks of joint data were required. For the construction of $\underline{A}^{1}_{1}$ all the degrees of freedom with known movements are omitted from the first block of joint data. In this manner the rows of $\underline{A}^{1}_{1}$ corresponding to these known movements are left out. In the second block of joint data, only the degrees of freedom for the known

movements are included so that there will be a row in $\underline{A}_2^1$ that corresponds to each known movement.

Care was taken to ensure that all the stiffness matrices $\underline{K}$ had the same order. This was achieved by considering the structure as a whole during the construction of the transformation matrices. Thus for each unknown degree of freedom in the structure there was a row in $\underline{A}_1^1$. Similarly $\underline{A}_2^1$ contained a row for each known movement in the structure.

In the case ofa plane frame the relationship $\underline{z} = \underline{AX}$ for a single member connecting joints i and j has the form:-

$$\begin{bmatrix} u \\ v \\ \\ \\ \psi_{R1} \\ \psi_{R2} \end{bmatrix} = \begin{bmatrix} -l_p & -m_p & o & --- & l_p & m_p & o \\ -l_q & -m_q & o & --- & l_q & m_q & o \\ & & & & & & \\ o & o & 1 & --- & o & o & o \\ o & o & o & --- & o & o & 1 \end{bmatrix} \begin{bmatrix} x_i \\ y_i \\ \theta_i \\ \vdots \\ x_j \\ y_j \\ \theta_j \end{bmatrix} \quad \text{(4.21.)}$$

end 1 at joint i — end 2 at joint j

To construct $\underline{A}_{lm}^1$ for the members, the joints are inspected in turn. Each member connected to a given joint is recorded under that joint by its number together with its relavent end number. For a given joint with no member connection $\underline{A}_{lm}^1$ contains as many blank rows as there are degrees of freedom in that joint data. These blank rows do not occupy any storage since sparse matrix type of storage is being employed.

For each member (i) there will be four columns in $\underline{A}_{lm}^1$. These will be column numbers 4i - 3, 4i - 2, 4i - 1 and 4i respectively corresponding to u_i, v_i, ψ_{Ril} and ψ_{Ri2}. Matrix $\underline{A}_2^1$ is constructed similarly, except, of course, the rows of this matrix are numbered from one upwards to correspond to the known movements in the second block of joint data. The construction of the member stiffness matrices is similar to that in chapter 3. here.

The construction of $\underline{A}_1^1$ and $\underline{A}_2^1$ for the plate elements follows the same procedure as those for the members. Except the columns numbers of these matrices are now given by:-

$$C_{ri} = 8i + 2k - 9$$
$$\text{and} \quad C_{r+1,i} = 8i + 2k - 8 \qquad (4.22)$$

where $k = 1,1,4$

for the rectangular elements and;

$$C_{ti} = 6i + 2k - 7$$
$$\text{and} \quad C_{t+1,i} = 6i + 2i - 6 \qquad (4.23)$$

where $k = 1,1,3$

Where i is the plate element number, C_{ri} and $C_{r+1,i}$ are the columns numbers and correspond to rectangular element number i while C_{ti} and $C_{t+1,i}$ are the column numbers for the triangular element i. In both equations (4.22 and 4.23) k refers to the corner numbers for the element under consideration. As it is expected in equation (4.22) there are 8 nodal movements for each rectangular element with 2 at each corner. Similarly each triangular element has 6 nodal movements, 2 of which at each corner.

The element stiffness matrices were formed for the plates so as to be adaptable for the case of plane stress or plane strain. The effect of orthotropy was also included. All these cases can be catered for by the alteration of the elasticity matrix, which takes the form:-

$$\underline{D} = \alpha_0 \begin{bmatrix} \alpha_{11} & \alpha_{12} & 0 \\ \alpha_{21} & \alpha_{22} & 0 \\ 0 & 0 & \alpha_{33} \end{bmatrix} \qquad (4.24)$$

where for plane stress, with $s_r = 0$:

$$\alpha_0 = E/(1-\nu^2)$$
$$\alpha_{11} = 1$$

$$\alpha_{12} = \nu$$
$$\alpha_{22} = 1 \qquad (4.25)$$
$$\alpha_{33} = (1-\nu)/2$$

On the other hand for plane strain with $e_r = 0$:

$$\alpha_0 = E(1-\nu)/(1+\nu)(1-2\nu)$$
$$\alpha_{11} = 1$$
$$\alpha_{12} = \nu/(1-\nu) \qquad (4.26)$$
$$\alpha_{22} = 1$$
$$\alpha_{33} = (1-2\nu)/2(1-\nu)$$

The terms of the element stiffness matrix can be evaluated as functions of the constants α_{ij} of the elasticity matrix. It is then straightforward in changing these constants depending on the type of analysis required.

This described the nonlinear iterative program. The next section shows how this was adapted to form a nonlinear incremental program.

4.5 Nonlinear Incremental Program.

In this type of analysis the loads are applied in small increments. For the first increment the displacements are found using elastic constants E_o, ν_o as in the iterative procedure. For the next increment the instantaneous or tangent modulus E_{ti} is used and the stresses and displacements are accumulated as the load increments are increased so as to give the final values at any position on the curve.

Fig. 4.4 gives a flow diagram for the incremental program. while table 4.3 summarizes the matrix operations. The general and element data is first read (block 1, fig. 4.5). The method of imposed deflections is not used in this program as the matrix $\underline{X}_2$ of the iterative program is used to store the accumulative displacements. There is therefore no second block of joint data. The load vector is now used as the load increments and is

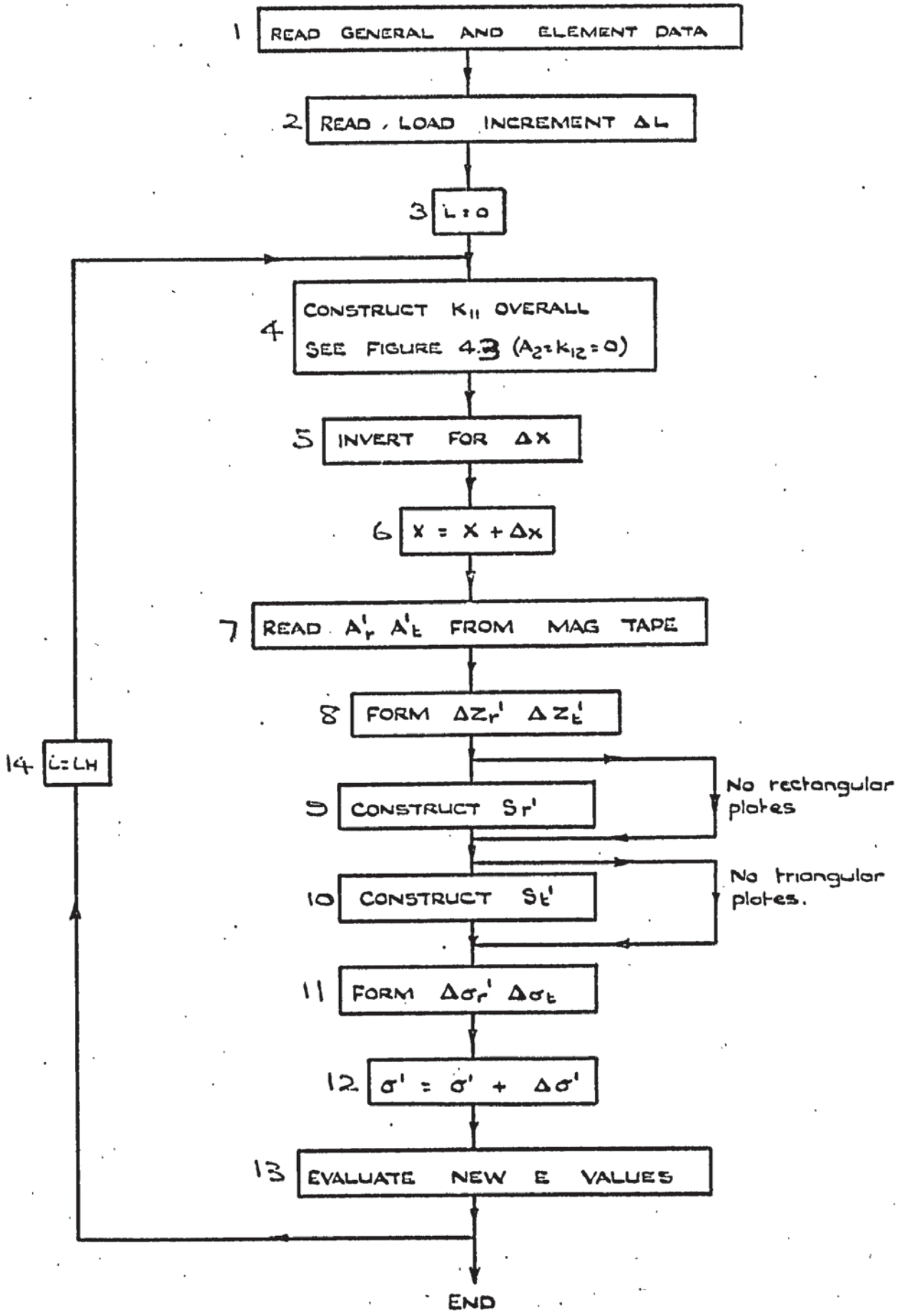

FIGURE 4.4. FLOW DIAGRAM FOR INCREMENTAL PROGRAM.

	OPERATION	1	2	3	4	5	6	7	8	9	10	11	REMARKS
1		$\Delta L'$	x'	k	0								K OVERALL FORMED $K_{12} = 0$
2	TRANS 2 → 6	$\Delta L'$	x'	k		ΔL	x						
3	CONTRACT 5-7 COMPOUND 3 & 8	$\Delta L'$	x'	k		ΔL	x'		ΔL	$K:\Delta L$			K COMPOUNDED WITH ΔL FOR INVERSION
4	REMOVE 3-9	$\Delta L'$	x'	$K:\Delta L$									
5	DIV. 3	$\Delta L'$	x'	Δx									INVERT 3 TO FORM Δx
6	TRANS 3 → 4 ADD 2+4	$\Delta L'$	x'	Δx	$\Delta x'$	$(x+\Delta x)'$							ACCUMULATE Δx
7	REMOVE 2-4 4 = 2	$\Delta L'$	$\Delta x'$	$(x+\Delta x)'$	$\Delta x'$								DUPLICATE $\Delta x'$
8	REMOVE 2	$\Delta L'$	$(x+\Delta x)'$	$\Delta x'$									
9		$\Delta L'$	$(x+\Delta x)'$	$\Delta x'$	A'_t		A'_r						READ 4-7 BACK FROM TAPE ($A_z = 0$)
10	MULT. 3 x 4 3 x 6	$\Delta L'$	$(x+\Delta x)'$	$\Delta x'$	A'_t		A'_r		$\Delta Z'_t$		$\Delta Z'_r$	0	$\Delta z' = \Delta x' A'$
11	REMOVE 4 - 8	$\Delta L'$	$(x+\Delta x)'$	$\Delta x'$	$\Delta Z'_t$		$\Delta Z'_r$						
12	REMOVE 5	$\Delta L'$	$(x+\Delta x)'$	$\Delta x'$	$\Delta Z'_t$	$\Delta Z'_r$							
13		$\Delta L'$	$(x+\Delta x)'$	$\Delta x'$	$\Delta Z'_t$	$\Delta Z'_r$	S'_r	S'_t					CONSTRUCT STRESS MATRIX
14	MULT 4 x 7 5 x 6	$\Delta L'$	$(x+\Delta x)'$	$\Delta x'$	$\Delta Z'_t$	$\Delta Z'_r$	S'_r	S'_t	$\Delta\sigma'_r$	$\Delta\sigma'_t$			$\Delta\sigma' = \Delta z' S'$
15	REMOVE 3-10	$\Delta L'$	$(x+\Delta x)'$										RETURN FOR NEXT INCREMENT

TABLE 4.3 MATRIX OPERATIONS FOR INCREMENTAL PROGRAM.

denoted by $\Delta\underline{L}^1$. The imposed deflection vector $\underline{X}_2$ is set to zero.

The overall stiffness of the structure is formed using the same matrix operations as the iterative program (fig. 4.3) but, as there are no imposed deflections, the matrices $\underline{A}_{2m}$, $\underline{A}_{2r}$, $\underline{A}_{2t}$ are set to zero. Therefore $\underline{K}_{12}$ also becomes a null matrix and $\underline{K}_{11}$ simply becomes $\underline{K}$ (stage 1, table 4.3). On inversion the increment of displacement $\Delta\underline{X}$ is solved for (stages 2 to 5). This is then added to the previous increment of displacement (stage 6 and block 6) and printed out so that a position on the curve can be plotted for every load increment. The transformation matrices are then read back from the magnetic tape (stage 9 and block 7) to form $\Delta\underline{Z}_r$ and $\Delta\underline{Z}_t$ (stage 10, block 8) which, when multiplied by the stress matrices give $\Delta\underline{s}_r$, $\Delta\underline{s}_t$ (stage 14 and block 11). These are the increments of stress in each element. These are then converted into strain increments using the appropriate elastic constants. Both the set of stresses Δs_p, Δs_q, Δs_{pq} and the set of strains Δe_p, Δe_q, Δe_{pq} are accumulated for each element (block 12) in additional arrays.

These accumulative strains can now be used to find the effective strain $\bar{e}$, which will give the new tangent modulus value as shown in fig. 4.1 (e). This curve is obtained from measurments on curve 4.1(d) and is fed into the computer in its piecewize linearised form. As $\bar{e}$ is continuously increasing the same routine can be used repeatedly to find E_t. The new value for Poisson's Ratio is also found, as before, and a new increment of load is applied. The program is limited to equal load increments but only small alterations would be necessary to read a new load for every increment. The computer is stopped after a specified amount of increments.

The description of the incremental program just given covers the establishment of the new elastic constants from a so-called effective strain. In chapter 7 this program is used to analyse a sand mass and a study of the stress-strain characteristics will be made before these values are

to be defined. In nonlinear iterative program is also used in chapter 7.as well as chapter 8 in the nonlinear analysis of a shear wall.

CHAPTER 5

COMPARISON OF TRIANGULAR WITH RECTANGULAR ELEMENT

5.1 Introduction

As a logical step from the development of the triangular element stiffness matrix described in chapter 2 it was necessary to assess the accuracy of the element independently. This was needed before progressing to its inclusion in complex analyses of three dimensional structures.

The rectangular element stiffness matrix is generally accepted to give reliable results in the analysis of simple cases of bending and 'in plane' actions. Melosh (10), Clough (21), Zienkiewicz (14) etc. have all used similar forms of the element with a high degree of success. The 'out of plane' stiffness matrices of Zienkiewicz and Melosh were used as a basis for comparison of results. Both have been mentioned in chapter 1 and it will suffice here to say that they conform for displacements but not slopes across their interfaces. The displacement function of Zienkiewicz shares with the triangular element a cubic expression and hence they will deform in a similar manner.

The 'in plane' rectangular element uses a linear displacement function similar to the triangular element. Again this has been used by numerous authors, among others, Argyris (7), Zienkiewicz (2), Przemieniecki (3), Clough (9). It also suffers from the lack of an 'in plane' rotational term.

The elastic analysis program was used in the comparison in two different forms. These were either to print out the plate forces on paper tape so as to be ready for use in the calculation of stresses, or to store the relevant matrices on magnetic tape so that stresses could be calculated from the stress matrices. Both these methods are described in detail in chapter 3.

The triangular element need not be symmetrical like the rectangular and, therefore, many different types of subdivision, or grid formations, can be used for a given problem. In this analysis three of the more common grid formations that can be expected were tried at various refinements of grid.

The main objects of this investigation were the comparison of rectangular with triangular element for different grid patterns with different refinements in calculating deflections. The two methods of evaluating the stresses are also compared. These analyses would also provide a useful check on the elastic analysis program.

5.2 Analysis of table

For the purpose of the comparison a table structure, shown in fig. 5.1, was used. This consisted of a flat top plate, ABCD, supported round the perimeter by edge beams which, in turn, were connected to columns at the four corners. These were fixed at the base. The structure was loaded laterally by two 10 ton loads at C and D. Vertical loading was applied by four one ton loads, symmetrically positioned on the table top as shown. The top was made to be $\frac{1}{4}$" thick and had a Poisson's ratio of .25. The members were given the relatively large dimensions of 3" square sections for reasons which will be given later. The value of Young's Modulus was 12,500 t.s.i. throughout. The properties are similar to those of steel.

This structure was decided upon for, although being three dimensional, the top plate action could be investigated independently. As the edge beams are so large, this plate will behave as if virtually 'built in' at the edges. The deflected form of the beams is different to that of the plates and this nonconformity might have affected the results.

The 'in plane' and 'out of plane' stiffness matrices are independent of each other. All movement in the XZ plane is therefore due

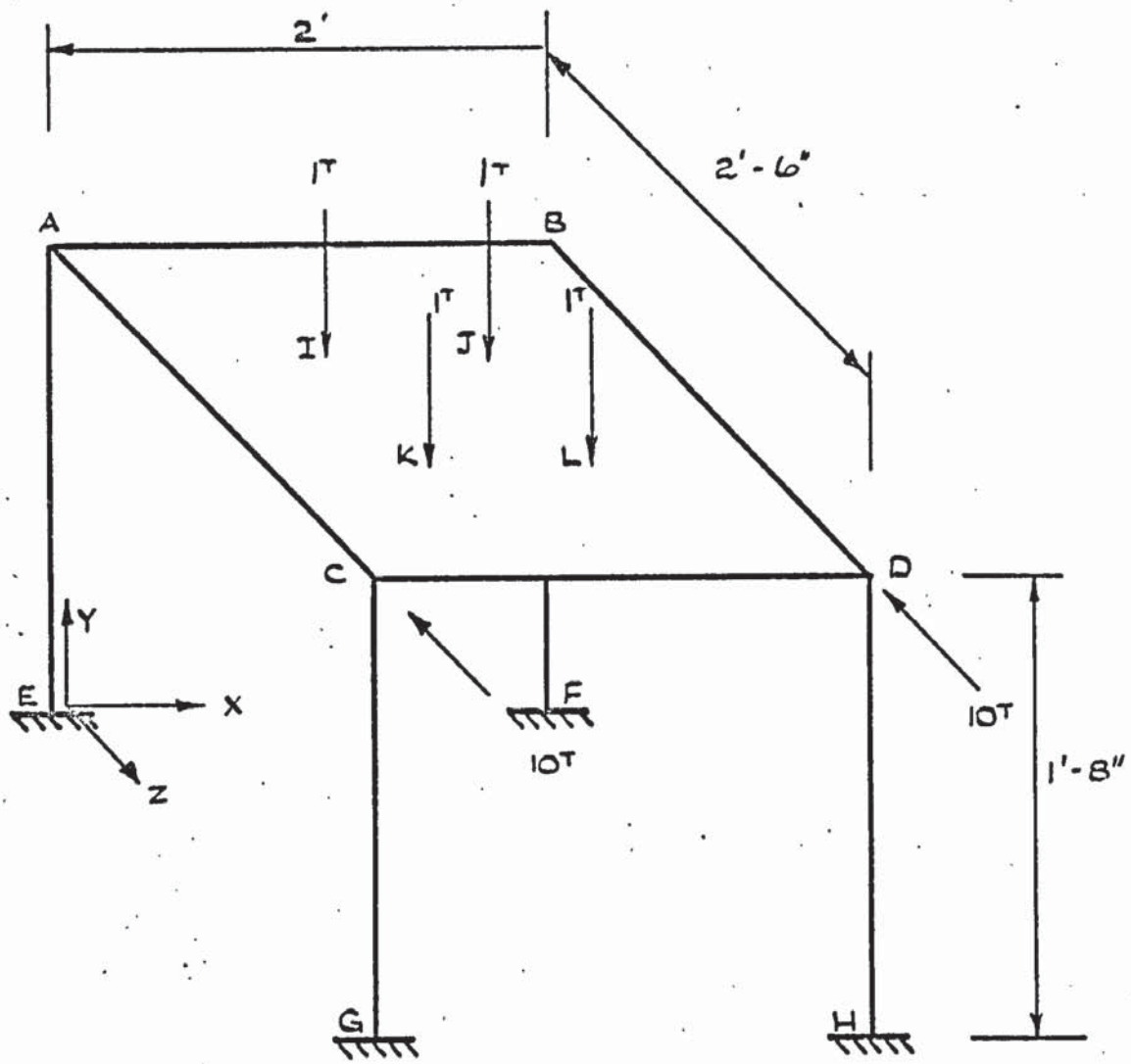

FIGURE 5.1. GENERAL VIEW OF TABLE

to 'in plane' action and all vertical and rotational movements are for the 'out of plane'. Thus the two matrices can be independently assessed.

The structure was analysed using five different types of grids for the table top as shown in fig. 5.2. The two rectangular grids were used to find out how quickly the elements converged to an answer. It also showed if this convergence formed an upper or lower bound.

The data for the analyses was punched in the form which appears in appendix 3. Having been run with the elastic program, the two different stress programs were run, using either the plate forces or the magnetic tape facilities. The matrices and storage requirements involved in the computation were small and hence such details as the numbering of joints will not be discussed in this instance.

Grid types 2 and 5 were split up into three joint groups, the other types only being in two. No computational difficulties were encountered and all analyses were performed in under three minutes. The stress analyses took half a minute. Although symmetry could have been used to analyse only half of the structure, a check on the symmetry of results was gained by analysing the whole. The 'in plane' rotational degree of freedom, θy, was suppressed for each interior node on the plate. No such terms exists for the 'in plane' stiffness matrix, and, if included, this would have resulted in the overall stiffness matrix of the structure becoming singular.

5.3 Comparison of results

The deflection of the table under load point J for the five different types of grid are shown in table 5.1. This position was common to all the grids and it was noticed that the results shown here were typical of those throughout the structure. The 'out of plane' deflections, in the Y direction, are examined first. The rectangular grids, 1 and 2, appear to be converging to an answer from a lower bound, as could be

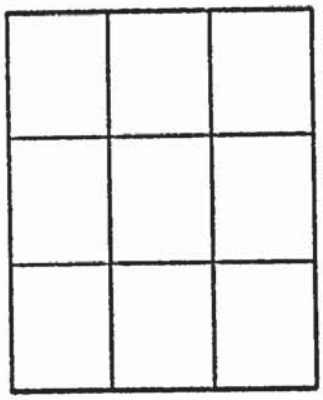

9 □ elements

16 members

GRID 1

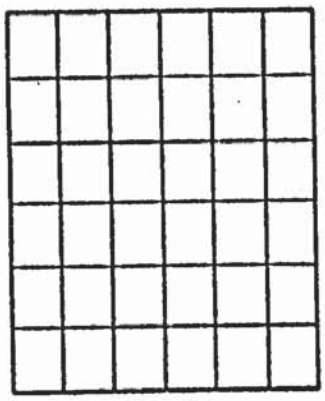

36 □ elements

28 members

GRID 2

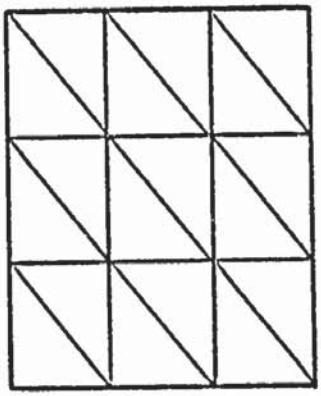

18 △ elements

16 members

GRID 3

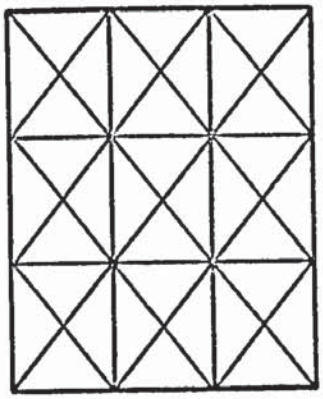

36 △ elements

16 members

GRID 4

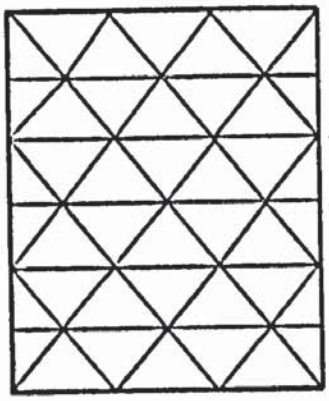

42 △ elements

22 members

GRID 5

FIGURE 5.2. SUBDIVISION OF TABLE TOP

X-direction

Rectangular		Triangular	
Grid 1	.000036	Grid 3	.000021 $\pm$ .000010
Grid 2	.000035	Grid 4	.000031 $\pm$ .000016
		Grid 5	.000032

Y-direction

Rectangular		Triangular	
Grid 1	-.28762	Grid 3	-.316455 $\pm$ .003500
Grid 2	-.29736	Grid 4	-.112085 $\pm$ .008500
		Grid 5	-.340841

Z-direction

Rectangular		Triangular	
Grid 1	-.063329	Grid 3	-.063312 $\pm$ .000015
Grid 2	-.063325	Grid 4	-.063300 $\pm$ .000002
		Grid 5	-.063320

TABLE 5.1 DEFLECTIONS UNDER POINT J

expected from the lower bound theory given in chapter 1. The triangular grids 3 and 4 were found to give unsymmetrical results and the average deflection is given followed by the amount of difference which was caused by this. It is noticable that the deflection of grid 4 is far out compared to grids 3 and 5. Ignoring grid 4, the other triangular grids would appear to be converging from a lower bound also. As all the elements are nonconforming one cannot say that the triangular elements are giving a result closer to the true answer. This is because of the kinking that would occur across interfaces and might even cause an overestimate of the true result. The rectangular deflections shown are those due to the Melosh stiffness matrix. It was found that the Zienkiewicz stiffness matrix gave higher results and almost equalled the triangular. Williamson (31) has compared the two rectangular matrices against experimental values and has found the matrix of Zienkiewicz to be slightly more accurate. The difference occurring in these analyses was too small to justify demonstration. The deflection of grid 4 is about one third of the other grids which is a surprisingly poor result. One possible explanation of this is the shape of the elements involved. For a given size, an element should span as little as possible in any direction across a continuum. This is inherent in their nature and the basic assumptions involved. The change in deflection and, in particular stress, across and element should be as little as possible. This is especially true in the latter case as stress discontinuities already exist across interfaces. Hence long thin elements should always be avoided.

As can be seen, the elements in this grid are of worse shape than those of the other grids. It is also evident that, of the two types of element used, one is also used with success in grid 5 and the other spans the same length as those used in grid 3. It can therefore be concluded that the grid pattern must have contributed to the poor results. The asymmetry of results was not expected for this symmetrical grid pattern.

This could have been caused by the random defining of the local axes in relation to the global axes. For grid 5, all local axes were made to lie in the same direction. All the elements P axes lay in the direction of the global X axis. The results were symmetrical. For the analysis of grid 4 this was not possible and some elements were made tolie at an angle to the X-Z directions. Although the displacement transformation matrix catered for this, the final terms in the overall stiffness matrix still depend on the unassembled stiffness matrix for the element derived with a different P-Q axis.

The 'in plane' displacements in the X and Z directions are next considered. The rectangular grids 1 and 2 appear to have converged and may even be forming an upper bound. As the elements conform completely the opposite would have been expected. This small discrepency is probably due to the element's interaction with the members which is more pronounced in the 'in plane' case. The triangular element grids 3, 4 and 5 converge from a lower bound and all give good results. The asymmetry of deflections in grid 3 was due to the pattern. A definite 'leaning' of the structure in the X - direction was noticed.

The values of the stresses obtained from the stress matrices are given in figs. 5.3 and 5.4. The stresses are shown only for the more refined grid patterns of type 2 and 5. These patterns gave the best results for deflections. The rectangular stiffness matrix of Zienkiewicz was used in this case as the stress program uses a stress matrix based on his displacement function. The stresses were calculated at the centre of gravity for each element hence they could not be compared at any one position. Stress values due to rectangular and triangular grids are marked and it can be seen from the contours constructed that no discontinuities arise between them. Only the stresses s_x, s_z, and s_{xz} are shown for the top surface of half the plate as they were symmetrical. The stresses on the bottom half were of a similar distribution as the 'in plane' stresses were found to be

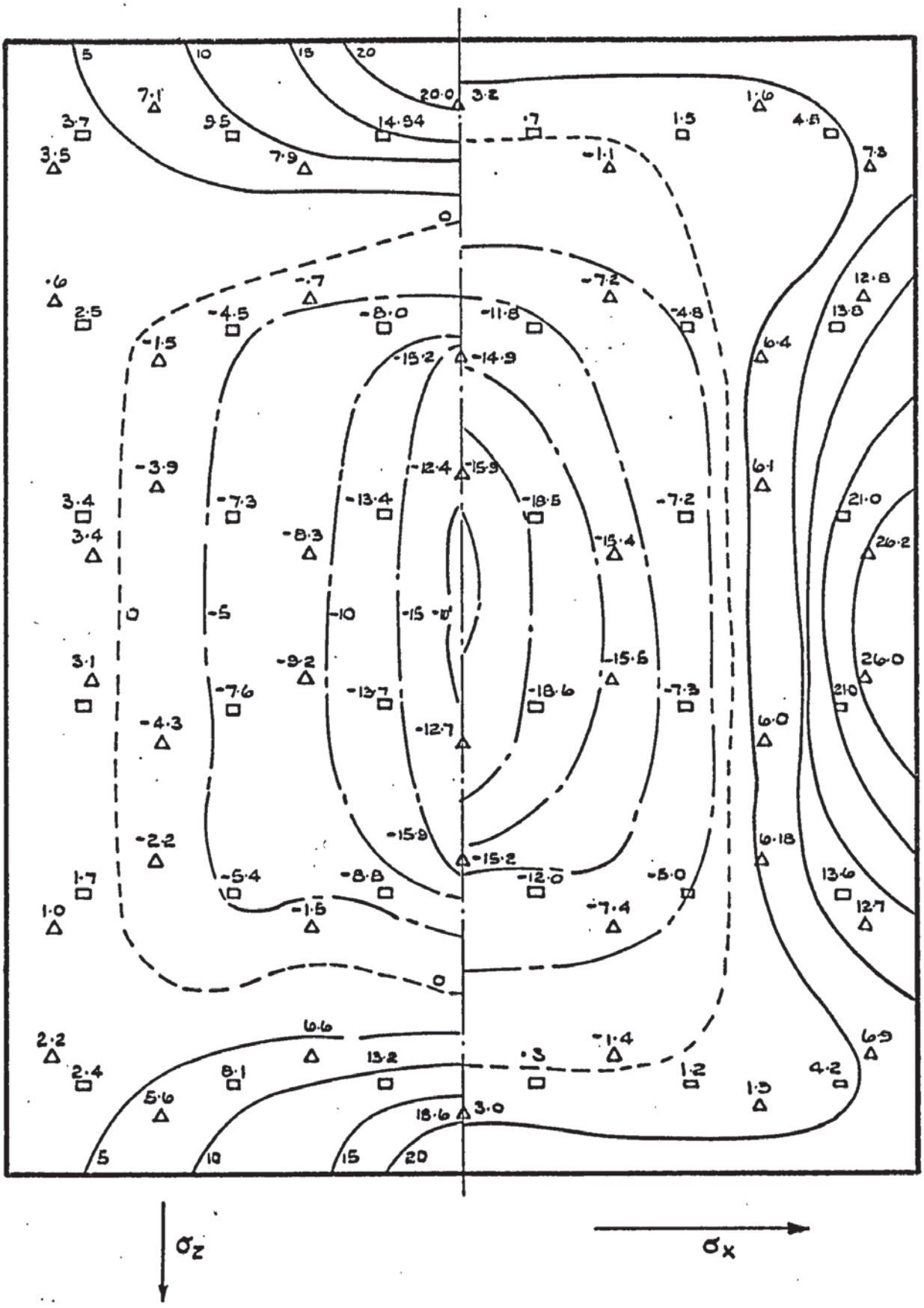

Tension Positive

△ Triangular plate stresses

□ Rectangular plate stresses

FIGURE 5.3. STRESS CONTOURS FOR TOP SURFACE OF TABLE

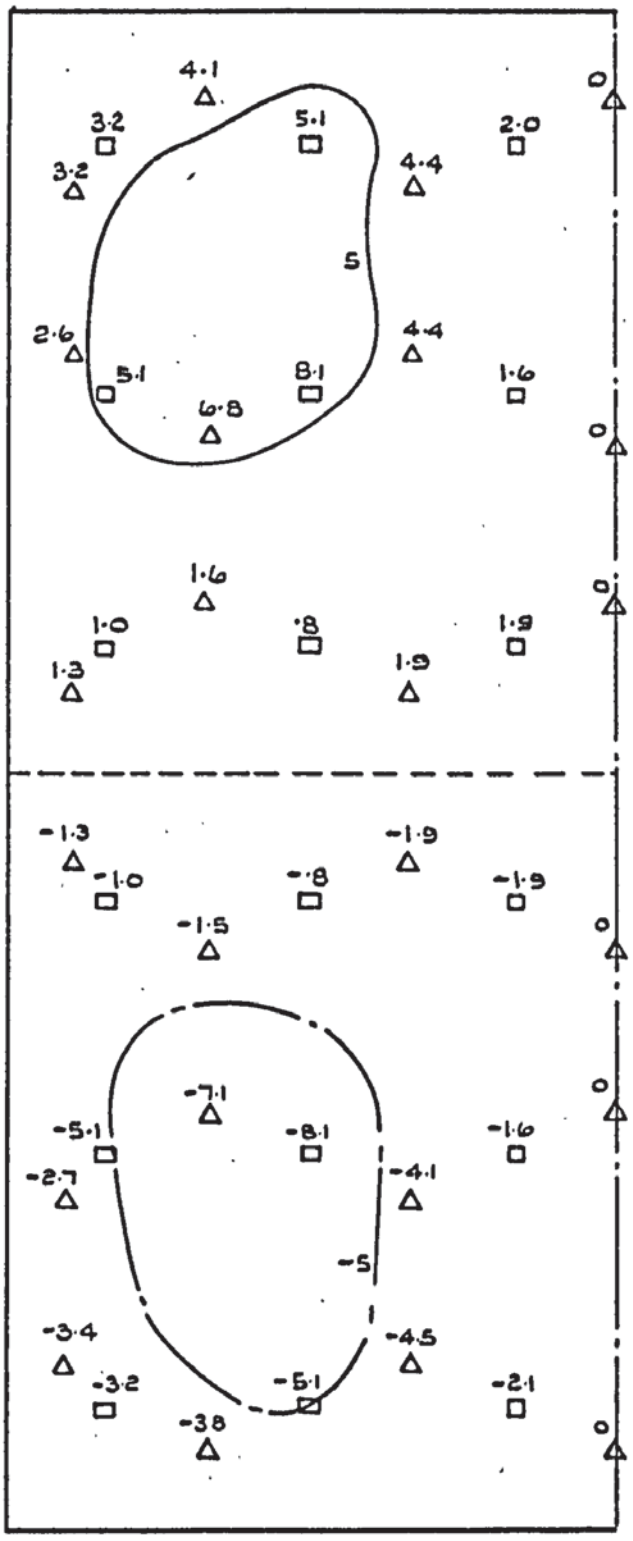

FIGURE 5.4 SHEAR STRESS CONTOURS FOR TOP SURFACE OF PLATE

small.

The stresses obtained from the plate forces are shown in figs. 5.5 and 5.6. These compare the direct stresses for rectangular and triangular grids in the Z and X directions respectively. The rectangular stresses were calculated at each corner of the plate and were found to be symmetrical. At the interior nodes the four values of stress (one for each adjoining corner) varied quite substantially in some cases. It was found that obtaining the values of stress at the centre of gravity by linear interpolation between corner values gave results identical to those obtained from the stress matrices. As already mentioned stress discontinuities do exist between interfaces and hence averaging the stresses at nodes where this condition was more serious may well give misleading results.

When the triangular stresses were plotted at the corners the discontinuities between elements meeting at a point were much more serious. The stresses at the centre of gravity of the elements are shown compared to the rectangular. These values were slightly asymmetric and are not in good agreement to the values obtained from the stress matrices.

From the agreement achieved elsewhere it would appear that the method of finding stresses from the nodal forces in the triangular case is in error.

For rectangular elements the shear stresses can be ignored when calculating direct stresses as explained in chapter 2. This may not be so for triangular stresses and hence the force on a node represents the summation of the direct and shear stresses on its adjacent sides which are sloping. For 'in plane' triangular stresses, which are constant throughout the element, Pope (36) assumed the nodal force to represent a stress distribution along the projection of a line joining the mid point of the adjacent sides. Although this assumption was empirical the results gained gave similar values to those given by the stress matrix. This distribution is shown in fig. 5.7 where

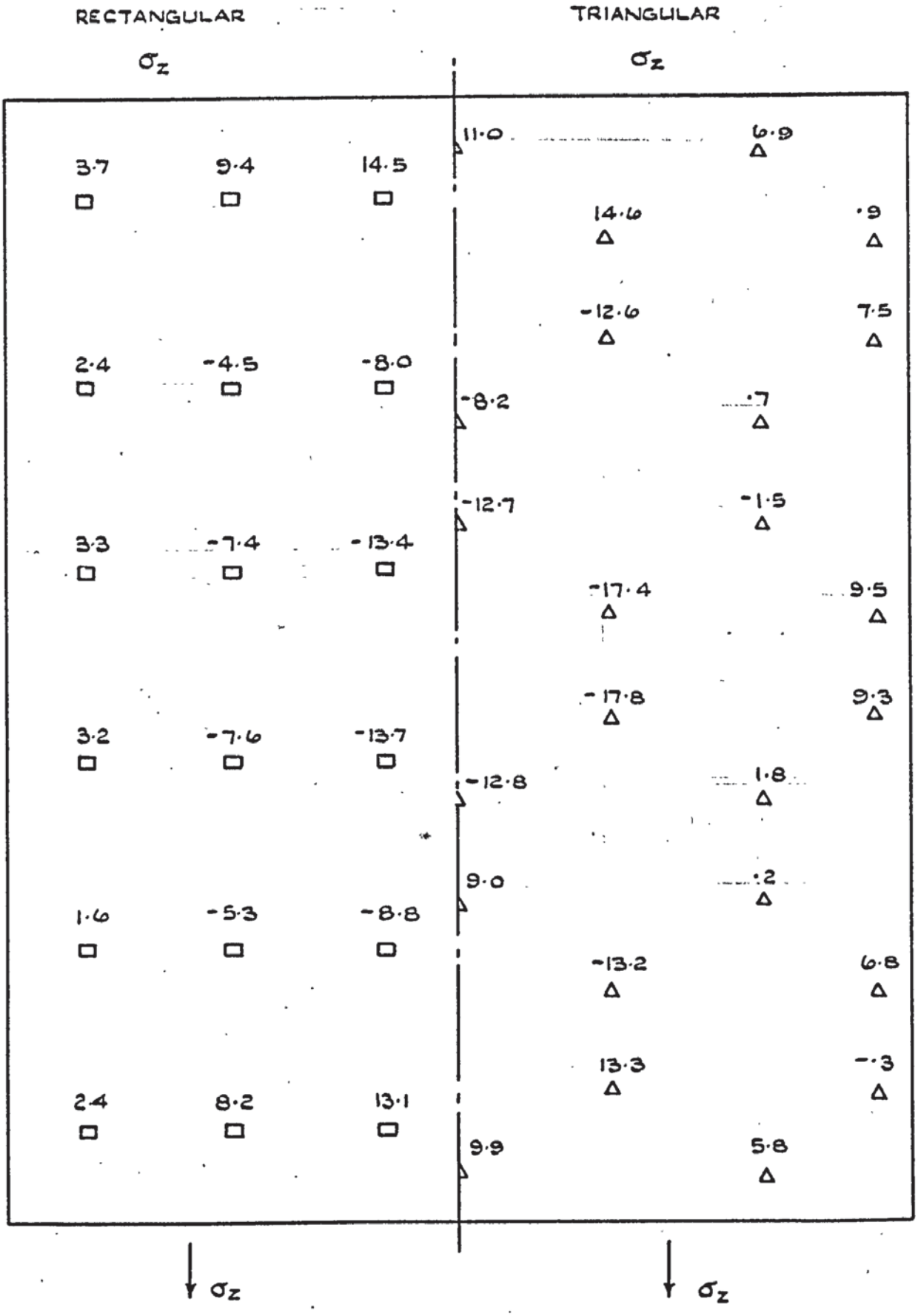

FIGURE 5.5 STRESSES IN Z DIRECTION DUE TO NODAL FORCES.

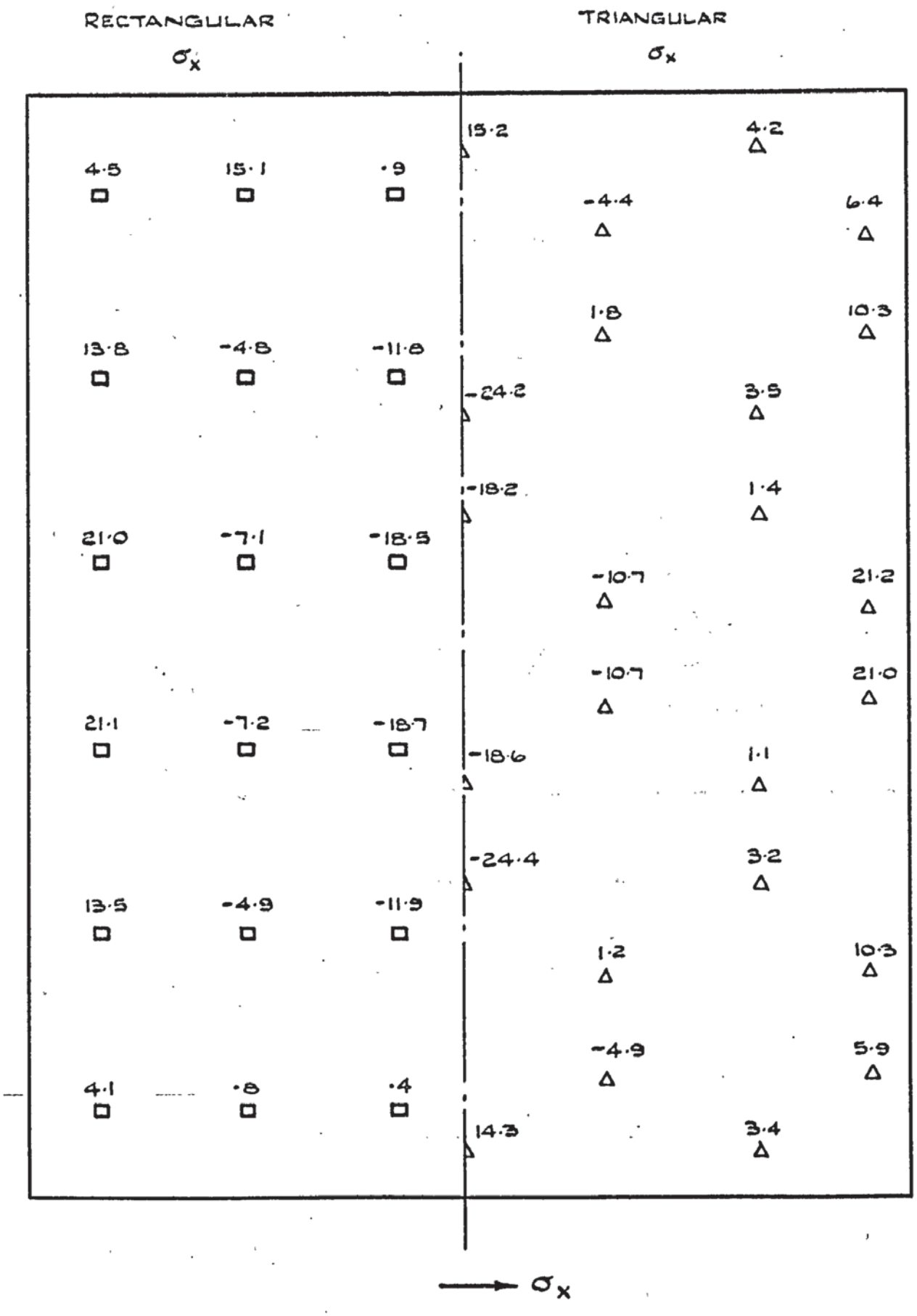

FIGURE 5.6. STRESSES IN X - DIRECTION DUE TO NODAL FORCES.

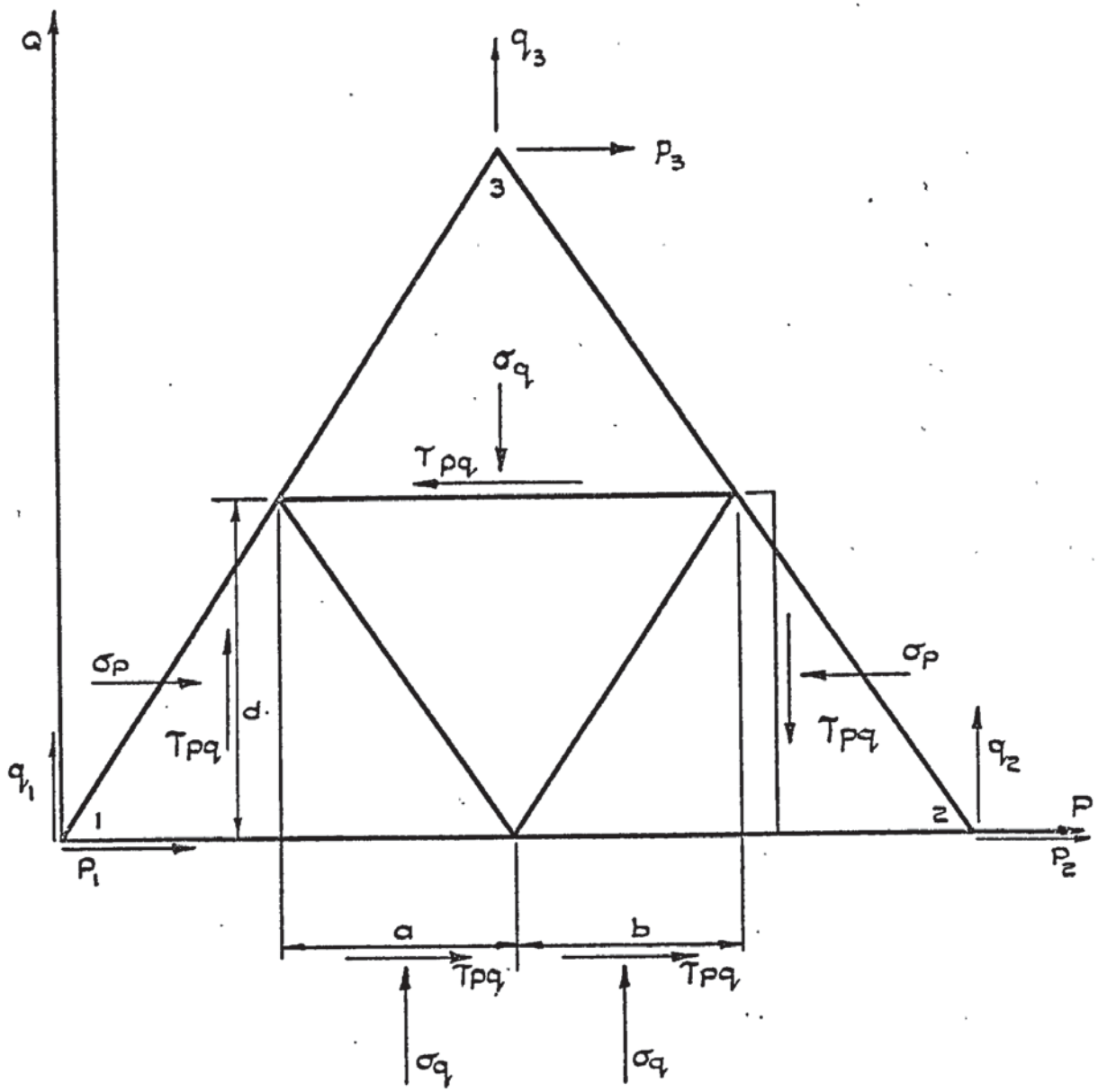

Element thickness 't'

FIGURE 5.7.

it is noticed that the equilibruim at each node gives:

$$s_q = -q_3/(a + b)t$$

$$s_{pq} = -p_3/(a + b)t \qquad (5.1)$$

$$s_p = (p_1 + p_3 a/(a + b))/at$$

It will be noticed, on examining the total six equations (two at each node), that the overall equilibrium is always satisfied.

Unfortunately this method could not be used for evaluating 'out of plane' stresses as the stress distribution varies linearly in this case. Therefore not enough equations are available. It is apparent that the shear stress must be included when calculating the direct stress from the nodal force of a triangular element which explains the general overestimation of stress in figs. 5.5 and 5.6.

5.4 Conclusions

The extent of the assessment of the triangular element in this chapter was rather limited but certain generalisations can be made on its performance. It is evident that the 'out of plane' stiffness matrix is sentitive to,

(i) The type of subdivision or grid.

(ii) The shape of the element.

(iii) The position of its local axes.

This latter case is not as significant as the first two. Ideally, for analysing structures, a triangle close to equilateral should be used in a subdivision pattern similar to grid 5, fig. 5.2. Coarse subdivisions, or subdivisions with only a few elements, give good values of deflections both in the rectangular and triangular elements. In this case they both form a lower bound and have a rapid rate of convergence.

The main advantage of refinement of meshes is in the calculation of stresses. The more elements there are in a given structure the less

serious will be the stress discontinuities between boundaries. For grids 1 and 3 it would not have been possible to plot stress contours and hence stress concentrations could easily be missed. The fact that the 'in plane' triangular element stiffness matrix is of constant stress does not impare its results in comparison with the linearly varying rectangular element.

The number of degrees of freedom in a structure shows the size of the overall stiffness matrix to be inverted in an analysis. The triangular subdivisions have a greater number of elements for a given number of degrees of freedom. Comparing grids 2 and 4, both have 36 elements, but the former has 269 degrees of freedom whereas the latter has 141. This is generally true of all triangular configurations and, hence, less computation is involved in its inversion. Convergence is only achieved by increasing the degrees of freedom of a structure to the real situation which is infinite. Therefore the number of elements does not determine the accuracy directly but, as convergence is so rapid, for a given number of degrees of freedom, triangular elements will give a better stress distribution due to their greater number. However it should also be pointed out that this is not strictly correct since the displacement function for a rectangular element with 12 constants should give better results than that given by the displacement function of a triangular element with nine terms.

For the calculation of rectangular element stress there is little to chose between the two methods compared. For triangular elements the evaluation due to the stress matrix was superior. The computing time in both methods was small but the 'stress matrix program' will take up more storage. This disadvantage is offset by the increased data handling which is involved in the other method.

CHAPTER 6

LINEAR ANALYSIS OF STRUCTURES

6.1 Introduction

This chapter describes the analysis of three structures using the finite element method. For large structures where, for practical and computational reasons, the element subdivision is relatively coarse, it is necessary to establish the order of accuracy that can be expected. This can only be achieved by either field measurements on an actual structure, which is very often impracticable, or the testing of an experimental model in the laboratory. This allows a direct comparison of values of stress and deflections for the computational and experimental results.

The first structure was therefore tested in the laboratory. The model consisted of a folded plate roof supported by two columns and the next sections of this chapter give a description of the problem followed by the details of the experimentation involved. The conclusions gained from the subsequent analysis were used to judge the accuracy which could be expected in the following structures.

A full size motorway bridge was analysed using the elastic analysis program. The computational difficulties encountered are mentioned here for the size of structure. The results of the analysis were compared with a straightforward beam analogy of the bridge.

The third structure was a steel electrofilter precipitator casing, the results of which are also given.

6.2 Analysis of Folded Plate Roof Structure

A folded plate roof structure, as shown in plate 6.1 was built and tested experimentally for values of deflection and stress under load. The results were compared with those obtained from the computational analysis. This structure can only be represented accurately by the flat triangular plate element. Hence the element formulated in chapter 2 was

PLATE 6.1 FOLDED PLATE
ROOF STRUCTURE

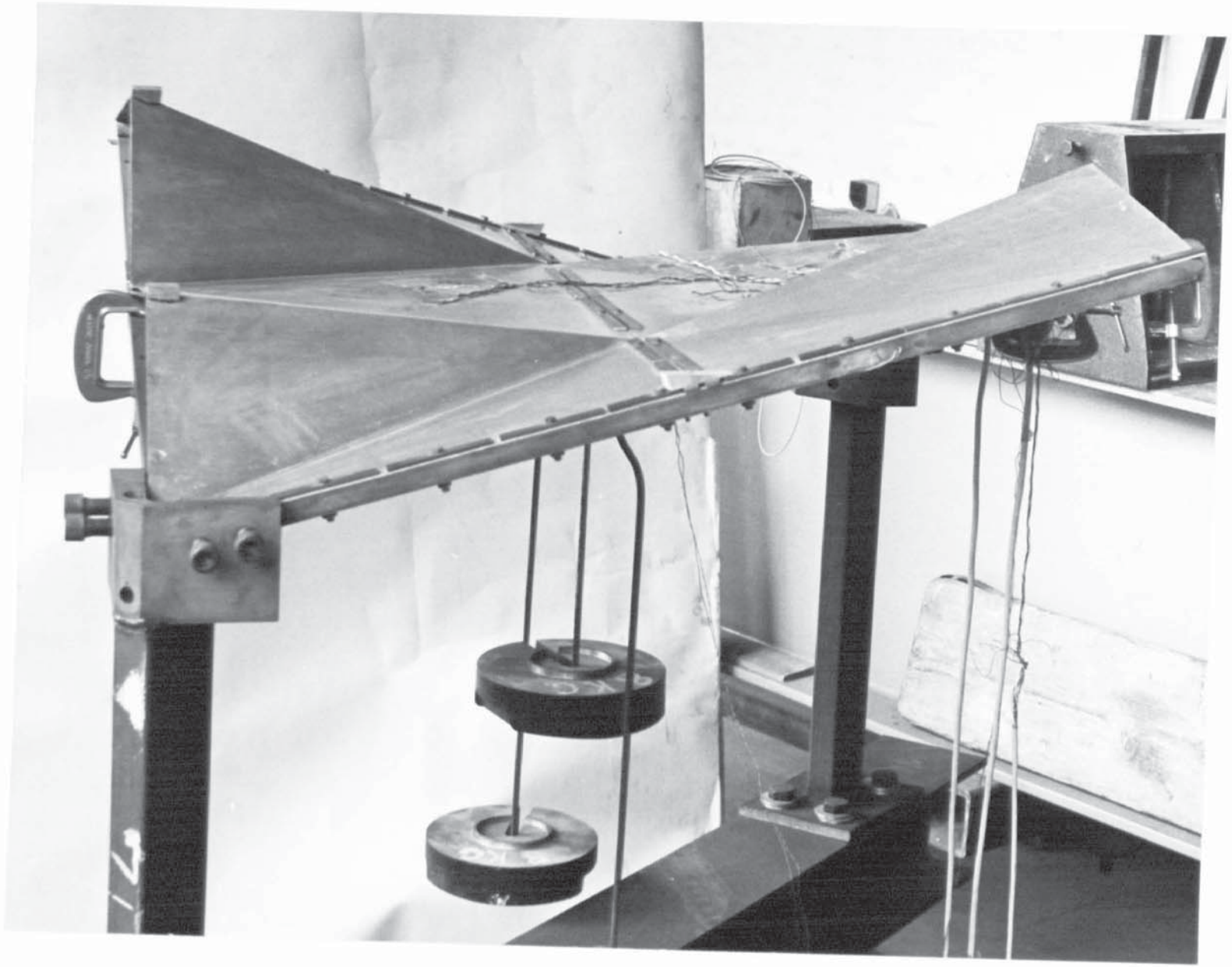

used and the deflections were calculated using the elastic analysis program described in chapter 3. For the calculation of stesses, the 'stress program', also described in this chapter, was used as its advantages over other methods have been pointed out in the previous chapter.

When analysing three dimensional structures of this type the non-conformity between certain elements will be more serious. If all elements lie in the same plane then it has been shown that conformity of displacement at least can be ensured. When two elements meet at an angle, then both will deform in their own planes and conformity of displacement as well as slope along the interfaces will be lost. An extreme case would be that of two elements meeting at right angles. Here, the 'out of plane' bending curve of one would not conform with the linear 'in plane' displacement of the other. Zienkiewicz (2) has successfully analysed shells as an assembly of flat plates but it can be seen that, as the subdivision of elements is refined in this case, the non conformity becomes less serious. This is not the case with the folded plate structure where non conformity will occur along the folds. However, Zienkiewicz's convergence criteria are not violated and hence one of the main objects of the experiment was to see if convergence to a true result occurred for various refinements of the element.

One of the analyses was performed mixing the rectangular with the triangular element. The rectangular element used was that of Melosh and, in this case, additional non conformity will arise between these elements.

The performance of the elastic analysis program is also investigated. It was desirable to know its limitations when analysing structures as regards storage capacity, speed of analysis and efficiency. Various ways of splitting up the structure into groups are discussed and the accuracy of the routine for solving the progressively larger number of equations is estimated.

6.2.1 Fabrication of Structure

Basically, the structure consisted of Aluminium sheeting, bent to

the desired configuration, and bolted down onto a frame made from mild steel beams. These edge beams were joined in such a way as to form the boundaries of a rectangular hyperbola and were connected at their two low corners to stanchions.

Fig. 6.1 shows an idealized drawing of the structure and gives the coordinates, in inches, of the main positions A-R. From hereon in this chapter positions and elements will be defined by the lettering used in this figure.

The stanchions, AB and QR, were of rectangular hollow box section $3\frac{3}{8}$" x 15/8" and .182" thickness. These were cut and machined square to a length of 20" and welded at one end to a 6" x 6" x $\frac{3}{8}$" thick base plate. The plates were bolted by four $\frac{3}{4}$" bolts to a heavy I-beam which ran between the two stanchion bases and was clamped in four places to a large rig.

The rectangular hyperbolic frame was made by welding together four mild steel bars, $\frac{3}{4}$" square in section, and 3' long. The slope of each bar from the horizontal was 1:4. This was connected to the two stanchions by means of end blocks which were welded onto the stanchions. The blocks were machined from solid pieces of steel. Two $\frac{3}{4}$" grooves, at right angles to each other, were made at the correct slope of 1:4 into the blocks. These received the corner of the frame. The central portion between the grooves was machined down so that the height of the groove on this side was a little less than $\frac{3}{4}$" high and hence the block would not interfere with the sheeting which was to be attached to the top of the frame. The frame connection could then be tightened in the grooves by four screws, two on either face, which passed through one side of the block. These are shown in Plate 6.1. These end blocks were considered to be the best method of attachment as they did not alter the properties of the edge beams at the connection.

In practice, in order to ensure a correct fit, the end blocks

were made first and connected the correct distance apart by bolting to a $\frac{1}{2}$" dia steel rod which ran between and through them. The four edge beams, cut ready for welding, were tightened into the blocks and checked for position. They were then tack welded together and removed. The subsequent welds at the corners were finished off allowing long time lapses between runs to avoid distortion. The frame was replaced into the end blocks which were then welded to the top of the stanchions. The central strap KG was of $1\frac{1}{4}$" x $\frac{1}{4}$" mild steel section and was welded in between the two edge beams BL and FQ at their mid points. Before doing this the strap had to be twisted through 28° so as to lie flat at each end with the edge beams. This was done by inserting a length of the steel into a hollow steel tube, just oversize, and clamping one end in a vice. The other end was twisted manually by clamping a piece of steel at right angles to the strap and through this applying a torque. The steel outer tube prevented any bending.

The Aluminium roof sheeting was made in two halves BFKG and QLKG both being bolted along the central strap KG, and was cut from a flat sheet .029" thick. In order to obtain the correct development, a cardboard 'mock up' was first made of the roof. This consisted of seven triangles of cardboard, BGH, BHC, CHD, HDJ, DJE, FEJ, FJK, sellotaped together along the joins for each half of the structure. Each apex of the roof was made to lie vertically over the edge beam at a height of 4". It was impracticable to bevell the sides of the cardboard at the joins and therefore the development could not be obtained on flattening the sheet. To overcome this a piece of paper was laid over the 'mock up' and marked appropriately for the development. The sheeting was bent with the help of a special machine. Not all the folds were accessable and some had to be bent manually over a hard corner. The sheeting was held in position by $\frac{3}{8}$" bolts at 4" centres along the edge beams and both the halves were held by $\frac{1}{8}$" bolts along the central strap. The holes for these bolts were drilled out on the frame and the sheeting clamped down with G clamps. The corresponding holes in

the sheeting were then made by hand drill. Where the edge beams entered the end blocks the holes were tapped and the sheeting screwed down.

Strips of 1/16" x $\frac{1}{4}$" flat steel section were used as 'washers' throughout to prevent any local stress concentrations or buckling to occur around the bolt holes. At points D and N, bolting of the Aluminium was impracticable and therefore it was clamped using small G clamps. Around the raised edges of the Aluminium sheeting, for example BCD, a small edge beam 5/16" x $\frac{1}{8}$" section was clamped to the Aluminium again using G clamps. The beam was in turn clamped to the frame by means of a small return piece which was welded to the edge beam as shown in plate 6.1. The purpose of these beams was to prevent any buckling which might occur along the free edges and to keep the folds of the Aluminium rigid. The method of analysis assumes rigid connections and, while this requirement is met elsewhere in the structure, the bending of the Aluminium could have caused a weakness along the fold, especially where the fold was made manually and therefore was not very sharp. Hall (26) carried out a study of rigid and semi-rigid connections and found that deformations within joints can influence the state of affairs considerably.

The loads were applied by hangers which were supported from the structure by means of small hooks which were welded to the underside of the central strap at H, I and J.

A framework of Dexian was built round the structure to support the dial gauges as shown in plate 6.2. The actual positions of the gauges are shown in fig. 6.2. The whole of the Dexian frame was securely clamped onto the supporting I-beam so that any relative movement of this beam or the rig would not affect the dial gauge readings. An exception to this was at points C and E. As can be seen in plate 6.2 these gauges are supported from the rig for convenience as the structural rigidity of the Dexian frame would have been impared by the necessary cantilevering needed for access to

PLATE 6.2. GENERAL VIEW OF APPARATUS.

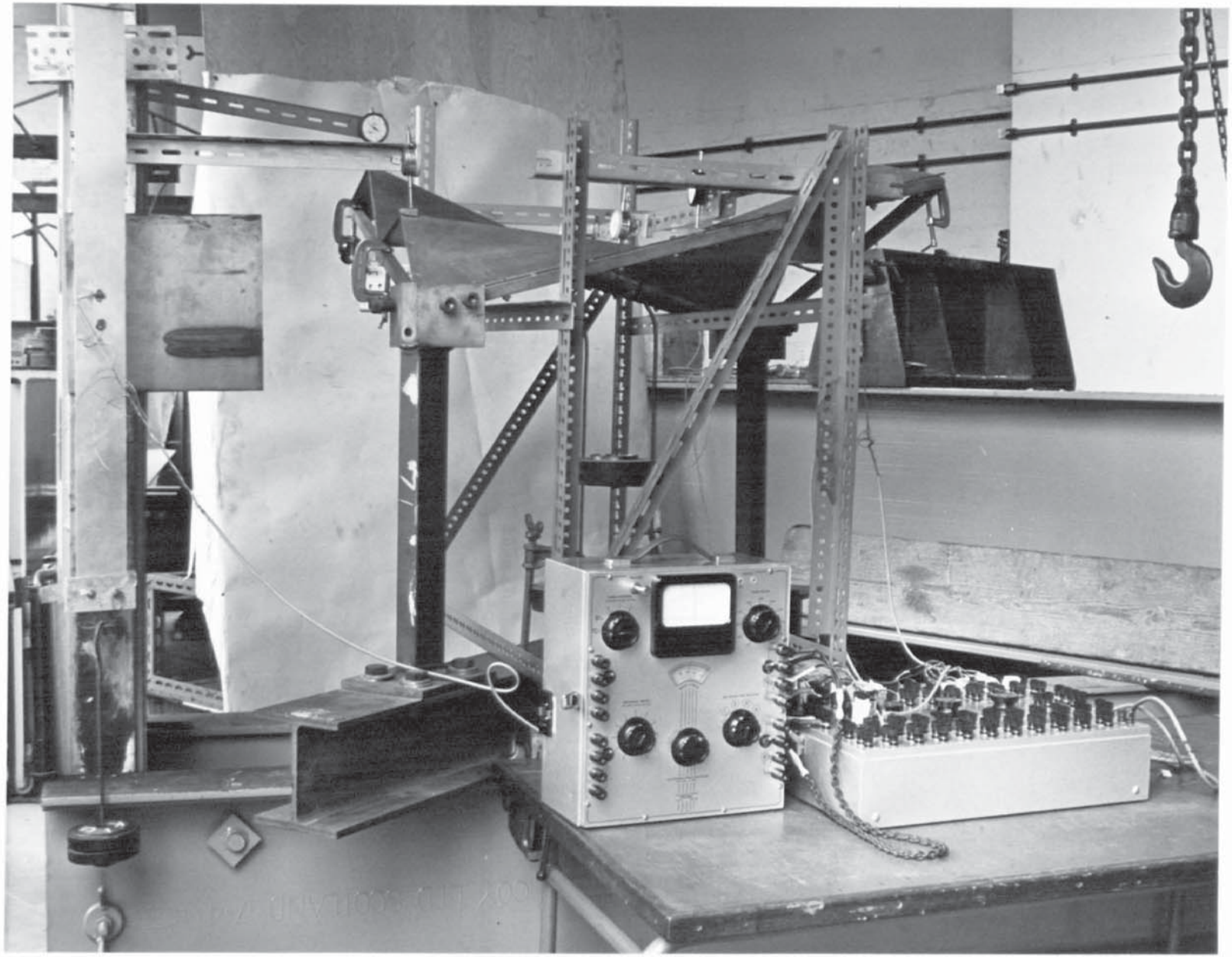

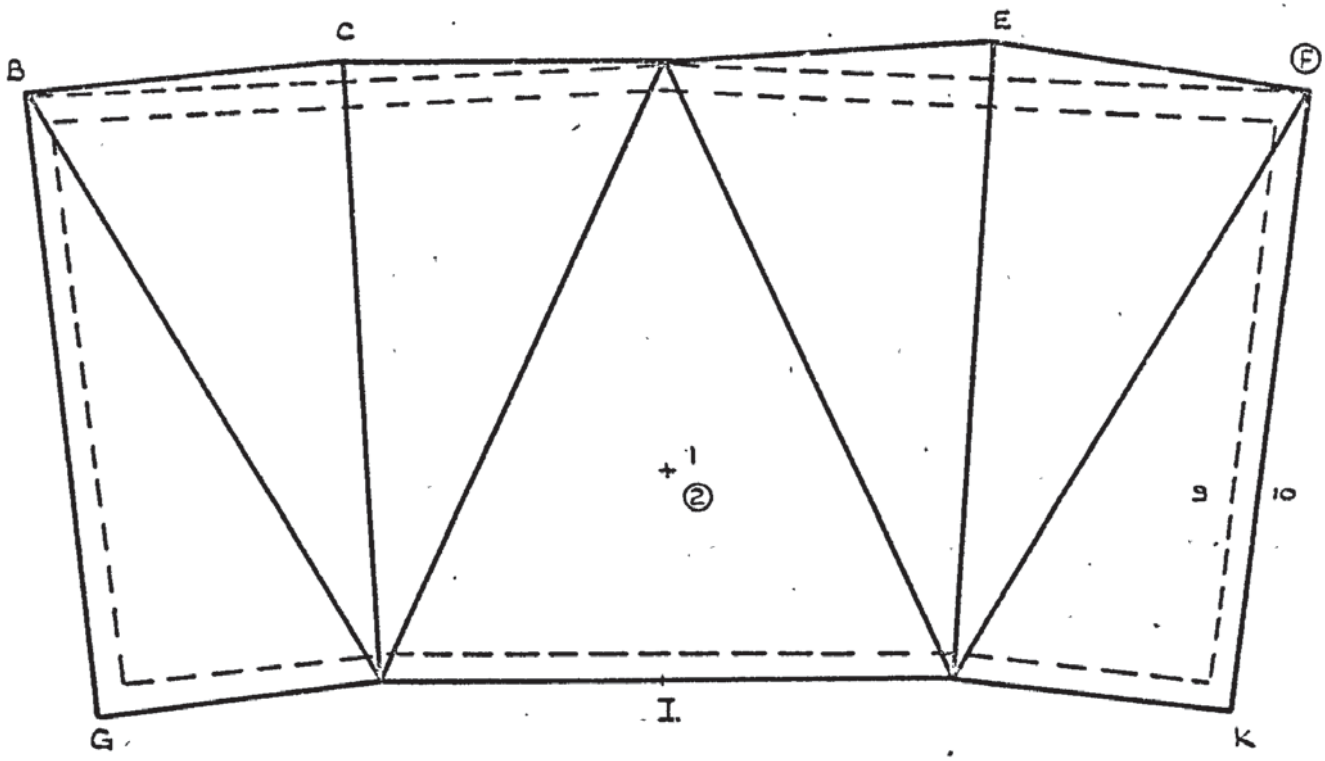

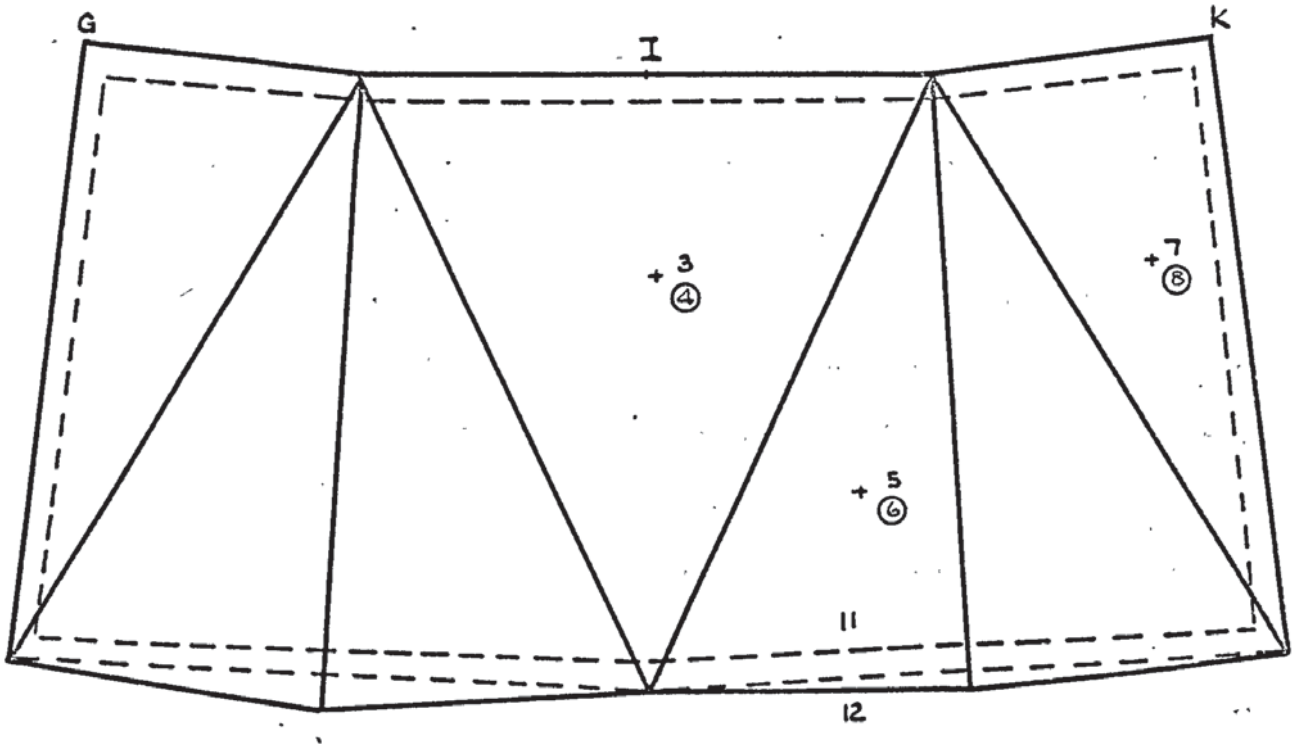

Dial gauge at positions C, E, Ⓕ, G, I, K.

1 - 8 Positions of 120° strain gauge rosettes

9 - 12 Positions of gauges on edge beams

encircled characters denote gauges on underside of structure.

FIGURE 6.2. POSITIONS OF STRAIN AND DIAL GAUGES.

these points.

Where the dial gauges met a sloping surface, small wooden blocks were glued with Araldite to the structure. These were carefully levelled so that the gauge was resting on a horizontal surface and small movements laterally would not effect the vertical deflection reading.

The control test of the Aluminium sheet was carried out by means of a tensile test on a strip 2' 6" long by $2\frac{1}{2}$" wide. In order to ensure uniform stress was passed into the strip when it was loaded, two plates of Aluminium, 3" x 2" x $\frac{1}{4}$" thick, were bolted onto either end by two $\frac{3}{8}$" bolts. The load was applied by a hanger which was hooked over strong wire attached to these bolt heads. The assembly was supported from a 2" diameter solid steel cantilever by wire attached to the top two bolts. This is shown on the left of plate 6.2.

6.2.2 Positioning of Strain Gauges

For access purposes, the gauges were glued to the Aluminium and soldered to multicore wire before the sheeting was bolted down to the frame. The gauges were $\frac{1}{2}$" long and all were from one batch with a gauge factor of 2.05. These were positioned in 60° rosettes on the top and bottom surfaces of the Aluminium at the centre of gravity of the main triangles as shown in fig. 6.2. Thus 'in plane' and 'out of plane' strains could be recorded. The positions were purposely kept away from the folds to reduce any local inaccuracies which might occur at these points. Gauges 1-4, 7 and 8 (fig. 6.2) were positioned where the stress would be relatively high. Gauges 5 and 6 were to investigate any loss of accuracy which might occure due to nonconformity on the sloping sides. At each position the surface was first rubbed down with fine Emery cloth and then cleaned with Carbon Tetrachloride and Ammonia. Two types of adhesive were tried for fixing the gauges, those of Budd and Eastman's 911 'quick-set'. It was found that, when Budd adhesive

was used in the control test, the amount of glue needed under the gauge was quite substantial and affected the results. The Aluminium sheeting was thin and hence this extra thickness of glue caused a misrepresentation of the strain. This was overcome by using Eastman's 911 adhesive where a thin layer of glue could be achieved more easily.

Strain gauges on the members were positioned on either side of the edge beams FK and NL as shown in fig. 6.2. More care was needed in the preparation of the surface as steel oxidises more easily and hence coarser Emery cloth was used followed by a finer cloth.

For the control test of Young's Modulus and Poisson's ratio of Aluminium two gauges were placed vertically in the centre of the strip and two horizontally. The gauges were placed on either side but not at the same point so that the extra thickness added to the plate by the gauge and its glue was kept to a minimum.

6.2.3 Experimental Procedure

The loads, W, were applied to the structure, equally on each of the three hangers, by increments of 20 pounds up to 140 pounds. After each increment the deflection of the dial gauges was noted and the strains were recorded using a Peekel strain gauge recorder. The process was repeated for the unloading cycle.

On the first testing it was found that the structure did not behave perfectly linearly and, when unloaded, it did not return to the original readings. The difference of readings between loading and unloading being about 10% in the worst case. This was found to be mainly due to the end block connections at the corners of the frame. These were loosened off and retightened for the next test and, on doing this, the structural connections at the end blocks and around the frame behaved elastically. The results shown later are for the final testing.

At the same time of loading the structure, the control test

on the Aluminium was carried out by applying equal increments of 40 lbs. up to 280 lbs. on to the aluminium strip. The four strain gauge readings were recorded after each increment. The results of this test are given in fig. 6.3. As can be seen the horizontal gauges gave virtually the same results but the vertical gauge readings differed consistently. This was probably due to the thickness of gauge adhesive. The averaging of the two results gave values of Young's Modulus and Poission's ratio similar to the maker's specifications.

The Aluminium plates were comparatively thin, so much so that it was found to give difficulty to test them in bending. This deficiency was later justified by the fact that the 'in plane' stresses were found to be more prominent in the structure. For this test therefore it was impossible to calibrate the strain gauges and calculate Young's Modulus independently. In order to compensate for these deficiencies, 1" wide strips of the Aluminium were cut and tested in a Denison tensile testing machine. Three tests were made and the result of one of them is shown in fig. 6.4. The values of the Young's Moduli obtained by the two alternative methods of testing were 10.06 psi and 10.01 psi respectively. This showed that no alteration was needed to the gauge factor.

No control test was thought necessary for the steel beams as these were considered of secondary importance to the plate roof. It was necessary though to find the value of Young's modulus and the shear modulus for the material. The Young's modulus was found by testing a sample of the $\frac{3}{4}$" square edge beam in a Denison machine. The result is shown in fig. 6.5 and leads to a value of 31.54×10^6 psi. To find the shear modulus of the steel, a specimen was tested in a Tequipment Torsion testing machine as shown in plate 6.3. A 6" length of the $\frac{3}{4}$" square steel edge beam was cut and its central portion, $3\frac{1}{4}$" long, was turned down to $\frac{1}{4}$" diameter. This was done very slowly so that the properties of the steel would not be affected by the

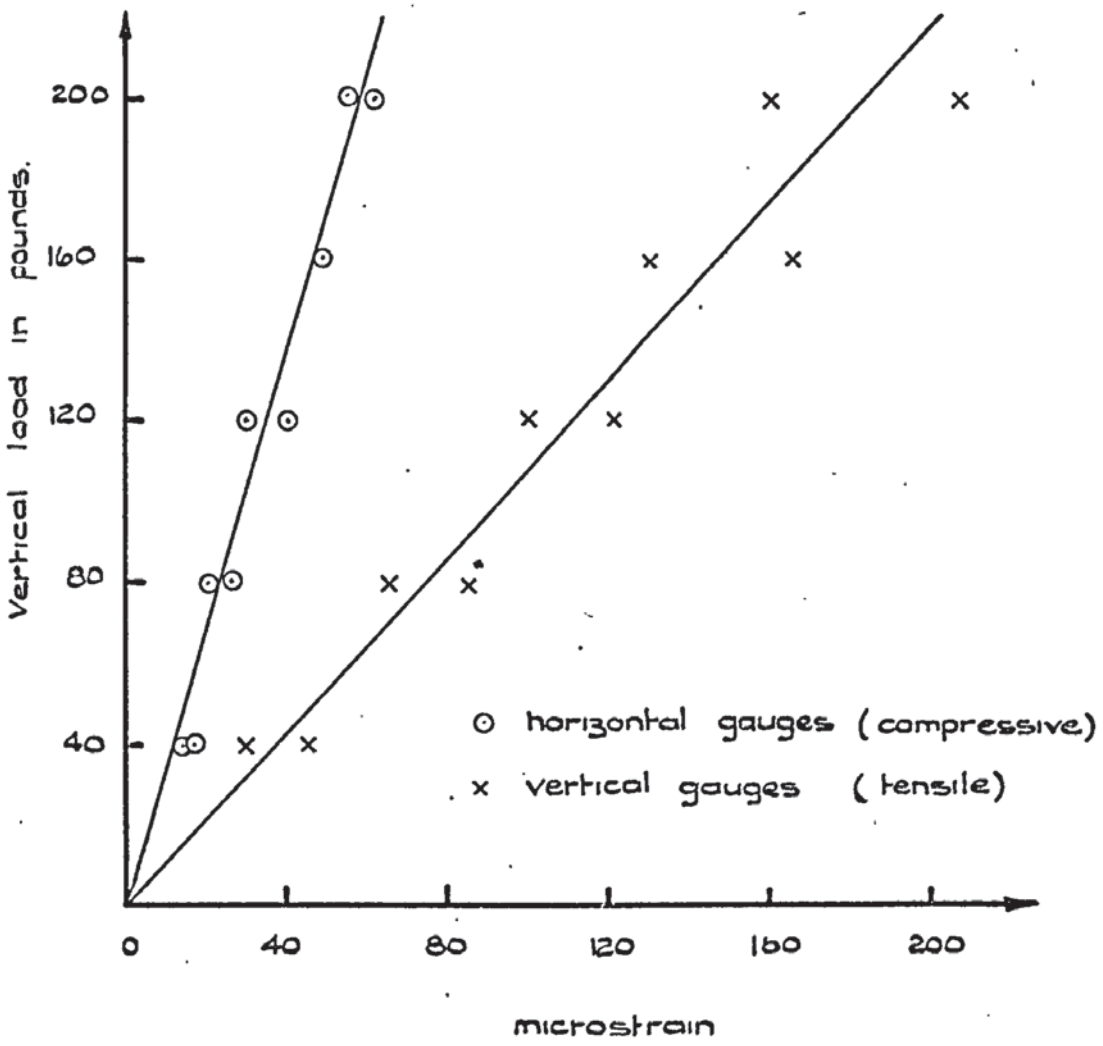

$E = 10.06 \times 10^6$

$\sigma = .311$

FIGURE 6.3. TENSILE TEST FOR YOUNG'S MODULUS. AND POISSONS RATIO OF ALUMINIUM.

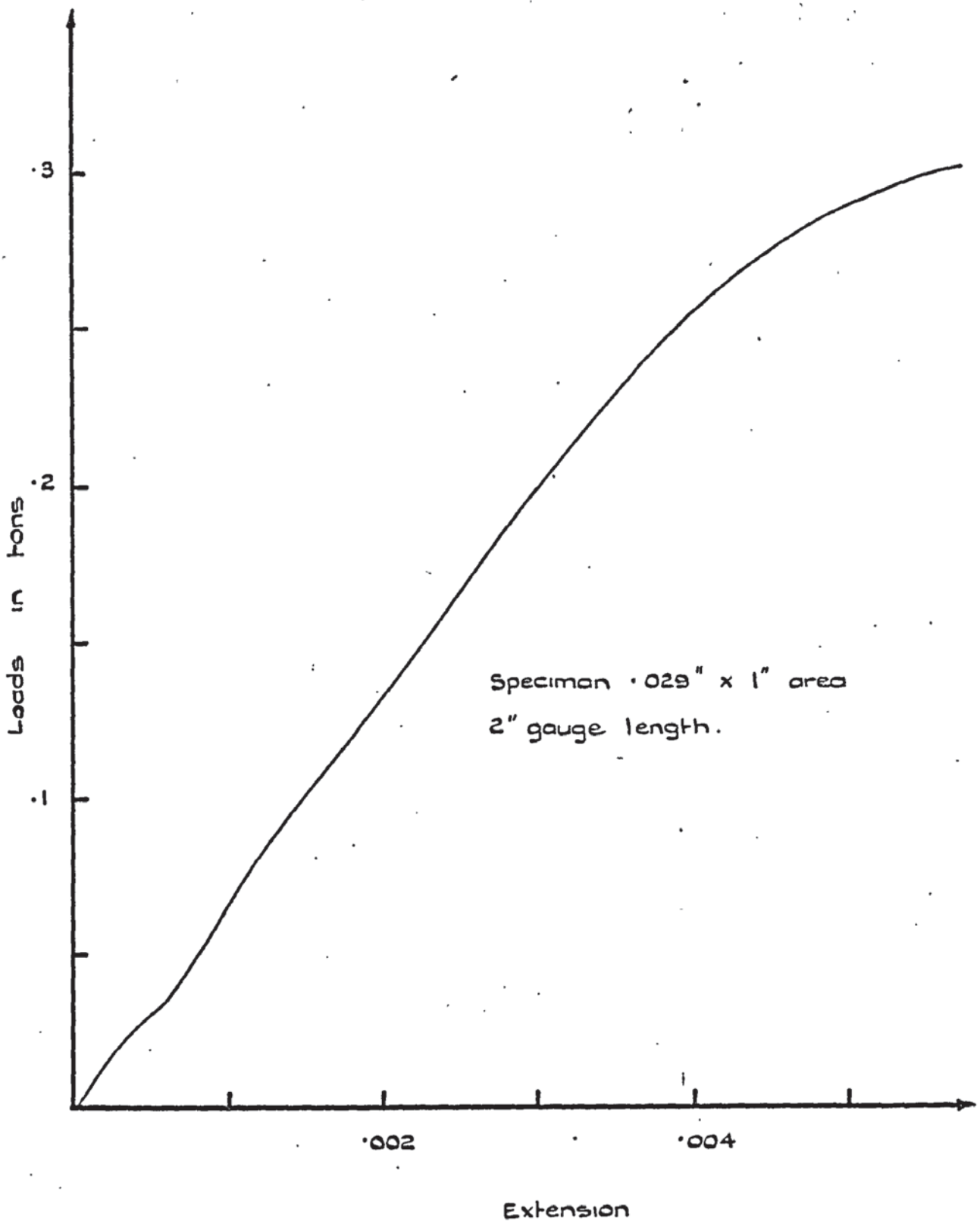

$E = 10{\cdot}01 \times 10^{6}$ p.s.i.

FIGURE 6.4. TENSILE TEST FOR YOUNGS MODULUS OF ALUMINIUM.

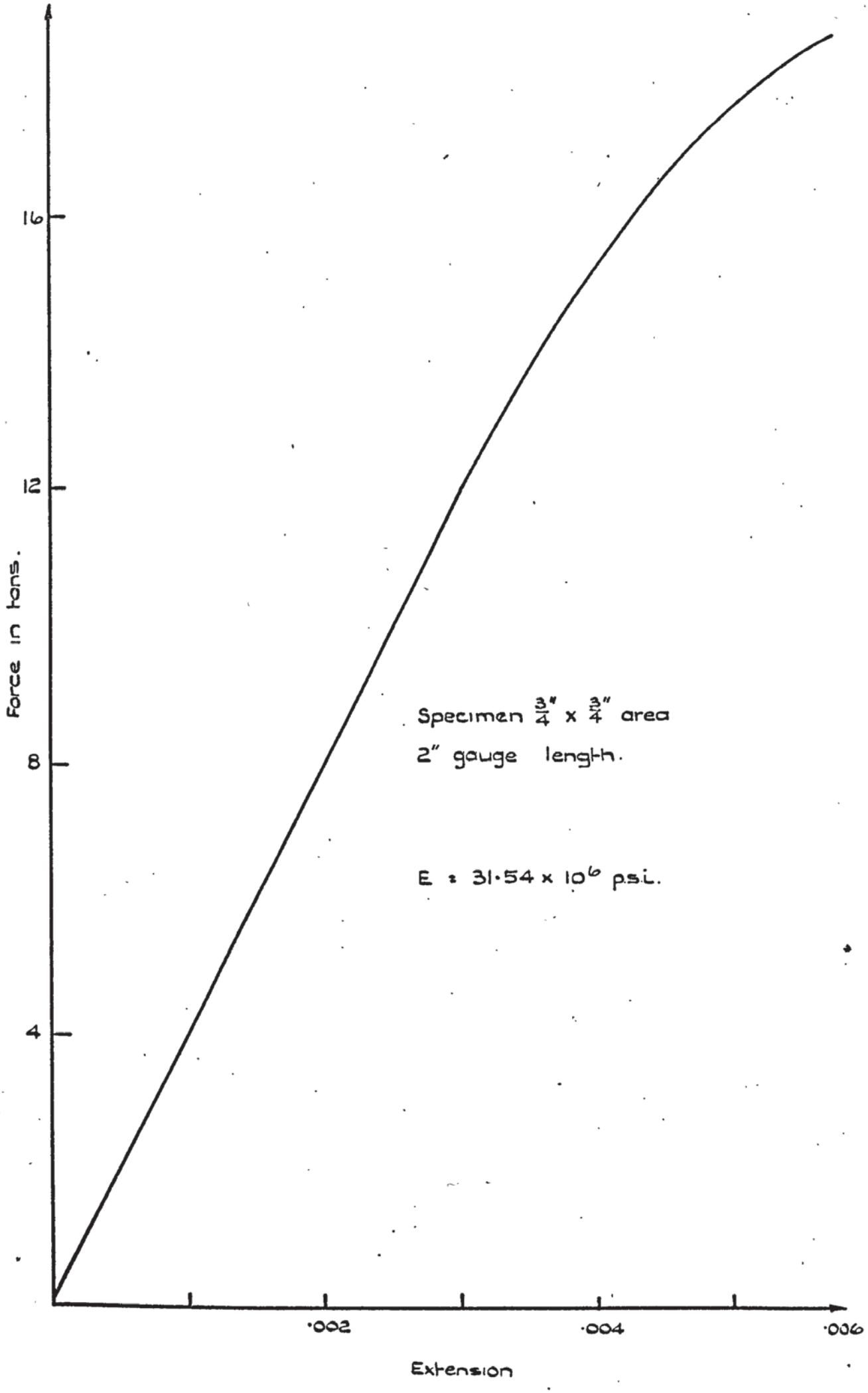

FIGURE 6.5. TENSILE TEST FOR YOUNG'S MODULUS OF STEEL.

PLATE 6.3. TORSION TESTING MACHINE

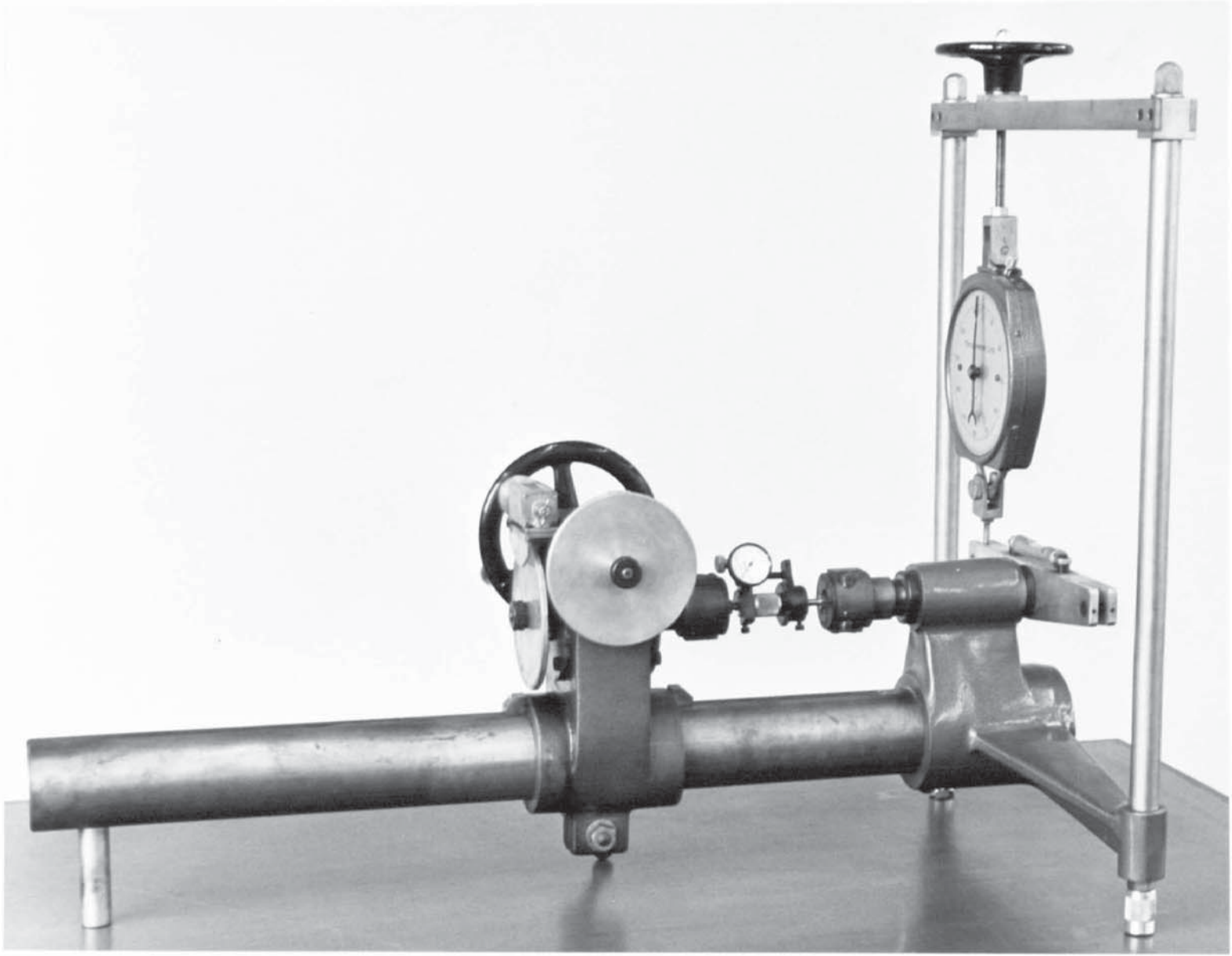

heat generated. Either end was filed octagonally to fit in the jaws of the machine. An angle of twist was applied to the specimen and the torque was measured by a spring balance shown on the right of the apparatus in plate 6.3. A torsiometer, clamped to the specimen, measured the relative movement in torsion over a 2" gauge length. The result is shown in fig. 6.6. G, the shear modulus, was calculated using the simple theory of torsion. For the linear portion of the graph $G = 11.48 \times 10^6$ psi.

6.2.4 Computational Analysis

It is apparent from the results shown in Chapter 5 that, in order to show convergence of results, the same element configuration must be kept for differing refinements of element and that the best results are obtained using an equilateral element or, at least, an isosceles element. It was also shown that the configuration given by grid 5 in fig. 5.2 gave the most reliable results. Consequently three types of triangular subdivision, i.e. coarse, medium and fine, were chosen as shown in figs. 6.7 - 6.9. Only half the plates are shown for each configuration as the pattern is symmetrical about line GK. Irregularities in the pattern had to be introduced in the coarse and fine subdivision so that a node was situated at the central loading position I. The corners of the triangles were numbered so that their P axis coincided with the overall X axis of the structure and the coordinates of the nodes were calculated by linear interpolation between the corner coordinates shown in fig. 6.1. All the member and plate properties were calculated from the control test results described earlier and the data for each analysis was prepared in the form given in appendix 3.

The method of splitting the structure up into groups influenced the computational problem to an appreciable extent. In general, the more groups there are in a structure the less will be the storage requirements but time for computing and magnetic tape usage will be increased. It would be desirable to find an optimum between time and store when splitting up the structure.

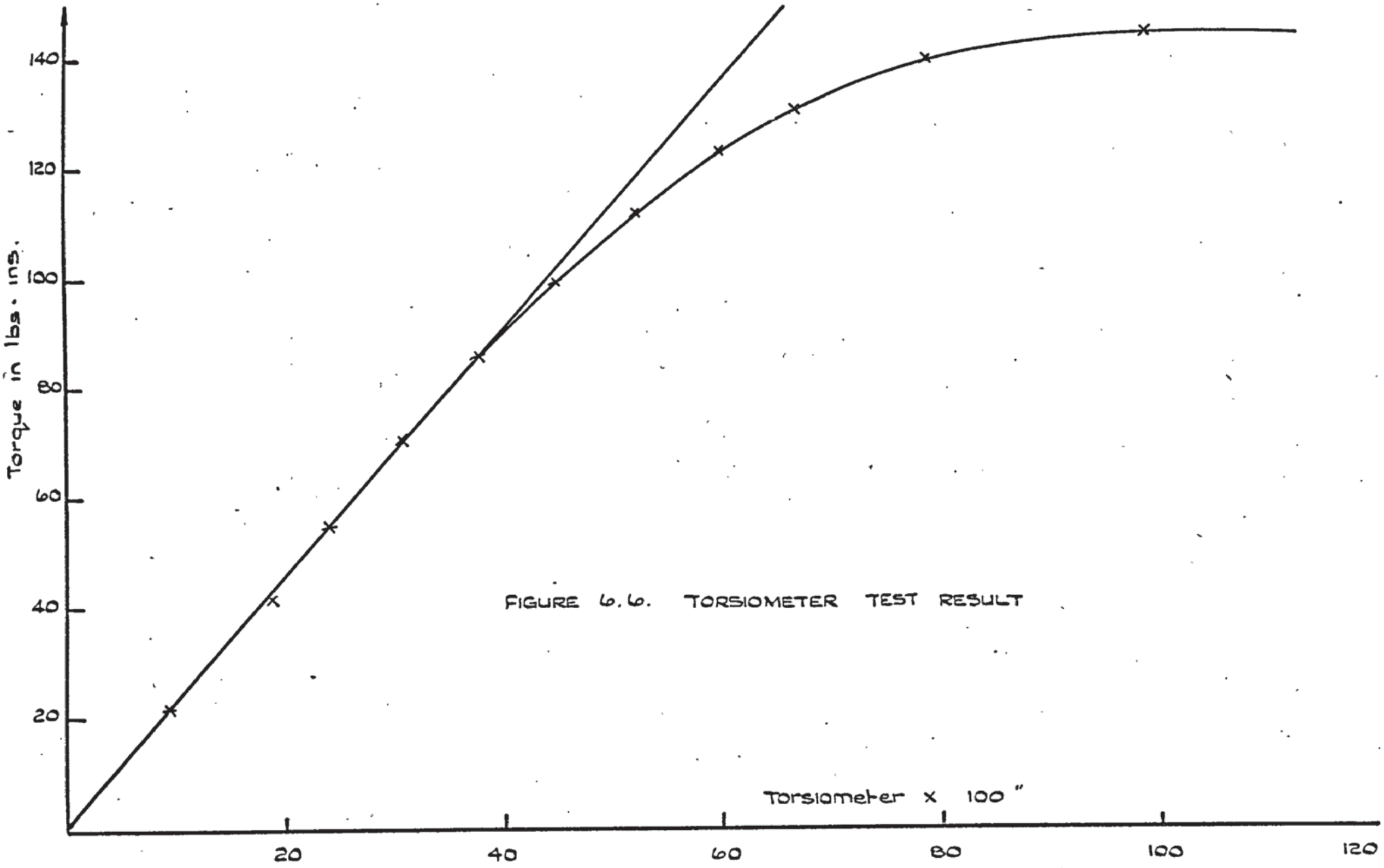

FIGURE 6.6. TORSIOMETER TEST RESULT

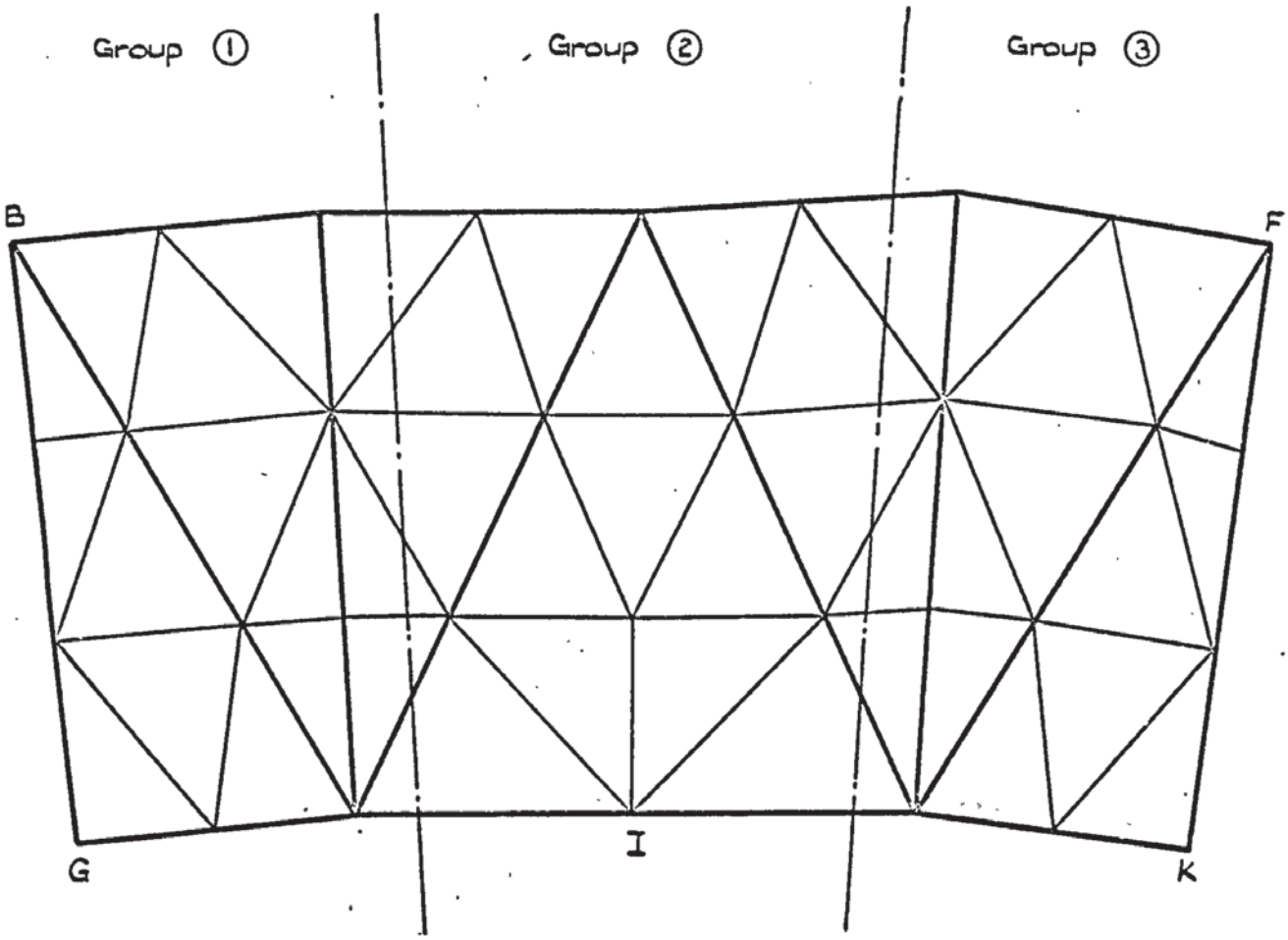

Groups	number of members	number of rect. plates	number of tri. plates	number of joints	No. of degress of freedom
Group 1	18	0	36	22	126
Group 2	19	0	28	17	100
Group 3	13	0	24	23	126
TOTAL	50	0	88	62	352

——·—— denotes group division lines

FIGURE 6.7. SUBDIVISION 1 (COARSE)

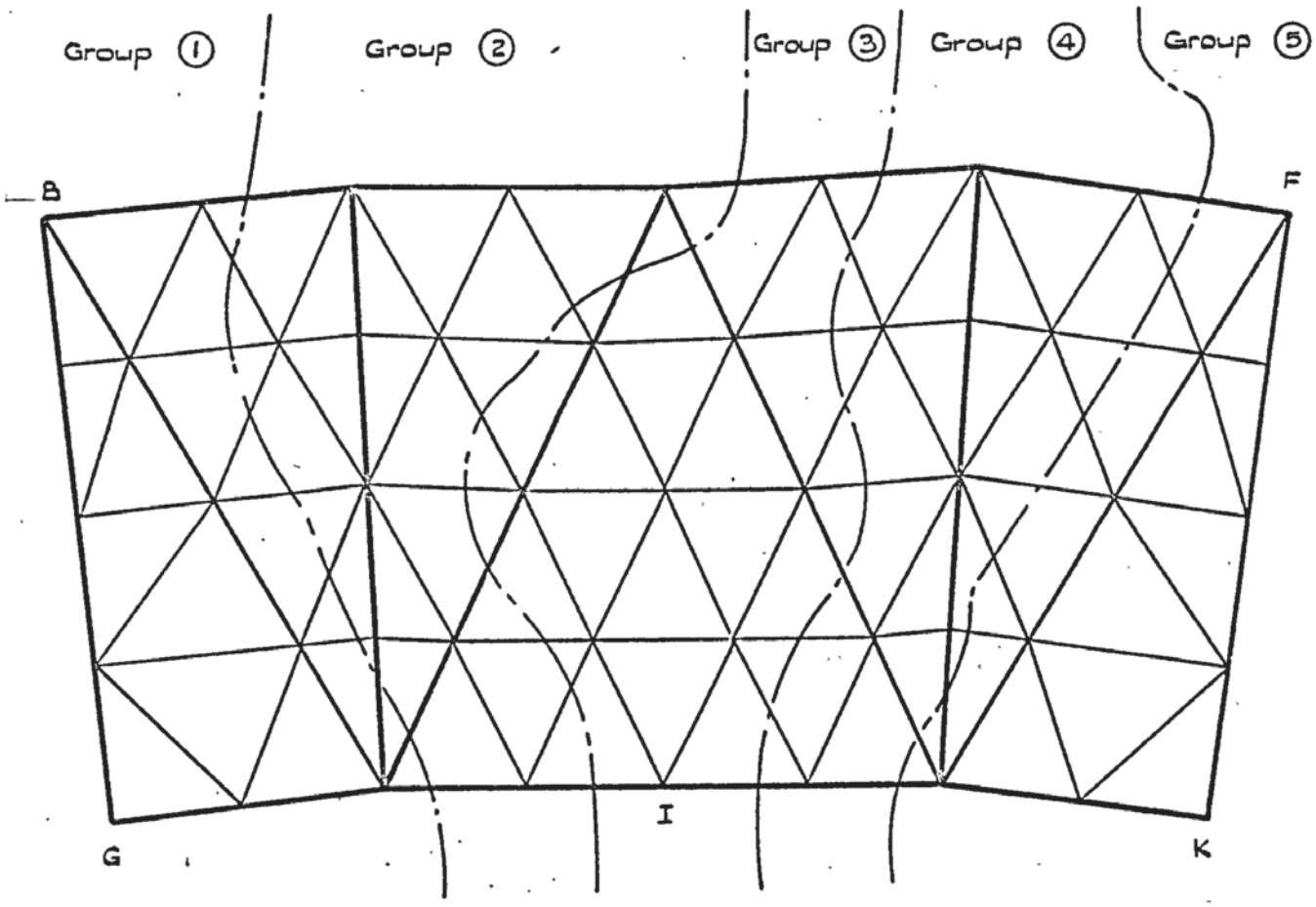

Groups	number of members	number of rect. plates	number of tri. plates	number of joints	N°. of degrees of freedom
Group 1	18	0	36	20	144
Group 2	9	0	32	20	114
Group 3	5	0	30	19	108
Group 4	7	0	30	21	114
Group 5	11	0	16	19	102
TOTAL	50	0	144	99	552

——·—— denotes group division lines

FIGURE 6.8. SUBDIVISION 2 (MEDIUM)

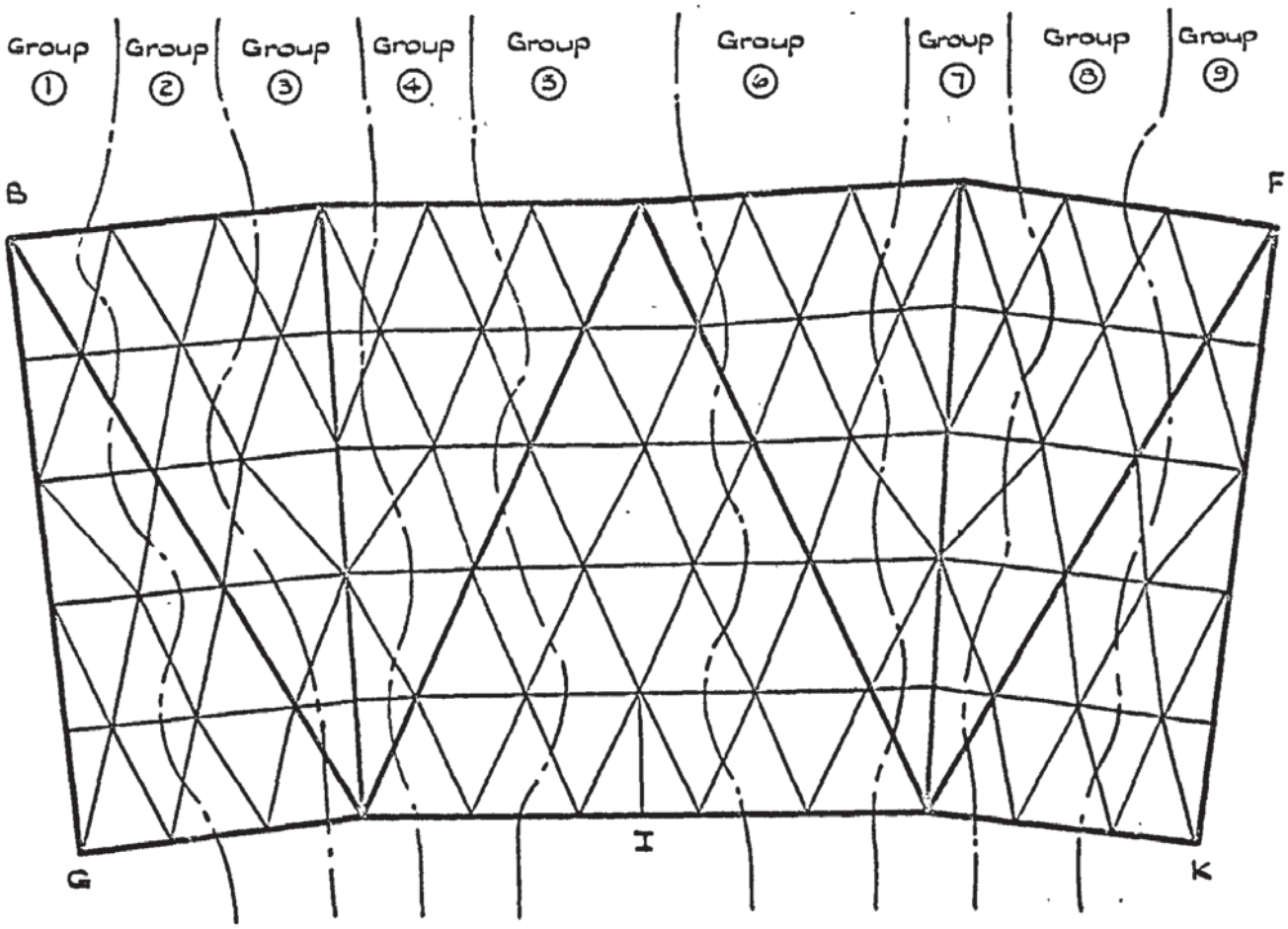

Groups	number of member	number of rect. plates	number of tri. plates	number of joints.	N°. of degrees of freedom
Group 1	17	0	34	19	108
Group 2	7	0	28	19	108
Group 3	5	0	30	20	108
Group 4	6	0	29	18	106
Group 5	8	0	33	18	100
Group 6	6	0	29	18	106
Group 7	6	0	29	20	108
Group 8	6	0	29	18	108
Group 9	13	0	15	21	114
TOTAL	74	0	256	171	966

——.—— denotes group division lines

FIGURE 6.9. SUBDIVISION 3 (FINE)

In practice, for the larger analyses, the number of groups are dictated by the shape and subdivision of the structure and storage is nearly always the limiting factor.

The structure was first divided up laterally, parallel to the X axis. This method became unmanageable for larger subdivisions and did not give as good results as those obtained when divided as shown by the dotted lines in figs. 6.7 - 6.10. In this way more control was possible on the size of group. The size of computer store which is used is governed by the sizes of the biggest three consecutive groups in a structure as only two are stored at any one time. Best results were obtained by making all groups equally large. The joints were numbered so that, within any joint group, the difference in the numbering around any element was kept to a minimum. This ensured that, for stiffness matrix $\underline{K}_{ii}$ of group i, which had to be inverted, the terms were grouped as close to the leading diagonal as possible. Figs. 6.7 - 6.9 also give a table showing the number of elements and degrees of freedom in each joint group. The number of elements, both beam and triangular, indicate the storage requirements whereas the degrees of freedom show the size of matrix to be inverted. While these two are quite interrelated for a given structure it was found that about 30 plates and 120 degrees of freedom in a joint group fitted into the Atlas computer quite comfortably and no difficulties in computation were encountered.

One analysis was performed mixing the triangular element with the rectangular. This subdivision is shown in fig. 6.10 and was decided upon by making as many of the elements as possible truly rectangular with the triangular elements filling in the necessary gaps. As can be seen, the elements boardering on edge BF are not quite rectangular. This would not affect the computation as the rectangular stiffness matrix is calculated using only two of the side lengths at right angles. The element corners were numbered so that the effective size of the element would be different to the true

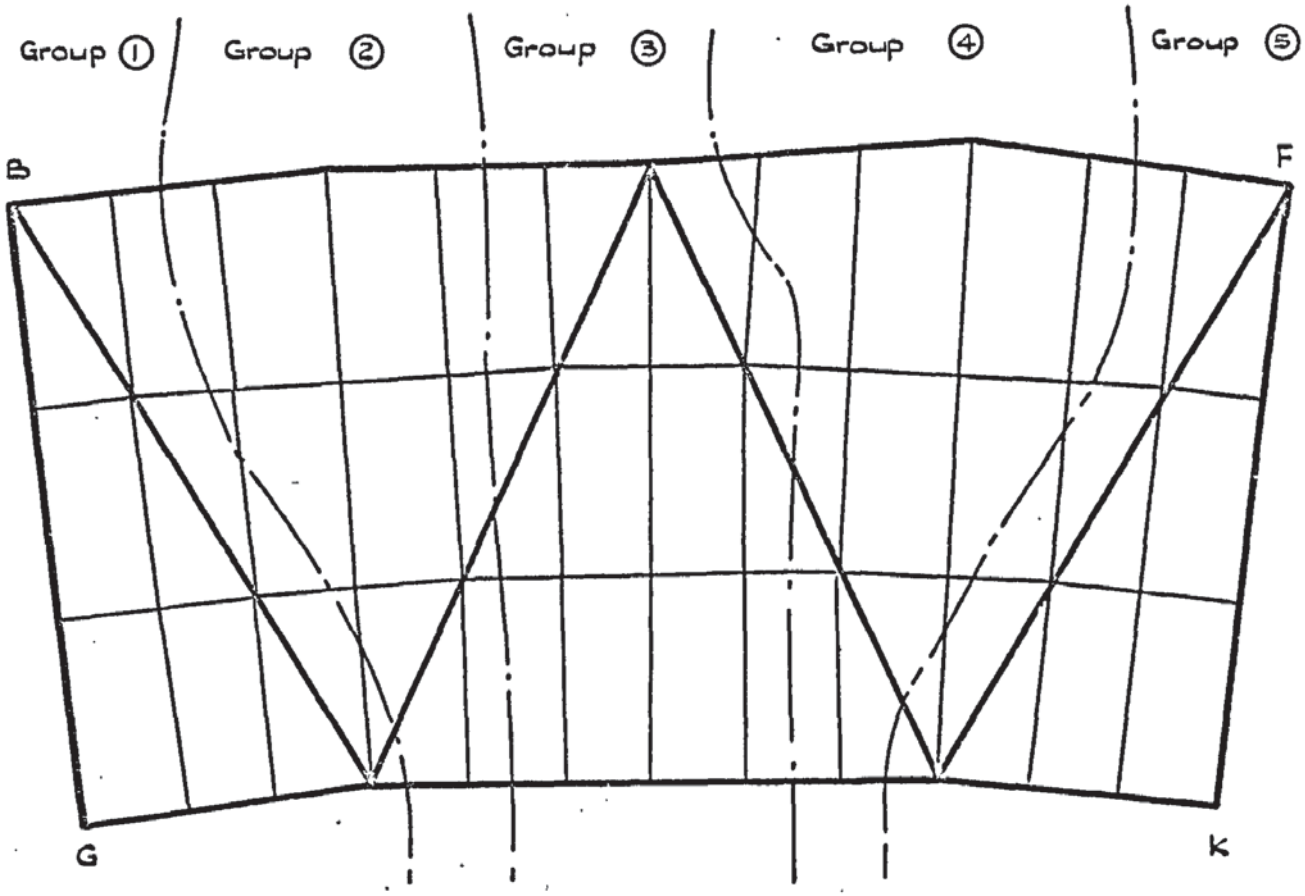

Groups	number of members	number of rect. plates	number of tri. plates	number of joints	No. of degrees of freedom
Group 1	17	10	16	19	108
Group 2	10	10	5	21	120
Group 3	9	12	11	19	106
Group 4	10	10	8	21	120
Group 5	12	6	8	20	108
TOTAL	58	48	48	100	562

—— · —— denotes group division lines

FIGURE 6.10. SUBDIVISION 4 (MIXED)

size but retain the overall symmetry of the structure without seriously impairing the stiffnesses.

There is no 'in plane' rotational term for the plate stiffness matrix and so, wherever the local axes of the plate coincide with the global axes and there is no member present at a particular node on a corner, the 'in plane' rotational degree of freedom has to be suppressed for that joint. This condition arises on plane HJD and HJN. Elsewhere in the structure no rotation needs to be suppressed as the global 'in plane' rotation of the structure θy at any such joint has contributions from local 'out of plane' stiffness terms due to their direction cosines.

The number of members had to be increased with the increase in number of plates so as to span between nodes and avoid separation of member and plate at any intermediate node. On edge beams BDF and QNL dummy joints had to be introduced along the length where more than one joint group division line cut the beam. As already stated a member can only be connected to its neighbouring groups. Thus, for instance BD was split up into 4 separate members in the fine subdivision. For most members the 'in plane' joint numbers which define the local PQ plane, had to be created outside the structure at the appropriate position for the member and given zero degrees of freedom. For the central strap GK which was twisted into position, this was approximated by altering the 'in plane' joint number along the member. This central strap had to be subdivided into separate members between each node. Therefore the 'in plane' joint number could be easily changed for each member and the analysis approximated to a series of straight members connected at a varying angle.

In order to estimate the influence the end blocks had on the structure, one analysis was performed using the coarse subdivision but suppressing the rotation θ_x and θ_z for the joints at B and Q. It was

supposed that the size of the end blocks connecting the edge beams to the stanchions might affect their freedom of movement at that particular joint.

6.2.5 Results

The graphs of deflection at the various dial gauge positions on the structure are shown in figs. 6.11 - 6.15. Fig. 6.11 gives the central deflection at I and shows that all three triangular meshes agree very closely to the experimental values. It is apparent that the analyses form an upper bound. Theoretically, a fully conforming element should form a lower bound but, due to its inherent nonconformity in slope and also along the folds of the structure, the subsequent relaxing of the structure caused an overestimate of the true solution. The rapidity of convergence is shown from the accuracy of the coarse sub division. The medium subdivision gives results almost exactly equal to the experimental value and the fine subdivision appears to be diverging again. This fact can be explained by the far greater number of equations needed to be solved for the analysis which was almost twice as many as the medium subdivision. More rounding off errors will occur in this inversion and may well account for the divergence. The analysis using the mixture of rectangular and triangular element can be seen to underestimate the true result. This analysis suffers from two defects, the irregularity of the rectangles as mentioned above and their length to breadth ratio which is rather large.

The analysis performed restraining the 'out of plane' rotations at the end block positions gives a more serious underestimation of the true result. This can be expected as it caused the edge beams to behave as if they were built in and the bending of the stanchions ignored. The results of this analysis were not plotted elsewhere as they were too erroneous and could be left out of the graphs for the sake of clarity. This does show

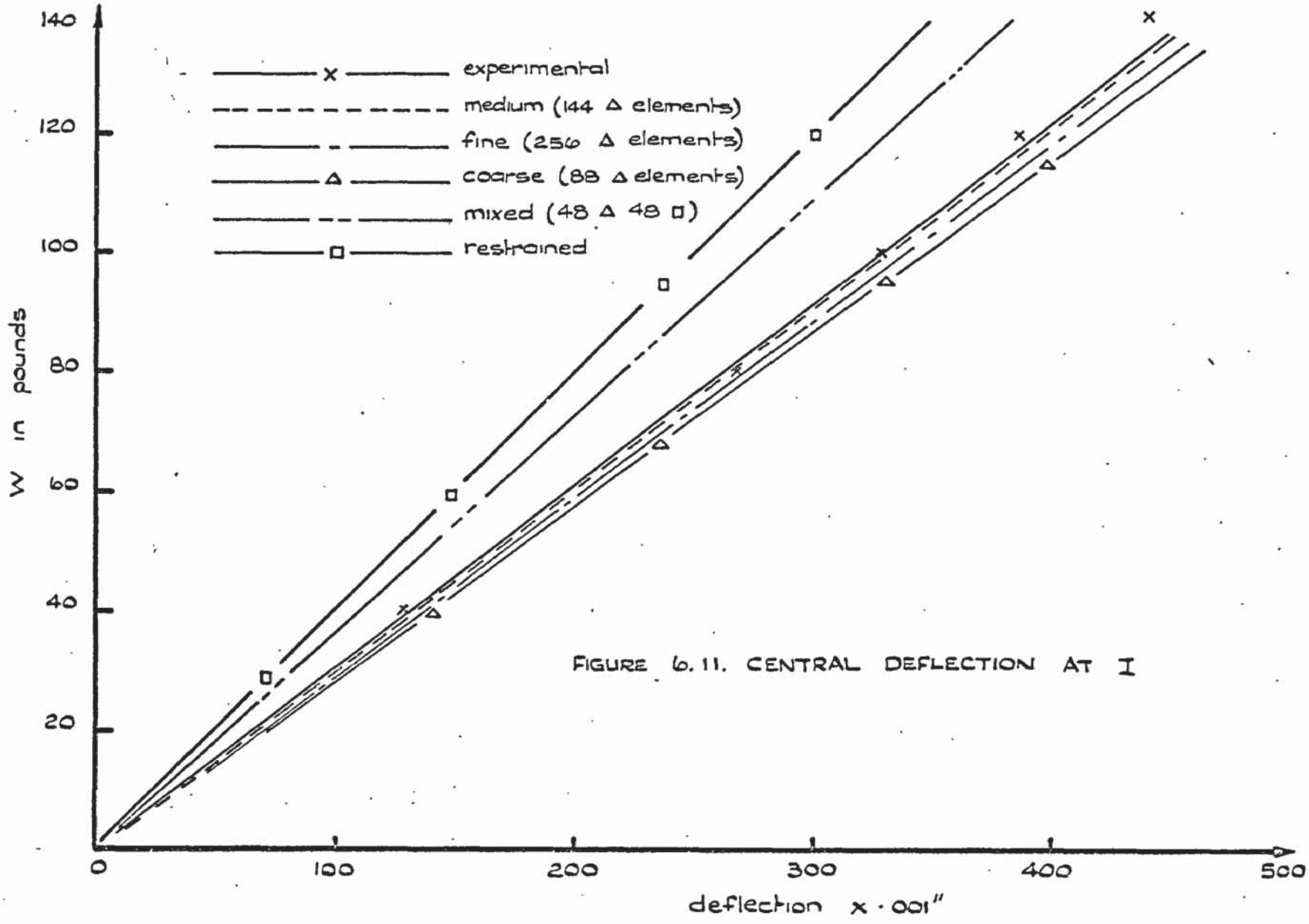

FIGURE 6.11. CENTRAL DEFLECTION AT I

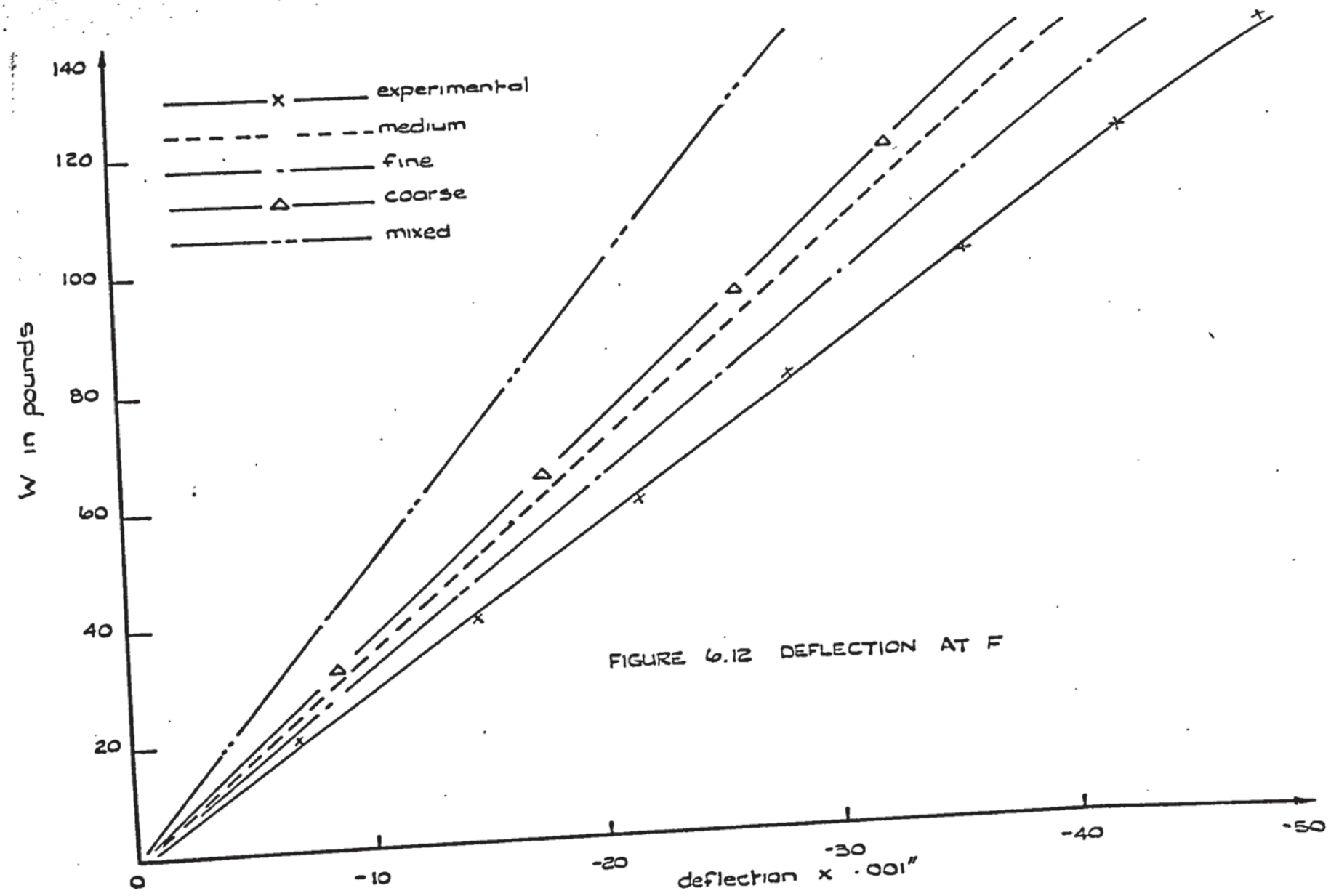

FIGURE 6.12 DEFLECTION AT F

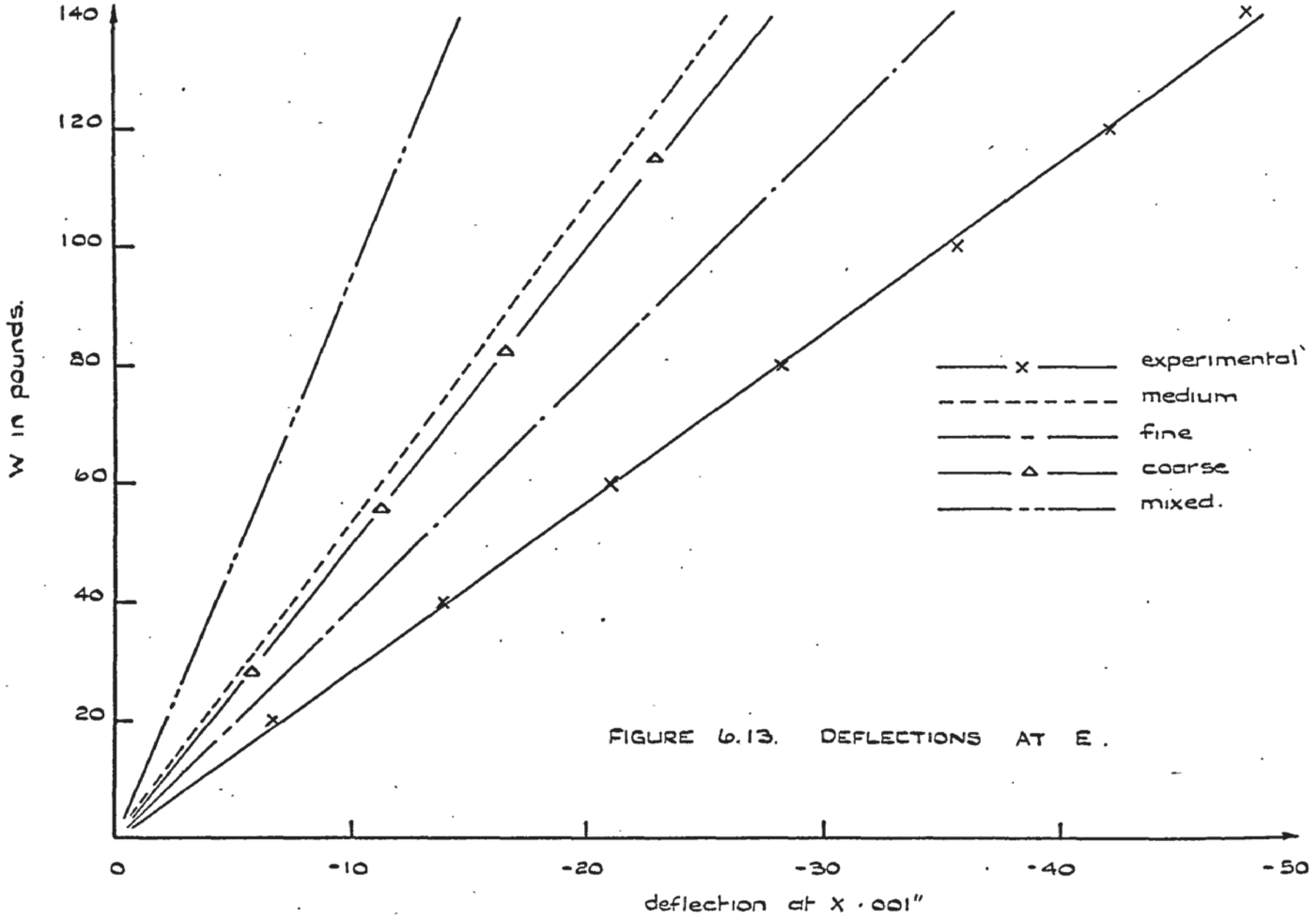

FIGURE 6.13. DEFLECTIONS AT E.

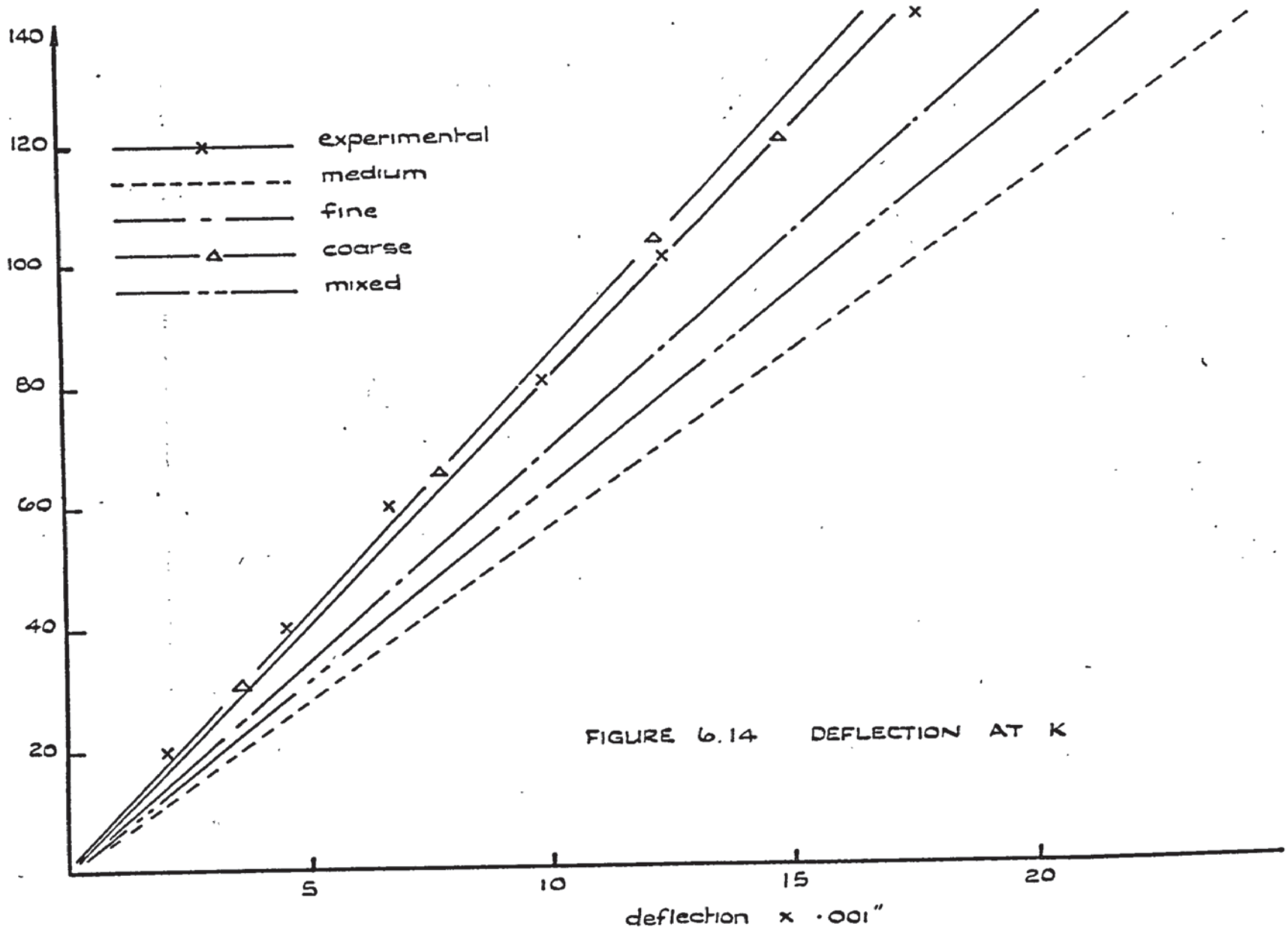

FIGURE 6.14 DEFLECTION AT K

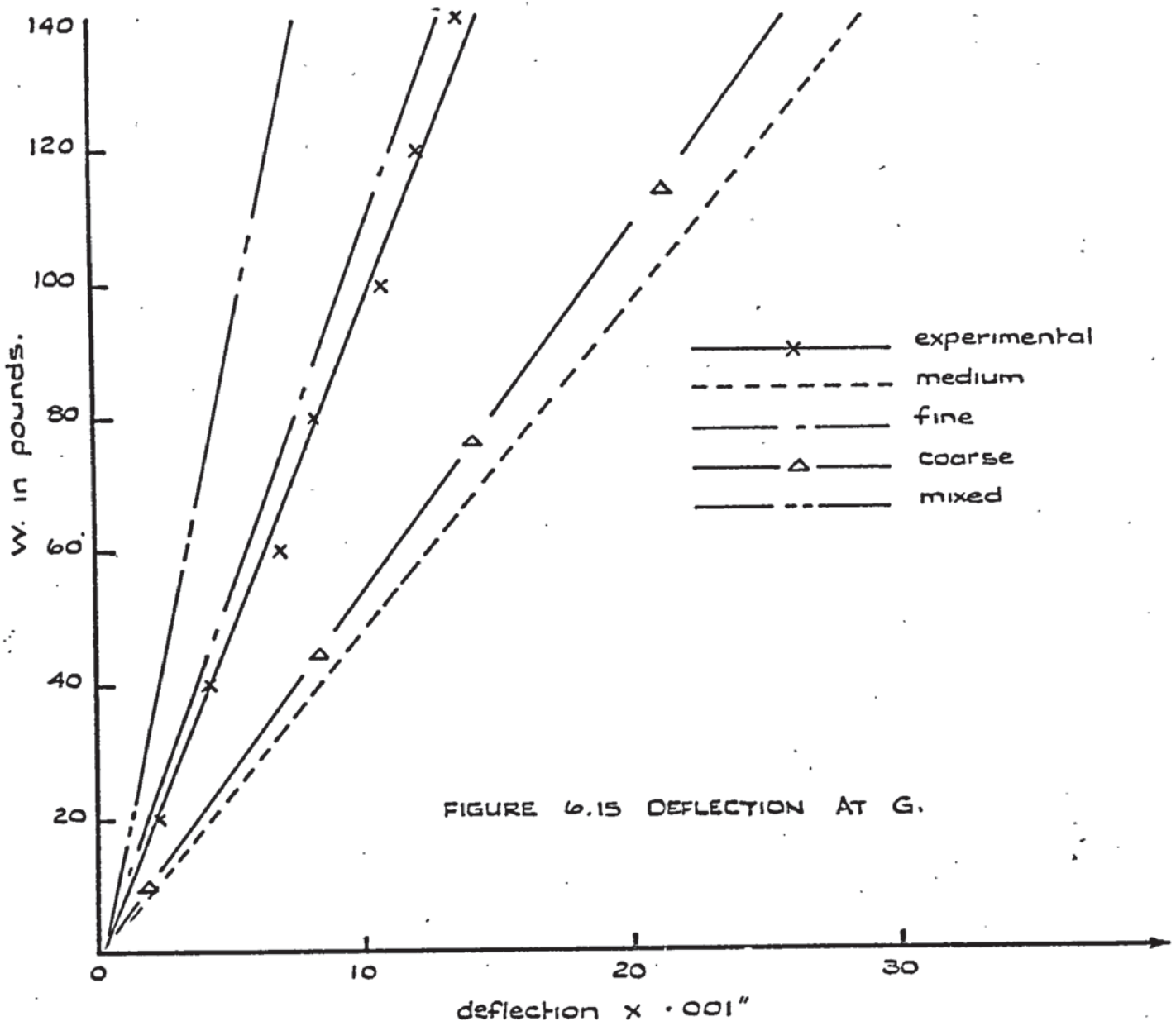

FIGURE 6.15 DEFLECTION AT G.

however the little effect the end blocks had on the freedom of movement of the edge beams beyond the connection. However this analysis shows clearly that it is wrong to idealize a complete structure by removing parts of it and replacing them with supports. It indicates that a complete structure should be analysed as it is and as a whole. A fact that is often overlooked by many analysts.

It was noticed during the loading cycle of the experiment, that the free corners F and L deflected vertically upwards whereas the central portion of the structure deflected downwards. This trend was repeated in the computer analyses and rising deflections are shown occuring at points F and E in figs. 6.12 and 6.13. The other positions of the dial gauges, at K and G, were found to be at almost neutral points, deflecting downwards slightly as shown in figs. 6.14 and 6.15. In all these positions the triangular fine subdivision gave the best results. For downward deflections the subdivisions would appear to be converging from above the true answer whereas, for upward deflections, the convergence is from below.

In general, it can be seen that, where the deflections are high, agreement between results is much better than positions of lower magnitude of deflection. At position G, for example fig. 6.15, the deflection is a twentieth of the central deflection and therefore those calculated at these points will be more sensitive to small data errors such as might occur when calculating the nodal coordinates and errors of inversion. Compared to the triangular element analyses, the mixed element analysis was not so accurate and showed a general trend to be overstiff. It is therefore likely that, on further refinement of subdivision better results would have been obtained.

The member stresses obtained at positions 9-12 (fig. 6.2) are shown in table 6.1. The experimental stresses were evaluated from the load-strain graphs obtained from the gauges and are shown for a load of W = 100 lbs. The analytical stresses were calculated from the appropriate member

SUBDIVISION	POSITION 9	POSITION 10
COARSE	-249.4592	689.8218
MEDIUM	-183.5736	688.6695
FINE	-202.0501	565.9433
MIXED	-488.3280	977.8282
EXPERIMENTAL	-294.25	742.19

SUBDIVISION	POSITION 11	POSITION 12
COARSE	-376.0602	583.4734
MEDIUM	-614.0612	875.3340
FINE	-339.7724	518.2752
MIXED	-93.0	333.7190
EXPERIMENTAL	126.31	473.31

All stress values given in psi.

TABLE 6.1 COMPARISON OF MEMBER STRESSES

forces. The axial stress was simply evaluated from the axial force and the bending stress was calculated by interpolating the end moments of the members. It can be seen, that the results, although somewhat erratic, are in reasonable agreement. An exception to this is the stresses obtained from the mixed element subdivision. The stress obtained experimentally at position 11 is obviously in error, probably due to the gauge not behaving correctly.

The plate stresses for positions 1-8 (fig. 6.2) are compared in tables 6.2 and 6.3 for a load of W = 100 lbs. The values of the principal stresses s_1 and s_2 and the angle α, of s_1 rotated from the X to Z direction are given for the various subdivisions as well as the experimental values. It can be seen that these values differ quite substantially in some cases. The reasons for this lie both on the experimental and analytical side. As already mentioned above, before screwing the Aluminium sheeting onto the frame, the strain gauges were affixed. Although the sheeting had been bent to the correct shape as far as possible, a fair amount of added twisting was necessary when bolting it down to the frame. Therefore there was quite large initial strains in the sheet and subsequent reorientation of the load-strain readings had to be carried out. The gauges did not behave very elastically which may have been due to local buckling, the folds not staying rigid, or even a 'tightening up' effect as mentioned earlier. It was noticed that some of the gauges did not immediately start recording for the first increment of load Hence it was quite difficult to arrive at the true strain reading. One faulty gauge in the rosette could affect the final principal values. The final stresses are only calculated for the centre of gravity of each element hence, where the rosette positions did not coincide with these positions, they had to be interpolated linearly from the neighbouring elements. The stresses throughout the structure varied substantially and this

POSITION 1

SUBDIVISION	s_1	s_2	α_{x-z}	
COARSE	52.868	-681.302	-40.187	*
MEDIUM	203.325	-859.371	-63.662	
FINE	288.373	-861.289	-81.006	
EXPERIMENTAL	292	-1320	-76	

POSITION 2

SUBDIVISION	s_1	s_2	α_{x-z}	
COARSE	470.002	-120.687	-28.600	
MEDIUM	843.538	-200.267	-25.263	
FINE	650.199	-139.419	-3.981	
EXPERIMENTAL	1020	-151	-46	

POSITION 3

SUBDIVISION	s_1	s_2	α_{x-z}	
COARSE	-100.230	-520.147	83.001	
MEDIUM	172.117	-836.924	65.169	
FINE	-70.501	-636.671	79.130	
EXPERIMENTAL	-208	-1360	89	

POSITION 4

SUBDIVISION	s_1	s_2	α_{x-z}	
COARSE	652.300	-150.562	12.010	
MEDIUM	821.390	-188.979	24.202	
FINE	860.746	-469.869	6.900	
EXPERIMENTAL	1560	-370	10	

All Stress values given in psi.

TABLE 6.2 COMPARISON OF PLATE STRESSES

POSITION 5

SUBDIVISION	s_1	s_2	α_{x-z}	
COARSE	533.684	174.154	-27.184	*
MEDIUM	263.061	33.136	-12.453	*
FINE	402.436	165.488	-69.037	*
EXPERIMENTAL	560	101	-72	

POSITION 6

SUBDIVISION	s_1	s_2	α_{x-z}	
COARSE	177.234	-238.229	16.253	*
MEDIUM	336.525	105.674	-71.752	*
FINE	256.038	-135.640	2.672	*
EXPERIMENTAL	358	-322	-81	

POSITION 7

SUBDIVISION	s_1	s_2	α_{x-z}	
COARSE	397.606	-1201.072	-28.751	*
MEDIUM	-284.603	-2506.124	-33.280	
FINE	169.042	-1160.539	-14.871	*
EXPERIMENTAL	352	-1581	-35	

POSITION 8

SUBDIVISION	s_1	s_2	α_{x-z}	
COARSE	-291.117	-1483.438	-33.216	*
MEDIUM	-704.091	-2633.525	-21.989	
FINE	-892.601	-1596.340	-34.432	*
EXPERIMENTAL	-952	-1820	-42	

All Stress values given in psi

TABLE 6.3 COMPARISON OF PLATE STRESSES

meant averaging between a number of elements. Two methods of averaging were tried. Either averaging the principal stresses, s_1, s_2, α, or the direct stresses, s_p, s_q, s_{pq}. The latter method gave the best results and from these values the principal stresses were calculated. Where stress interpolation was employed the values of stresses are marked with an asterisk. It is seen that these values give the most error in general.

Considering the fact that the triangular element is formed on a displacement function and hence the stresses across its boundaries are discontinuous, and for the reasons given above, the disagreement should not be considered with alarm.

Figs. 6.16 - 6.18 show stress contours in the Z direction for the top half surface of the structure BFKG. These are coarse, medium and fine respectively. These contours show the advantage of a finer subdivision when studying stress concentrations around certain points. In fig. 6.16 the elements are relatively large and only an approximation can be made to the exact positions of the contours. Where these were undefined they were left open. In the medium subdivision, fig. 6.17, the position of the major contours is now fixed and a stress concentration can be seen to be building up at position H, one of the loading points. This did not show up for the coarse subdivision as only the average stress throughout the relatively large element could be plotted. In fig. 6.18 the final stress contour is shown for the fine subdivision. The full stress concentrations at H and J are apparent. At position H the stress value is about twice that shown in the coarse subdivision. The detection of these stress concentrations, as well as the general pattern of the stress distribution, by the computer indicates the qualitative values of the analytical approach.

Table 6.4 shows the size of computation involved for the three comparable triangular element subdivisions. Considering the analysis program,

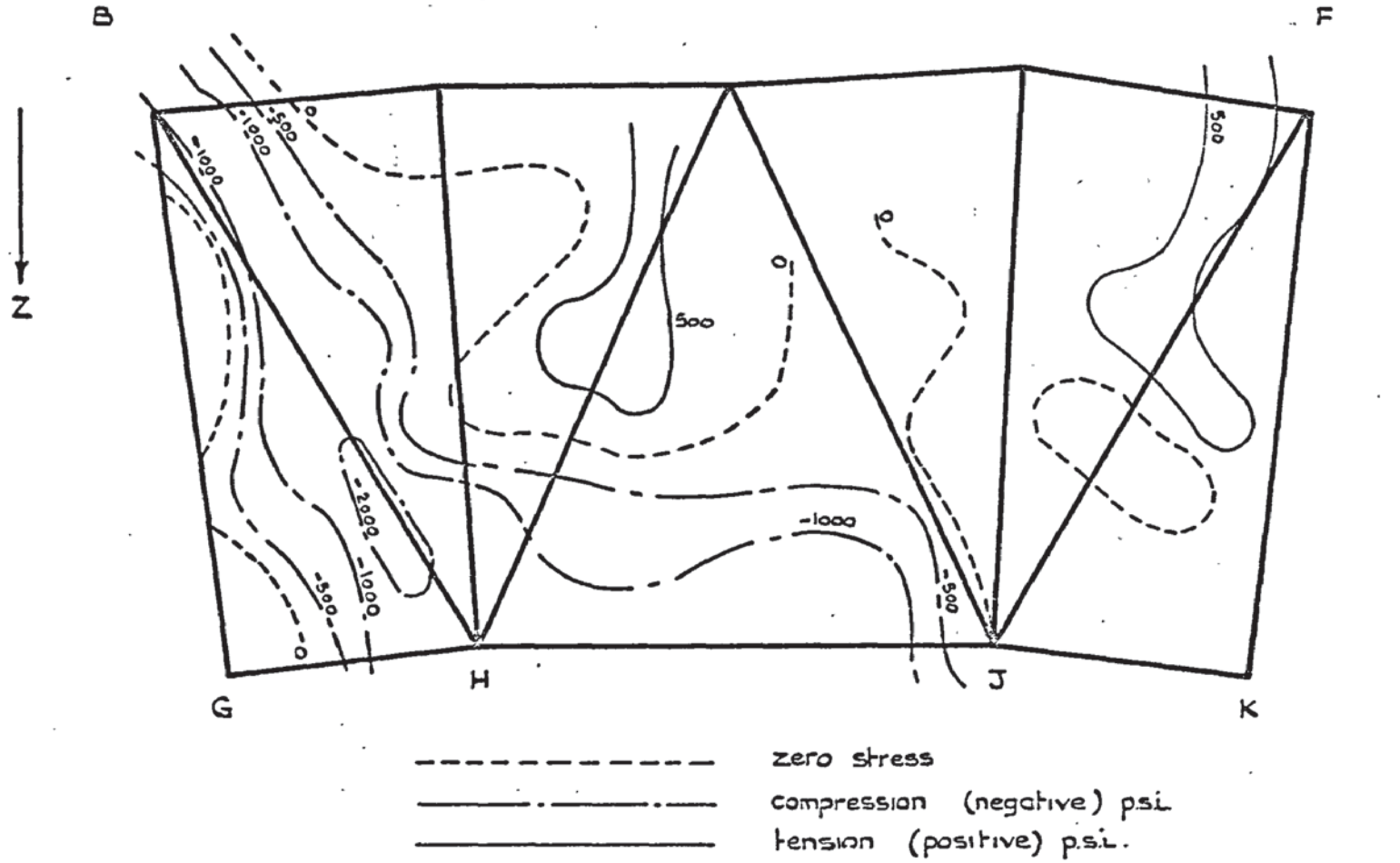

FIGURE 6.16. CONTOURS OF σ_z FOR TOP SURFACE OF COARSE SUBDIVISION

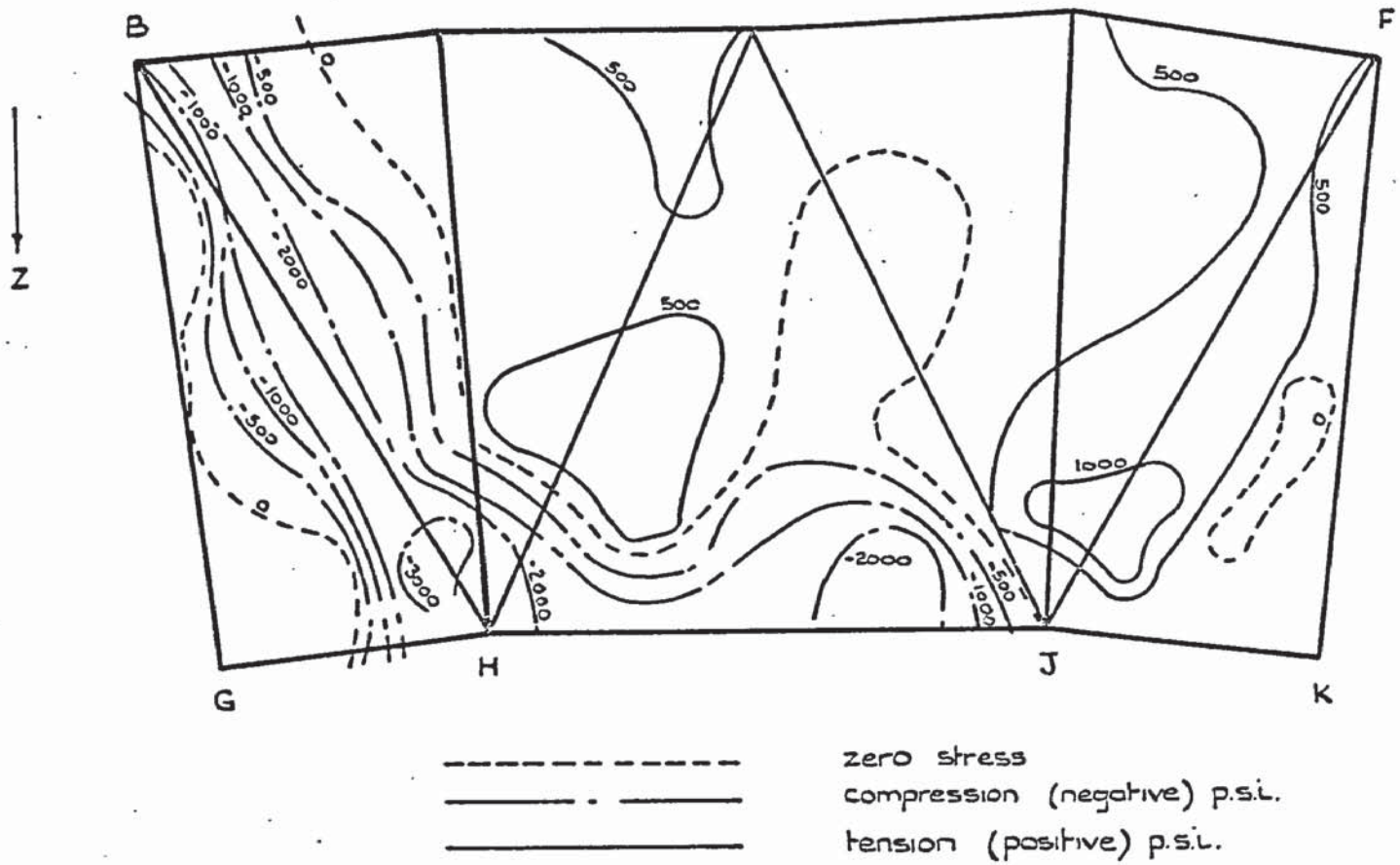

FIGURE 6.17. CONTOURS OF σ_z FOR TOP SURFACE OF MEDIUM SUBDIVISION.

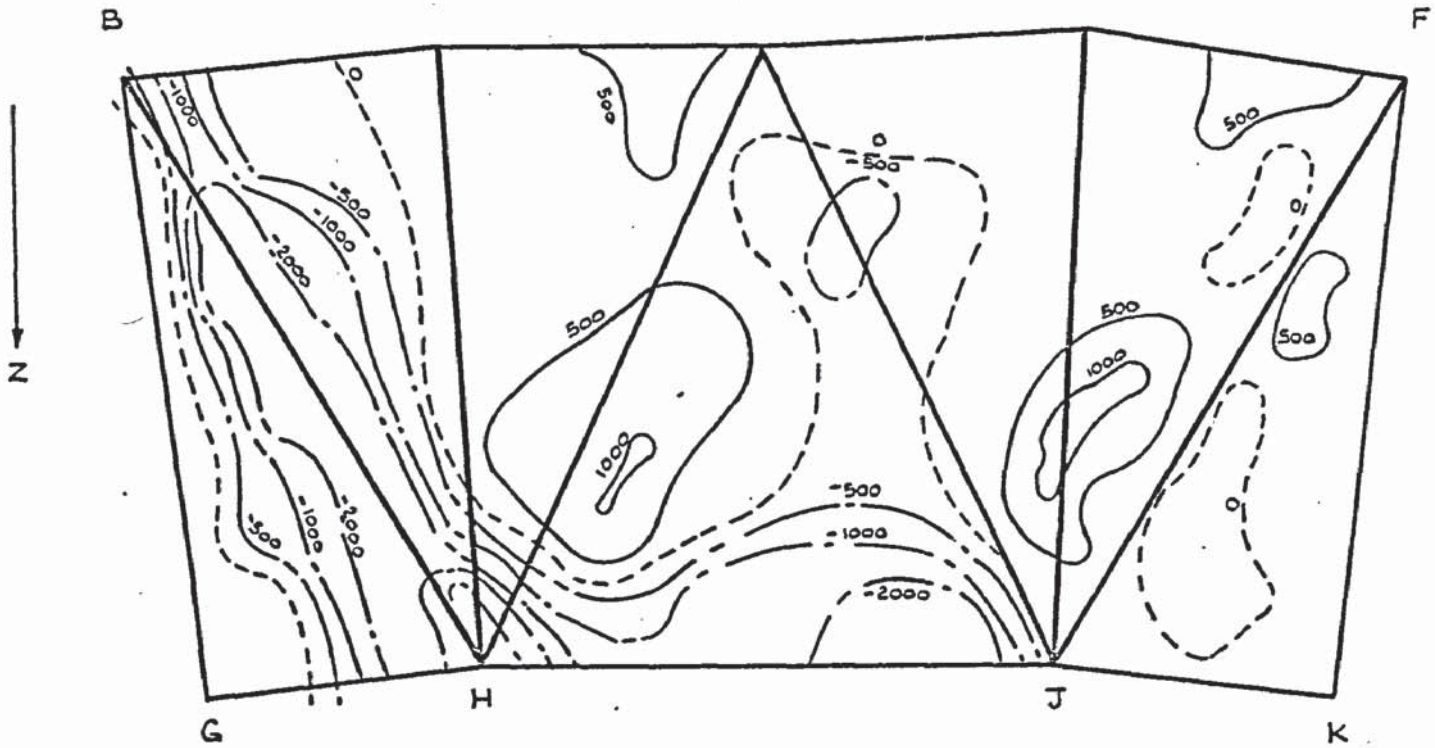

FIGURE 6.18. CONTOURS OF σ_z FOR TOP SURFACE OF FINE SUBDIVISION.

ELASTIC ANALYSIS PROGRAM			
SUBDIVISION	COMPUTING TIME (MINS)	WAITING TIME (MINS)	STORE (BLOCKS)
COARSE	8.9	1.0	174
MEDIUM	20.2	2.3	185
FINE	37.3	5.2	192

STRESS PROGRAM			
SUBDIVISION	COMPUTING TIME (MINS)	WAITING TIME (MINS)	STORE (BLOCKS)
COARSE	.40	1.08	63
MEDIUM	.65	2.33	85
FINE	1.1	6.10	124

TABLE 6.4. COMPUTATION INVOLVED

the store involved rises only slightly for increase in the number of elements. This is due to the suitable arrangement of joint groups mentioned previously. The computing time increases almost linearly with the total number of degrees of freedom of the structure. These values can only be taken as a very rough guide to estimating the computing time for analysis of other structures as they also depend on the number and type of elements involved. The waiting time is the time used over and above the computing time where the computation was held up while the magnetic tape was being rewound. This time was virtually all due to the storing required for later use with the stress program.

The computing time used in the stress program was very small, even for the fine subdivision. The waiting time was comparatively large but this is only to be expected with the amount of magnetic tape manipulation involved. The maximum store used in the stress analysis occurs when the stress matrices for 'in plane' and 'out of plane' elements have just been constructed. This store is proportional to the total amount of elements to be analysed. This program therefore, although very fast to run, will only accommodate 550-600 triangular elements for 'out of plane' and 'in plane' stressing.

6.2.6 Concluding remarks

The results show that this method of analysis can be used for a structure as awkwardly shaped and complicated as the folded plate structure described above with a good degree of success. This is especially true in predicting deflections where even the coarser grids will give good results. It would appear that the higher degree of nonconformity which occurs in such structures does not impair the accuracy to any appreciable extent and therefore it would be reasonable to assume that differently shaped structures could be also analysed successfully.

The obvious advantage of a coarse grid is the saving in computation which is a .significant factor in storing such problems. On the other hand it has been demonstrated that stress concentrations could be underestimated, and that stress interpolation could be misleading. These defects can be improved by using a stress function as opposed to a displacement function in deriving the stiffness matrices. As it stands, the results of the computer analysis could be improved by use of a grid which is more refined atpositions where the stress is expected to be critical. In this case the triangular element has an advantage over other shapes as its size can be graded over a surface area with little inconvenience.

The results of the mixed element analysis were rather disappointing but the approximations involved have already been pointed out. It is clearly advantageous to be able to use the more reliable rectangular element for orthogonal type structures with the triangular element inserted in places where irregularities of geometry occur.

In analysing complete structuresit was of interest to note the effect of subdivision on the prismatic member elements. It was noticed that member forces on the central strap close to the plates were appreciably affected and also this influence was carried down to the fixed base of the main columns. However it was apparent that, at this point the effects were dampened.

The elastic analysis program has been shown to cope with large structures or large numbers of degrees of freedom. Theoretically, the limiting feature is the amount of fast store which is available. It has been shown that most structures could be analysed as long as the number of joints and elements per joint group can be kept at a reasonable level. This is also true of the stress program with respect to the total amount of elements present.

The next sections of this chapter give two examples of the use of

the program for analysing such structures. The accuracy of the results can only be judged with regard to more conventional techniques and the more practical computational difficulties which arise are also discussed.

6.3 Analysis of Road Bridge

The elastic analysis program described in chapter 3 was used to determine the deflections and stresses of a motorway bridge of which the more relevant details are given in figs. 6.19 and 6.20. Half the cross section was analysed up to the centre line as shown in fig. 6.20. The two carriageways acted independently as they were totally separated and acted as two independent bridges.

The bridge was to be built of prestressed concrete and basically consisted of two box beams, A and B supporting the motorway deck. The ends were supported on rollers and the legs pinned at their base.

The object of the analysis was to determine the deflections and stresses under various combinations of imposed loading which consisted of HA and HB loads and could be added to the prestressing in the concrete. Obviously no comparison to a true answer could be made and hence the method of analysis and representation was investigated and the structural details are not given here. The results however were compared with another computation analysis program called 'Strudl' which idealises the structure to a space frame.

All three types of element were used in the representation and the subdivision is shown in fig. 6.21. The total number of elements involved were 512 rectangular plates, 88 triangular plates and 88 members. The box beams were represented by the rectangular plates being one plate in depth. The sides were, on elevation, trapezoidal but these were approximated to rectangular with little loss in accuracy. These were numbered in such a way as to be symmetrical about the legs and therefore not to cause any additional

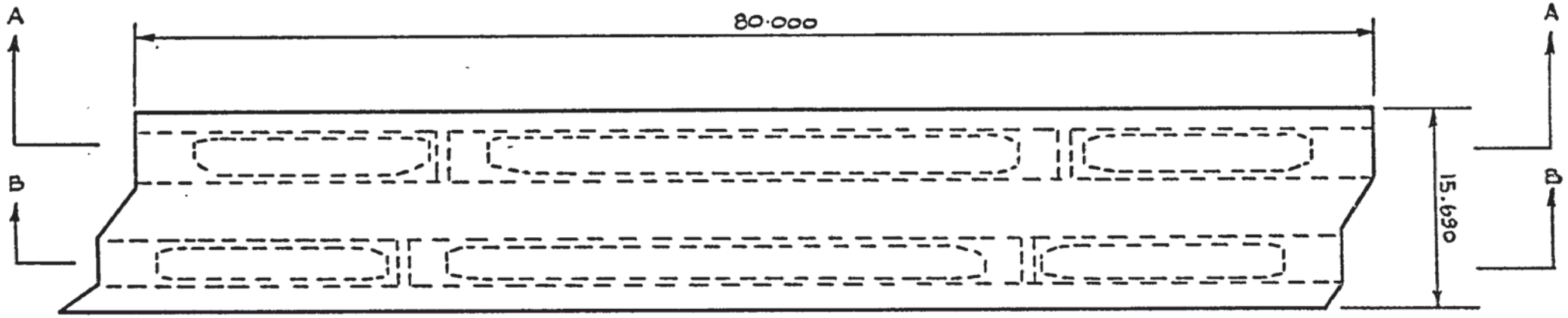

Plan of Deck Slab

Section A-A

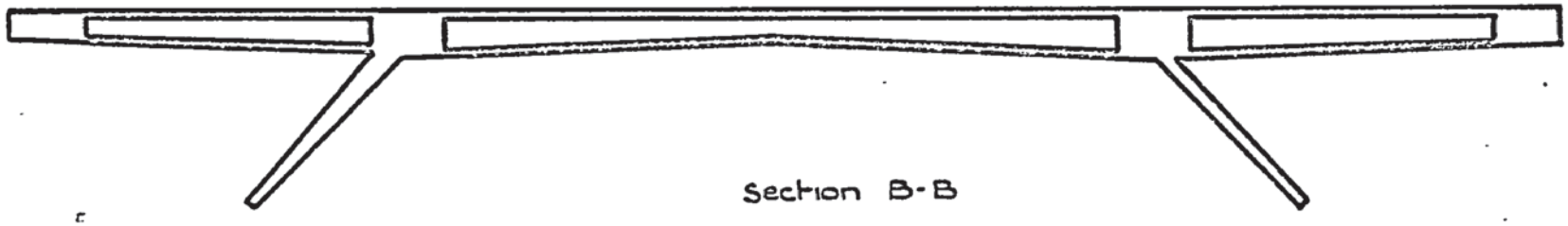

Section B-B

FIGURE 6.13 DETAIL OF ROAD BRIDGE.

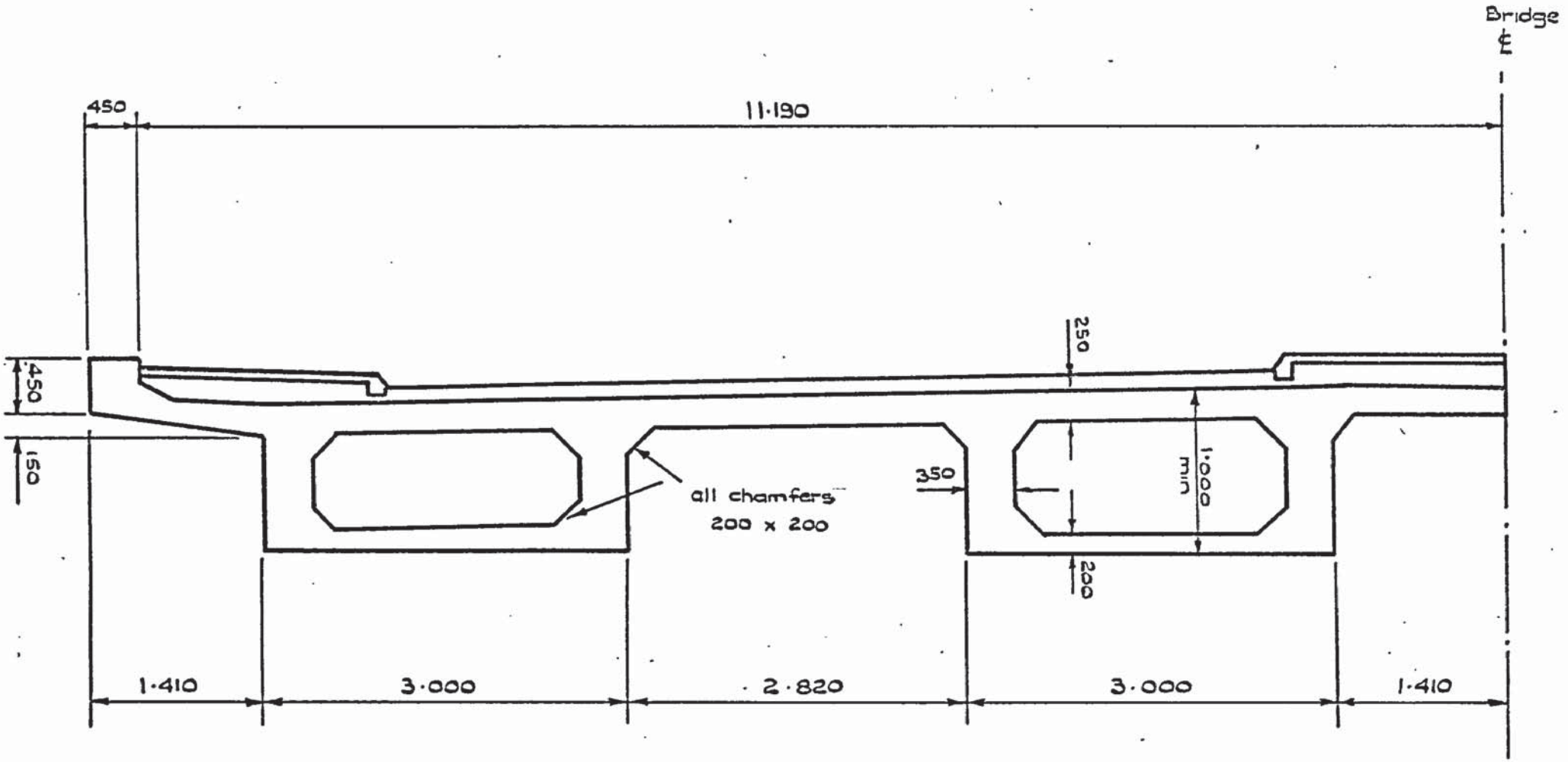

FIGURE 6.20 TYPICAL CROSS SECTION OF BRIDGE.

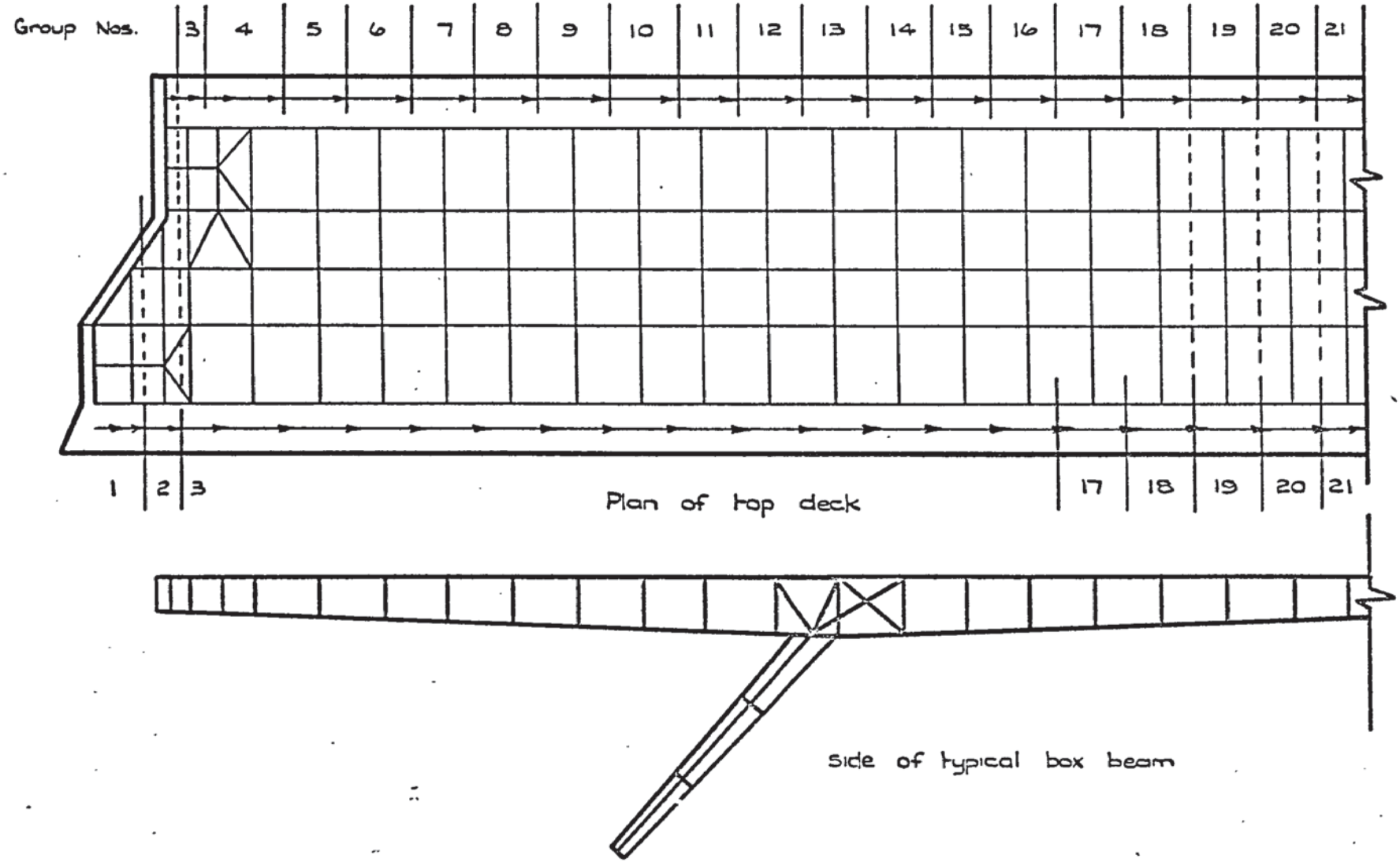

FIGURE (2) FINITE ELEMENT REPRESENTATION OF HALF THE BRIDGE

sway due to geometrical errors. Member elements were used to represent the two sides of the bridge where only little stress was involved. The appropriate offsets of the member from the position of the joint to which it was attached were calculated and these compensated for the thickness of the element. Experience had shown that the use of these elements helped to make the stiffness matrix more stable besides including an 'in plane' rotational term.

The box beams were to be of solid concrete construction at either end and under the supports in order to carry the high stresses which were expected at these positions. It was decided to represent these areas as an assembly of plates acting vertically and at angles through the thickness as shown. The thicknesses of the plates were arranged so that the total volume of concrete was filled. By this means, the torsional and 'in plane' action of the block could be catered for. It was necessary to use the triangular element in these regions. About half their number were used as dummy plates in groups where no such elements existed and hence did not affect the analysis to any appreciable degree.

The supports were made up of three rectangular plates each. The subdivision would appear to be rather coarse especially around the box beams but even so, this resulted in 2599 degrees of freedom. Therefore this number of simultaneous equations had to be solved. Any more refinement of mesh may well have precipitated large inversion errors and, as was later found, would have overflooded the main store of the computer.

The joints of the structure were divided into 43 groups as shown. The maximum number of joints in a group were 13 which was rather lower than the number previously used but made it possible to store all the plate data etc. which was permanently kept in the machine throughout the analysis.

6.3.1 Computational Analysis of Bridge

The data required for such an analysis was very long and a program

developed by Bray (55) was used to assist in checking the vast quantity of figures in an effort to overcome the human errors which could only be expected.

Originally four loading cases were to be used on one run but it was found that this overflooded the main store and therefore they had to be run independently. Even so it was found that, during the backsubstitution cycle, the forces vector grew to such an extent that the store was again overfilled. It was therefore decided that the kA matrices would not be brought down for each group and a member forces program was written to bring back the relevant matrices and form the element forces after the elastic analysis program had been used.

The bridge was therefore analysed using four programs:-

(i) A program to check the data.

(ii) Elastic analysis program to determine the deflections and store relevant information on the magnetic tape.

(iii) Element forces program to use the magnetic tape in the calculation of member and plate elements.

(iv) Stress program to use the magnetic tape to calculate the plate stresses.

For the elastic analysis program it was clear that a run time of over one hour on Atlas was necessary to evaluate the displacements. During this time it is quite possible that machine faults could develop or a data error be discovered after some time in the reduction cycle. To avoid losing all the calculations done so far and save computing time the facility for storing the main store arrays on the magnetic tape if further time was not available (see chapter 3) was also used so that this information was written up every fourth reduction loop.

For this analysis therefore the magnetic tape held S_i, $\underline{kA}_i$, $\underline{A}_i^1$ for each group, general data after every fourth group, $\underline{X}_i$ for each group written up in the backsubstitution loop and general data for the stress program. It was found that a prohibitive amount of rewinding of the magnetic tape was needed in the backsubstitution process in collecting $\underline{S}_i$ from one end and writing $\underline{X}_i$ to the other. The time taken to do this was almost as long as that used in the reduction process and very often resulted in the magnetic tape failing. To overcome this therefore a disc was used in conjunction with the tape. With a disc no rewinding is necessary and direct access is available to every position. At the end of the analysis all the information on the disc was copied onto the magnetic tape for storage. The deflections were printed out and the locations of the $\underline{kA}$ and $\underline{X}$ matrices made available for use with the forces program.

The stress program described in chapter 3 also had to be altered to cater for the large number of elements and the long rewinding time which would be of the same length as the analysis program. The latter effect was achieved by first writing all the displacement arrays $\underline{X}_i$ from the tape onto a disc. In order to form $\underline{Z}_i$ during the running of the program the displacement transformation matrices $\underline{A}_i^1$ were read off the tape and the $\underline{X}_i$ matrices off the disc therefore preventing unnecessary rewinding of the tape. The storage capacity of the program was also increased with the use of the disc. As soon as the nodal displacement vectors had been constructed they were written to the disc before being cleared out of the store. The stress matrices were also transferred as they were constructed. These two matrices were then brought back and multiplied to form the stresses for each individual type of element before considering the next type. They were then added and subtracted as before to obtain top and bottom stresses.

The element force program worked on a similar procedure to the stress program. A disc was used onto which the $\underline{X}_i$ matrices were written

from the tape. The matrices $\underline{kA}_i$ and $\underline{X}_i$ were brought back alternatively from magnetic tape and disc and multiplied together to form $\underline{P}_i$. These force vectors were added together in the same manner as that used by the backsubstitution loop.

For a fully populated vector three numbers have to be stored for each element using the sparse matrix scheme. These are, row number, column number, element value. To cut down the storage of the vector it was stored in its transposed form $\underline{P}^1$ where only the column number and element value need be stored with one row number. The storage was therefore reduced by one third.

The reactions could be evaluated manually by resolving the forces at a joint. The above three programs could thus be used to analyse the structure completely.

6.3.2. Results of Bridge Analysis

The deflections and stresses are shown in figs. 6.22 and 6.23 for two of the four loading cases. These are representative of the other two types of loading. The 'Strudl' space frame program which was used as an alternative analysis represented the two box beams as tapering members, the centre portion of the decking as another member and the four supports as members. Cross members joining the box beams were used to similate the torsional stiffness of the assembly.

Fig. 6.22(a) shows the finite element model as being stiffer than the 'strudl' in both box beams under this loading. The stresses in the longditudinal direction are shown for the top and bottom of each box beam. It was noticed however that these were very close to the stresses given by 'strudl'.

The main difference between the two results occurred in the side loading in fig. 6.23(a). Here the 'strudl' model showed a greater tendency to sway whereas the finite element model remained much more rigid. It would

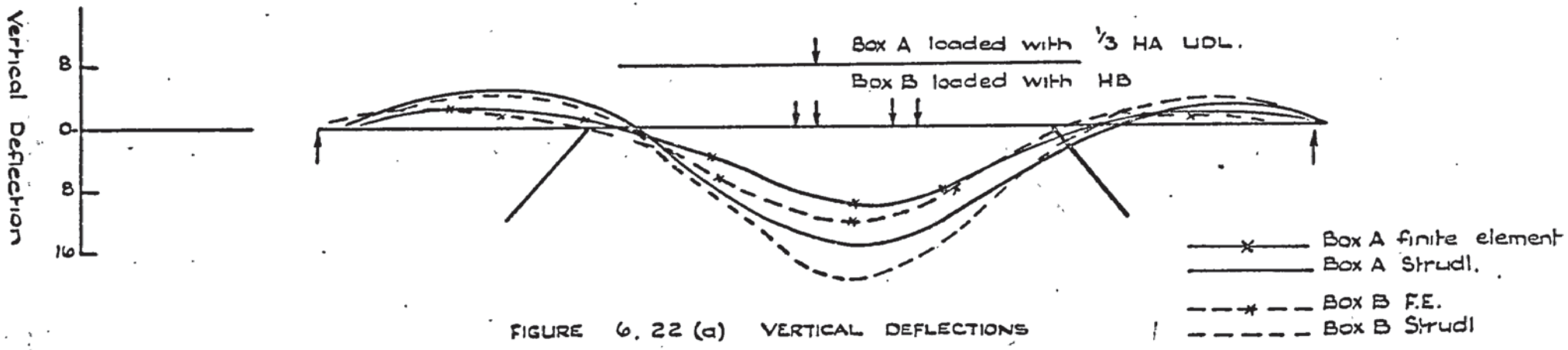

FIGURE 6.22 (a) VERTICAL DEFLECTIONS

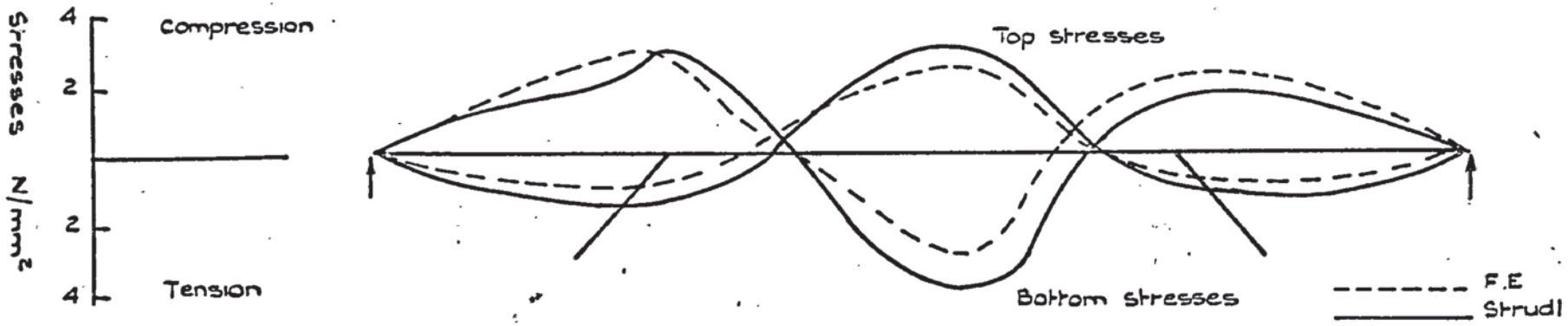

FIGURE 6.22 (b) LONGDITUDINAL STRESSES Box A.

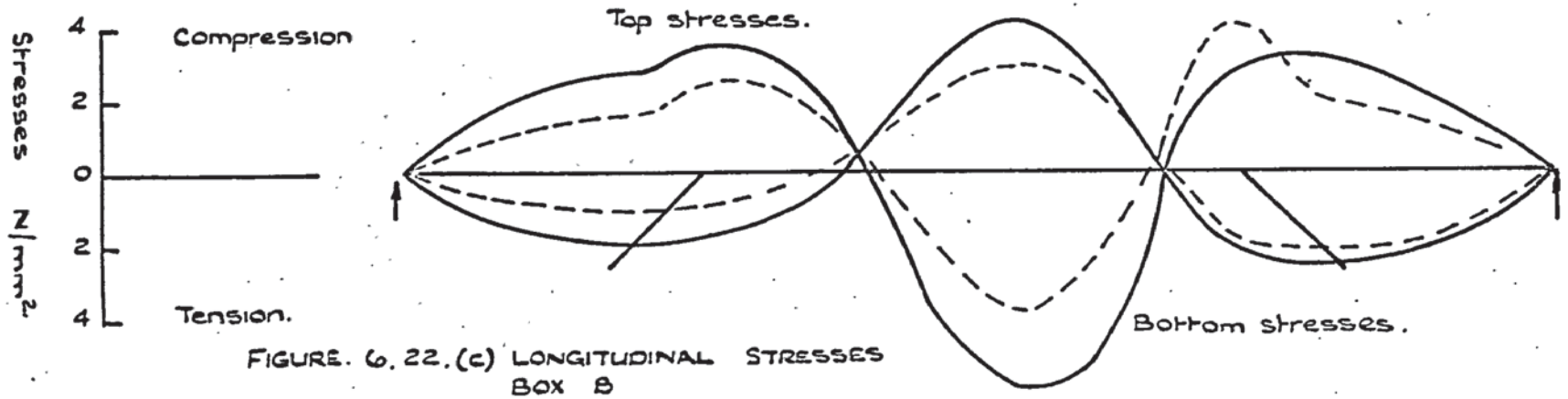

FIGURE. 6.22.(c) LONGITUDINAL STRESSES BOX B

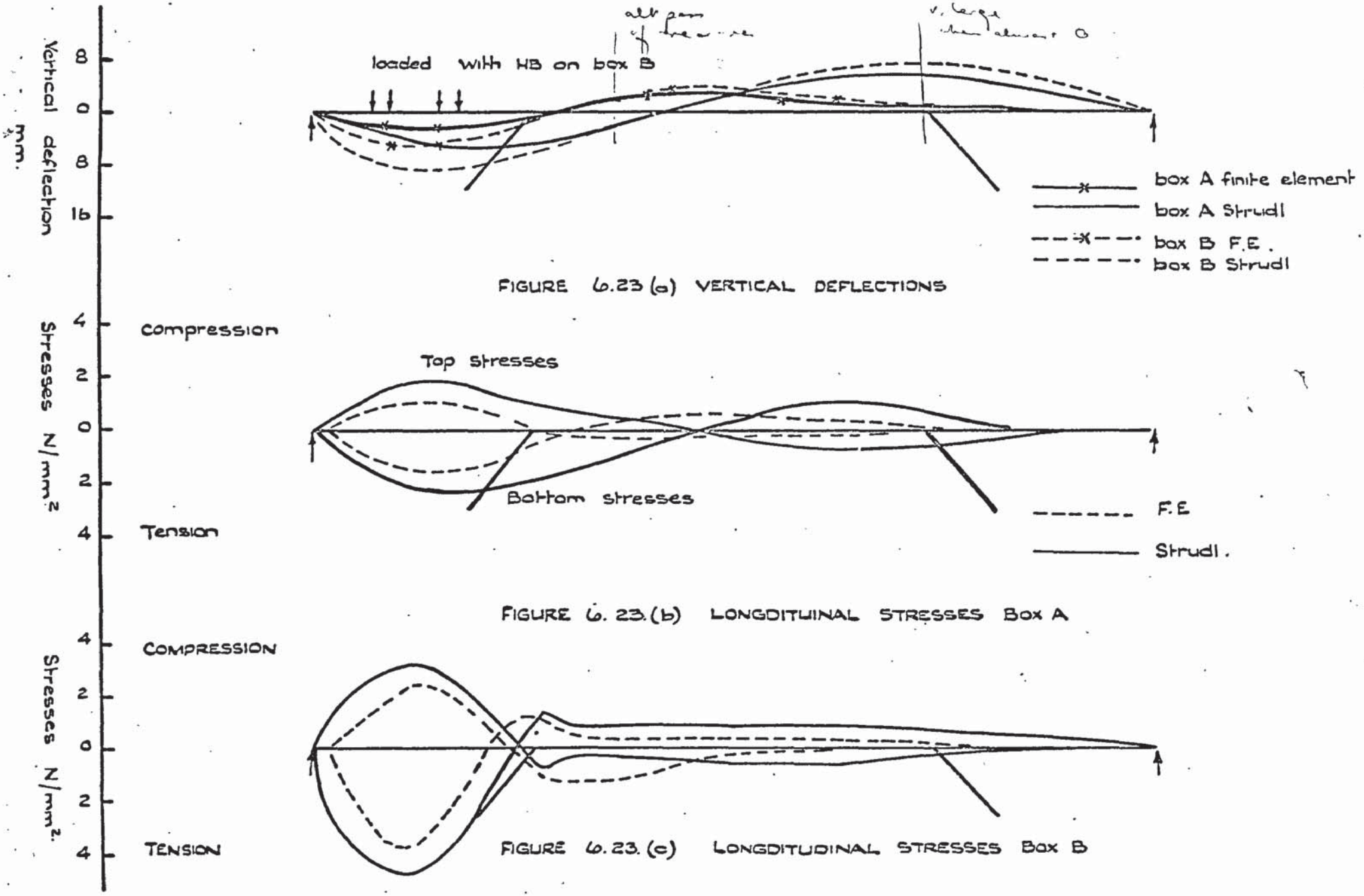

FIGURE 6.23 (a) VERTICAL DEFLECTIONS

FIGURE 6.23.(b) LONGDITUINAL STRESSES Box A

FIGURE 6.23.(c) LONGDITUDINAL STRESSES Box B

be misleading to make a direct comparison between the two due to the different assumptions which have been used in each. The main source of error for the finite element analysis would be in the inelastic properties exhibited by concrete and the application of thin plate theory to such a structure. It can be seen from the cross section of the bridge that the box beams are relatively thick as regards their span and this is also true in the representation of the supporting legs.

6.4. Analysis of Precipitator Casing

Plates 6.4 and 6.5 show the finite element representation of the electro-filter precipitator casing. Basically, its function is to collect dust particles electrostatically from exhaust gases which pass through it. The dust collects at the base in a hopper from which it can be transported away. These kinds of structures will normally take a similar shape and hence an analysis is desirable to ascertain at which positions the amount of steel could be saved. Only a quarter of the structure, as shown, needed to be analysed as it was symmetrical about the X and Z axes. Two cases of loading were investigated that of the vertical dead and superimposed loading and the horizontal wind loading. The former was represented by loads on the joints of the structure to simulate the dead load of the steel, the live load on the filter roof, the weight of a full hopper, and a suction on the sides of the structure due to the passage of 'exhaust' through it. The wind loading was applied to the projection of the face of the structure in the direction of the global X axis. The degrees of freedom of the joints on the perimeters of the structure were altered accordingly for each load case.

6.4.1 Computational Analysis of Casing

The inherent geometrical shape of the structure was found to limit the finite element representation and joint grouping which was

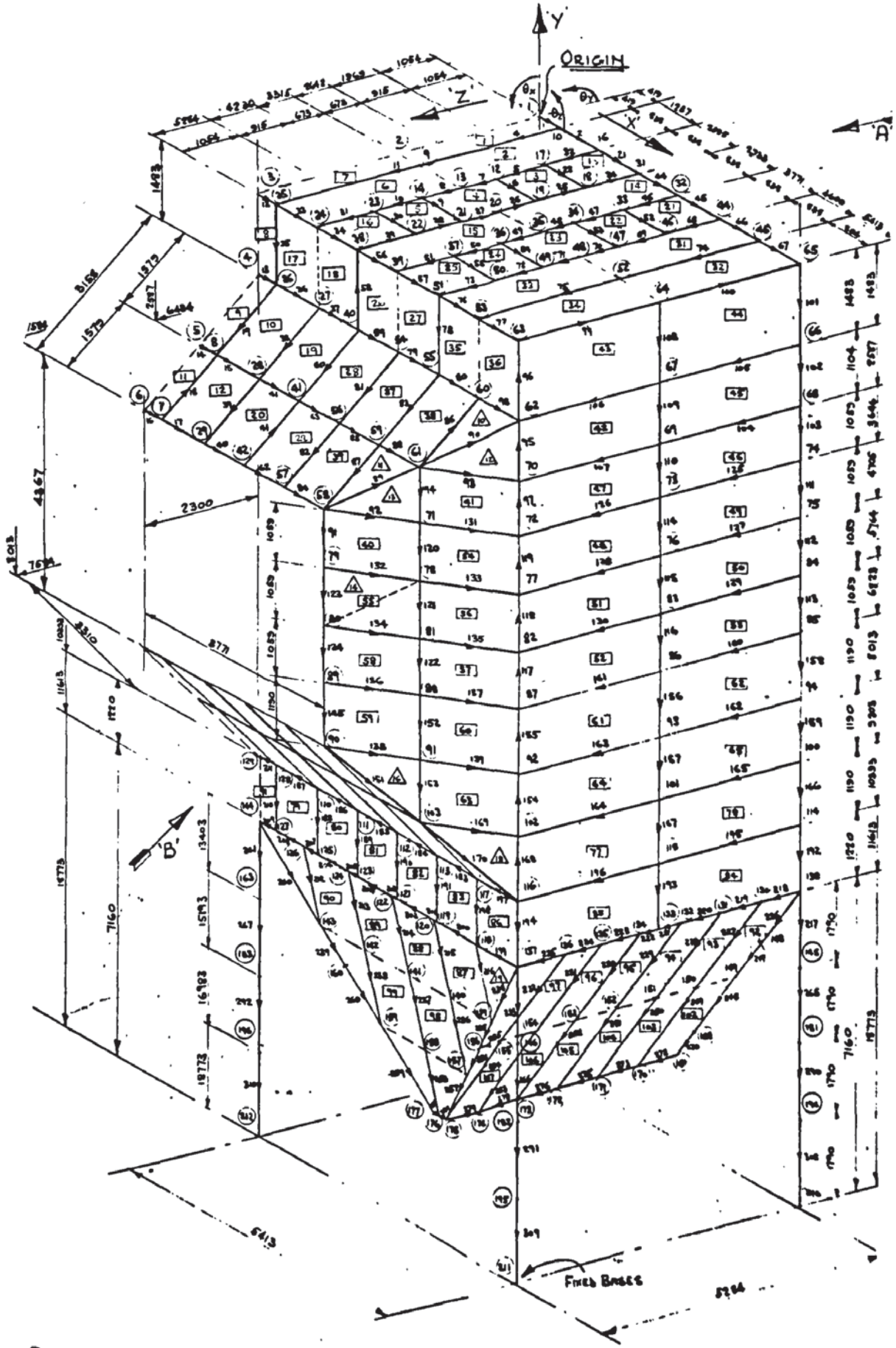

PLATE 6.4 QUARTER SECTION OF FILTER.

PLATE 6.5. DETAILS OF FILTER

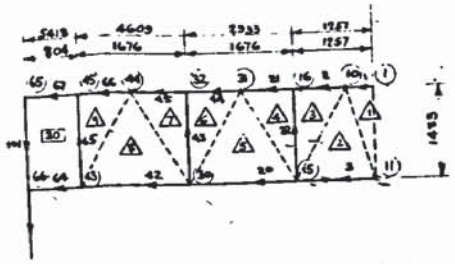

ROOF BEAM - ARROW 'A'

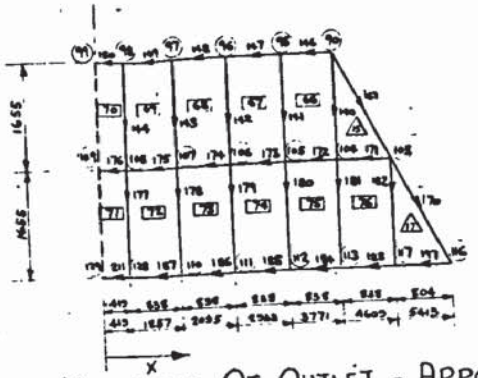

UNDERSIDE OF OUTLET - ARROW 'B'

GROUPS	∠ PLATES	JOINTS	□ PLATES	MEMBERS	TOTAL
1	1 - 3 = 3	1 - 14 = 14	1-12 = 12	1 - 19 = 19	48
2	4 - 5 = 2	15 - 29 = 15	13-20 = 8	20 - 41 = 22	47
3	6 - 8 = 3	30 - 44 = 15	21-29 = 9	42 - 63 = 22	46
4	9 = 1	45 - 57 = 13	30-39 = 10	64 - 85 = 22	45
5	10 - 13 = 4	58 - 70 = 13	40-47 = 8	86 - 110 = 25	44
6	14 = 1	71 - 84 = 14	48-58 = 11	111 - 135 = 25	43
7	15 - 16 = 2	85 - 99 = 15	59-70 = 12	136 - 163 = 28	42
8	17 - 18 = 2	100 - 113 = 14	71-78 = 8	164 - 191 = 28	41
9	19 = 1	114 - 129 = 16	79-86 = 8	192 - 216 = 25	40
10	20 = 1	130 - 144 = 15	87-98 = 12	217 - 243 = 27	39
11	21 = 1	145 - 159 = 15	99-107 = 9	244 - 267 = 24	38
12	22 = 1	160 - 179 = 20	108-113 = 6	268 - 292 = 25	37
13	23 = 1	180 - 196 = 17	114-119 = 6	293 - 310 = 18	36
14	24 = 1	197 - 212 = 16	120-123 = 4	311 - 324 = 14	35
	24	212	123	324	610

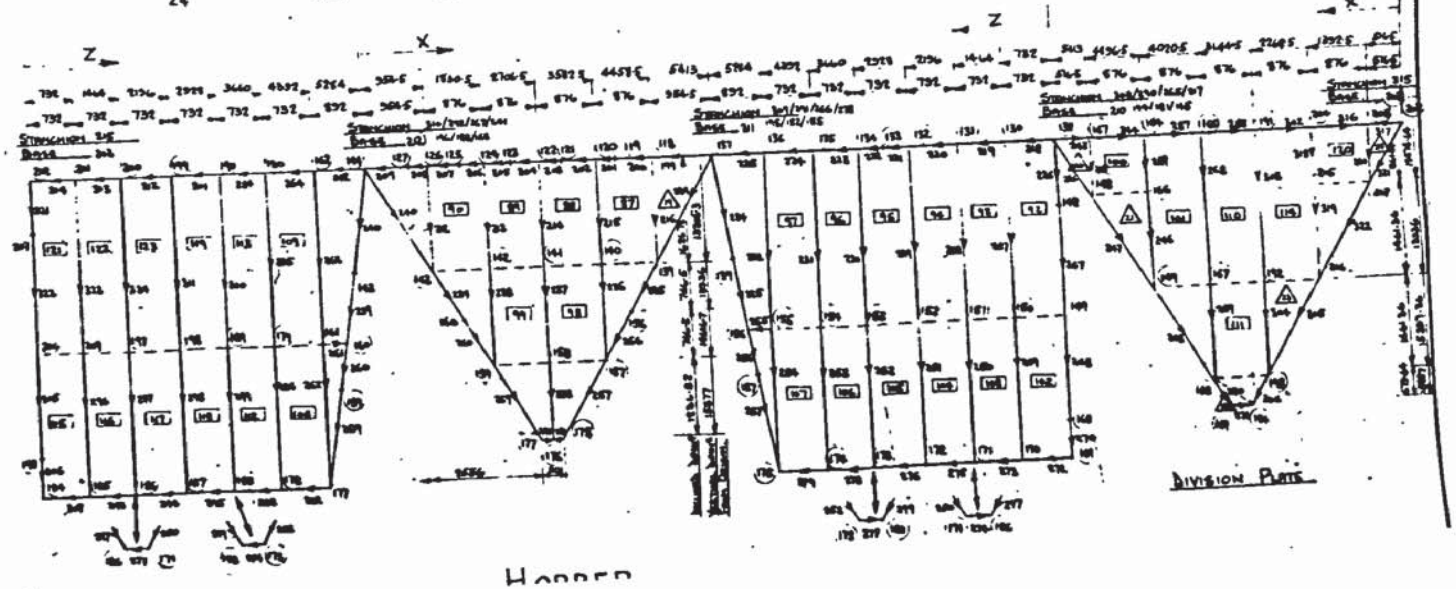

HOPPER

necessary for the analysis. It was intended to investigate the stability of the structure as a whole and, in particular, the deformations and stresses throughout the hopper as this region consistutes the major load bearing area. This led to two difficulties. In refining the mesh size round the hopper this meant that the larger plates on the side of the structure spanned across several joints as can be seen in plate 6.4. Also the increased number of joints in this region made their grouping more difficult.

The finite element representation was largely dictated by the structural components. These consisted of members of varying size as shown covered with steel sheeting 0.6" - 1" thick. It is difficult to estimate the stiffening effects of this sheeting by conventional means. Various methods of grouping the structure were attempted with little success due to the fact that the number of joints per group had to be limited to about 18. The final idealization was decided upon in view of the following factors:-

(i) All member elements were to be included.

(ii) In general, plates were formed from the member boundaries and, where possible did not have a length to breadth ratio greater than 2.

(iii) The maximum number of joints per group kept to about 18.

Using these criteria it was possible to split up the structure into 14 groups which totalled 324 members, 123 rectangular plates and 23 triangular plates. Even so the joint grouping round the back of the hopper had to be carefully arranged to avoid overflowing the main store of the computer. There were altogether 1069 unknowns in the problem.

The analysis took just under half an hour to give the values of deflections and element forces. The plate stresses were found from the

forces at the nodes of each element.

6.4.2 Results of Casing Analysis

Plate 6.6 shows the deflected form of the casing under vertical loading. The deflections are full scale. Similarly, plate 6.7 shows the deflections for the wind loading. It can be assumed that the structure is quite rigid enough under these loadings.

The results for the plate stresses appeared to be less reliable. Where the node of the plate was considered to be restrained in rotation, i.e. along the lines of symmetry of the casing, the stresses were very high, often well above the permissable. It was also noticed that along some edges of the structure certain stresses would be discontinuous or erratic. In the former case this high stressing at a restraint is due to the plate bending theory and the other stress irregularities were overcome by plotting stresses along a line and interpolating the stresses which were obviously in error at a certain position.

It was apparent that the values of stress were much more sensitive to irregularities such as change in element shape or size than the deflections. On the underside of the outlet, shown by arrow B, plate 6.4, all plates appeared to be overstressed. This could only be expected in view of the irregularities and it was found that badly shaped triangles as used along the corners of the hopper also made the deflections untrustworthy. Because of this it was not possible to make any significant saving on the steel plate but it was found that the member steel could be reduced by as much as 20 per cent.

Before leaving this subject it is worth noting one major discreprency which occured in the member forces. It was noted that the four stanchions only took the load of the top half of the structure and ignored the hopper. Efforts were made to overcome this by dividing them up into five members, one for each group in the hopper, but still the total loads in the stanchions did not balance the applied loads. This would

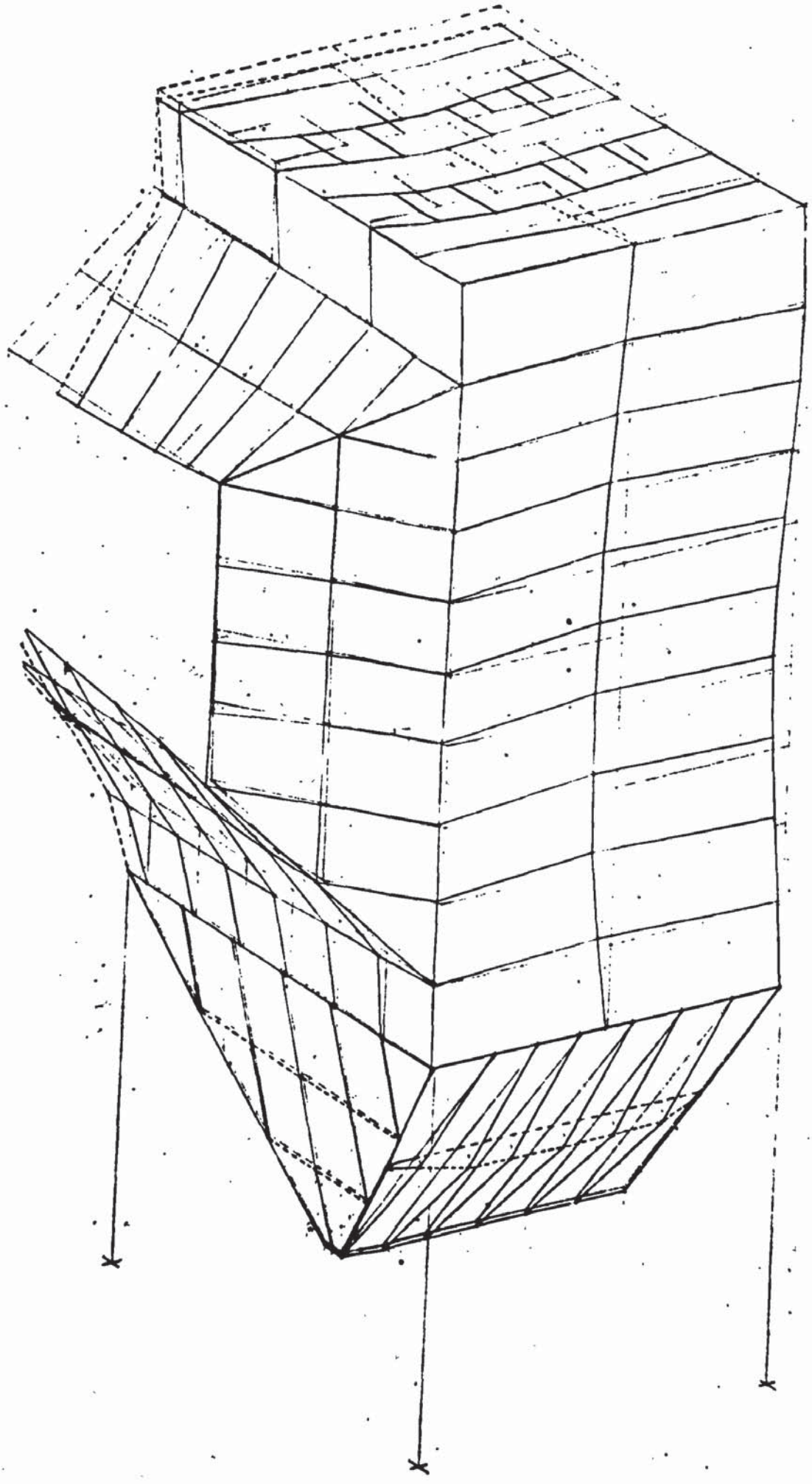

PLATE 6.6. DEFLECTED FORM OF FILTER DUE TO DEAD LOADING.

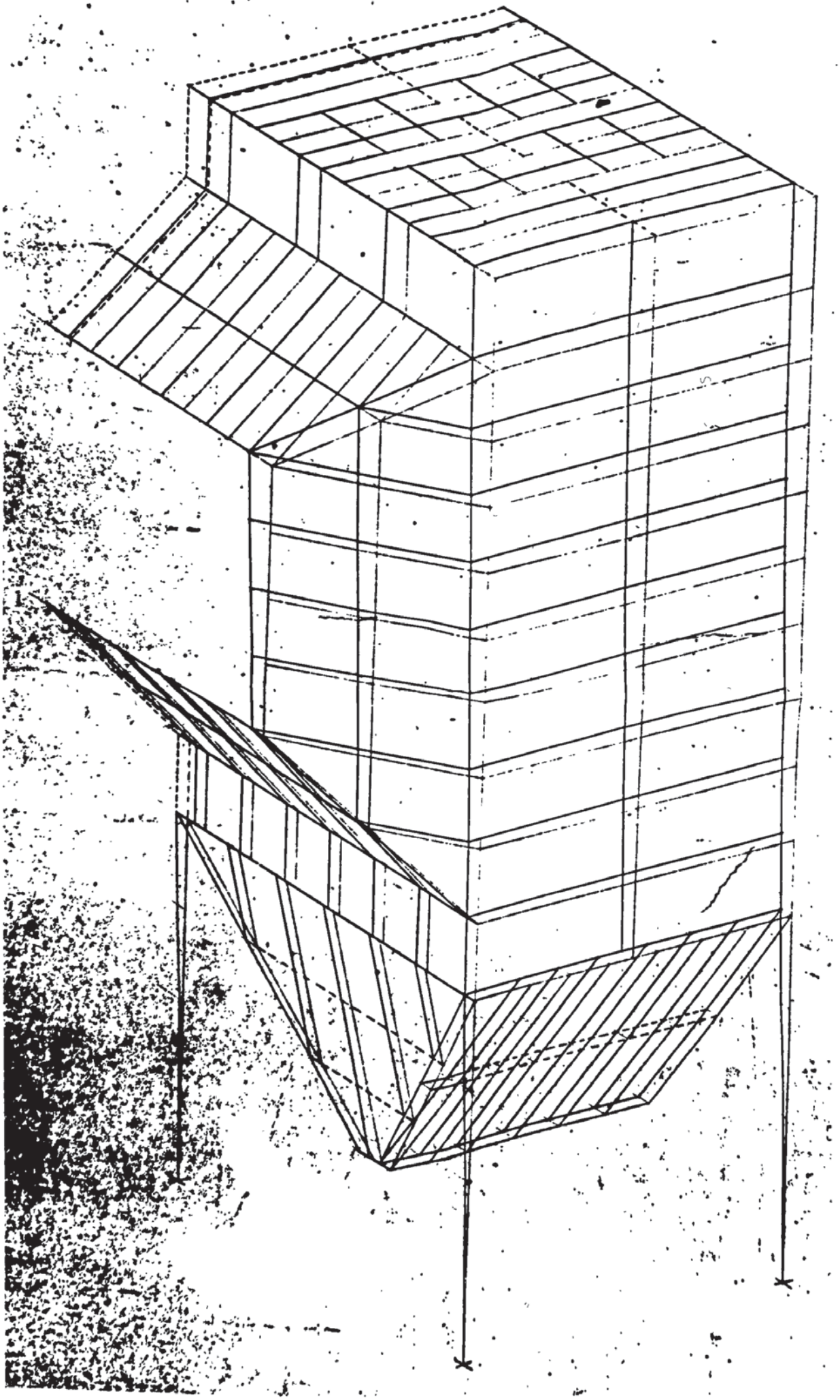

PLATE 6.7. DEFLECTED FORM OF FILTER DUE TO WIND LOADING

appear to be a drawback of the tridiagonalisation process where irregular grouping is necessary and care must be taken in the division of the structure.

CHAPTER 7

NONLINEAR ANALYSIS OF A FOOTING LOADED ON A SAND MASS

7.1. Introduction

This chapter describes a complete method of analysing the deformation of a footing when loaded on a sand mass. An experiment was carried out to investigate the validity of the theory and a comparison is also made of the strain distribution throughout the medium.

The next section deals with the theoretical justification of the stress-strain relationship which was used in conjunction with the nonlinear analysis programs described in chapter 4. The properties of the sand are next established by testing specimens in a specially designed triaxial apparatus.

Section 7.4 deals with the laboratory testing of the footing itself and is followed by the computational analysis and comparison of results.

7.2. Stress-Strain Relationship for Sand.

For the elastic-plastic analysis of a continuous isotropic material such as steel, the elastic range is well defined and its extent can be determined with the use of a Yield criterion. This is usually a function of the principal stresses which defines a yield surface beyond which additional plastic deformation will take place. This criterion can be used in conjunction with a flow rule, which determines the extent of plasticity which has taken place, to analyse such continua. It is generally accepted that, for such materials, a purely hydrostatic stress causes change in volume and a deviatoric stress, change in shape. Also it is usually proposed that failure will not take place under hydrostatic stress. For the case of sand which is a cohesionless granular medium there exist certain

basic differences which make this type of analysis impracticable. Firstly, there is no well defined elastic range of a conventional form. Secondly, due to its granular nature, sand will dilate on the application of shear force and therefore volume change will take place.

In order to define the state of stress in a continuum a three dimensional principal stress space can be used as shown in fig. 7.1. This shows the three principal stresses s_1, s_2 and s_3 as axes and any condition of stress can be plotted as a point P which is given in the figure. A line can be constructed passing through the origin which is equi-angular to the axes. This is called the space diagonal and on this, $s_1 = s_2 = s_3$. Any plane, on which P lies, which is at right angles to the space diagonal, is called the octahedral plane. Such a plane cuts the space diagonal at some point P^1. Using the octahedral plane and the space diagonal, the condition of stress at any point in a body can be represented by OP^1, PP^1 and an angle θ, relative to one of the axes. The line OP^1 represents the amount of hydrostatic stress and PP^1 the deviatoric stress. It can be shown that,

$$OP^1 = \sqrt{3}\sigma_{oct}$$
$$PP^1 = \sqrt{3}\tau_{oct} \qquad (7.1)$$

where σ_{oct} and τ_{oct} represent the octahedral normal and shear stresses respectively. Also,

$$\sigma_{oct} = \frac{s_1 + s_2 + s_3}{3}$$
$$\tau_{oct} = 1/3\sqrt{(s_1-s_2)^2 + (s_2-s_3)^2 + (s_3-s_1)^2} \qquad (7.2)$$

The corresponding octahedral normal strain and shear strain, which are denoted by ϵ_{oct} and γ_{oct}, are defined as:-

$$\epsilon_{oct} = \frac{e_1 + e_2 + e_3}{3} \qquad (7.3)$$

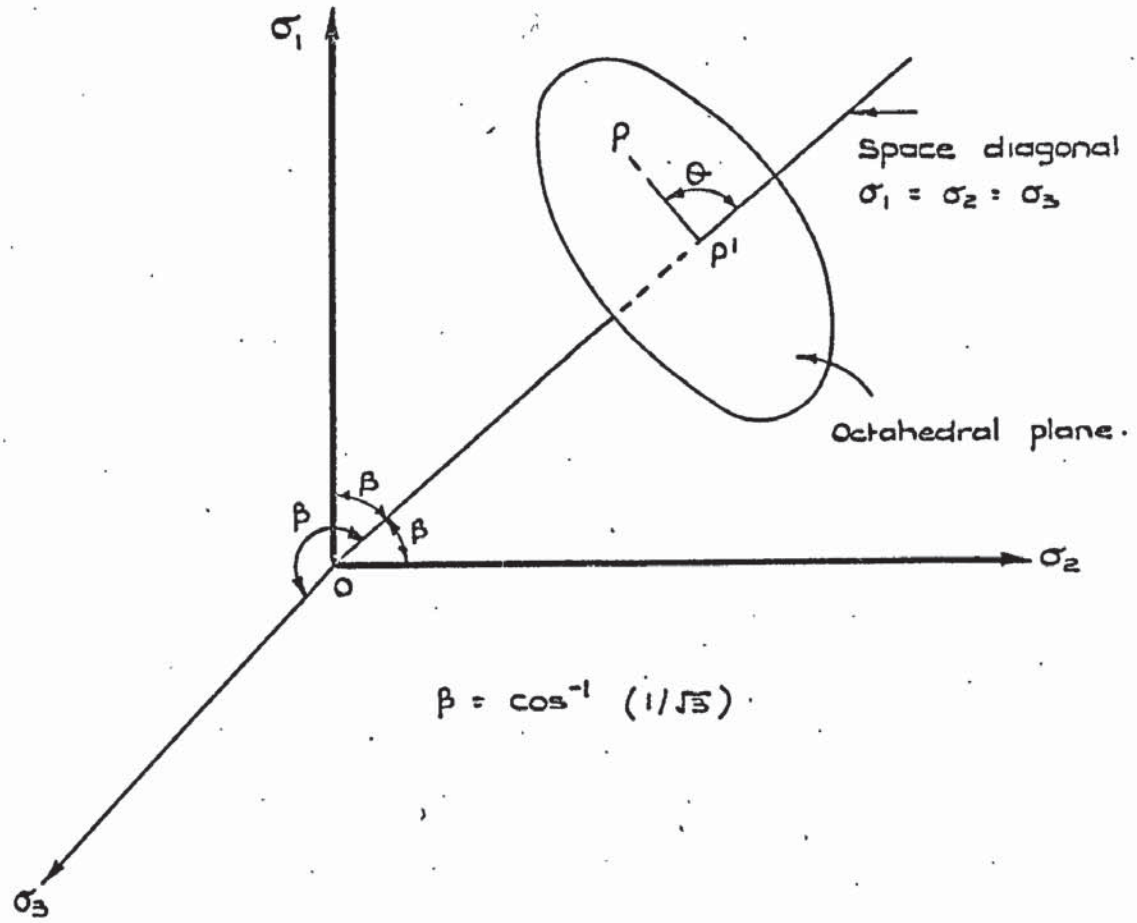

FIGURE 7.1. THREE DIMENSIONAL STRESS SPACE

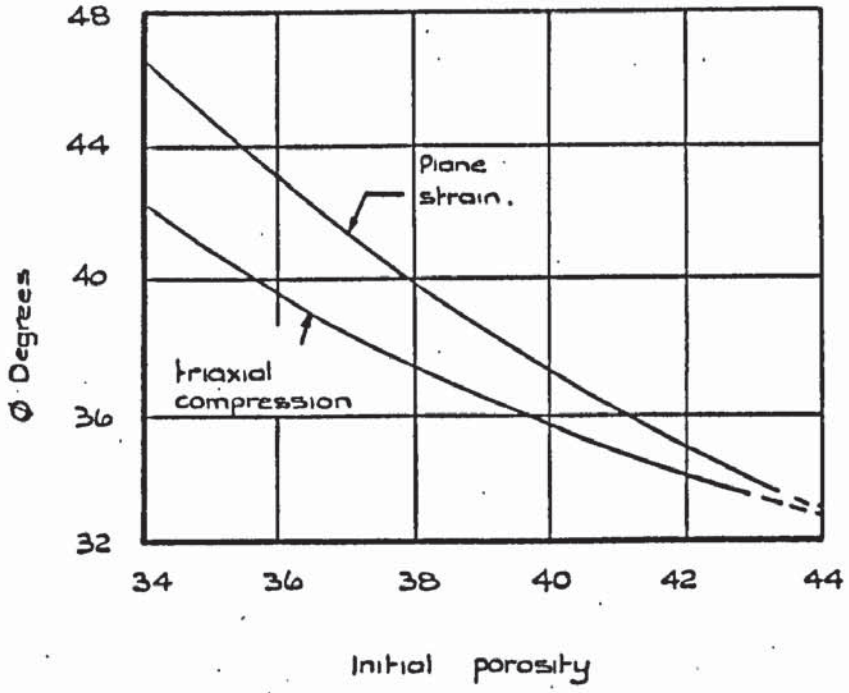

FIGURE 7.2. COMPARISON OF PLANE STRAIN AND TRIAXIAL RESULTS

$$\gamma_{oct} = 2/3\sqrt{(e_1-e_2)^2 + (e_2-e_3)^2 + (e_3-e_1)^2}$$

where e_1, e_2 and e_3 are principal strains. One of the advantages in the use of these quantities is their relationship with material constants.

$$\sigma_{oct} = 3K\epsilon_{oct}$$
$$\tau_{oct} = G\gamma_{oct} \qquad (7.4)$$

where K and G are the bulk and shear moduli respectively and:-

$$K = \frac{E}{(1-2\nu)}$$
$$G = \frac{E}{2(1-\nu)} \qquad (7.5)$$

The bulk modulus, K, is the measure of compressibility of the medium while, G, measures its deformability.

If a specimen of sand is loaded hydrostatically in a triaxial testing machine it is noticed that after a small initial volume change the sand will behave as virtually incompressible for higher pressures. Whereas if a deviatoric stress is applied in the form:-

$$s_1 > s_2 = s_3$$

then large deformations and failure will occur. It can be concluded therefore that the greatest part of deformation in sand is due to the deviator stress and the sand behaves incompressibly under hydrostatic stress.

In using a yield criterion to determine the failure of a material it would seem reasonable to assume that the function of the stresses would also govern the deformation characteristics until, at failure, the medium becomes unstable. A material such as sand can be considered to be yielding continuously. Therefore the stress path of the sand is passing through a series of failure envelopes and the deformation of the sand will depend on the yield criteron which is obeyed.

A substantial amount of work has been done in the investigation of various criteria for the limit analysis of soil mechanics problems.

Even so, for the majority of this, the testing of sands has been limited to the well known triaxial testing in which the conditions exist that $s_1 > s_2 = s_3$. The main criteria under consideration are:-

1. Mohr-Coulomb criterion. Mathematically this can be stated as:-

$$s_1 - s_3 = \text{Sin } \phi \ (s_1 + s_3) \qquad (7.6)$$

2. Extended Tresca criterion:-

$$s_1 - s_3 = \alpha(s_1 + s_2 + s_3)/3 \qquad (7.7)$$

3. Extended Von Mises criterion:-

$$\sqrt{(s_1-s_2)^2 + (s_2-s_3)^2 + (s_3-s_1)^2} = \alpha(s_1+s_2+s_3)/3 \qquad (7.8)$$

As the soil which is to be investigated is dry sand the influence of pore pressure can be neglected and no differentiation is made between total and effective stress. It is also assumed that:-

$$s_1 > s_2 > s_3$$

The Mohr-Coulomb failure criterion is perhaps the most commonly used for the investigation of triaxial conditions and is found to be reliable. The quantity $\sin\phi$ is a constant for the material. The extended Tresca and extended Von Mises criteria are both similar to the ones usually applied to isotropic continua but now differ in that they contain the influence of the so called mean stress or octahedral normal stress. Hence, in the case of the Von Mises yield criterion the yield surface changes from a cylindrical shape, passing through the origin, to a conical shape with its apex at the origin. Again, α is a constant.

It is apparent that these latter two criteria are the only ones to include the influence of the intermediate principal stress s_2. The Mohr-Coulomb criteron includes no terms involving s_2 and therefore assumes no difference between the axysmmetric conditions which exist in the triaxial test and the plane strain conditions. From the rather limited data available on plane strain testing, Bishop (52) made a comparison of the two conditions. Fig. 7.2 shows a graph of ϕ, which can be regarded as

the strength, against the initial porosity of sand for the two conditions of plane and axysymmetric strains. It can be seen that its strength in plane strain is consistently higher, especially as the porosity decreases. The sand used in the model testing, which will be described later, is medium dense and also will have a rather low porosity. There was no apparatus available to measure ϕ in plane strain and thus the graph shown in fig. 7.2 indicates that, if the Mohr-Coulomb yield criterion were used, then the results would probably be an underestimation of the soil strength.

By rearranging equations (7.6 - 7.8) a comparison of the three criteria can be made regarding the strength of the material as influenced by variations of the intermediate principal stresses. This is shown in fig. 7.3 where ϕ is now plotted against the ratio $\frac{s_2 - s_3}{s_1 - s_3}$. It is noticed that when $s_1 = s_2$ this ratio will equal unity. On the other hand when $s_3 = s_2$ as is the case under triaxial conditions, then this ratio equals 0. All three criteria give the same value under triaxial conditions for a dense sand where $\phi = 40^{\circ}$ and $\alpha = 1.636$. Three measured values are shown on the graph. These are for compression, plane strain and extension conditions. It is seen that for the condition of plane strain, the Extended Tresca or Von Mises criterion gives the better results but, these do not give meaningful results for an extension test. This is perhaps the major drawback of these two criteria. This is explained by consideration of the differing failure surfaces as seen when viewed from a point on the space diagonal. This is shown in fig. 7.4 in which plane D_1, D_2, D_3 is coincident with the octahedral plane and its apexes lie on the s_1, s_2 and s_3 axes respectively. The crossections of the three criteria take the form of an irregular hexagon, a regular hexagon and a circle for the Mohr-Coulomb, Extended Tresca and Extended Von Mises respectively. These are shown in the figure where it is noticed that the Extended Von Mises and Extended Tresca failure envelopes pass outside the boundaries of D_1 D_2 D_3 as shown by the dotted lines.

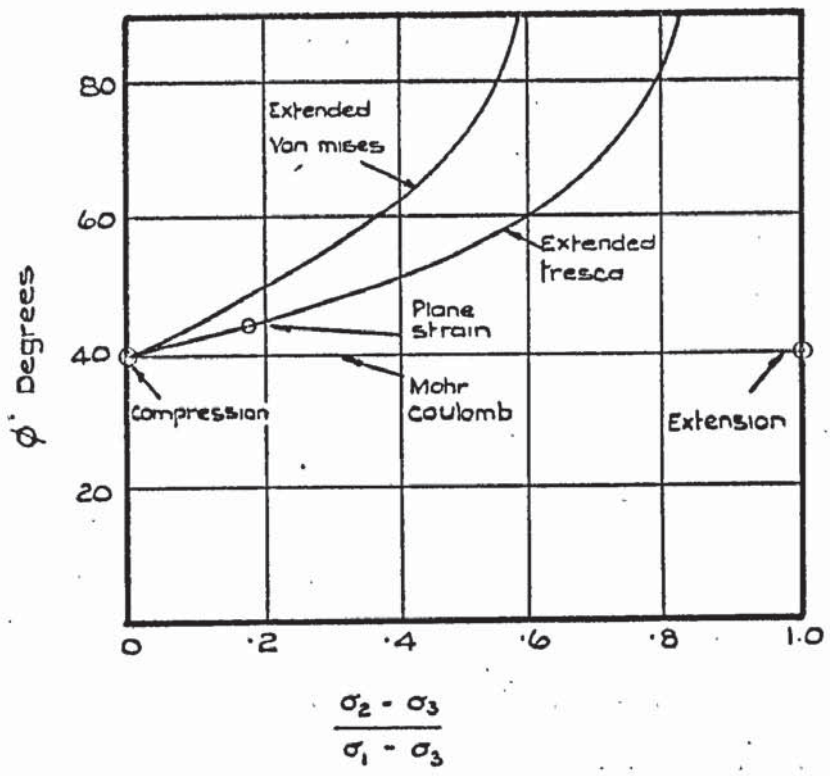

FIGURE 7.3 OBSERVED AND PREDICTED VALUES OF ϕ'

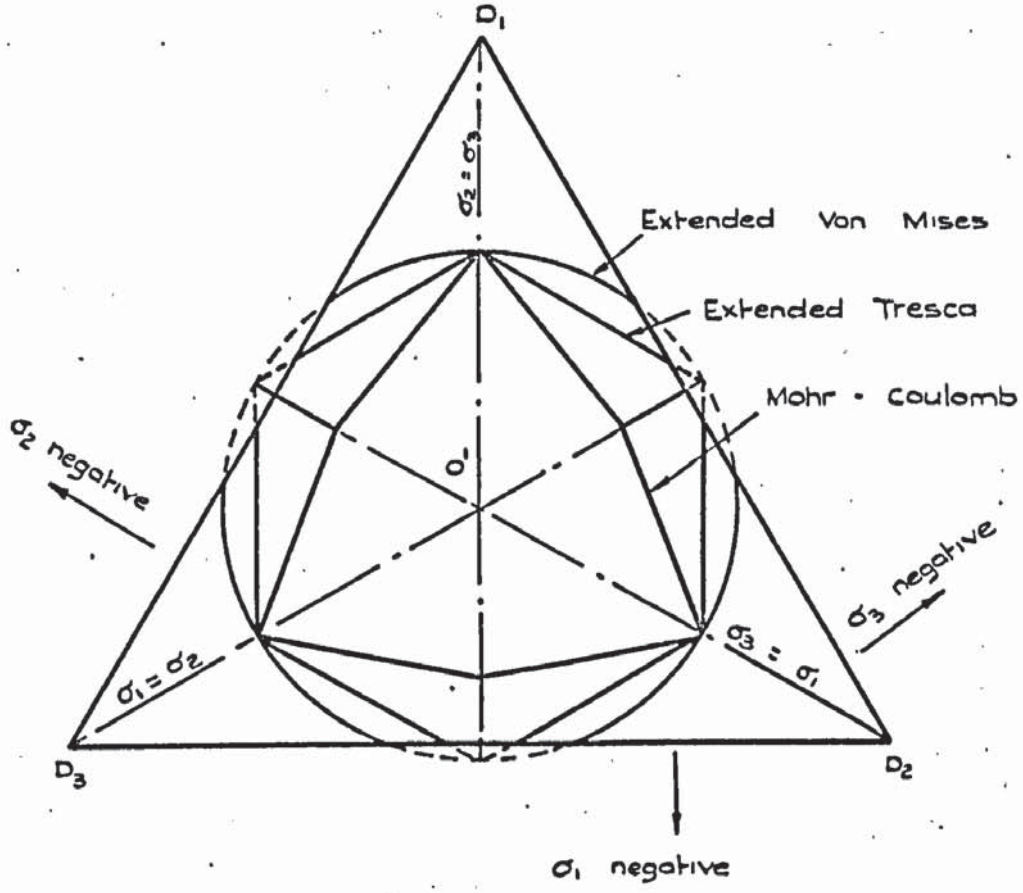

FIGURE 7.4 FAILURE CRITERIA IN PRINCIPAL STRESS SPACE

They are therefore in negative stress space in these regions. As a cohesionless soil such as sand cannot withstand any tension this state of stress cannot exist.

Only triaxial test results were available and it was desirable to choose one of the criteria which included the influence of the intermediate principal stress. These two were very alike and there was little to choose between them. As there was little evidence to suppose that the yielding in sand would depend on a third parameter, such as θ of fig. 7.1, it was decided to use the Von Mises criterion.

The deformation in sand is primarily due to shear strain and it was assumed that the shear stress would cause the total change in volume whereas the sand was virtually incompressible under hydrostatic stress. From equation (7.5) it can be shown that Poisson's ratio should not be greater than half. However, the finite element method in plane strain is limited to a Poisson's ratio of not more than 0. 48, as will be shown later. It follows that the value of $\frac{s_2 - s_3}{s_1 - s_3}$ in fig. 7.3 will never be greater than .5.

Other researchers (55) have suggested that the settlement of footings is mainly due to shearing action and therefore for this and the reasons given above it was decided to base the stress-strain relationship on the shear modulus. It is well known experimentally that the deformation of a triaxial specimen is linearly dependant on the confining pressure. Therefore there would be a unique nonlinear relationship between the quantity $(s_1 - s_3)/s_3$ and the axial extension e_1 for triaxial specimens which are loaded under different cell pressures. In a similar manner therefore, use can be made of equation (7.4) to determine the shear modulus by plotting the quantity $(\frac{\tau_{oct}}{\sigma_{oct}})$ against γ_{oct}. This should give a unique relationship for the computation of the shear modulus. As can be seen

from equations (7.2) and (7.8) this stress ratio is the same as that of Von Mise's. Once the shear modulus has been found the Young's Modulus can be obtained from equation (7.5).

The experimental testing involved in establishing such a relationship and the calculation of Poisson's ratio are now described.

7.3 Triaxial Testing

The model footing whichwas to be analysed was 4" in width and situated on dry medium dense sand. It was estimated that a horizontal pressure of not more than 3-4 psi could be expected under the footing. It was thought necessary to test at this order of confining pressure in a triaxial machine. Although it is known that shearing is linearly proportional to confining pressure at higher pressures, this may not be the case for the very low values expected here.

7.3.1 Apparatus and Testing

The normal triaxial testing machine is designed for cell pressures of about 15-30 psi at the lowest and to test in a range of 0-4 psi would be impracticable due to the frictional problems occurring around the loading system. In order to overcome this an apparatus was developed in such a way that an internal suction was applied to the sample instead of an externally applied cell pressure. Thus low pressures of around .25 psi could easily be simulated in the sample. This apparatus is shown in plate 7.1.

A conventional triaxial cell base was used to hold a 4" diameter sample. This was sealed in a rubber membrane and held between the base plate and top cap by rubber 'O-rings'. The top cap was made from Perspex, 1" thick and 4" diameter. The loading hanger was screwed into this by means of a previously drilled and tapped hole. The hanger assembly was made from Aluminium so as to be as light as possible. This consisted of two crosses of Aluminium jointed together by 3/16" diameter steel rods which were threaded at either end so that the assembly could be dismantled after

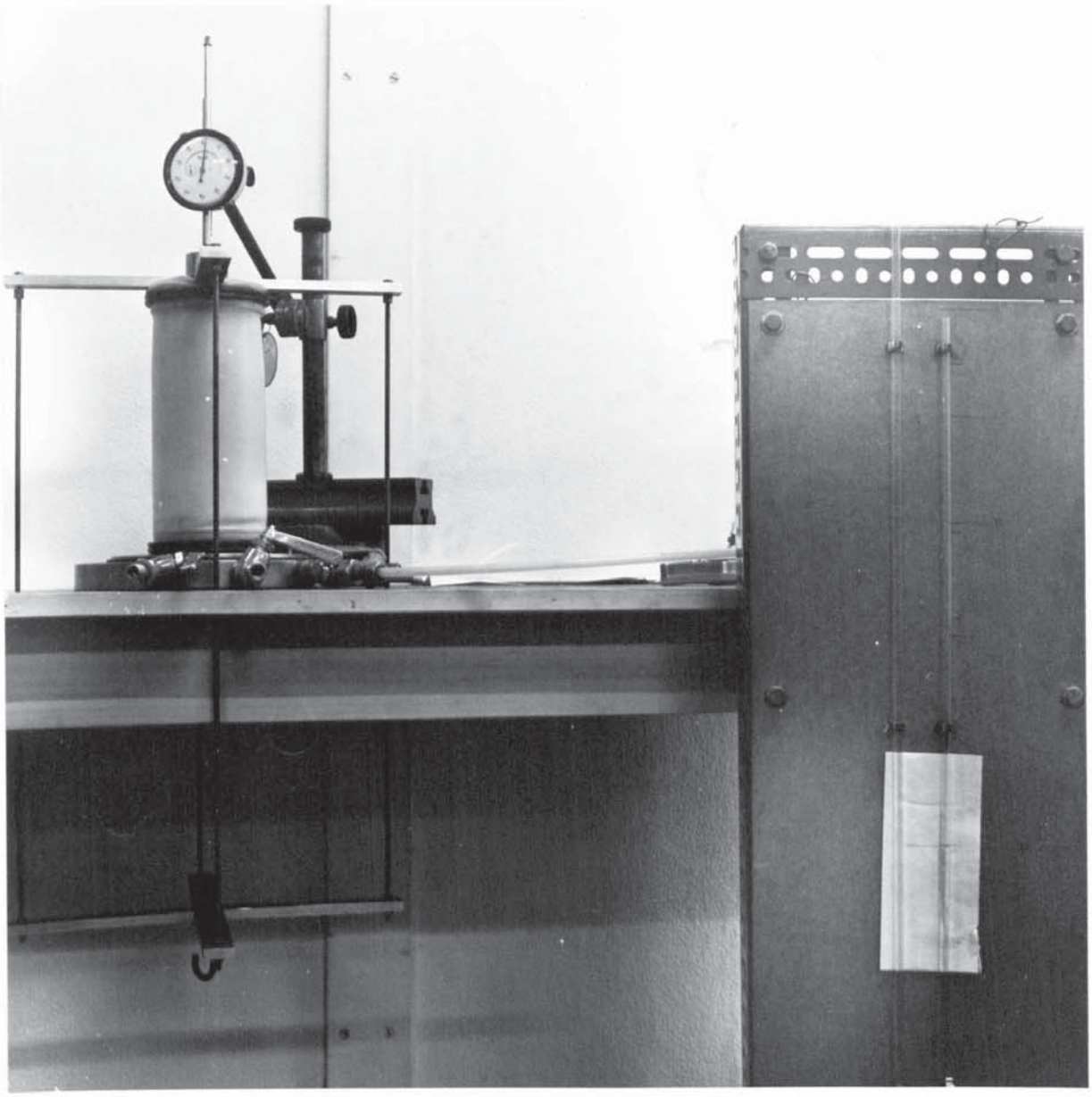

PLATE 7.1. TRIAXIAL APPARATUS

each experiment. The hanger took the form of a cage and the rods passed through specially made holes around the base plate. As shown the lower cross had a hook welded to its underside so that a normal hanger could be used to apply the weights. This arrangement prevented any tilting of the top cap which might occur on loading, thus keeping it horizontal. A 2" dial gauge was positioned on the top cap to record the vertical deflection.

The central drainage hole in the base plate was connected to a manometer shown in the right of the photograph. A suction could thus be applied to the sample through the right hand arm and its magnitude measured by the head of water which was raised in the manometer. All the joints were well covered with Vaseline to ensure that there were no air leaks.

The sand sample was prepared in an 8" high Brass former which was lined with the rubber membrane. A $\frac{1}{4}$" thick porous stone was positioned at the base. The testing density decided upon was 100 p.c.f. and moderate tamping was necessary to achieve this. The specimen was first weighed and then attached to the apparatus by securing the membrane to the base plate with 'O-rings'. The top cap and hanger assembly were similarly attached and the dial gauge was positioned. The required suction was then applied to the sample through the manometer and this was maintained for about 10 minutes in order to ensure that there were no air leaks. The hanger was propped up and the Brass former unclipped and removed. The height of the sample was measured with a rule and its radius checked with calipers. These measurements were later used in the accurate calculation of the density.

When the hanger was unpropped, this acted as the first load increment and from thereon the loads were applied in 1 lb. intervals allowing half a minute between each loading. At the same time the change in height in the manometer was recorded so as to give a measure of the volumetric change in the specimen. The height was then readjusted to its original value before

the next loading so that the suction remained constant. The vertical deflection was also measured with the dial gauge. All the specimens failed in shear and plate 7.2 shows a typical case for the higher cell pressure. The density of 100 p.c.f. was used as loose sands tend to be unstable and too dense a sand also becomes impracticable for laboratory tests. These tests were carried out on similar samples at cell pressures of $\frac{1}{4}$, $\frac{1}{2}$, 1 and 2 psi. Testing was found to be impracticable outside this range. From the dimensions and weight, the density of the specimen was first calculated. The internal diameter of the manometer was measured with a travelling microscope so that its area and hence the volume change at each load increment could be measured.

7.3.2 Results

For triaxial conditions, it can be shown from equations (7.2 and 7.3) that:-

$$\tau_{oct} = \frac{\sqrt{2}}{3}(s_1 - s_3)$$

$$\sigma_{oct} = (s_1 + 2s_3)/3 \qquad (7.9)$$

$$\gamma_{oct} = 2\sqrt{2}\, e_1(1+\nu)/3$$

where e_1 is the axial strain and Poisson's ratio is calculated from the volumetric strain $\frac{\Delta v}{v}$ which was also measured. This is given by:-

$$\frac{\Delta v}{v} = e_1 + 2e_2$$

Therefore:-

$$\nu = \tfrac{1}{2}\left(1 - \frac{\frac{\Delta v}{v}}{e_1}\right) \qquad (7.10)$$

As soon as the sand began to dilate due to shearing the value of Poisson's ratio was taken to be constant at a half.

From equations (7.9) and 7.10) it was possible to plot graphs of $\left(\frac{\tau_{oct}}{\sigma_{oct}}\right)$ against γ_{oct} for the various values of initial cell pressure. These are shown in fig. 7.5. As s_1 is increased in the test so was σ_{oct}

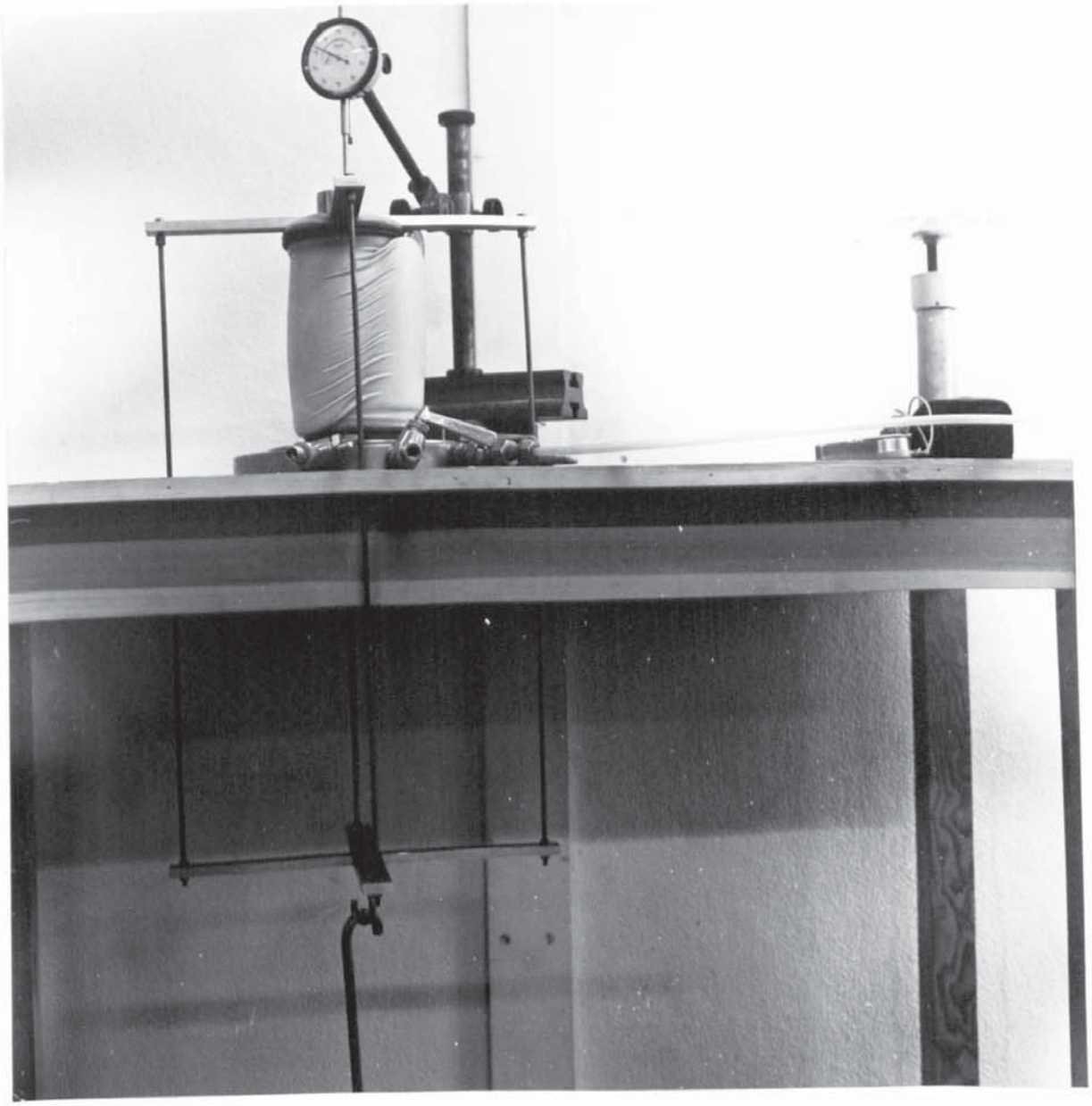

PLATE 7.2. FAILURE OF TRIAXIAL SPECIMEN

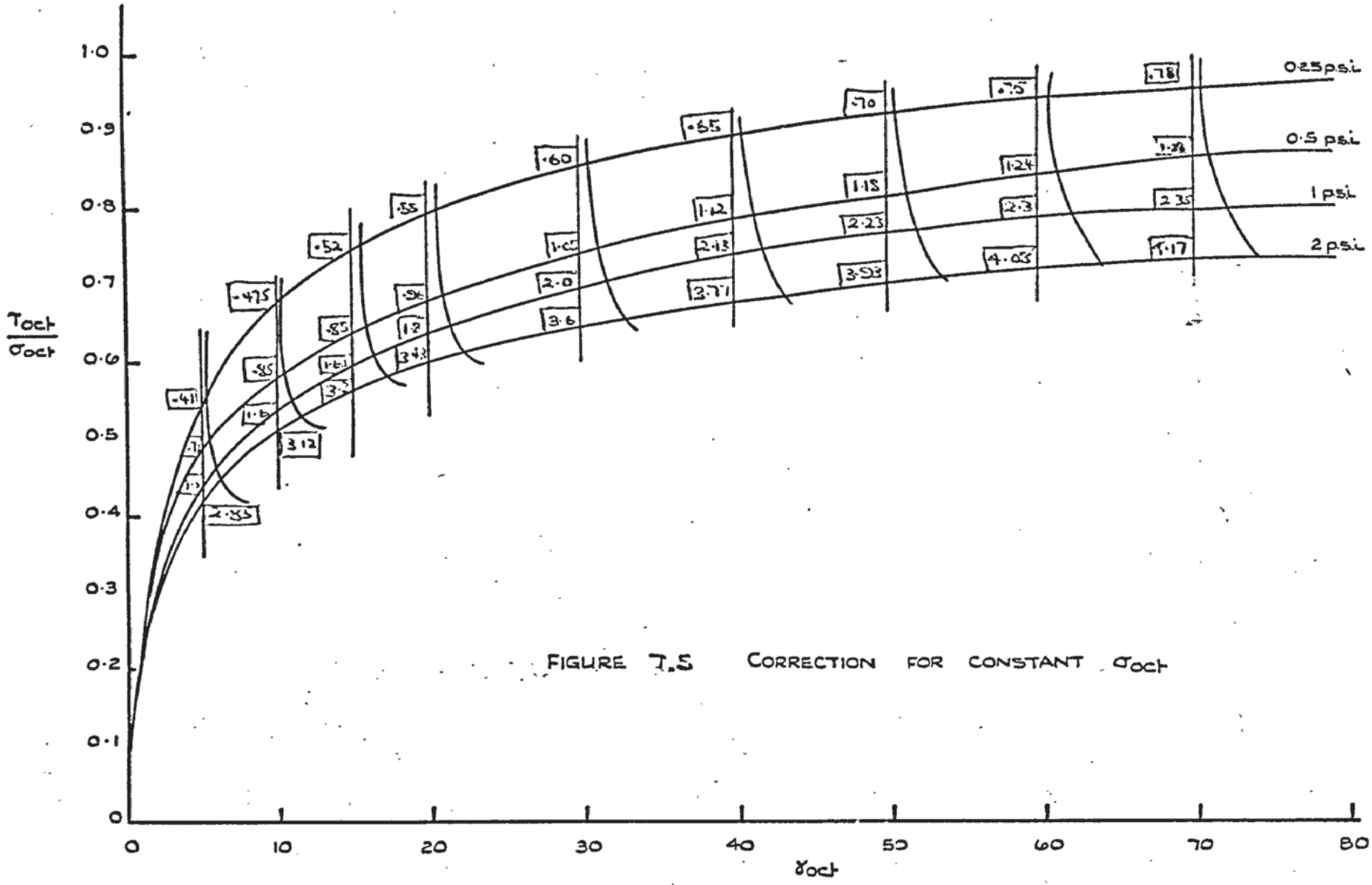

FIGURE 7.5 CORRECTION FOR CONSTANT σ_{oct}

and therefore these curves need to be corrected so as to represent values at a constant σ_{oct}. This is necessary as the value of σ_{oct} will also vary substantially under the footing as it is loaded and the instantaneous value of σ_{oct} will be calculated for use with these curves. To achieve this, a graph of instantaneous σ_{oct} against γ_{oct} was drawn and these values plotted on the original curves. At various values of γ_{oct} the instantaneous σ_{oct} values were plotted for each curve horizontally. These are shown in the square boxes in fig. 7.5. The best curve was then drawn through these points so that a particular value of σ_{oct} could be found on the curve. At these values of γ_{oct} values of the instantaneous σ_{oct} at .5, .75, 1, 2, 3 psi were marked and points of equal σ_{oct} joined together to give the new curves of $\frac{\tau_{oct}}{\sigma_{oct}}$ against γ_{oct} for values of constant σ_{oct}. These are shown in fig. 7.6. It is apparent now that this graph does not give a unique curve. The curves at the lower confining pressures become rather more divergent, whereas, as the pressure increases, the curves would appear to converge which may suggest that in the normal range of testing they might well be unique.

It would have been possible to input this family of curves into the computer and then use the appropriate curve depending on the value of octahedral normal stress which was required but, to save added computation it was decided that a more satisfactory solution would be arrived at by applying a corrective function in order to give a unique curve. It can be seen that, for this pressure range, σ_{oct} is not linearly proportional to the strength so this function will be of σ_{oct} such that the graph of $f_n(\sigma_{oct})\ (\frac{\tau_{oct}}{\sigma_{oct}})$ against γ_{oct} will be unique for all confining pressures. This variation of σ_{oct} would appear logarithmic and hence, in order to establish this empirical function, a graph of $\log_e(\sigma_{oct})$ against $\frac{\tau_{oct}}{\sigma_{oct}}$ was

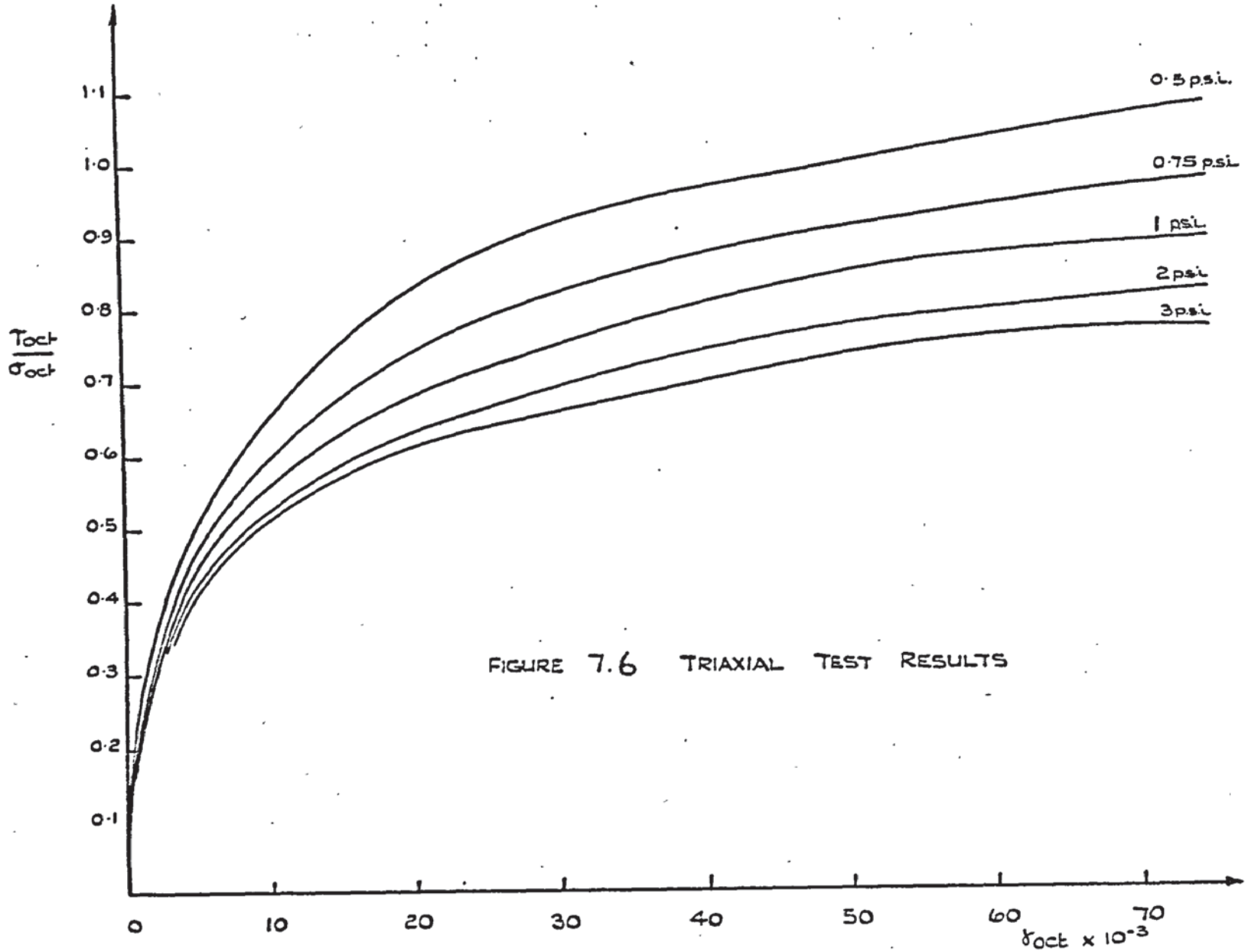

FIGURE 7.6 TRIAXIAL TEST RESULTS

drawn for positions of constant γ_{oct} varying between .5-7 as shown in fig. 7.7. These are seen to be almost parallel for values of σ_{oct} above 1. Below this value the variation is more marked but these results are less reliable due to their more difficult interpolation from fig. 7.5. As this value of σ_{oct} was about the average that was expected in the model it was decided to form a function to make the curves converge on that of $\sigma_{oct} = 1$. The average slope of the curves $\frac{\Delta\gamma_{oct}}{\sigma_{oct}} / \log_e \sigma_{oct}$ was found to be .145 and therefore the function which was used was:-

$$\text{fn}\ (\sigma_{oct}) = 1 - 0.145 \log_e (\sigma_{oct}) \qquad (7.11)$$

In order to check this function the curves of fig. 7.6 were replotted in the form of $\text{fn}(\sigma_{oct})\left(\frac{\gamma_{oct}}{\sigma_{oct}}\right)\sigma_{oct} = 1$ against γ_{oct}. For $\sigma_{oct} = 1$, $\text{fn}(\sigma_{oct}) = 1$ and therefore this curve is unaltered. For $\sigma_{oct} > 1$, $\text{fn}(\sigma_{oct}) > 1$. Therefore, for this empirical function:-

$$\left(\frac{\gamma_{oct}}{\sigma_{oct}}\right)\sigma_{oct} = i = \text{fn}\ (\sigma_{oct} = i)\left(\frac{\gamma_{oct}}{\sigma_{oct}}\right)\sigma_{oct} = 1 \qquad (7.12)$$

where i takes the values for these tests of .5, .75, 1, 2, 3, psi. Fig. 7.8 shows the final graph for the calculation of the stress-strain relationship. As is apparent, the function produces a unique curve for $\sigma_{oct} > 1$ but there is some divergence for values less than one. However, this is only for much higher values of σ_{oct} when failure is being approached.

Fig. 7.9 shows a graph of volumetric strain against octahedral shear strain. It is seen that all specimens start as being slightly compressible and, according to confining pressure, dilate increasingly rapidly up to failure. For a cell pressure of .25 psi dilation starts at .05% strain and for 2 psi at 1.2%. At these positions the pseudo-elastic

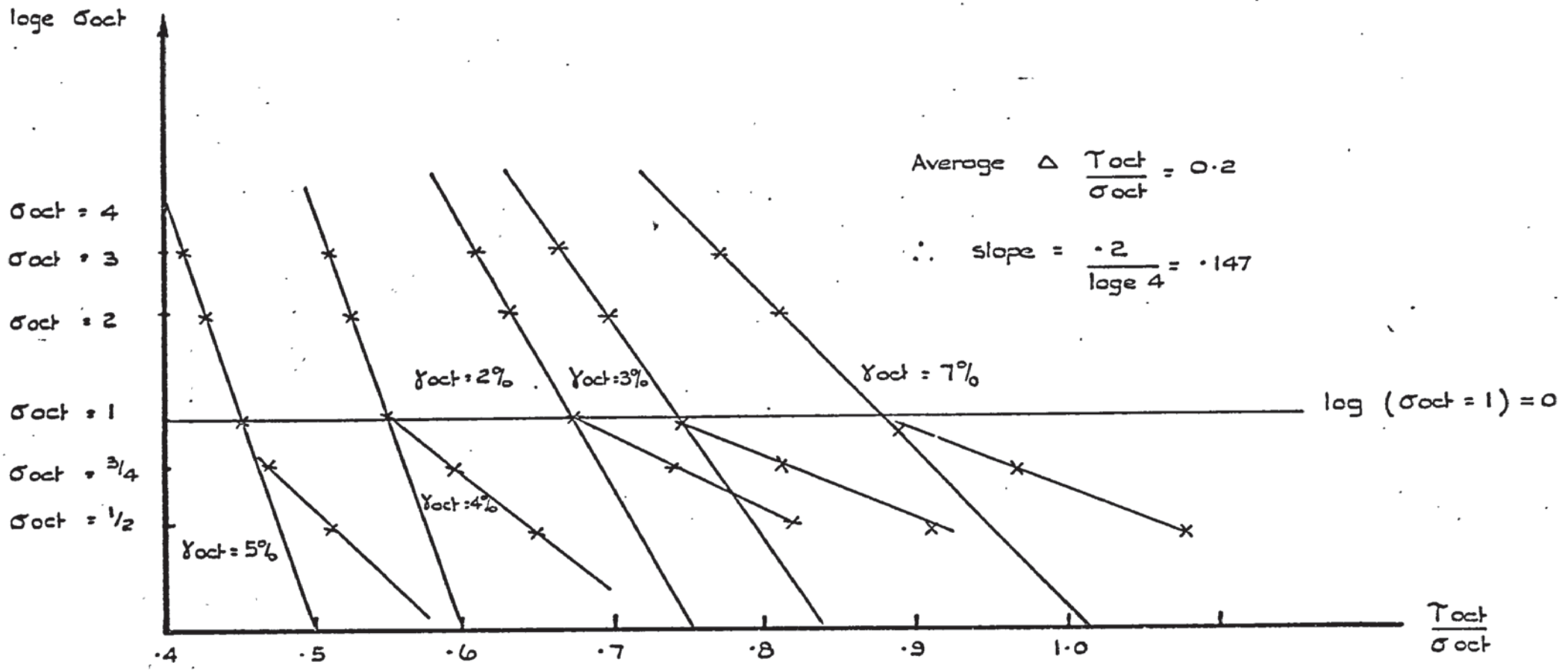

FIGURE 7.7. DETERMINATION OF FUNCTION OF σ_{oct}

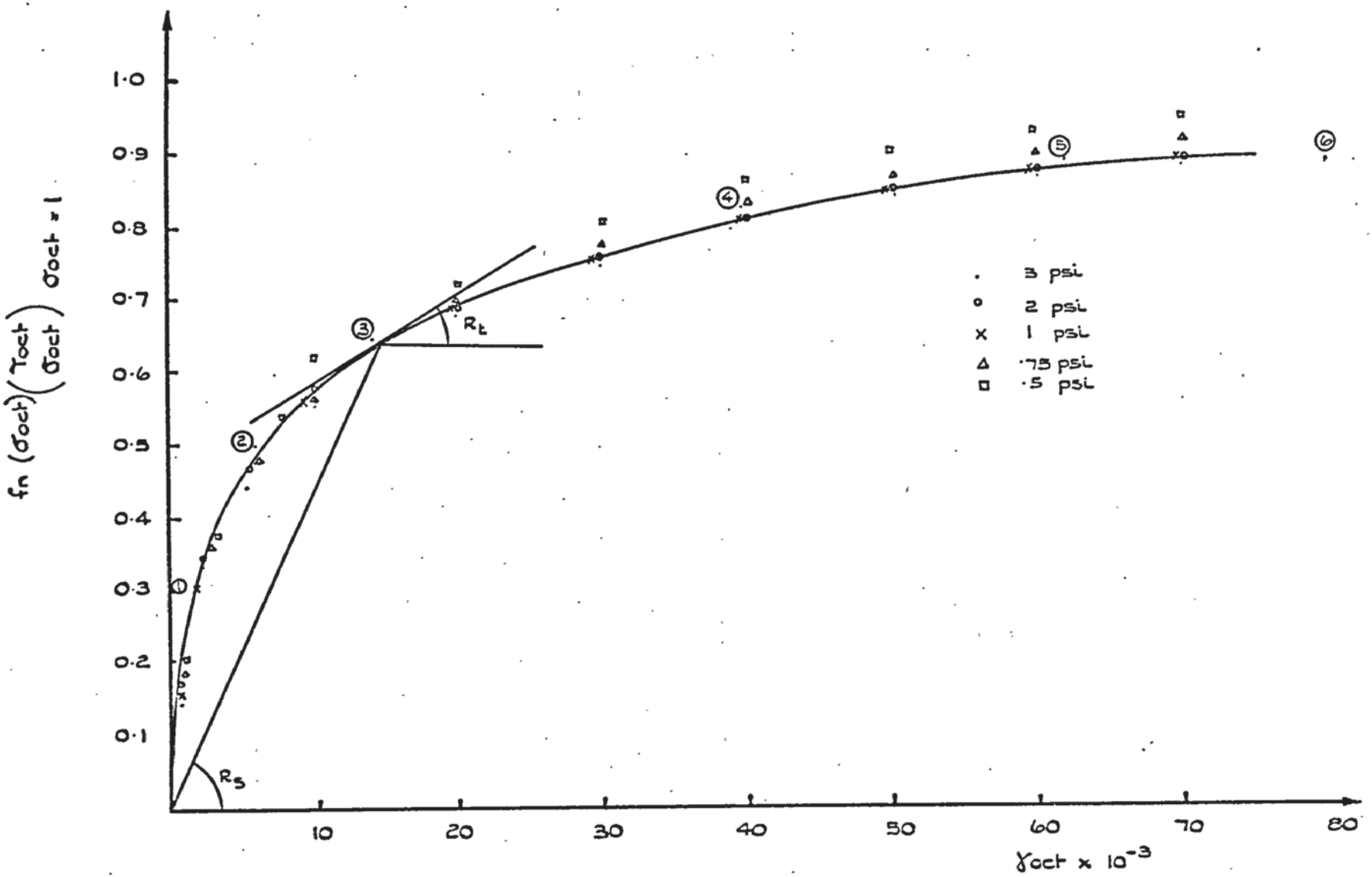

FIGURE 7.8 FINAL EMPIRICAL STRESS - STRAIN RELATIONSHIP

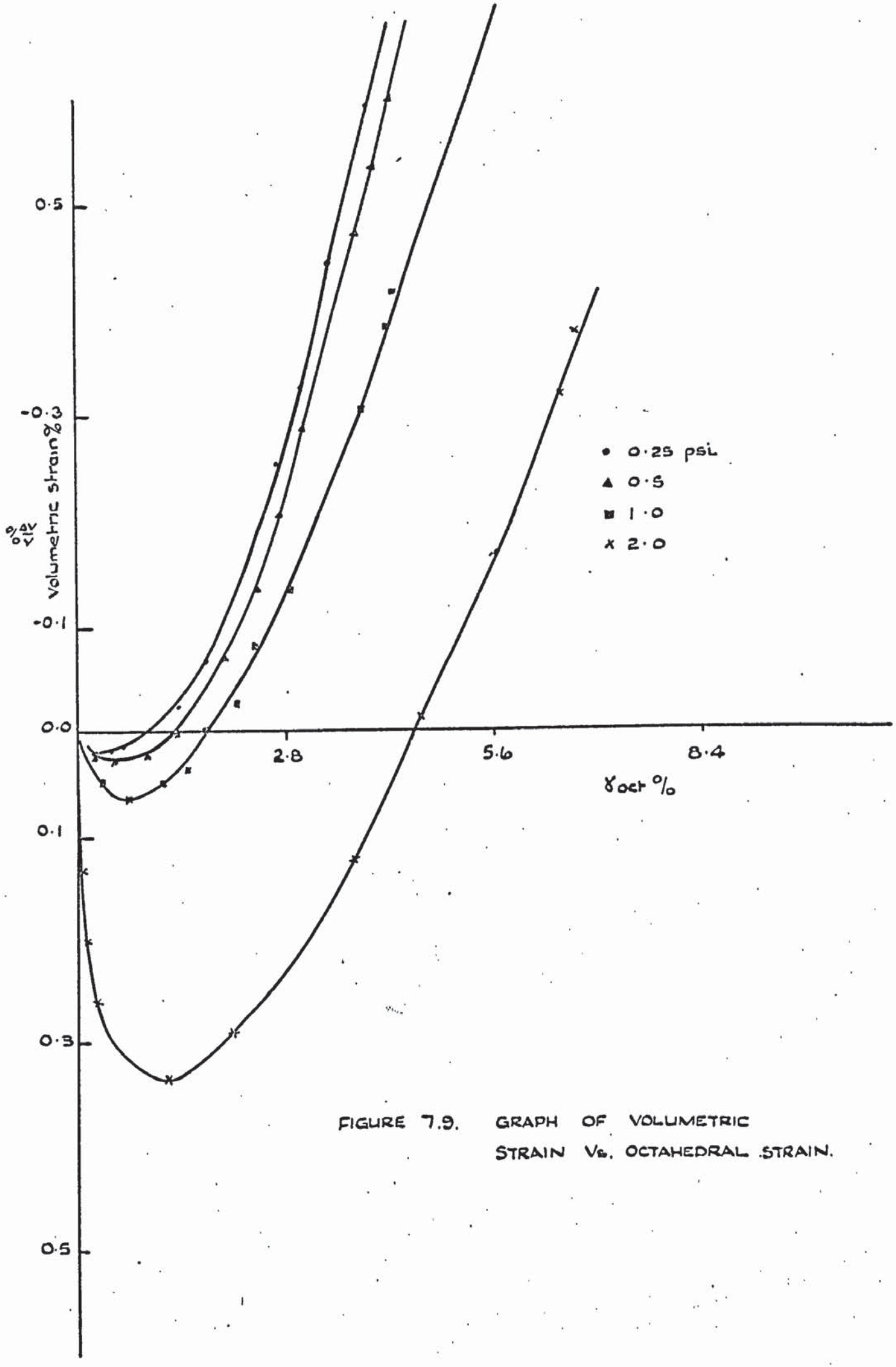

FIGURE 7.9. GRAPH OF VOLUMETRIC STRAIN Vs. OCTAHEDRAL STRAIN.

Poisson's ratio takes the value of .5. After this it increases more rapidly until, at failure, values of 2 or 3 have been recorded. This cannot be catered for, as previously mentioned,but it should be pointed out that from consideration of figs. 7.8 and 7.9 dilation does not commence until approximately 80% of peak strength has been reached and therefore the sand is near failure. The influence of dilation is therefore not as serious as it may first appear. The affect of these graphs on the calculation of the pseudo-elastic constants will be discussed in the section on the computational analysis of the model footing, but first the experimental work carried out on the footing is described in the next section.

7.4 Tests on a Model Footing

The object of the experiment was to test a strip footing over a mass of uniform dense sand under conditions of plane strain. It was required to know the load settlement characteristics of the footing and the distribution of deflection and strain throughout the sand under the footing. These were to be compared with the results of a subsequent computer analysis based on the properties of the sand which were determined in the last section.

7.4.1 Apparatus

A complete assembly of the apparatus which was used and is ready for testing is shown in plate 7.3. Basically, this consists of a tank, 30" wide, 15" in length and 38½" deep. This was filled with sand on top of which rested the model footing. At each corner of the tank stanchions were bolted to a base plate and these ran up its height and were interconnected by ¾" diameter bolts. At the top they supported the loading system for the footing. The load was applied through a 1" diameter steel rod which was driven vertically downwards by a 'constant rate of Penetration machine' as shown in the top of plate 7.3. This load was passed through a proving ring which had been previously calibrated and the central deflection of the footing was measured by a dial gauge.

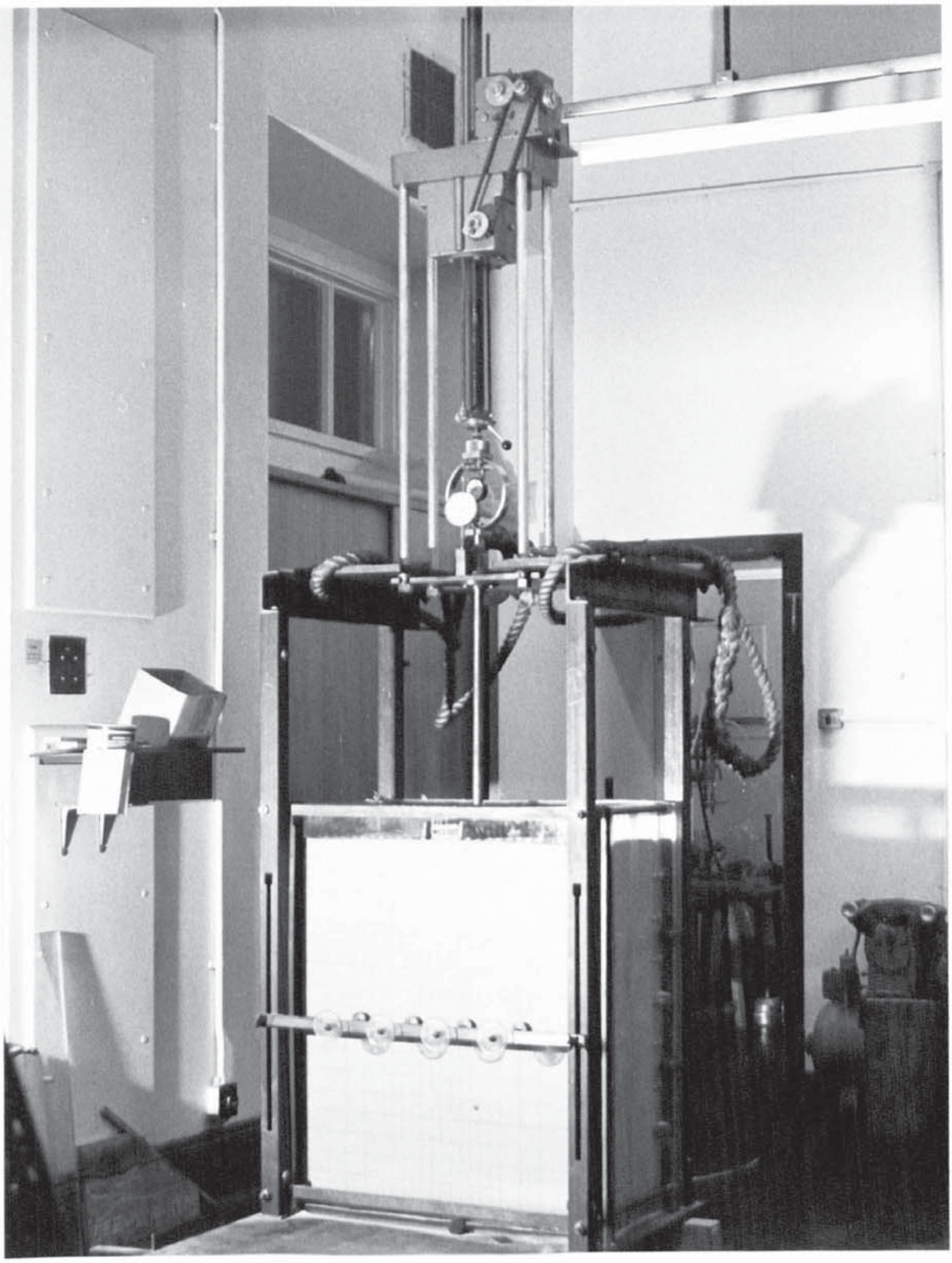

PLATE 7.3. GENERAL VIEW OF EXPERIMENTAL APPARATUS.

The main considerations given to the design of the apparatus were that:-

(i) True conditions of plane strain existed under the footing.

(ii) A reliable method of determining the strain distribution under the footing was available.

(iii) The footing would be uniformly loaded and therefore would not tilt into the sand.

(iv) The sand used would be uniformly dense and homogeneous.

In order to obtain plane strain conditions there must be no strain between the back and the front faces of the tank along the length of the footing. Furthermore, as this is a unit strip of footing, these faces must have no other influence on the experiment and must therefore be as frictionless as possible. This was achieved by using two sheets of polished plate glass as the tank faces. The front plate was $\frac{3}{4}$" thick and the back, which was also supported by a Perspex sheet, was $\frac{1}{4}$" thick. The coefficient of friction between sand and polished glass is known to be low enough and not to affect its movement. The sides of the tank should also be far enough away from the loaded area so as to have no influence on the experiment. These were of 1" thick perspex sheeting. The ratio of the width of the footing to the width of the tank was 1:7. The excessive depth of the sand is noticable but has no adverse effect on the tests. It will be shown in the results that the two sides of the tank had little or no influence on the footing. The whole tank was bolted together by bars between four 2" square steel section stanchions and further steel bars were placed across the face of the glass with adjustable spacers as shown in plate 7.3 so that no bulging of the glass face would occur.

The front two stanchions and the $\frac{3}{4}$" glass plate front were removable and on the inside of the glass a rectangular grid was drawn

with marking ink. This consisted of a 1" square grid to a depth which the loaded footing could influence. In order to be able to measure the distribution of strain throughout the sand, markers were fixed to the inside of the glass with Vaseline. This was done at every point on the grid before the sand was poured. When the apparatus was assembled and the footing loaded, the markers would be displaced with the sand. By measuring the movement, the strain can be calculated. The markers themselves were made from glass beads with a small wire 'tail', about $\frac{1}{8}$" long, which protruded into the sand and ensured that the marker gave a true representation of the sand's movement.

The model footing was made from a 4" x 2" channel section as shown in detail in fig. 7.10. This was cut so that it just fitted between the glass plates but without touching them. The edges were bevelled so that slight tilting would not cause any jamming. The inside of the channel was machined flat and two $\frac{1}{2}$" steel plates, which were separated by rollers, were used to distribute the load evenly onto the floor of the footing. A 1" diameter steel rod was attached to the penetration machine, and rounded at the end. Through this the load was applied to the footing at the mid point of the top of the $\frac{1}{2}$" plate and was located by a specially drilled indentation at this position. As the footing was so rigid, it could be assumed that this point load was evenly distributed over the whole area of the footing. It was required to develop high frictional forces between the footing and the sand. To create these a 4" strip of coarse sandpaper was glued to the underside of the footing.

The constant rate of penetration machine was attached to a steel base plate which could be disengaged from the top of the stanchions and lowered to the ground by a winch whenever access was needed for pouring sand into the apparatus. The density and uniformity of the sand depended on the speed and method of pouring. Plate 7.4 shows the sand pouring

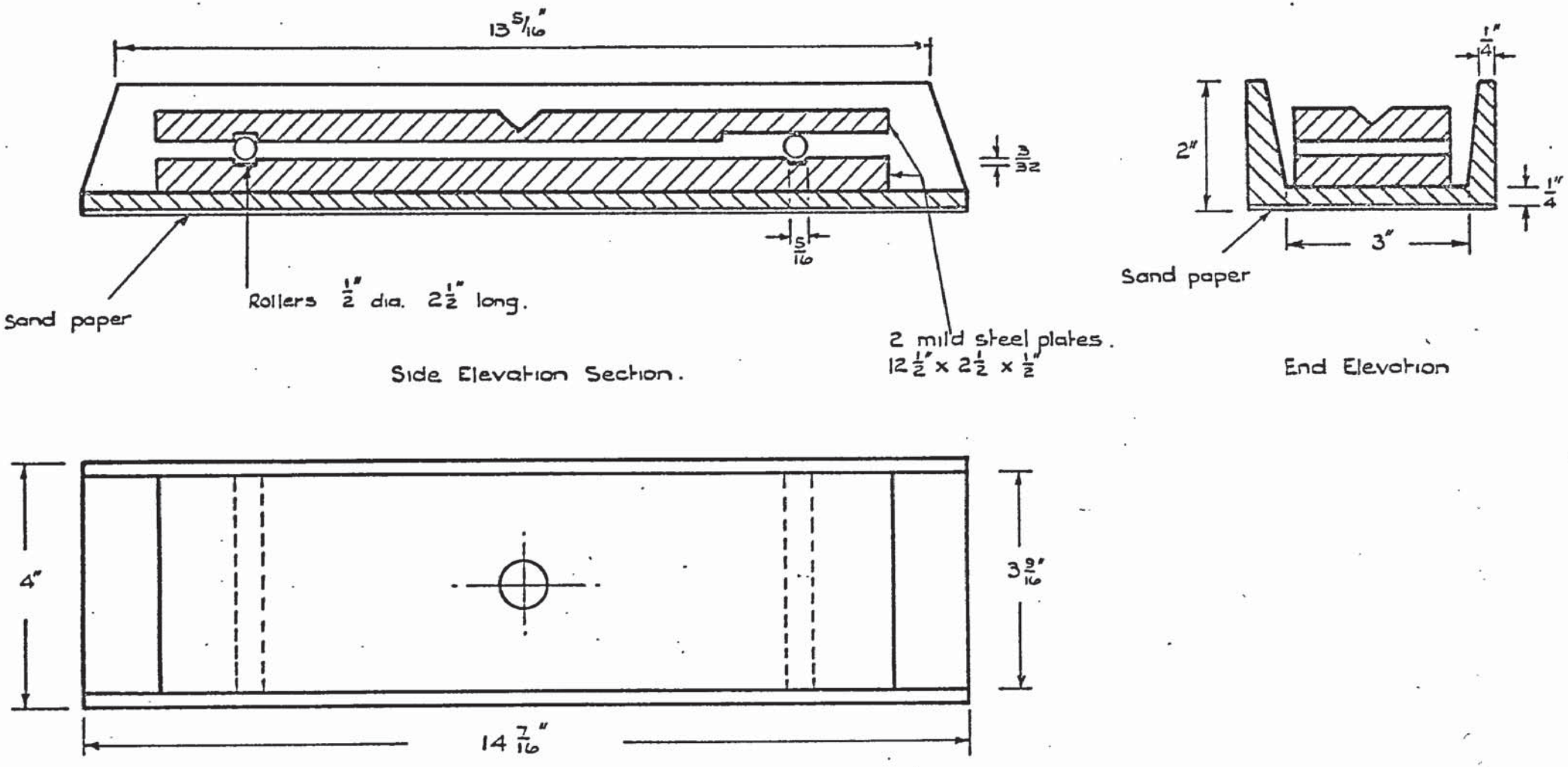

FIGURE. 7.10. DETAIL OF MODEL FOUNDATION.

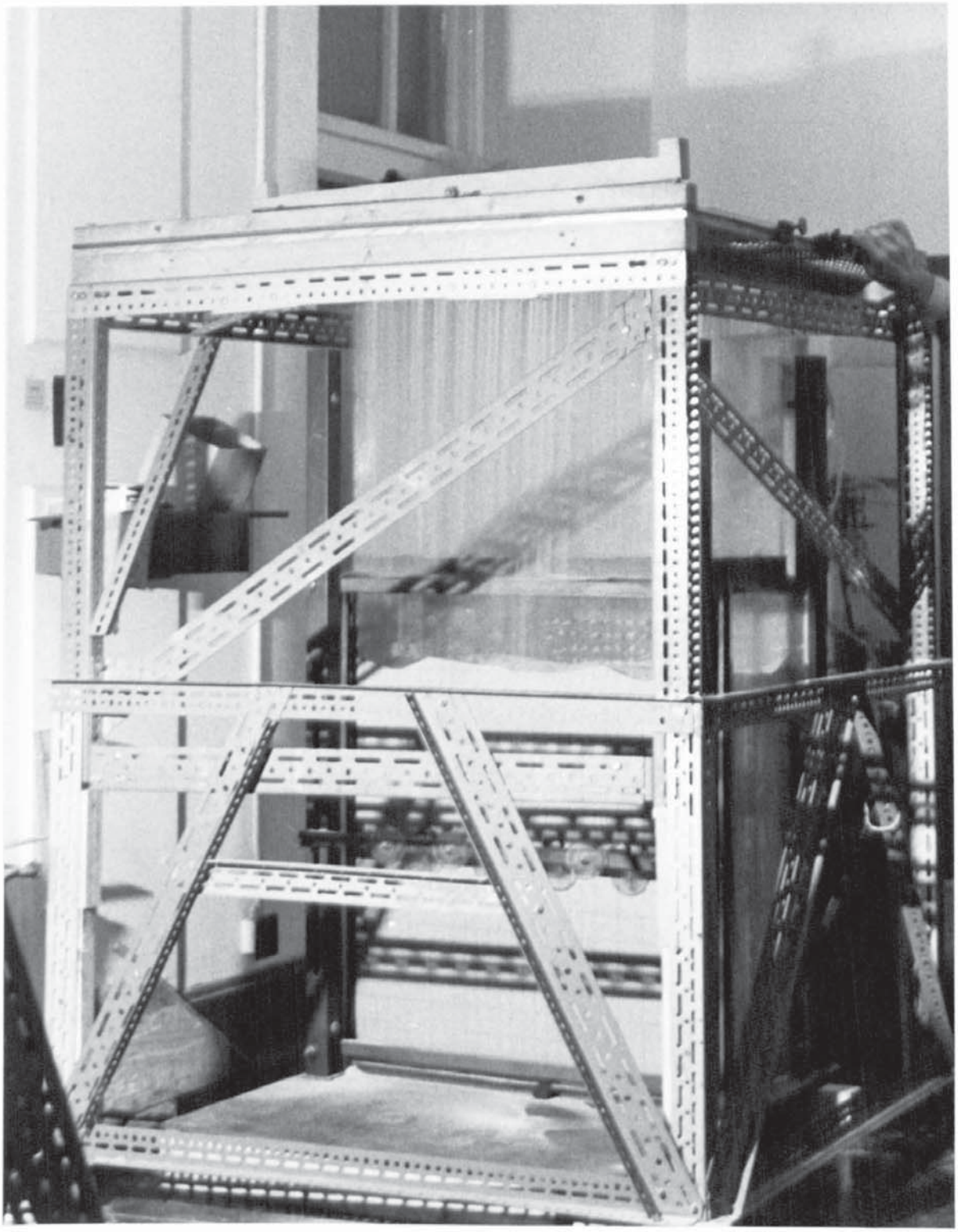

PLATE 7.4. POURING APPARATUS.

apparatus. This consisted of a Dexian frame supporting three sheets of Aluminium which were drilled with $\frac{1}{2}$" diameter holes at 1" centres. The lower sheet was $\frac{1}{2}$" thick and attached to the frame. The middle sheet was $\frac{1}{8}$" thick and adjustable over the lower sheet so that the holes could be made to be small or, at the largest, $\frac{1}{2}$" diameter. The top sheet, 1/16" thick, was also adjustable and was used to open and close the prearranged apertures of the bottom two sheets and hence allow or prevent the flow of sand. This sand was poured in three inch layers by first filling a 3" high wooden former above the sheets and then opening the apertures. These were then closed and the former refilled for the next pour of sand. It is apparent that the smaller the aperture used the denser will be the pour of sand into the tank. For a uniform sand mass the pour must not be disturbed in any way. It was therefore necessary to pump out the displaced air through the bottom of the tank as the sand was poured. This prevented upward rising air causing eddy currents and subsequent uneven distribution of the sand. For this, the Perspex bottom of the tank had channels cut into it and wire netting, covered by fine gauze, acted as a false bottom to the tank about $\frac{1}{8}$" off the Perspex. A hole was drilled through the side of the tank under the gauze and a suction supply was introduced. As the sand was poured on to the gauze the displaced air could be sucked through the sand and out of the bottom of the tank.

7.4.2 Experimental Procedure

The experimental procedure in setting up the apparatus needed to be precise. The constant rate of penetration machine and the glass front were removed from the tank. The markers were affixed to the glass using the minimum amount of Vaseline so as to prevent smearing as the sand moved. This was then replaced and the pouring apparatus wheeled into position over the tank. The Aluminium sheets were adjusted so as to give a pour of approximately 100 lbs/cu. ft. This was done by trial and error. The suction pump was started and the pour commenced. It was found that

this was not uniform to start with and the surface of the sand was therefore uneven after each pour. This was due to eddy currents which were set up in the tank and it was also noticed that high electrostatic charges were being built up on the tank, probably due to inter particle friction. The tank was earthed in an effort to prevent this. However, for the last 18" of pour under the footing these effects were negligable and, as will later be shown, the loaded footing did not influence the sand beyond this depth to any noticable degree. At various layers of pour cyclindrical Brass density pots were placed on the sand surface as shown by plate 7.5 so that, after the experiment had been completed, they could be carefully removed and weighed in order to ascertain the density of sand in the tank accurately. Obviously this density had to be as close to that used in the triaxial tests as possible. Three layers of density pots were used and their average density taken to be that of the whole mass. The pots were not used less than 14" below the footing to prevent any effects they may have had on the results.

The surface of the sand was carefully smoothed flat using a former and the model footing accurately positioned on the top. The constant rate of penetration machine was hoisted into position and the steel rod, which was attached to the proving ring, was located in the proper place on top of the footing. Great care was taken to ensure that all the apparatus was symmetrical and vertical. To do this a theodolite was used to check that the grid and steel rod were vertical. This would help to prevent tilting of the footing on application of load.

The movement of the markers was to be recorded at intervals by taking photographs of the front face. A Hasselblad camera was set up about 6' from the apparatus so as to get a clear photograph of the markers.

A rate of penetration was selected which, at an estimation, would correspond to the rate of strain in the triaxial test. The proving ring

PLATE 75 DENSITY POTS

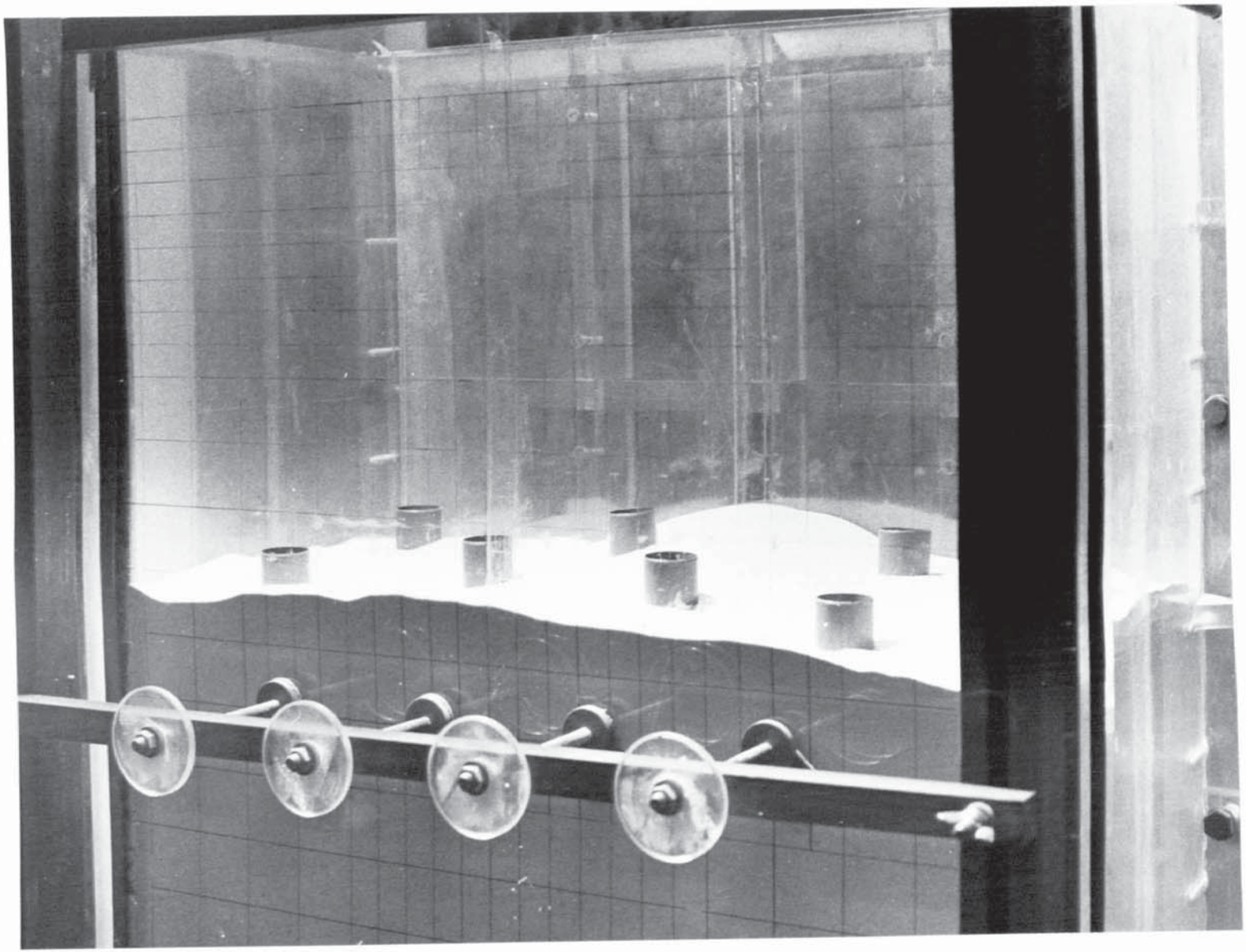

and dial gauge were read every 5 minutes and still photographs taken every 30 minutes. The test was stopped after the footing had travelled about 2" into the sand. At regular intervals the footing was checked to make sure it was travelling horizontally. Plate 7.6 shows a print of a picture of the markers at the end of the experiment. A good indication can be obtained from this as to the influence the footing had on the sand. A small amount of heave occurred along the top surface. At the same time it can be seen that the sand has fallen back against the side of the footing due to its cohesionless nature. The grid was made bigger where it was thought that strains were less critical. The movement of the markers at the sides of the grid was very small which suggests that the influence of the sides of the tank is also small. The markers below the footing were noticably influenced to a depth of about three times the breadth of the footing.

In order to determine the movement of the marker from the photographs, a Wild A7 Autograph machine was used. It can be calculated that distortion of the photograph due to reflection through the glass is negligable. The main source of error would be the stretching of the print during development and therefore all readings were made off the negatives.

The first photograph of the footing at rest was set up with the help of fine cross-wires in the machine. This was also connected to a coordinate plotter and a drawing table. With this apparatus it was able to take each marker in turn and manually punch its reference position. The machine then automatically plotted the position on the drawing table and at the same time printed out its coordinates. This was done for all the negatives of one experiment and hence on overall picture of the movement of the markers was built up along with all their coordinates. From these measurements the movements of the markers can be converted into strains. This will be discussed later in the next section which also gives the method of anlysis of the footing.

PLATE 7.6 MOVEMENT

OF MARKERS

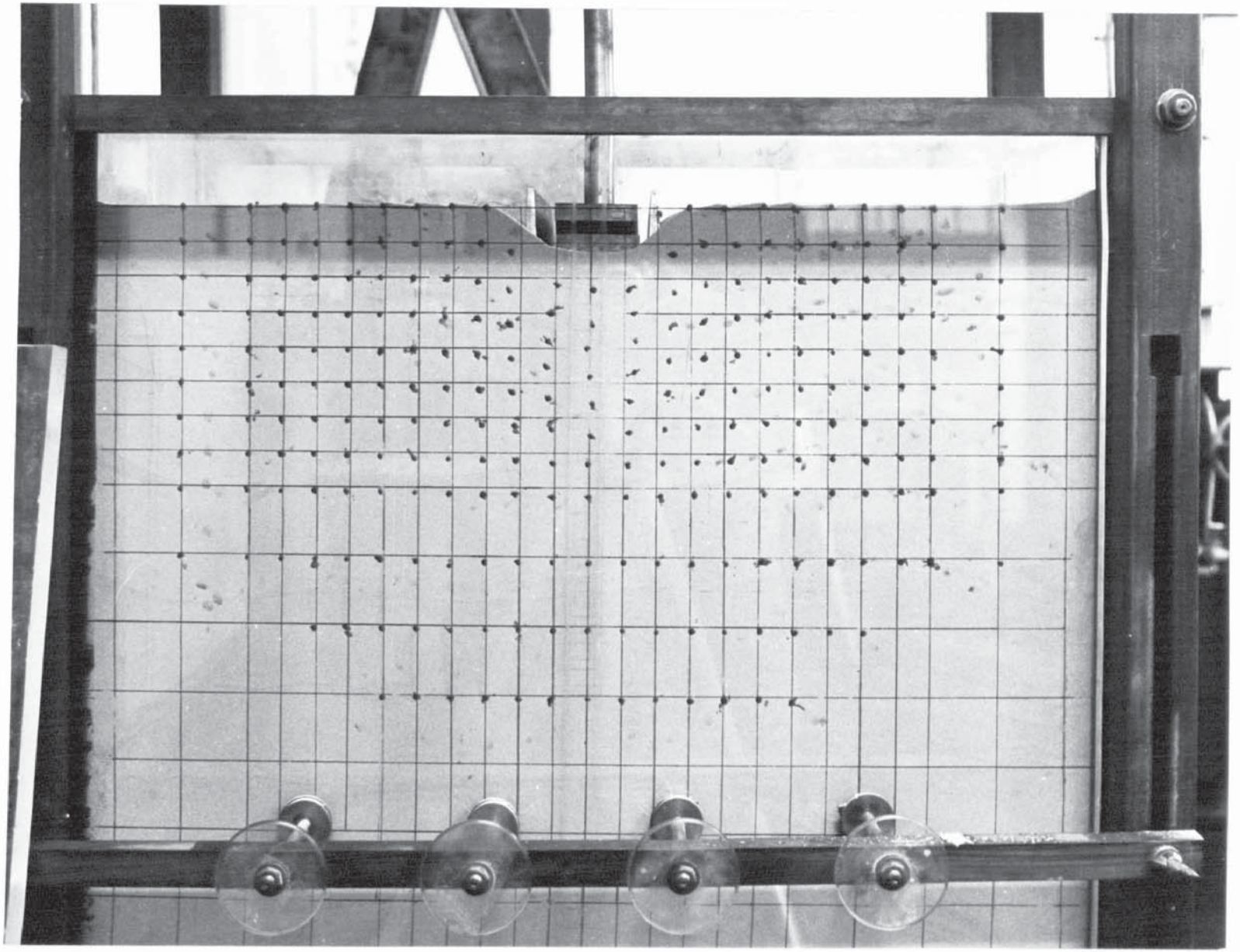

7.5 Computational Analysis of Model Footing

An attempt was made to use both the nonlinear iterative and incremental programs which were described in chapter 4. The iterative program had first to be slightly modified to suit the stress-strain theory and the type of analysis which had been carried out.

7.5.1. Iterative Analysis

Fig. 7.8 shows the dimensionless graph which was used to represent the 'stress-strain' behaviour of the sand. As before, initial values of Young's Modulus and Poisson's ratio were assumed throughout the medium and the stress was calculated in every element. The strain could therefore be calculated and, from this the octahedral shear strain. This was used as it was the only practical parameter near failure on the curve. Each element of sand was assumed to be isotropic and therefore the same curve was fed in twice for the local P and Q directions. The curve had to be represented by a series of straight lines, and for this, it was split up into seven parts. The points, whose coordinates were fed in are shown encircled in fig. 7.8 and labelled 1-6. Based on this value of γ_{oct}, a value for the secant 'modulus' R_s can be found where:-

$$\left(\frac{\tau_{oct}}{\sigma_{oct}}\right)_{\sigma_{oct}=1} = R_s \gamma_{oct} \qquad (7.13)$$

Therefore, using this curve of $\sigma_{oct} = 1$ and rearranging equations (7.13) and (7.12) gives:-

$$\frac{\tau_{oct}}{\gamma_{oct}} = R_s \cdot \sigma_{oct} \cdot fn(\sigma_{oct}) = G \qquad (7.14)$$

From equation (7.5) the expression for Young's Modulus in each element becomes:-

$$E = 2(1+\nu) \cdot R_s \cdot \sigma_{oct} \cdot fn(\sigma_{oct}) \qquad (7.15)$$

From the normal stresses in each element the principal stresses were found.

Hence the principal strains and σ_{oct} were found, and the evaluation of γ_{oct} straightforward. The quantity of fn(σ_{oct}) can be evaluated from equation (7.11) and therefore all the parameters were known for the evaluation of Young's Modulus.

The self weight of the soil was not treated as an imposed load as any displacement caused by this has already taken place before the testing started. This effect though was fed into the computer along with the plate data as the initial confining pressure on each plate. This could be added to the pressure.induced by that of the footing.

For the first iterative analysis a rectangular mesh was used as shown in fig. 7.11. This was arranged so that the joints coincided with the positions of the markers and therefore a comparison could easily be made of the experimental and computed results. A relatively coarse mesh was used so that, when large deformations took place the geometry of the elements beneath the footing would not alter appreaciably and change the stiffness of the continuum. As the footing was symmetrical about its centre line, only half the semi-infinite medium needed to be analysed. No 'in plane' rotational terms are included for the element and so this face was allowed to move vertically only as shown. In a similar manner it was decided to permit the other vertical and horizontal faces to move solely in the vertical and horizontal directions respectively. By this means it was possible to judge if the loaded footing was having any influence on the outer edge of the Perspex box and hence determine whether plane strain conditions were being met. The grid was taken to the same depth of the markers where only small amounts of movement were measured experimentally.

The thickness of the member and plate elements was assumed to be one inch and hence all the properties of the elements could be fed in to the computer in a similar manner given by appendix 4. The nodes connecting the member elements included a rotational stiffness and hence the member

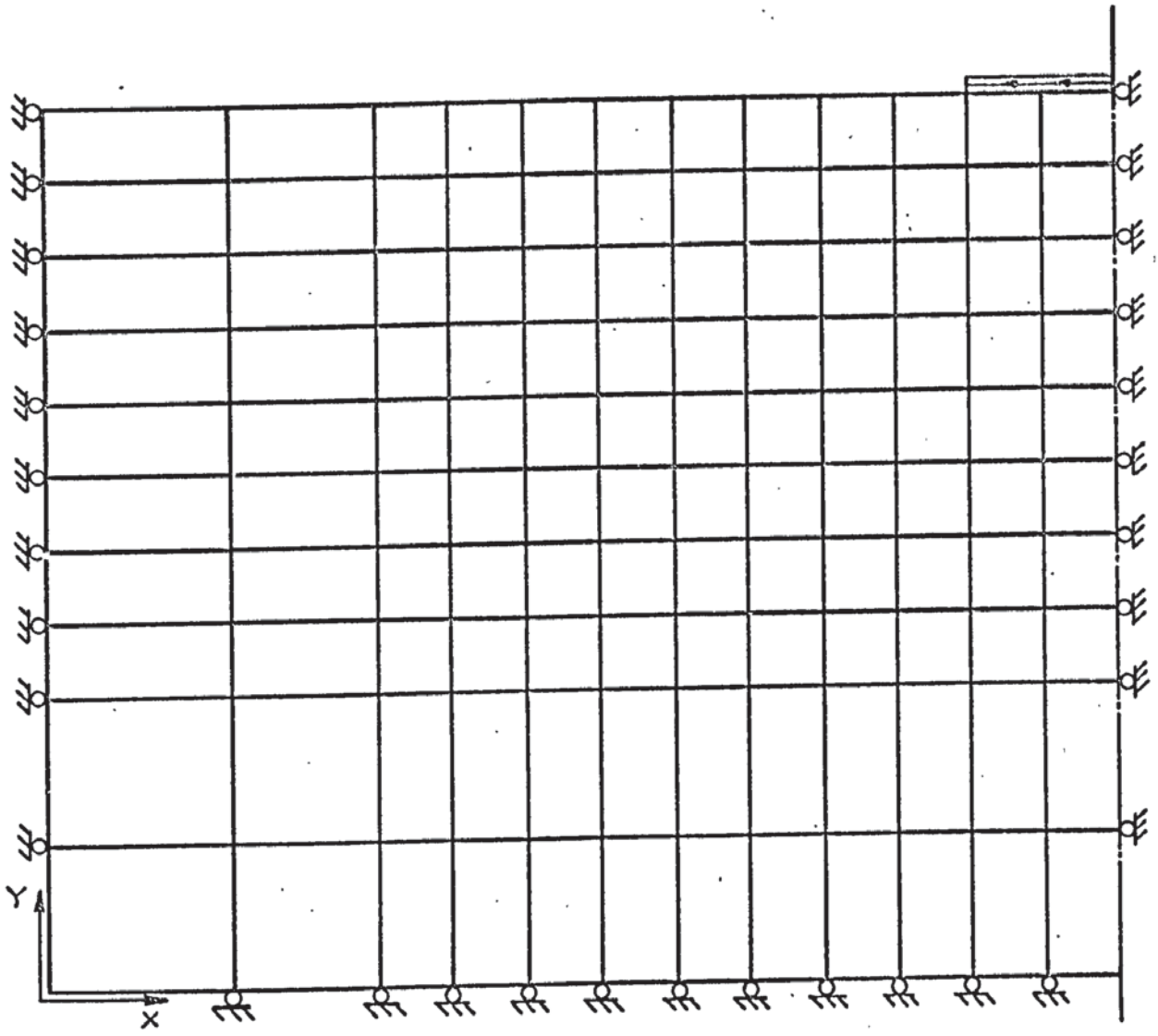

FIGURE 7.11 RECTANGULAR MESH

elements were given the material properties of steel and sectional properties for area and second moment of area for a 1" x $\frac{1}{4}$" rectangular section. For each element (σ_{oct}) initial was calculated from the formula.

$$(\sigma_{oct}) \text{ initial} = \rho h \left(\frac{3\nu}{1-\nu}\right) \qquad (7.16)$$

where ρ, the density, was known to be 100 p.c.f. and h was the vertical distance from the centre of each element to the free surface.

The coordinates of the stress-strain curve were fed in from fig. 7.8 and it is apparent that this cannot be used to determine the initial value of Young's Modulus. It was therefore necessary to supply an assumed value after this data for the local P and Q directions. Therefore the elements were given a Young's Modulus of 90 p.s.i. This is a reasonable value as used in the more straightforward calculations of settlements using the Boussinesq equations. This therefore ensured that the result of the first iteration was near the expected deflection and prevented any abnormal behaviour of the iterative procedure due to unrealistic deformations.

The representation of Poisson's ratio for sand is complicated by its tendency to dilate. It can be seen from equation (4.13) that, under these conditions this ratio will affect the constant α_{33} of the elasticity matrix. For an incompressible medium $\alpha_{33} = 0$ and, on dilation, α_{33} will be negative. This would introduce a zero or negative number on the loading diagonal of the stiffness matrix and prevent its inversion. For coarse or even medium fine grids the results obtained using a value for Poission's ratio greater than .48 are untrustworthy. For every fine girds values of up to .495 can be used but the additional accuracy involved does not justify the greatly increased computation which is needed. Fig. 7.9 gives the graph of volume change, which is proportional Poisson's ratio, against octahedral shear strain. This ratio will therefore vary with

octahedral shear strain and stress. The Young's Modulus varies in a similar fashion and it was assumed to a first approximation that the Poisson's ratio varied with Young's Modulus. The lowest recorded value was .4 under small strain and this was made to vary linearly up to .48 for sand near failure (i.e. of low modulus value).

From equation (7.15) it is apparent that, when σ_{oct} is negative (or tensile), then this will result in a negative value of Young's Modulus. This is clearly inadmissable and therefore a lower limit of .05 was put on σ_{oct} in case zones of high tensile stress developed. This might be expected near failure.

An analysis was carried out under a quater of the total load that was eventually applied to the footing. The tolerance parameters tol and tol^1, as described in chapter 4, were set to .04 and .08 respectively. Six iterations were completed in ten minutes computing and by this time over three quarters of the elements had acceptable modulus values with the remainder rapidly converging.

On examination of the deflection of the footing it was found that this was only one quarter of the experimental value. The stresses throughout the medium were nearly all compressive which was satisfactory as tensile stresses in a cohesionless soil would be meaningless. An exception to this was along the surface of the sand where a certain amount of heave was observed. It was also noticed that the values for Young's Modulus was high 600 - 700psi in the lower regions of the medium where the initial octahedral stress was high and especially in the region directly under the footing. This was therefore being supported on a stiff column of sand of about the same width of the footing and failure was only occurring in the elements at the free surface away from the footing.

The reason for this was due to the interaction of footing and sand which had been assumed. The footing behaved as if it was virtually rigid and did not extend or rotate to any noticable degree under the load. The analysis assumes no movement between the underside of the footing and the sand contact. For this reason the sandpaper had been glued to the footing for complete friction. On this coarse grid therefore the elements under the footing were not allowed any lateral movement. From the position of the markers in the experiment it could be seen that, at a small distance below the footing, this movement had taken place. For a virtually incompressible medium this theoretical confinement of the elements under vertical pressure was interpreted in the analysis to be due to a high lateral compressive stress which in turn caused a large value of σ_{oct}. From equation (7.15) it is evident that this will cause a high value for Young's Modulus and will tend to prevent any more movement on the next iteration. Any allowance of movement of the particles under the footing cannot be theoretically justified and it was therefore decided to refine the mesh in the area of the footing so as to give individual elements more freedom of movement. For such refinement, the rectangular element is not suitable as this will result in badly shaped elements in regions where stress is less significant. A triangular distribution, as shown in fig. 7.12 was therefore used. The same basic configuration was used as was successful in chapter 5 although this resulted in some rather badly shaped elements. It was now possible to make the mesh even coarser at positions of low stress. The analysis was taken to a greater depth as the results of the rectangular grid indicated that the lower boundary stresses were significant and therefore this boundary could influence the deflections. The stresses in the elements on the vertical sides were small enough to be ignored. Another advantage of the triangular element in such nonlinear analyses is that it is a constant stress element and no partial yielding can

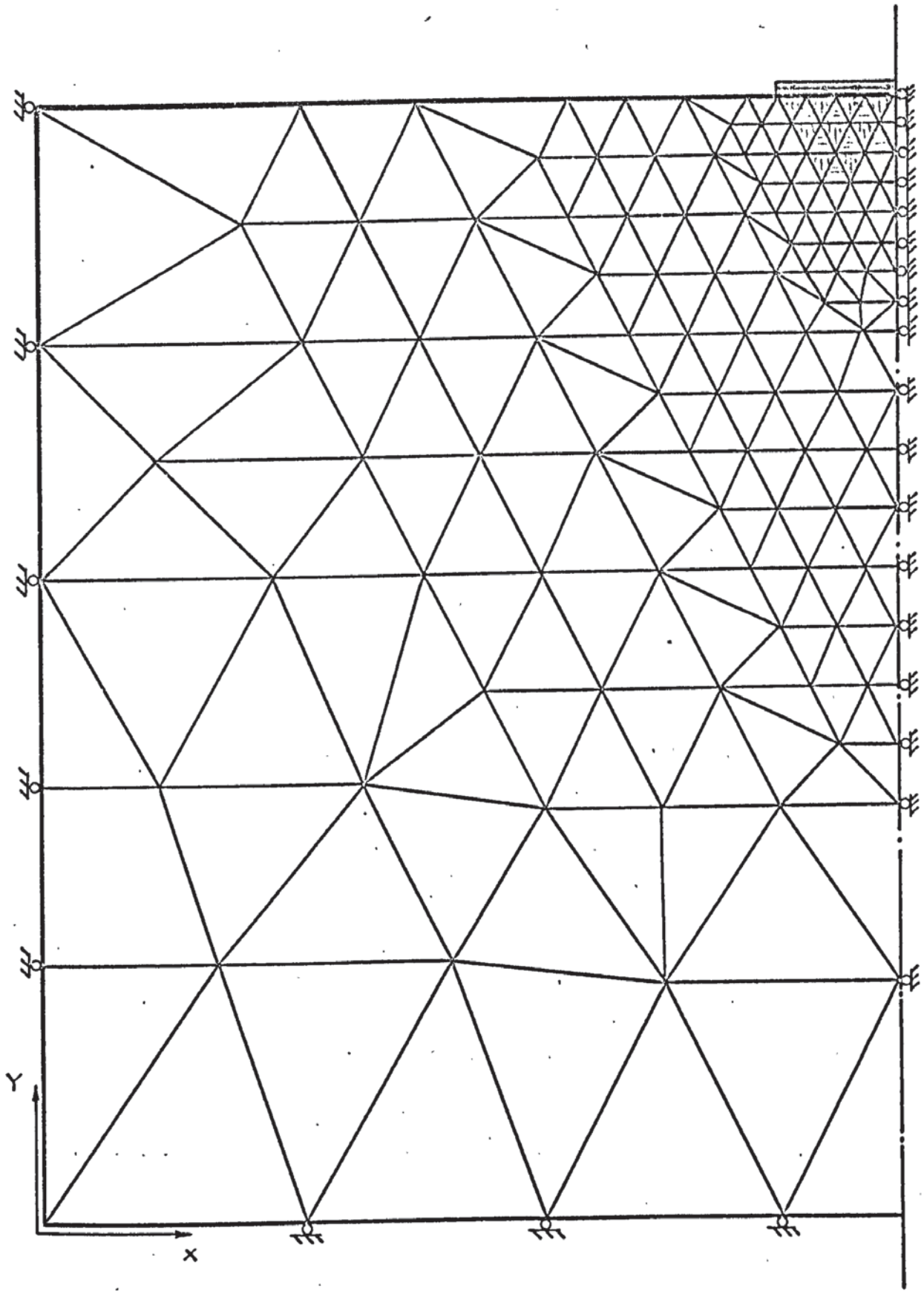

FIGURE 7.12 TRIANGULAR MESH.

take place within its boundaries as the state of stress is fixed.

Again the value of (σ_{oct}) initial was calculated at the centre of gravity of every element and the load was applied equally distributed between the nodal loads. Loads of a quater, half and three quarters the experimental load were used on the mesh. It was found that no convergence could be obtained in the elements. Differing initial modulus values were tried between 50-300 psi but the elements behaved in a similar pattern each time. The first iteration gave the type of results which could be expected for a beam on an elastic continuous half space. The elements nearest the footing had virtually no lateral movement due to its rigidity and the octahedral stress therefore rose giving high elastic moduli and stresses. This relieved the load on the neighbouring elements and their stiffness consequently fell. After only two iterations a definite trend was already established with the moduli of the vertically shaded elements, in fig. 7.12, rising increasingly sharply. Those of the horizontally shaded elements on the other hand were falling off to their minimum value. The remaining elements had rather high values of 200 psi further down under the footing but continuity was established to a certain degree across elements. The subsequent discontinuities under the footing led to erroneous answers and only about a quater of the elements converged to a steady modulus of elasticity value. The continuum behaved as an assembly of triangles connected at their apexes and with gaps existing between them. Clearly this was not the case experimentally. At first it was thought that this might have been simulating an 'arching' condition where, if the sand is confined laterally as well as vertically it can take up the configuration of an arch which will relieve the pressure on the lower strata. It is apparent that this is very unlikely as no definite arch is defined. The deflections obtained were again about a quarter of the experimental values. One analysis was attempted where an imposed deflection was put on the footing at each of the five nodes rather than a loading condition. The results were

similar but it was noticed that the divergence was not so acute. This was due to the initial deflection causing high shear strains under the footing and these tended to compensate for the high values of octahedral stress.

It was concluded from these analyses that this method of iteration was not suitable for this type of problem, due to its inadequacy to represent the footing/sand interface. The high influence which σ_{oct} had on the modulus value was also noticable. During the earlier stages of loading and even up to half the full loading this value was high enough to increase the stiffness of the elements so that the deformations were reduced appreciably. It was therefore decided to use the incremental program described in chapter 4.

7.5.2 Incremental Analysis

The discontinuities which arose when using triangular elements under the footing have already been pointed out and hence it was decided to revert to the use of a more refined rectangular grid under the footing. The triangular element was used outside the footing as such a mesh can be graded to give large elements where stress is of less importance. The mesh which was used is shown in fig.7.13 and hence member, rectangular and triangular elements were used. The interface between rectangular and triangular elements might have caused some discontinuities but both have linear displacement functions and therefore are compatible.

For this type of analysis the tangent modulus R_t in fig. 7.8 is used. It was found more convenient to rearrange this graph into a plot of R_t against γ_{oct} as shown in fig. 7.14. It is now clearly visible that the values of R_t decreases rapidly from (R_t) initial = 200 under no strain, down to 25 for $\gamma_{oct} = 0.5\%$. For $\gamma_{oct} = 6\%$ failure has occurred and $R_t = 0$. When using the secant modulus R_s this effect is less pronounced.

The joint and element data were fed into the computer along with the initial confining pressures (σ_{oct}) initial for each element. The initial

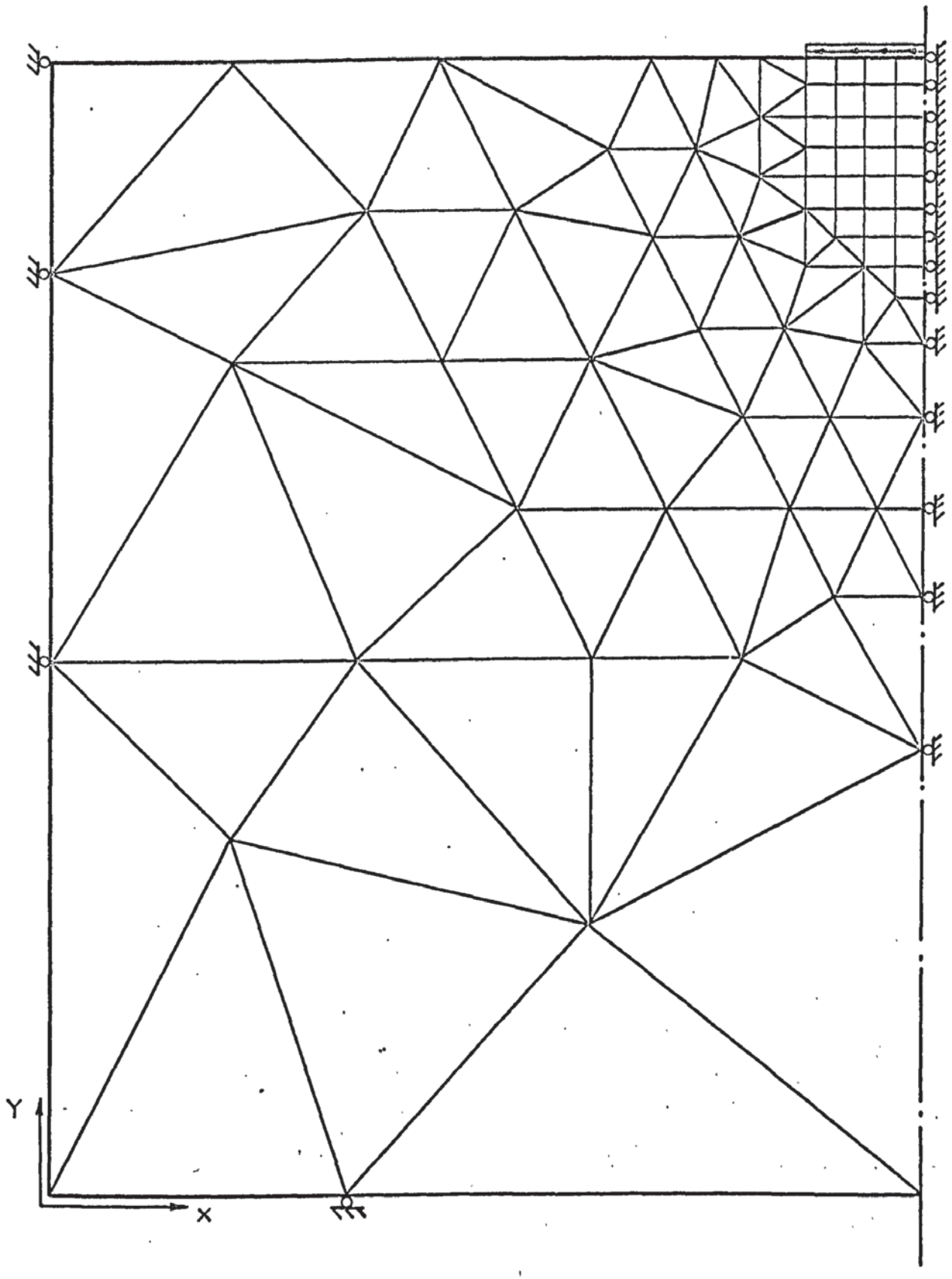

FIGURE 7.13 RECTANGULAR AND TRIANGULAR MESH.

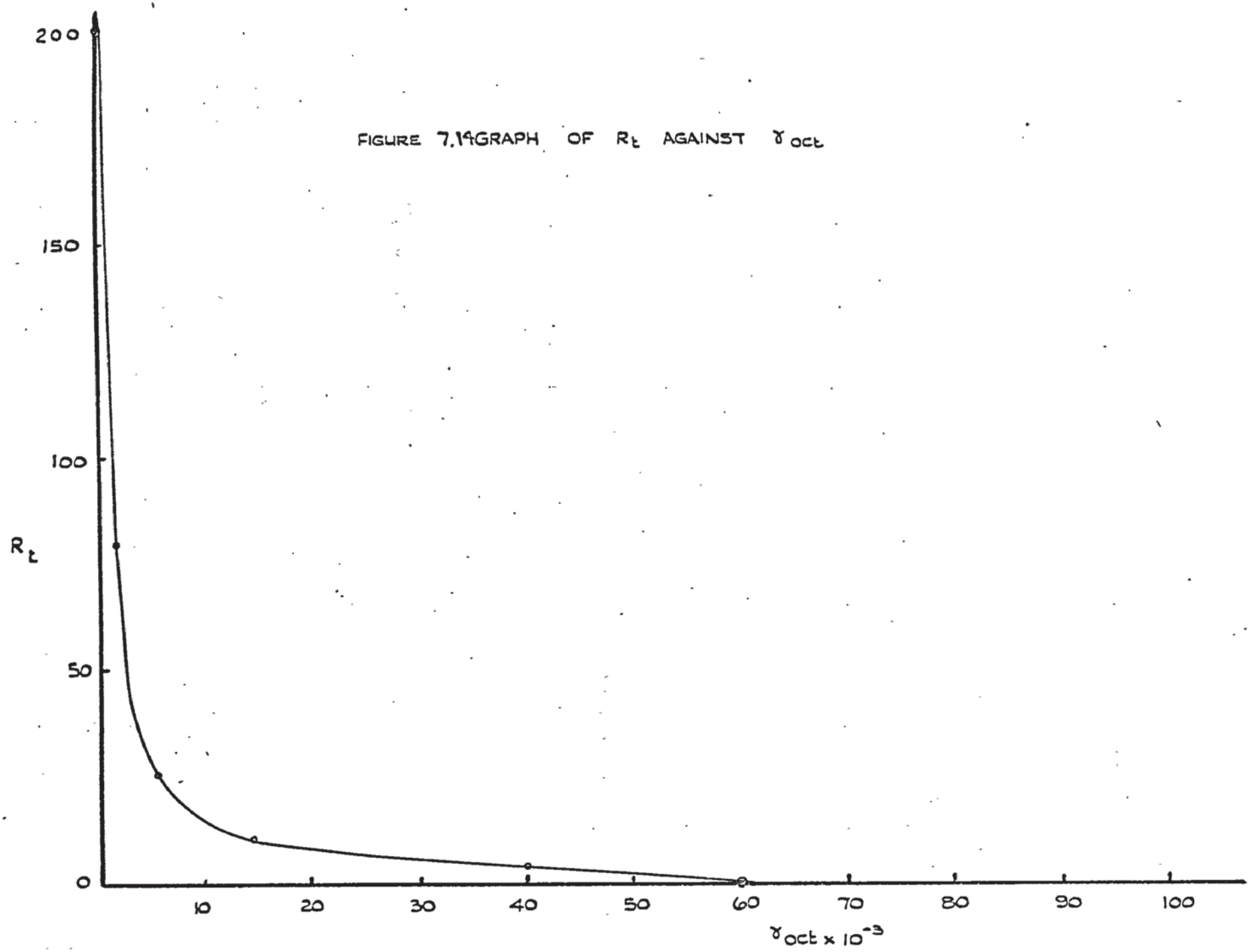

FIGURE 7.19 GRAPH OF R_t AGAINST γ_{oct}

modulus values for the first increment could then be calculated from:-

$$E_{ti} = 2(1+\nu_i)\, R_{ti}\, (\sigma_{oct=i})\, Fn(\sigma_{oct=i}) \qquad (7.17)$$

where suffix i refers to initial conditions. As could be expected, the stiffness of the elements was now graded according to the depth. From the load increment ΔL the first increment of deflection ΔX_1 was found. This lead to the calculation of $(\Delta\sigma_{oct})_1$ and $(\Delta\gamma_{oct})_1$. The fig. 7.14 had been fed into the computer in a piecewize coordinate form and hence the calculations of R_{t1} and E_{t1} and ν_1 for each element was straightforward. In the next load increment the value of ΔX_2 was found using these pseudo-elastic constants and $(\Delta\sigma_{oct})_2$ and $(\Delta\gamma_{oct})_2$ were subsequently determined. The total values of octahedral stress and shear strain in the element were found using the following two equations:-

$$\sigma_{oct} = (\Delta\sigma_{oct})_2 + (\Delta\sigma_{oct})_1$$
$$\gamma_{oct} = (\Delta\gamma_{oct})_2 + (\Delta\gamma_{oct})_1 \qquad (7.18)$$

and thus values of R_{t2}, E_2 and ν_2 were calculated. The same procedure could be used for the next load increment. In the general case the state of stress and strain on each element for the calculation of elastic moduli E_{j+1}, ν_{j+1} was found from:-

$$(\sigma_{oct})_j = \sum_{j=1}^{j} (\Delta_{oct})_j$$
$$(\gamma_{oct})_j = \sum_{j=1}^{j} (\gamma_{oct})_j \qquad (7.19)$$

Limits had to be put on these quantities to prevent the moduli becoming zero or negative. A lower limit of .01 was used for σ_{oct} and an upper limit of .05 for γ_{oct}.

The results of this analysis are shown in fig. 7.15, which is labelled "Computed incremental i". It is clear that this computed load-deflection curve is of a similar form to the experimental.

The analysis just described used a load increment of 110 lbs. where this represented the experimental load on the footing. As an

improvement a smaller load increment was used. Clearly the use of 'previous increment' moduli in the current increment would tend to overestimate the stiffness of the soil. The program does not allow for the rotation of principal strains which was thought to be of secondary importance. The quantity γ_{oct} is a function of the principal strains and therefore its accumulation to find the total shear strain implies that principal strains are independent of rotation. As an extra refinement therefore the direct strains e_p, e_q, e_{pq} were accumulated and from these values the octahedral shear strain was calculated. The value of σ_{oct} is independent of the rotation of principal stress and since:-

$$(s_1 + s_2 + s_3)/3 = (s_p + s_q + s_r)/3 \qquad (7.20)$$

it follows that σ_{oct} can be accumulated directly. The load increment was reduced to 60 lbs., which was about half its previous quantity. The results of the load-deflection computation is also given in fig. 7.15 under the heading "Computed Incremental 2", and will be discussed in the next section. At the end of each step the quantities e_{max}, α, s_1 and s_2 were printed out for each element. Here $e_{max} = e_1 - e_2$ is the maximum shear strain, while the principal stresses are s_1 and s_2, with their rotation α being measured from the local axes of the element. These will be compared with the experimental observation later on. The values of σ_{oct}, γ_{oct} and fn (σ_{oct}) were also printed our for checking purposes.

7.5.3 Strain Analysis

Before leaving this section there follows a description of the program which was written to calculate the maximum shear strain from the experimental results. This was done using the movement of the markers which had been calculated from photographs taken at various stages indicated as P_o, P_1 ... P_4 in fig. 7.15.

As the origin of the plotted coordinates was remote from the marker grid, the movement of these markers at any position i could be obtained simply by subtracting the coordinates of each point at P_i from those at P_o. The grid was rectangular with each rectangle defined by a marker at each corner. The displacements (u_1, v_1 .....u_4, v_4) were known and therefore, assuming a linear displacement between markers, the strains at the centre of the elements could be found using equation (1.11). For a rectangular element of dimensions a and b as before, the strains can be found from $\underline{e} = \underline{B}\,\underline{Z}$, thus:-

$$\begin{bmatrix} e_p \\ e_q \\ \delta_{pq} \end{bmatrix} = \frac{1}{2ab} \begin{bmatrix} -b & o & b & o & -b & o & b & o \\ o & -a & o & -a & o & a & o & a \\ -a & -b & -a & b & a & -b & a & b \end{bmatrix} \begin{bmatrix} u_1 \\ v_1 \\ u_2 \\ v_2 \\ u_3 \\ v_3 \\ u_4 \\ v_4 \end{bmatrix} \qquad (7.21)$$

The maximum shear strain can then be found from consideration of Mohr's circle.

The program was written in Fortran and a flow diagram appears in fig. 7.16. The coordinates of the positions P_o and P_i were first punched as data on cards and arranged row by row from the surface and from left to right. Only the rectangular portion of the grid was considered and extended over 23 markers across, 10 markers deep. The two sets of coordinates were first subtracted to find the vertical and horizontal displacements of each marker. The value e_{max} was found and printed for each element in turn by cycling through the rows. The dimensions were calculated from the coordinates at P_o and the strains from equations (7.21). The maximum strain e_{max} is simply twice the radius of the Mohr's circle. By this means it was possible to plot the experimental strains throughout the rectangular gird

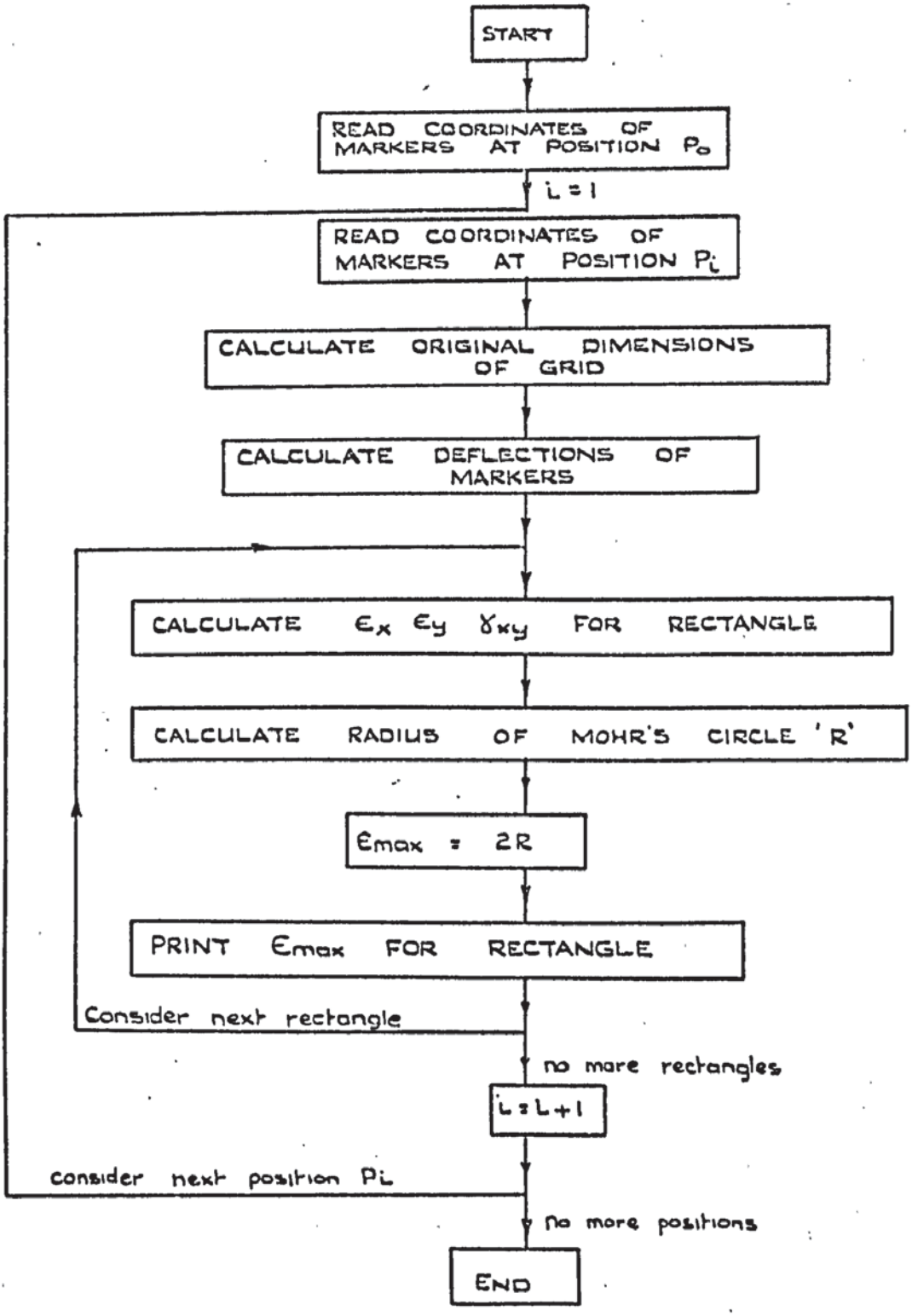

FIGURE 7.16 FLOW DIAGRAM OF PROGRAM TO CALCULATE ϵ_{max}

of elements. The program was so arranged to consider another position of markers after the first had been evaluated.

7.6 Comparison of Results

The general shape of the experimental load-settlement graph for the footing, which is shown in fig. 7.15, is as expected from studies of this type. As the footing is first loaded it experiences a certain amount of elastic and then inelastic deformation until, at the settlement of .4", it deflects at a uniform rate. It is noticable that there is no sudden failure due to a slip plane forming in the classical Terzaghi manner. This suggests that the sand sample under load was homogeneous and hence there was no tendency of the footing to tilt even though it was free to do so. Probably a more significant explanation for this was that, as the deflections of the footing became quite substantial, the overburden of sand at its sides acted as an imposed loading and caused an upthrust on the underside of the footing. At any event, if the word "failure" is to be used to describe this behaviour, then it should be only limited to points beyond P_2. This additional dead weight also prevented the rotation of the footing. Both the incremental results show a marked degree of similarity to the experimental results. In the lower regions of loading, 'incremental 2' follows the experimental curve exactly. The better result given by this analysis is almost entirely due to the application of small load increments during the analysis. It will be shown later that the principal stresses did not change their directions by any appreciable amount.

This suggests that the stress-strain relationship which was used could be valid even though it is known to include approximations. This does not explain however, the good agreement achieved even after "failure". The computational method did not take the effect of overburden of sand into account. It was found that the theoretical results depended upon the small

residual elastic moduli left in the element after failure. At the beginning of the analysis the values of the elastic moduli were very small for elements near the surface and rose to values of 550 psi in the lowest element. As the load was increased, the effect of increasing σ_{oct} and γ_{oct} tended to cancel each other out under the footing and this remained at about 20-40 psi. In the triangular elements at the edge of the footing failure occurred quickly while the lower elements remained unaffected. As further load was applied the elements under the footing also began to fail which meant that the value of γ_{oct} was put to .057. As σ_{oct} was very high the residual modulus value remained reasonably high under the footing. The elements around the footing continuously failed right up to the end of the analysis. There was therefore a spreading failure zone around the footing with relatively high modulus values of 15-30 psi in the rectangular elements underneath. An analysis was attempted limiting γ_{oct} to .0595. The results were practically the same for deflections up to .7" but thereon the computed deformation was greater than experimental. It was thought that, although the sand was failing through shear, its modulus of elasticity is not necessarily zero and may well depend on the confining stress in a similar fashion to that used in this analysis.

The iterative technique failed due to its inability to take into account the high values of σ_{oct} under the footing. Even when the rectangular and triangular element mesh was used, no or very little, convergence was noticable. As before the modulus values remained too high for the shear strain to develop.

The experimental and the theoretical maximum shear strains were compared at positions P_1 and P_3, Point P_1 is in the nonlinear elastic range while point P_3 is beyond the stage of failure, which was considered to take place at P_2.

Figures 7.17 and 7.18 show contours of e_{max} obtained experimentally and by computer at the two positions. The computed contours were well defined but the experimental values had first to be averaged around the centre line of the footing and were less clear. This could have been due to faulty markers. The failure of one marker to move with the soil would affect four results. Even so a definite pattern qualitatively similar to the computed results is evident. Maximum strains developed from the point of singularity at the edge of the footing and it was noticable that, symmetrically under the footing, maximum strain did not develop until some distance down, particularly at position P_3. The measured strains were larger under the footing than the computed especially at P_1. This is probably due to the fact that large deformations were not considered in the finite element method and also because of the inaccuracies introduced in representing the footing/sand interface. Elsewhere in P_1 and generally in P_3 the contours agreed quite closely. In the latter case, values of e_{max} were much larger after the development of steady conditions concerning the movement of the markers.

Figs. 7.19 and 7.20 show plots of the computed major and minor principal stresses and their orientations at various positions. It is apparent that both the major and minor principal stresses in both cases are high to a substantial depth under the footing. These stresses, however, gradually fall off with the depth of sand. As soon as the stresses are rotated from the vertical, which occurs beyond the edge of the footing, their values fall appreciably. In some of these regions small tensile stresses were developed and are denoted by 'T' in the figures. In these regions the principal stress ratio s_1/s_3 is very high and failure has obviously occurred whereas, under the footing this ratio is lower even though larger stresses are involved. It can be concluded from the computational analysis that the

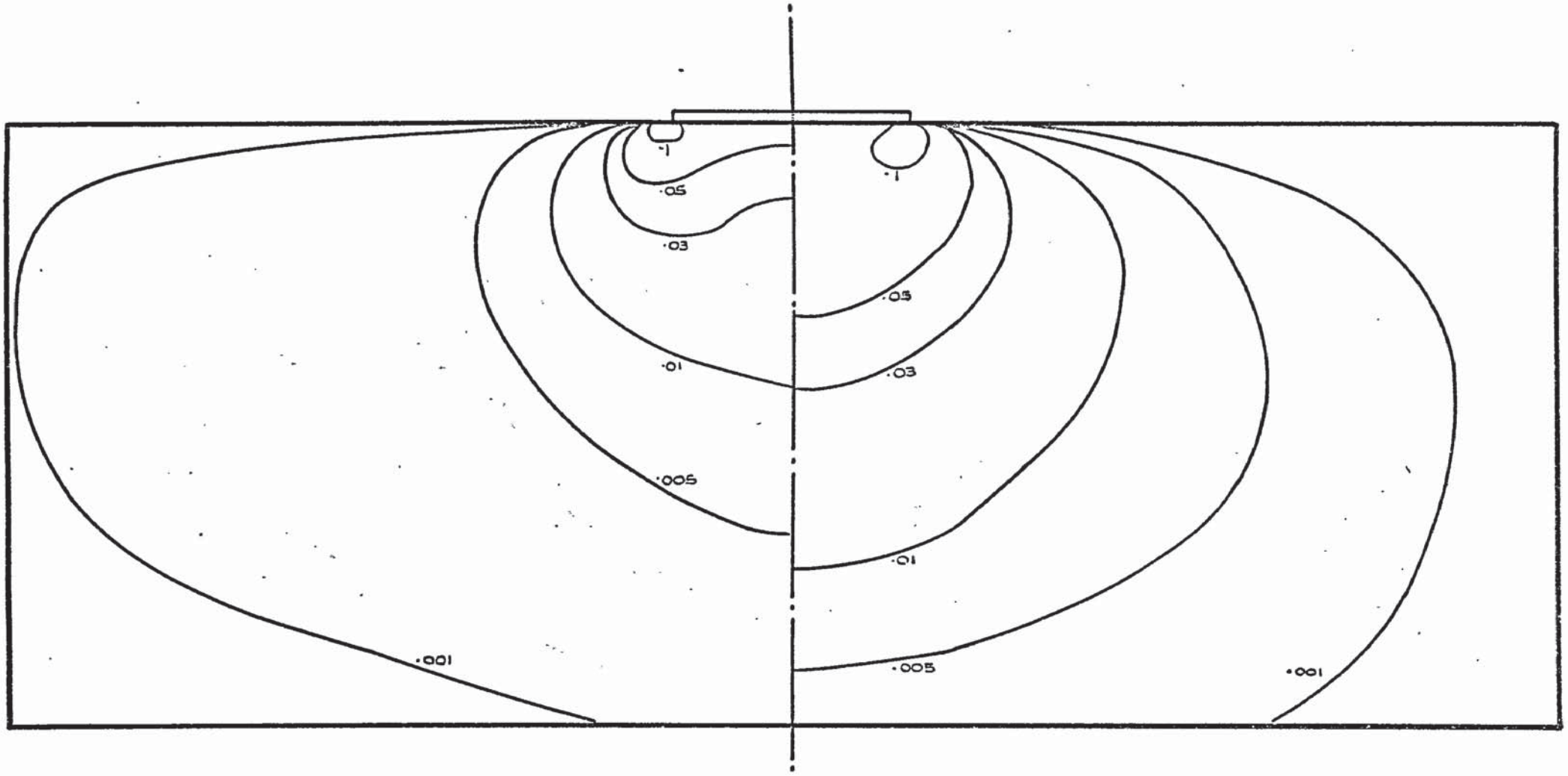

FIGURE 7.17 CONTOURS OF $\epsilon_{max.}$ AT POSITION P_1

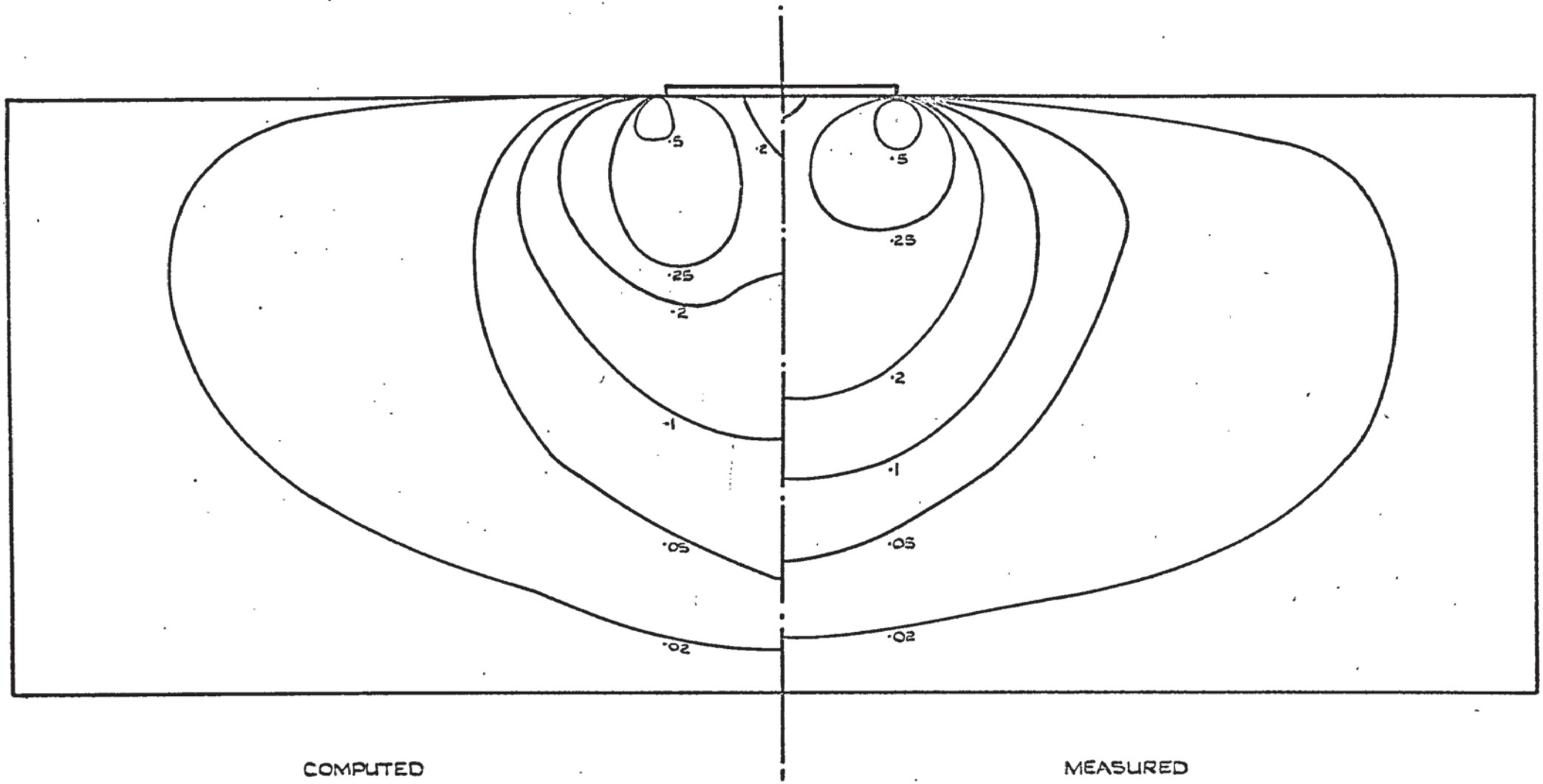

FIGURE 7.18 CONTOURS OF ϵ_{max} AT POSITION P_3

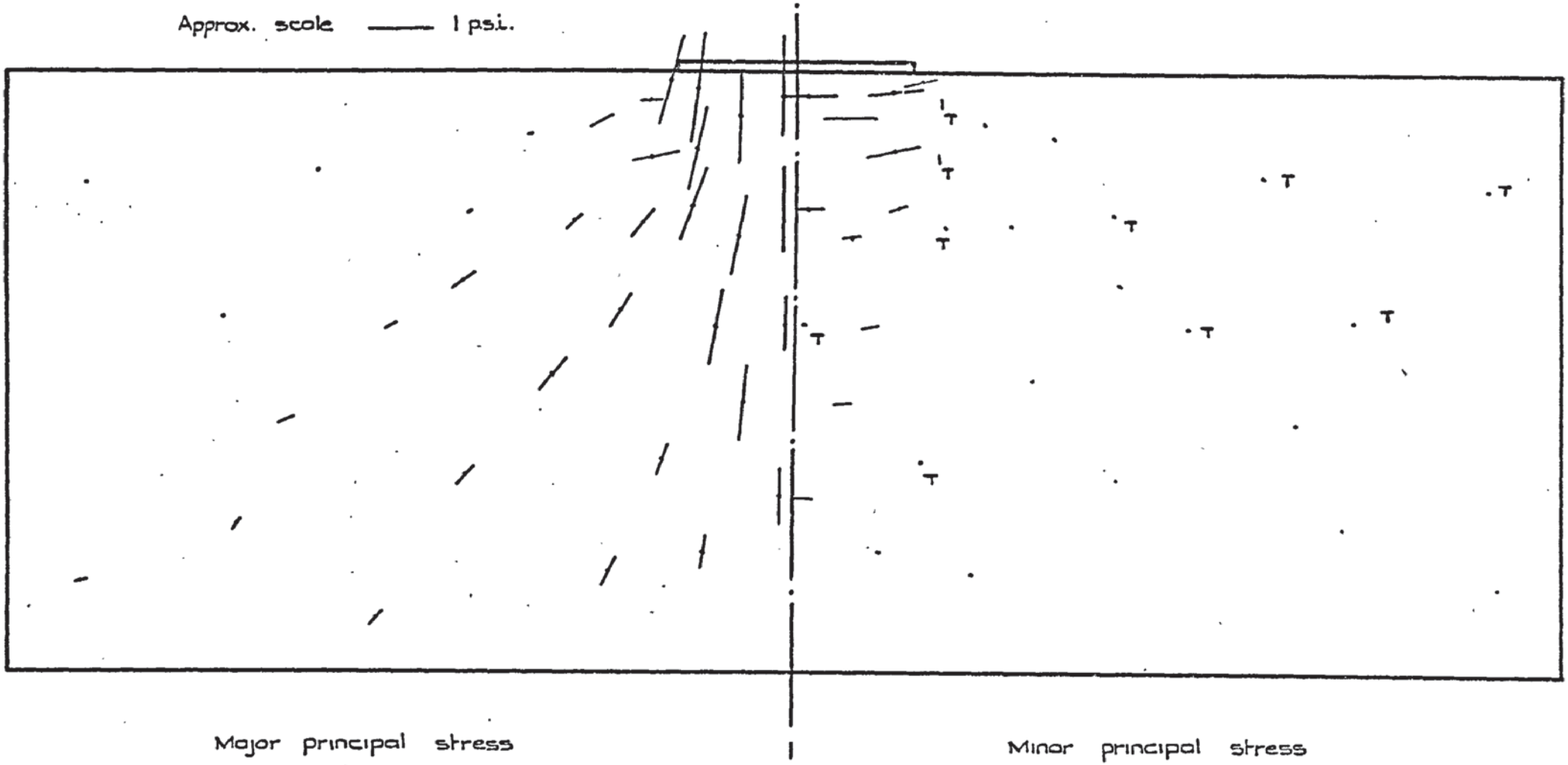

FIGURE 7.19 PLOT OF PRINCIPAL STRESS AT POSITION P_1

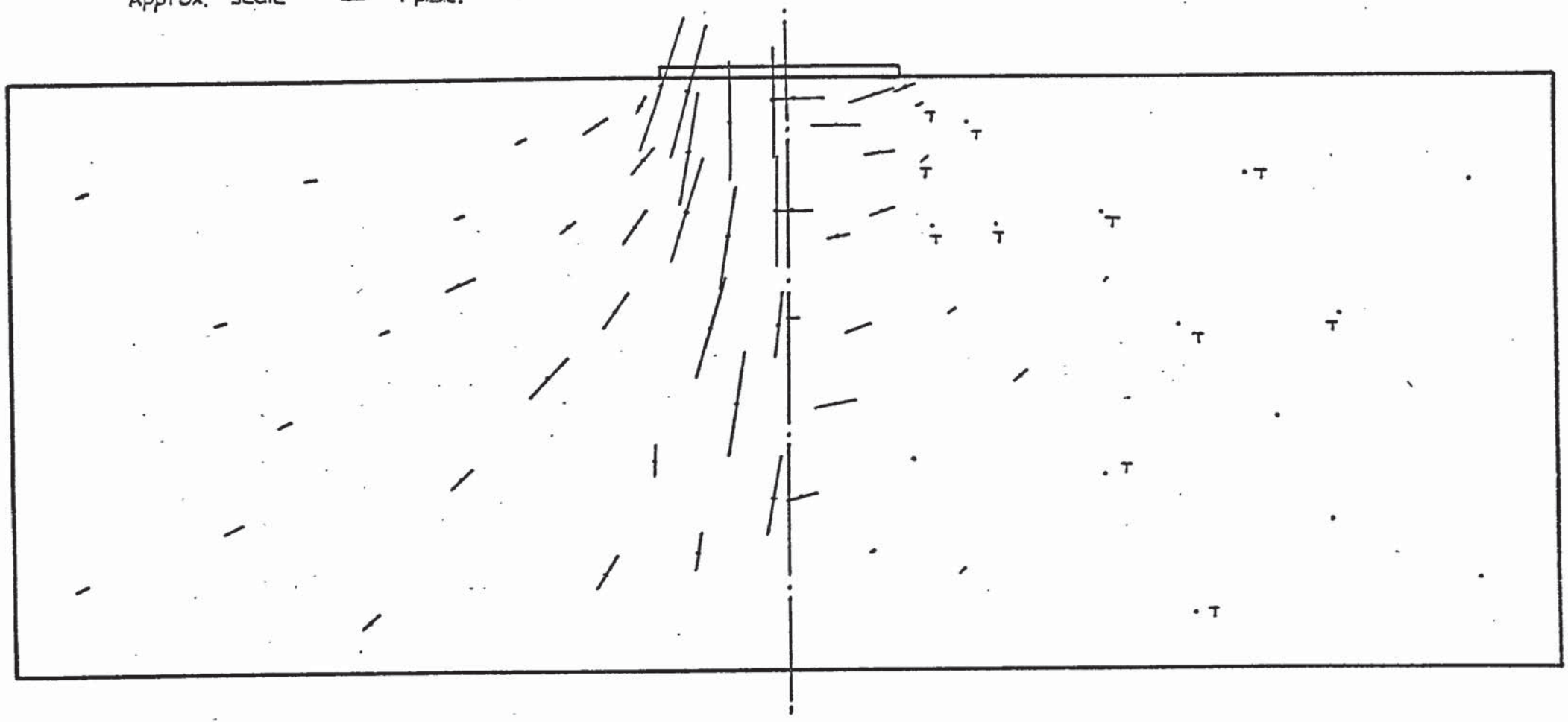

FIGURE 7.20 PLOT OF PRINCIPAL STRESSES AT POSITION P_3.

footing is being mainly supported by a column of sand approximately equal to its width to a depth of approximately between twice and three times the breadth of the footing. It can also be seen by comparison of these two figures that, as the loads are increased, little rotation of the principal stresses takes place. It is of interest to note that an increase in vertical stress occurs at the edge of the footing. It has been mentioned earlier that, at this position, the contact pressure is theoretically infinite. This analysis suggests a sharp decrease of pressure with depth due to the failure zone which develops around the edge. Change of pressure which occurs on deformation is therefore accommodated.

Fig. 7.21 shows the displacement field of the markers as they moved through positions $P_o - P_4$. Except for a few, all the markers moved away from the axis of symmetry of the footing and show that the influence of the loading of the footing was confined laterally to just over its own breadth on either side and therefore the width of the container was adequate for plane strain conditions to be developed. The symmetry of the field shows that the sand was homogeneous.

The displacements of the mesh, as obtained theoretically and experimentally are shown in fig. 7.22 for position P_3 where they were large enough to be significantly plotted. The computed displacements were not able to reproduce the very large deformations given by the markers at the edge of the footing (Points c and c^1). These could be misleading due to the tendency of loose sand to fall back into the side of the footing on large settlement. However the agreement between the theoretical and the experimental displacements is exceptionally remarkable. It is interesting to notice that the form of the free surface of the sand obtained theoretically on the side of the footing (see portion bc) becomes inclined just as was observed experimentally as indicated by $b^1 c^1$ in fig. 7.22. Furthermore the theoretical analysis

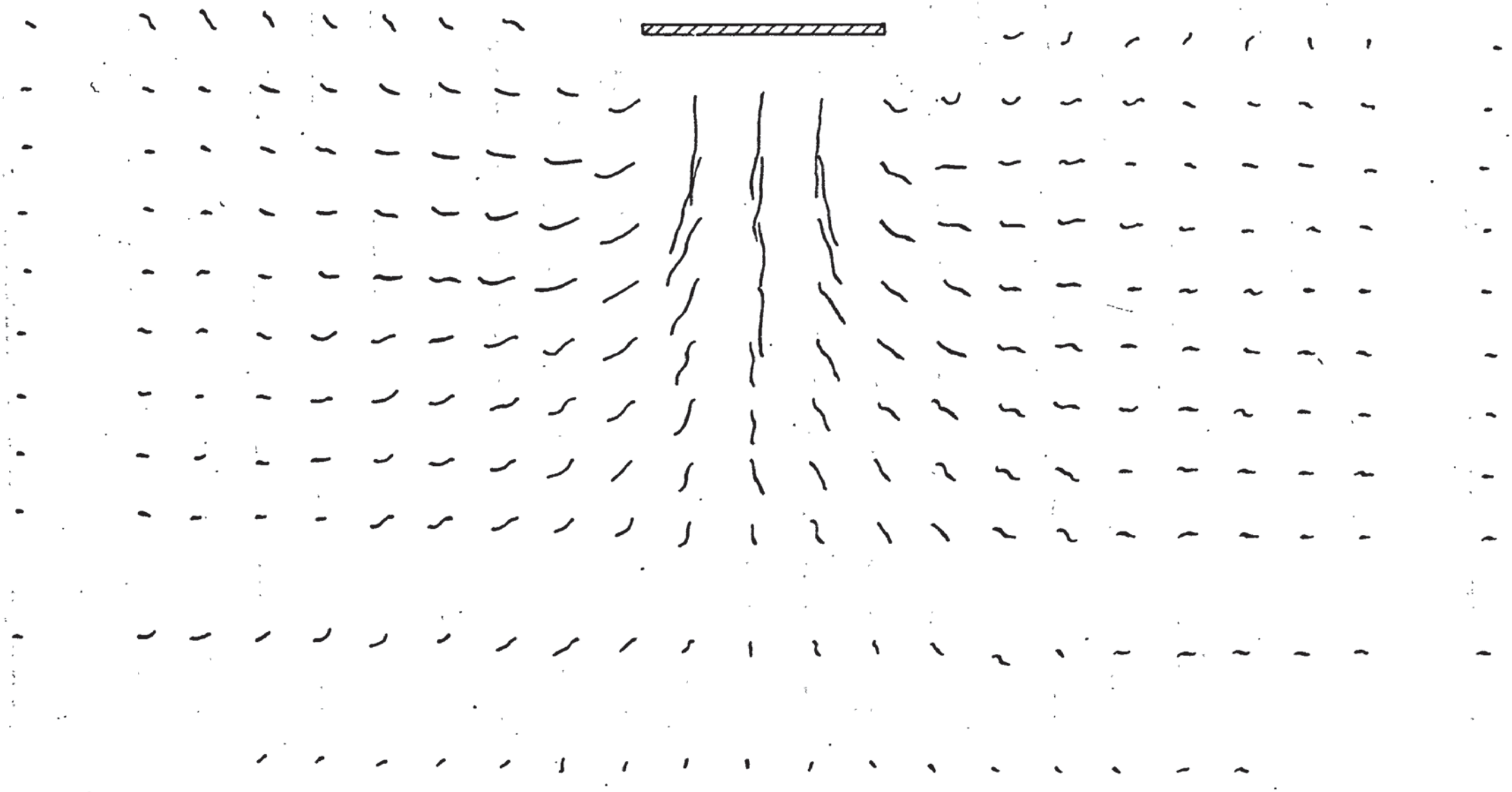

FIGURE 7.21 PLOT OF DISPLACEMENT PATHS OF MARKERS.

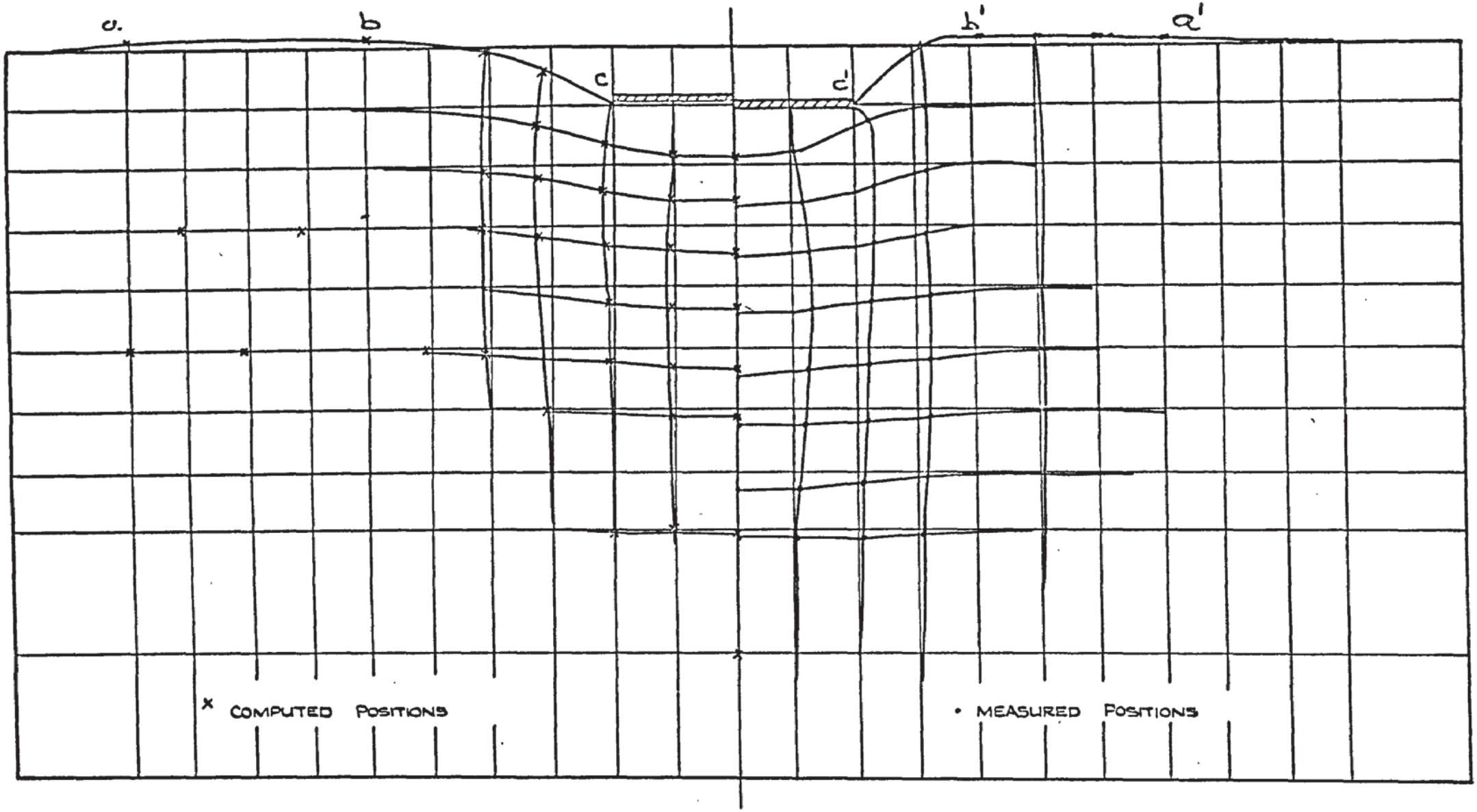

FIGURE 7.22 COMPARISON OF COMPUTED AND MEASURED DEFLECTIONS AT P_3

proved to be capable to indicate a rise in the level of the free surface of the sand at points, such as the region ab, away from the footing. The comparison between regions ab and $a^1 b^1$ is also remarkably favourable.

7.7 Conclusions:-

On the experimental aspect it can be seen that the load taken by the footing is not spread out into the sand as is commonly accepted and no passive failure is indicated to the side of the footing. The velocity field is therefore not in agreement with Terzaghi's bearing capacity model near its outer boundaries.

Both these phenomena are confirmed by the computed results which also give good values for the settlement of the footing. These are especially reliable in the lower regions.

It is therefore concluded that the stress-strain relationship which was developed gave a good approximation to the state of the sand but the method has obvious disadvantages to reproducing the actual discontinuous medium. A clear anomology that arises is the developement of theoretical tensile stresses at certain points marked in the sand. However these points are well away from the footing and in elements which had recorded a state of failure.

It is noticed that the theoretical approach discussed in this chapter and chapter 4 gives more realistic solutions to settlement problems than the more classical ones of the Boussinesq type.

CHAPTER 8

NONLINEAR ANALYSIS OF A PERSPEX SHEAR WALL

8.1 Introduction

This chapter describes an investigation which was carried out to predict the nonlinear behaviour of a Perspex shear wall. A model of the wall was built in the laboratory and tested under load for deflection and stress. A theoretical analysis was carried out using the nonlinear iterative program. Two different stress-strain curves were used in the nonlinear analysis and the results are compared with those obtained experimentally.

The application of the finite element method in analysing such walls would appear to be necessary. Over the last decade they have featured prominently, replacing to a large extent, the 'frame built' structures. Hand methods of analysis are confined to assumptions regarding the amount of bending or shear which is present. Some difficulty was experienced in obtaining meaningful results for this problem, even when using an elastic analysis program and hence a section of this chapter is devoted to the suitability of the method in their solution.

The Perspex material was chosen for its nonlinear characteristics which depend on many different factors and, for this reason an investigation of its behaviour is examined in the next section.

8.2 Nonlinearity of Perspex

In order to investigate the behaviour of Perspex under stress, tests were carried out on a strip of the material $1\frac{1}{2}$" wide and $\frac{1}{4}$" thick. The beam was simply supported in two positions as shown in fig. 8.1(a). The equal overhang of 7" from each support gave a constant bending moment over its middle span which deflected in the form of a circular arc. The weights were applied from hangers via a knife edge and the central deflection D_c was

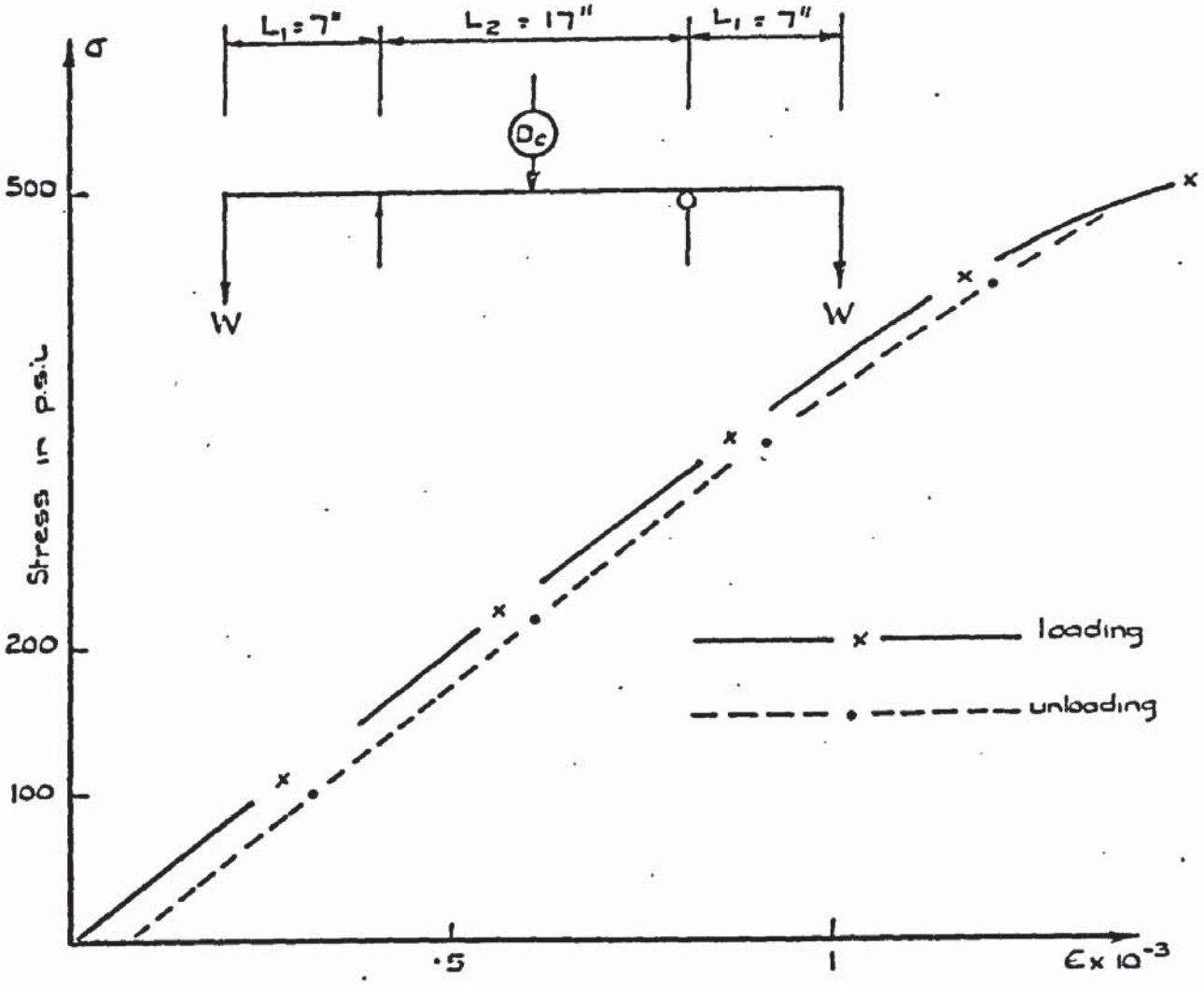

FIGURE 8.1 (a) FAST LOADING

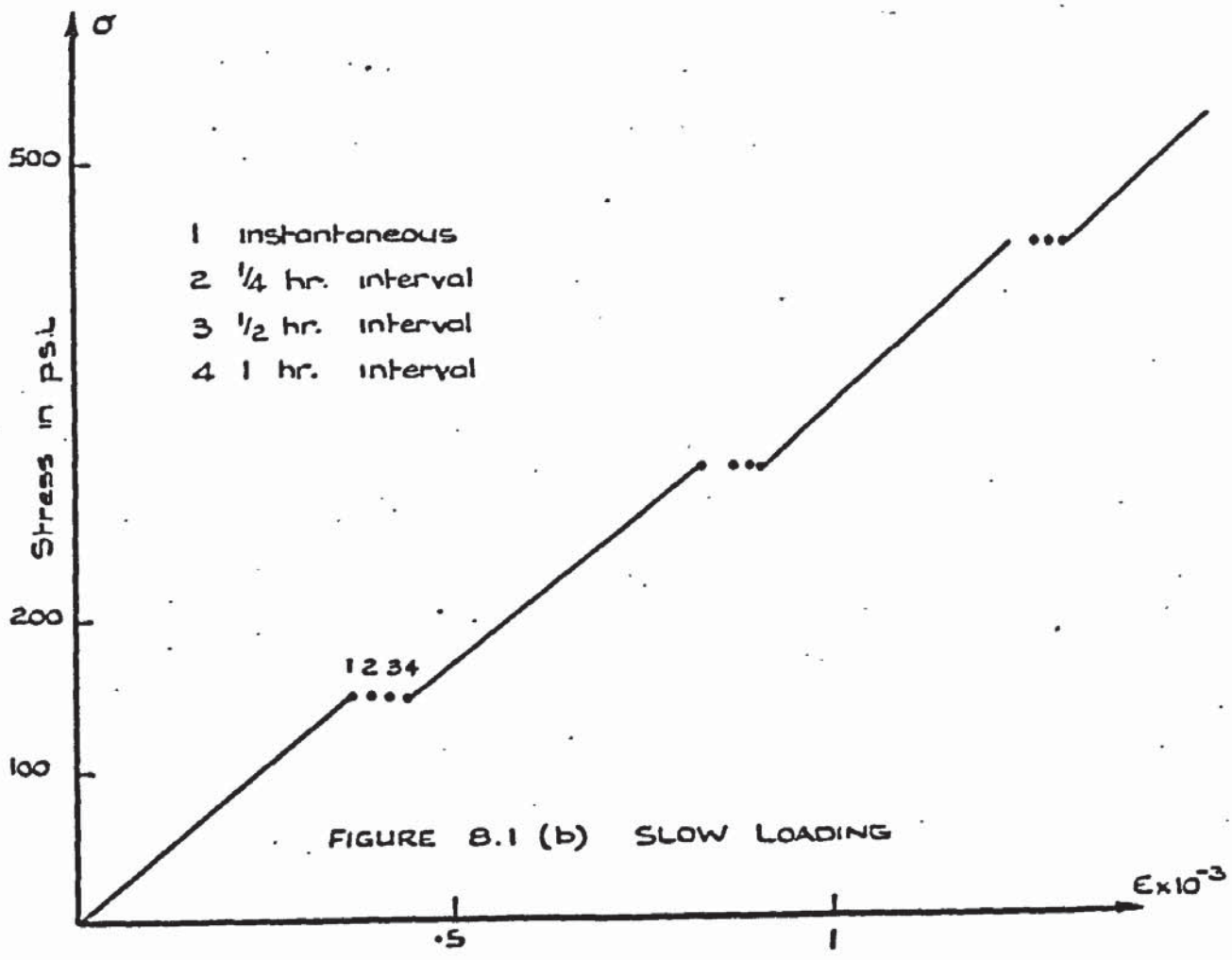

FIGURE 8.1 (b) SLOW LOADING

measured with a dial gauge. It was found that the high flexibility of the material and the membrane forces which were present on loading prevented the beam from deflecting fully, when loaded on two knife edge supports. Consequently one was changed to a roller bearing as shown.

Strain gauges were placed longditudinally and laterally on the beam at the third point in the middle span to measure Poisson's ratio and also so that they could be calibrated. Although the shear wall problem is purely an 'in plane' one, this bending test was justified for a number of reasons. For instance, the calibration of the strain gauges, which proved to be extremely sensitive on Perspex, could be somewhat improved using a bending test. The various factors affecting the stress-strain relationship, such as, stress level and stress history, which were considered to be very significant to the extent that they should be accounted for realistically, were found to be easily controlled by bending tests. This was particularly the case as sufficient numbers of direct testing equipments were unavailable. Furthermore, it is impractical to measure the behaviour of Perspex in compression with the aid of a tensile test. However, the replacement of a bending test for a direct test, in the case of Perspex, is not considered to be misleading since the material properties of Perspex are not considered to vary for bending or direct stress problems. This was investigated in a pamphlet on Perspex issued by the manufactures (53).

The beam was first loaded as quickly as possible to reduce its tendency to creep. The deflections were also noted for the unloading cycle. The stress in the central portion of the beam was found from the formula:-

$$s = \frac{6WL_1}{bt^2} \qquad (8.1)$$

where, for this case $L_1 = 7"$, $b = 1\frac{1}{2}"$ and $t = \frac{1}{4}"$.

Similarly, the strain was calculated from:-

$$e = \frac{4t\,D_c}{L_2^2} \qquad (8.2)$$

where $L_2 = 17"$ and D_c is the measured deflection.

Fig. 8.1(a) shows the stress-strain graph for the loading and unloading of the beam. The initial region of the graph is reasonably linear but nonlinearity is more pronounced as the stresses increase. On unloading, the curve follows a similar form but it can be seen that some creep had taken place due to its failure to return to the origin.

It was decided to investigate the nature of creep in Perspex and for this the same apparatus was used except the loads were applied at varying time intervals in order to ascertain the increase in strain under constant stress. Increments of load were applied and values of central deflection were recorded instantaneously, and after 15, 30 and 60 minutes. These are shown on fig. 8.1(b). Creep, in general, is known to depend on time, temperature, stress level and stress history. The effect of temperature is neglected in this instance although it proved to influence the experiment. It is apparent that the majority of the creep occurs quite quickly as can be seen from the difference in strain between the half hour and hourly intervals. Its magnitude would appear to be independent of stress level but this observation was easily established as being due to a strong dependence on stress history. Therefore the creep at a certain stress level depended on how much and in what form the material had been loaded to obtain the level. During the unloading stage, it was noticed that the strain was recoverable to a considerable extent with time. Thus the material retained its elasticity. The observations just described are typical of the phenomenon of 'viscoelasity' which has been studied in different forms by various authors.

Although empirical laws could be established to define the extent of creep by further testing, the problem of the inherent nonlinearity shown by the fast loading would be more difficult to account for. It was intended to use the nonlinear iterative program in the analysis of the shear wall to judge its suitability in analysing more complex problems where convenient theory is not so readily available. This would make the incremental 'initial load' type analyses impracticable.

In order to make the nonlinearity as pronounced as possible, the shear wall was loaded with varying stress and time increments.

It is clear that under such general conditions a stress-strain relationship could not be based on that of fig. 8.1(b) for the reasons given above. This problem was to be overcome by using a series of control tests which were loaded with the model in an attempt to overcome temperature changes which proved to give considerable difficulty. These tests could be utilized in the following manner.

Consider the case of four test beams loaded concurrently with the model. For the first load increment of the model, the test beams are subjected to different loads and hence a state of stress and corresponding strain is found from each beam test. This is illustrated diagramatically in fig. 8.2, where the four states of stress are marked as 1, 2, 3 and 4. The horizontal portions of the diagrams represent the creep strain which has occurred during or since the application of the load. The model is then loaded with another increment over a certain time. The same ratio of load increments is then applied to the test beams, thus establishing points 5, 6, 7, 8. This process can be repeated for as many loads as is required in the model and the four stress-strain relationships can be evaluated for creep, either under constant stress or under any strain rates.

The stress-strain relationship for the first load case is arrived at by taking positions 1, 2, 3 and 4 from the control tests and

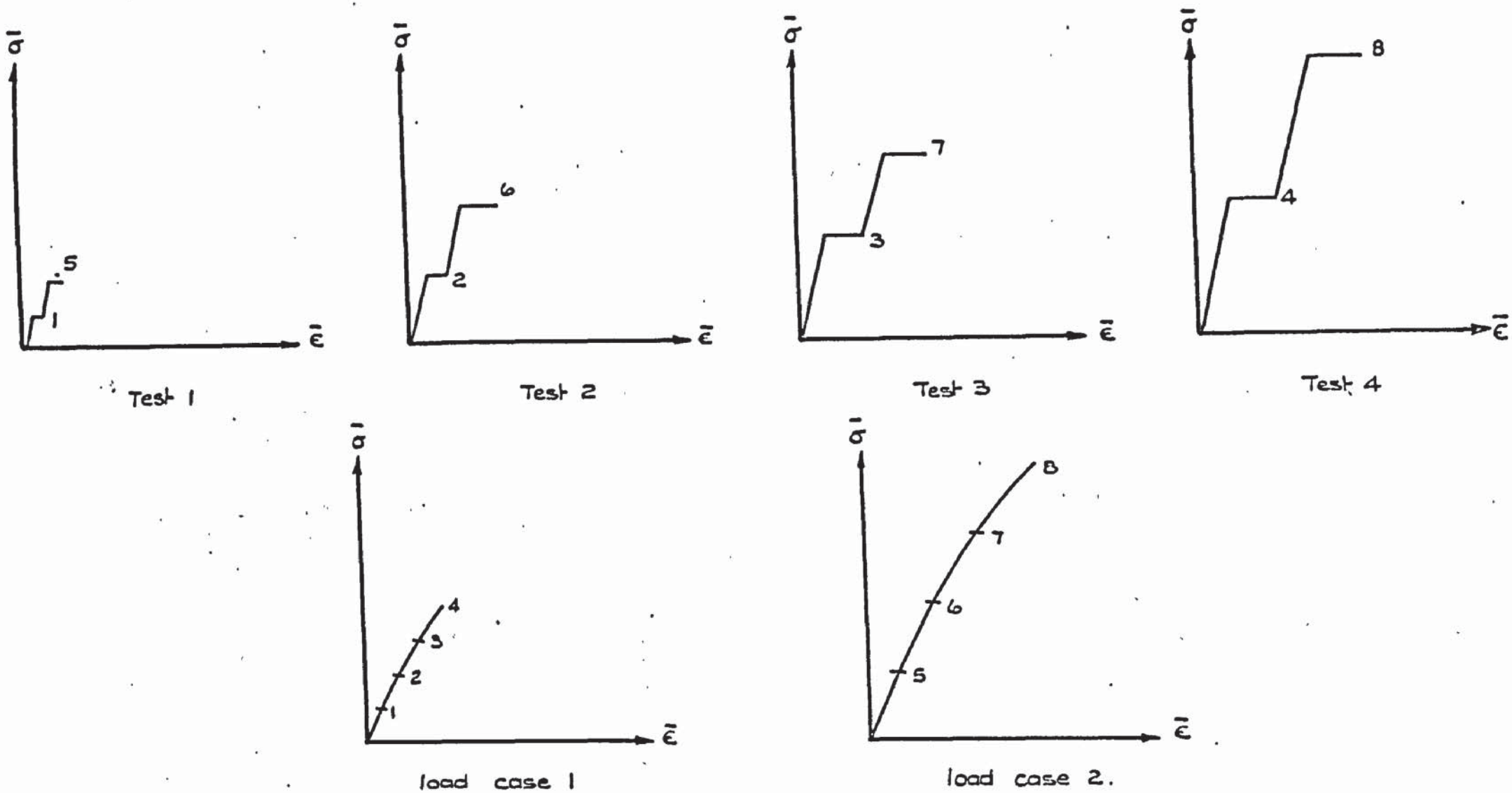

FIGURE 8.2. STRESS - STRAIN CURVES.

plotting a stress-strain graph which is used in conjunction with the model. Graphs of this type are also shown in fig. 8.2. The stress-strain relationship for the second case is given by points 5, 6, 7 and 8. Naturally these can be extended for the number of required loadings.

For the first loading case, the amount of strain depends on time and stress level and hence these are truly accounted for in the first graph obtained from points 1, 2, 3 and 4. For the second load case the strain will also depend on stress history. At a position in the model, any stress at, say point 6, on the stress-strain graph would have previously passed through position 2 in the previous increment. This is assuming that the stresses behave elastically. It can be seen that both these positions are on the same control test 2 and hence the stress history of the point is closely followed. That the stresses are not dependant on time is a well known result of viscoelasticity and hence it can be expected that they will behave elastically.

The greater the number of control tests which are performed, the better will be the accuracy as it is possible to establish more positions on the graphs. The first load increments can be evenly spaced so as to give a good distribution of points on the final stress-strain curves.

The shear wall was therefore to be analysed using a different relationship for each load condition. It is necessary to establish the magnitude of the stress which can be expected in the model under a given load so that the order of the loading in the control tests can be adjusted to give the best stress-strain relationships. For this reason it was decided to use the finite element method in a initial elastic analysis, using average elasticity constants, obtained from these tests. This initial analysis gave the expected order of maximum stresses in the model, which

were used to adjust the control tests so that the stresses developed are of the same order as those of the model.

8.3 Analysis of Shear Walls

It is worthwhile at this stage to mention briefly some of the difficulties encountered in the analysis of shear walls using the finite element method.

When analysing shear walls which, through necessity include openings, it becomes necessary to include prismatic member elements to represent the lintels between these openings. Fig. 8.3 shows a typical shear wall ABCD in which the member elements are represented by the dotted lines EF, GH and IJ. An analysis was performed on this type of structure which consisted of three member elements and 72 rectangular elements. It was found that this type of problem could not be solved directly as the presence of members gave rise to linearly dependent equations inthe overall stiffness matrix. Even when the rotation was supppressed at each end of the member, this difficulty was not overcome. This problem could be solved however by including an 'in plane' rotational stiffness term into the rectangular element (56) or by using a purely pin-ended member. This latter method would not give a true representation of the structure. For 'in plane' problems therefore member and plate elements can only be mixed when the members lie along the side of an element in the manner used in the previous chapter.

This shear wall analysis had therefore to be limited to those of a type where the 'lintels' are thick enough to be represented by plate elements. Another analysis was performed using 114 rectangular plate elements without any prismatic members. It was found that although inversion of the stiffness matrix took place the matrix became unstable and hence the results were meaningless, even though the band width was reduced to a

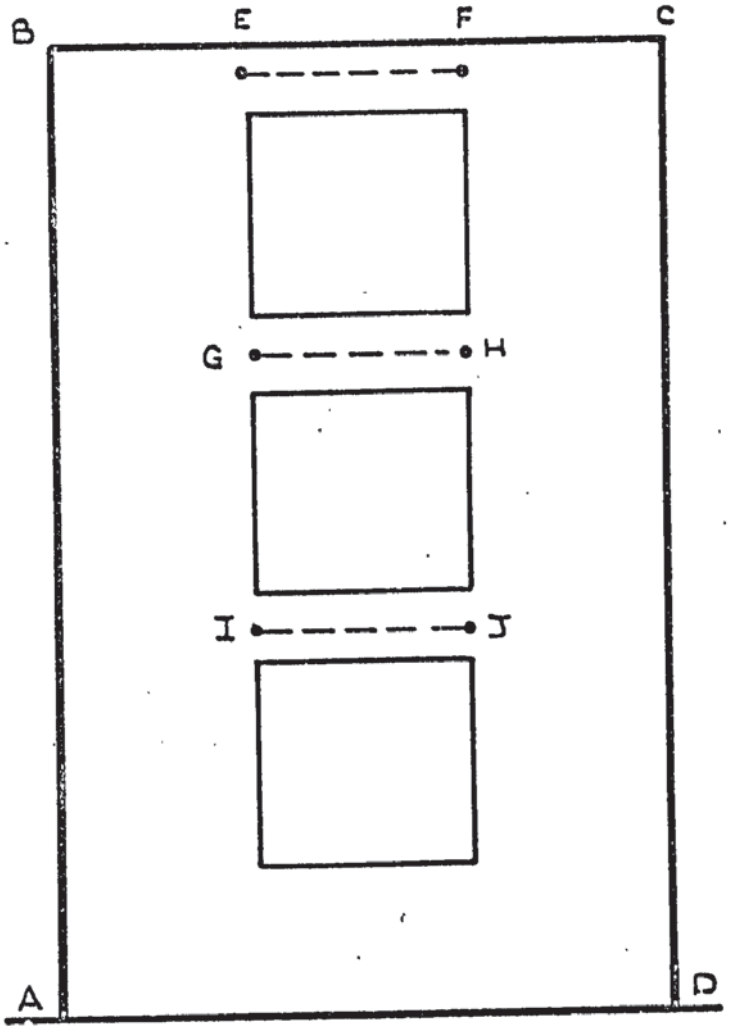

FIGURE 8.3. TYPICAL SHEAR WALL

minimum to make it as well conditioned as possible. The same problem was attempted on the elastic analysis program which makes us of tridiagnolisation. This gave successful results but it was apparent that the conditioning during inversion was becoming critical.

This phenomenon of instability has been often neglected by many authors, but similar occurrences have been noted when trying to analyse shear walls by the finite difference method. It was thought that the size of the stiffness matrix might affect the inversion and therefore a series of tests were tried on differing numbers of elements. When 42 elements were used the matrix was still unstable and stable results were obtained only when very small numbers of elements in the region of ten were used in the form of a solid wall. It was found however that no difficulty was encountered if all vertical movement of the joints was suppressed and hence this only allowed deformation due to shear. By neglecting the bending action of the wall it is evident that serious underestimation of the vertical stresses would occur especially around positions A and D, shown in fig. 8.3. An analysis was therefore tried by considering a portion of the outer perimeter ABCD to be member elements which would have no difficulty in taking into account the bending action. The inside portion of the wall consisted of rectangular plates as before. Again the inversion was unsuccessful.

Up till now only rectangular elements had been used as their linear stress distribution made them more desirable for accuracy than the triangular elements and also the geometric configuration of the wall was more adaptable to this sort of element. It was concluded that this element was not able to reproduce to any extent the bending action of the wall due to its basic shape. It is noticed that the difficulty of using 'in plane' rectangular elements in the analysis of problems involving bending and shear

deformations, is due to ill conditioning arising from the rotation of all the edges of these elements. Suppressing some of the degrees of freedom of these elements, for the case of shear deformation, prevented such rotations and gave rise to well conditioned equations.

For the above reasons it was decided to try the triangular element for the next analysis. The wall was subdivided into 30 elements and the inversion was successful. It was notable that the conditioning parameter during the inversion was of the same order as that in the elastic analysis program using tridiagonalisation. A routine was also included in to the program to clear out all the small elements in the stiffness matix which had arisen from similar sized stiffness terms almost cancelling each other out. Hence unnecessary operations on these negligable terms were eliminated before the inversion.

The final configuration which was chosen is shown in fig. 8.4 and consists of 114 triangular elements with 182 degrees of freedom. The inversion was successfully carried out and the expected order of stresses in the model was found. It was now possible to proceed with the experimentation and control testing which is now described.

8.4 The experimental procedure

Plates 8.1 and 8.2 show the Perspex shear wall in position, which was firmly fixed at its foundation. The wall was manufactured from a solid $\frac{1}{4}$" thick sheet of Perspex. The shape was cut out using a jig-saw and then all the surfaces were machined to the exact sizes as given in fig. 8.5. The inner corners of the openings were given a small radius to prevent stress concentrations building up at these positions. The loads were to be applied by hangers acting at the lower edge and for this purpose three $\frac{1}{4}$" diameter holes were drilled, as shown, through which these hangers could conveniently be looped.

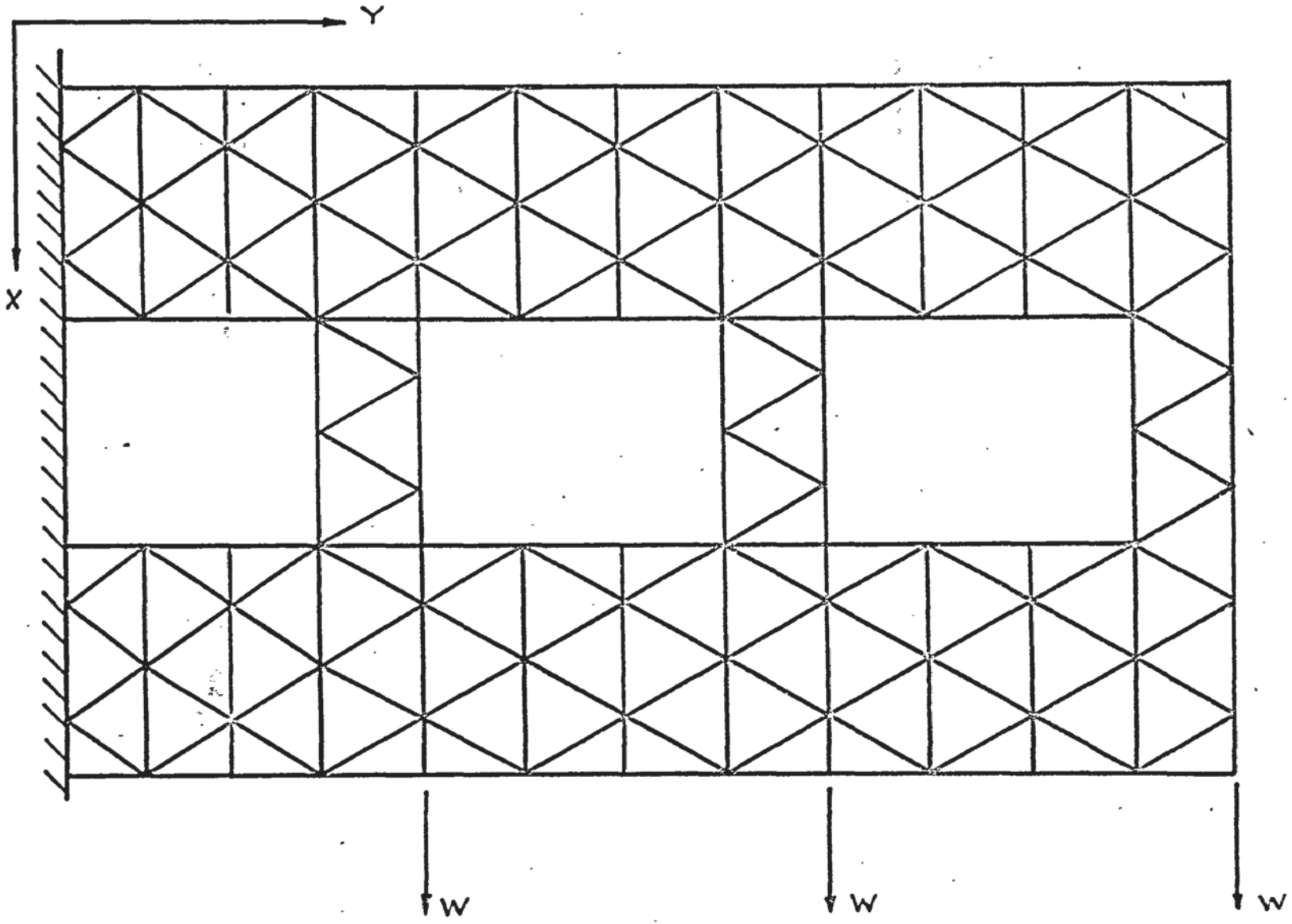

FIGURE 8.4. FINITE ELEMENT REPRESENTATION OF SHEAR WALL

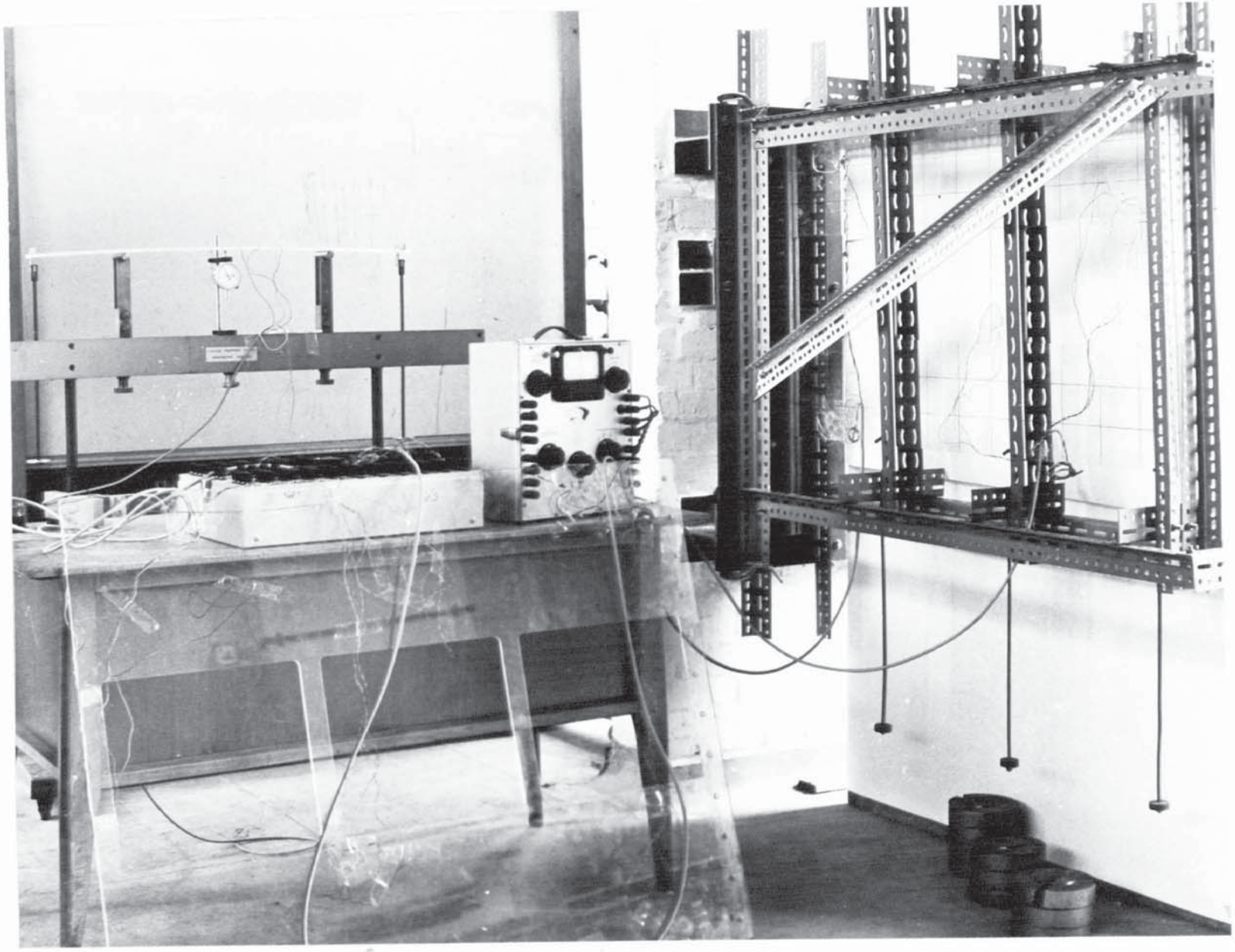

PLATE 8.1. GENERAL VIEW OF APPARATUS.

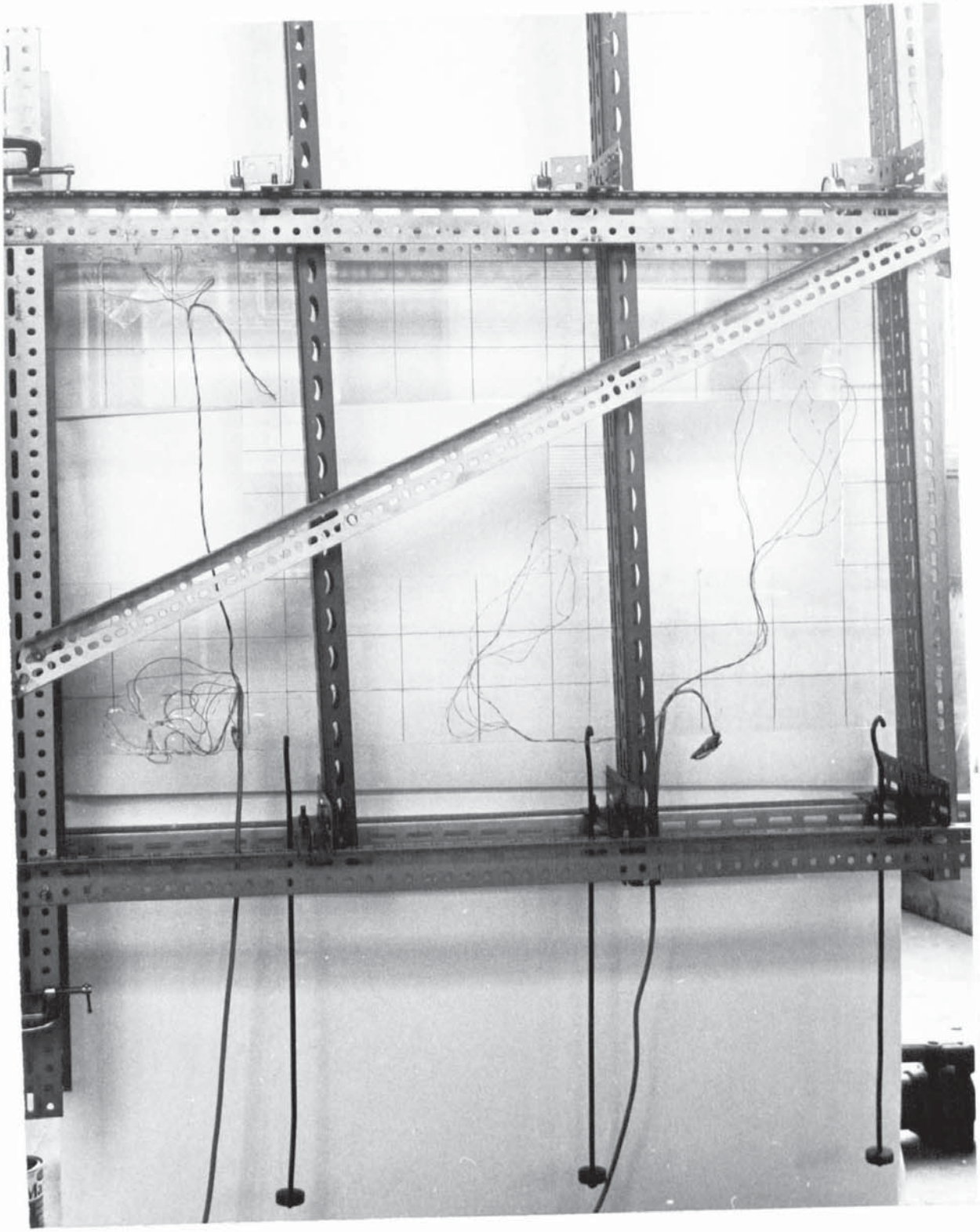

PLATE 8.2 SHEAR WALL

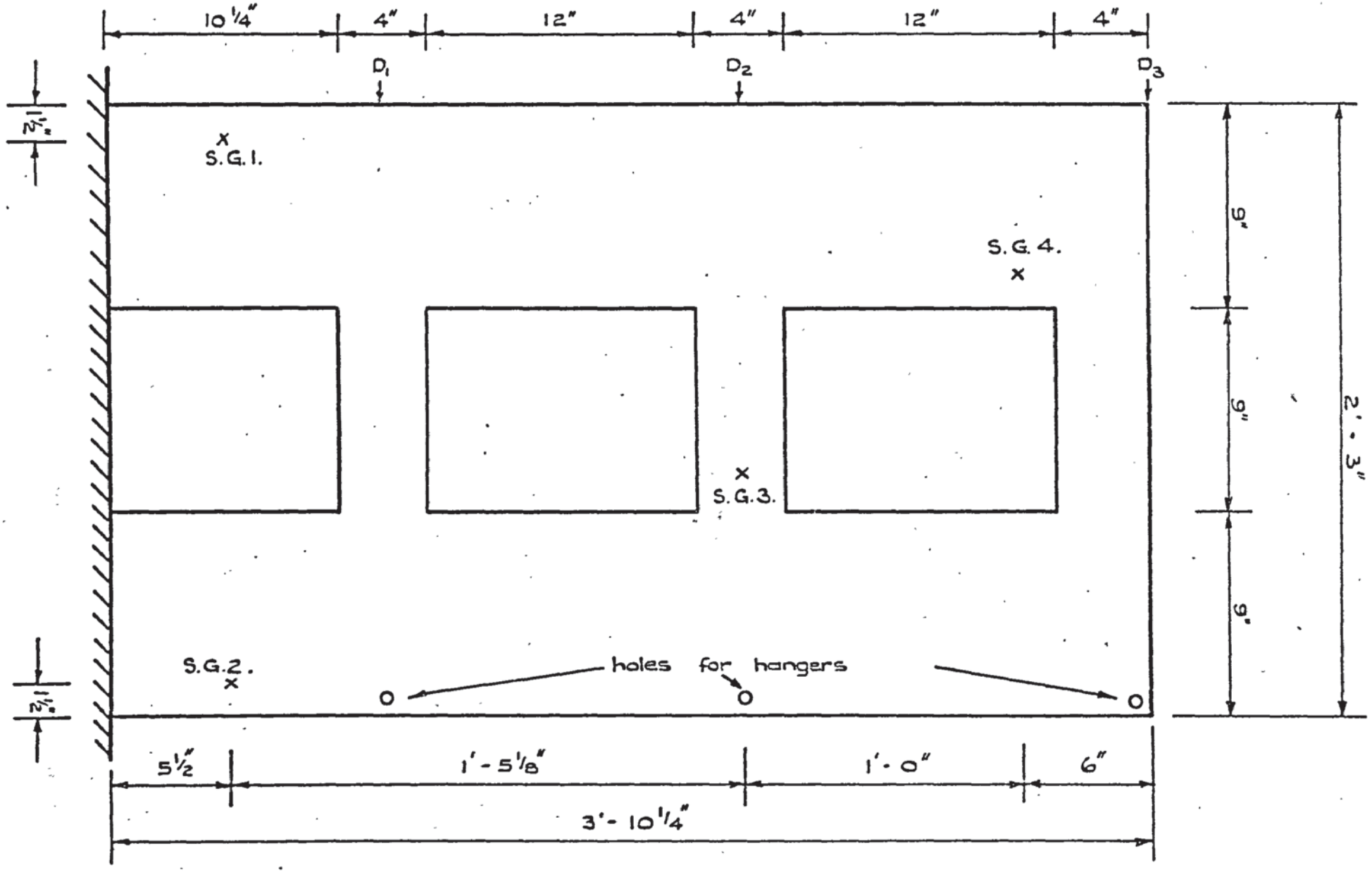

FIGURE 8.5. DIMENSIONS OF SHEAR WALL

The base of the wall was a continuous strip of the material $1\frac{3}{4}$" in width and this was clamped between two pieces of angle iron along its whole length by $\frac{1}{4}$" bolts at 2" centres. The other arms of the angle were in turn bolted to a $\frac{1}{2}$" thick steel plate. As can be seen in the photograph this plate was securely bolted to three I-beams running longditudinally along the laboratory wall. It was considered to be important that no movement of the base should be allowed during the loading and hence great care was taken in ensuring that all components were rigidly bolted. In order to set up the shear wall for uniform fixity, the bolt holes in the steel plate were slightly elongated. The wall was first fixed between the angles and the bolts tightened. The bolts connecting the angle to the plate were then tightened through the elongated holes to allow for any movement.

A Dexian frame was built around the shear wall for two reasons. Firstly, this frame could hold the dial gauges D_1, D_2, D_3 in position and therefore this was supported from the same plate as the wall. Any movement of the plate would hence have no effect on the deflection readings. Secondly, in addition to the frame which followed the outer perimeter of the wall, three vertical pieces were bolted at equal intervals of length across the width of the wall on either side. These were arranged to run along the 'lintels' at a small distance away without actually touching the shear wall. The presence of these prevented the wall from swaying and hence causing 'out of plane' bending stresses. It would also impede the tendency of it to buckle should the stresses become critical. The frame is shown in plate 8.1 which gives the general layout of the apparatus.

Before mounting the wall, the strain gauges were fixed in the positions shown in fig. 8.5 marked S.G.1 to S.G.4. These were fixed in the form of 45° rosettes so that s_x and s_y could be calculated directly and the shear stress evaluated from Mohr's circle. These could be

conveniently compared with the finite element stresses. The Perspex surface was prepared first by 'roughing up' with fine sand paper to give the glue better grip and then cleaning with Ammonia and Carbon Tetrachloride. Again Eastmann's 911 glue was found to be the most suitable. The gauges were connected up by soldering to multicore wire before fixing the wall in position.

The gauges were connected through a Peekel strain gauge recorder. It was found that one dummy gauge was needed for each active as the gauges were very sensitive to heat. On passing a current through a new gauge, this warmed up and the change in temperature in the Perspex caused an unsteady reading. The dummy, which has a current passing through it almost continuously, had by this time a steady resistance. By using one dummy for every active, as the current is passed through each pair in turn, they both warm up simultaneously and give a steady reading. The presence of body heat was enough to affect the gauges considerably. Even the dummy gauges had to be fixed to a similar sized sheet of Perspex to that of the wall so that heat dissipation would be similar. Nevertheless, the total effect of heating was found to be significant and difficult to avoid.

As the nature and extent of nonlinearity was to be reasonably regular it was decided that four control tests would be adequate. These were to be of a similar form as the beam test described earlier and hence four specimen strips were cut from the Perspex sheet and carefully machined to an identical width of $1\frac{1}{2}$". For clarity, only one of these is shown in plate 8.1 which also shows a 'dummy shear wall' to which the dummy gauges were fixed. In order to obtain a measureable amount of nonlinearity the loads were to be applied in unequal increments at varying time lapses, thus causing creep strain. It is necessary that the maximum load was not so great as to cause buckling. On the other hand it should be large enough to demonstrate the effect of creep. The time intervals were also limited to

decrease the chances of temperature changes. Although this factor should be compensated for by the control tests, the great sensitivity of these gauges on Perspex made this impracticable and hence could not compensate for, say, the sudden intervention of sunlight.

With these factors in mind it was decided to load the wall initially with W = 8.8 lbs. The deflections and gauge readings were recorded and the load increased to W = 22 lbs (see fig. 8.4). A time lapse of 10 minutes was allowed before the readings were noted. W was then made to be 52 lbs. and the time lapse increased to 1 hr. The last increment of load was up to 105 lbs. and a large increment of time, 17 hours was waited before the final readings were taken.

It had previously been calculated from the finite element analysis described in the last section that the maximum stress to be expected would not exceed about 600 psi and thus it was possible to arrange the loading of the control test accordingly. From this the maximum stress in the first load increment was worked out and arranged so that one beam was loaded up to this stress. The remaining three beams were loaded to a proportion of $\frac{3}{4}$, $\frac{1}{2}$, $\frac{1}{4}$ of the stress respectively. For the next load increment the loads which were, say, $w, \frac{3w}{4}, \frac{w}{2}, \frac{w}{4}$ originally were increased to, $\frac{5w}{2}, \frac{15w}{8}, \frac{5w}{4}$ and $\frac{5w}{8}$. After the time lapse, the loadings were increased in a similar fashion in the same proportions to that of the shear wall increments.

The experiment was carried out one evening and overnight on a day when little temperature variation was expected. It was next possible to 'plot' the load deflection pattens for the three gauges and evaluate the strains for each loading.

The results of the control tests are shown in the form of stress against strain and Octahedral shear stress against Octahedral shear strain

for the four test beams in table 8.1. The reasons for using octahedral stresses and strains will become apparent in the next section. Throughout the tests Poisson's Ratio was measured by strain gauges fixed longitudinally and laterally on the beam. Surprisingly little variation was recorded and was sometimes rather erratic due to gauge sensitivity. It was therefore decided to use an average value of 0.351 throughout the analyses.

8.5 Stress-Strain Relationships

The stress-strain curves which were derived from the control tests can only be representative of the nonlinear relationship for uniaxial states of stress. When stress systems become biaxial or triaxial the effects of the minor principal stresses are not taken into account and hence these stress-strain graphs have to be adapted so as to apply to the two or three dimensional cases. In this section two methods of doing this are described which are later used and compared in the computational analysis.

The first method is known to engineers and is based on the Von Mises breakdown theory. This takes a similar form to that used in the last chapter. In its simplest form it states that the total strain energy in a three dimensional body which is acted upon by the principle stresses s_1, s_2, s_3 can be split up into strain energy due to change in volume and strain energy due to change in shape. The stresses have also two components. These are:-

$$s_v = (s_1 + s_2 + s_3)/3$$

and,
$$s_s = \tfrac{1}{2}\sqrt{(s_1 - s_2)^2 + (s_2 - s_3)^2 + (s_3 - s_1)^2} \qquad (8.1)$$

which are known as the first and second stress invariants respectively. The stress s_v accounts for change in volume while s_s causes change in shape. It is well known that under a hydrostatic pressure most continuous materials behave elastically and are not time dependent. Most nonlinear effects such as plasticity and creep depend on the deviatoric stress which causes change of shape, and hence this function of the principal stresses will govern the

TEST 1				TEST 2				TEST 3				TEST 4			
s	e	τ_{oct}	γ_{oct}	s	e	τ_{oct}	γ_{oct}	s	e	τ_{oct}	γ_{oct}	s	e	τ_{oct}	γ_{oct}
12.3	.0318	5.80	.0406	24.6	.0635	11.6	.081	36.88	.0960	17.4	.123	49.2	.127	23.1	.162
30.7	.0827	14.45	.1053	61.50	.1650	29.00	.2125	92.25	.254	43.40	.323	123.0	.343	58.0	.436
73.50	.2180	34.70	.2775	147.5	.443	69.50	.5630	221.5	.673	104.0	.856	295.0	.924	139.0	1.175
147.50	.510	69.50	.6490	295.0	1.04	139.0	1.325	442.5	1.59	208.0	2.023	590.0	2.18	278.0	2.775

Values of $\dot{e}$ and γ_{oct} are x 10^{-3}

TABLE 8.1 RESULTS OF CONTROL TESTS

nonlinearity in the material due to creep.

As was explained in the last chapter, it is more convenient to use the Octahedral shear stresses and strains due to their simple relationship with the shear modulus. The pseudo-elastic value for Young's Modulus can be derived from this in a straightforward manner.

The other proposed method is to consider the material as orthotropic at an angle corresponding to the direction of the principal stresses. The stress-strain curve was used from the direct measurements and therefore two values of Young's Modulus were found for each element corresponding to the principal stresses. If the angle at which these act is calculated, the direction of orthotropy is known relative to the local axes in each element. The influence of the intermediate principal stress is ignored but in such a plane stress problem its value is known to be zero. An obvious approximation is introduced which implies that the element is taking up the form of a layered structure in the plane of its principal stresses which has two elasticity constants E_1 and E_2 in the respective directions. In effect this approximation is acceptable as long as the change of modulus is the same as that in the material as the planes are rotated from direction 1 up to 2.

An elasticity matrix can be simply written down relating the principal stresses in directions 1 and 2, to the strains. As before in general terms matrix $\underline{D}$ will be given by:-

$$\underline{D} = \alpha_o \begin{bmatrix} \alpha_{11} & \alpha_{12} & \alpha_{13} \\ \alpha_{21} & \alpha_{22} & \alpha_{23} \\ \alpha_{31} & \alpha_{32} & \alpha_{33} \end{bmatrix}$$

where, $\alpha_o = E_2/(1 - \nu_2^2 E_1/E_2)$

$$\alpha_{11} = E_1/E_2 \qquad (8.2)$$

$$\alpha_{21} = E_1 \nu_2 / E_2 \qquad (8.2)\ \text{(Contd.)}$$

$$\alpha_{22} = 1$$

$$\alpha_{33} = G_2/E_2(1 + \nu_1)(1 - \nu_1 - 2\nu_2^2 E_1/E_2)$$

$$\alpha_{13} = \alpha_{23} = 0$$

These values refer to the principal directions and therefore the elasticity matrix must first be transformed back to the local directions P and Q of the element before it is used in the stiffness matrix. This will involve a rotation through an angle B which is the angle of rotation from P to Q of the principal stress.

This transformation is analogus to that of the unassembled stiffness matrix and if a transformation matrix $\underline{H}$ can be found relating the strains in the principal plane $\underline{e}_{1,2}$ to those in the PQ plane $\underline{e}_{p,q}$ in the form:-

$$\underline{e}_{1,2} = \underline{H}\, \underline{e}_{p,q} \qquad (8.3)$$

then the elasticity matrix $\underline{D}_{p,q}$ in the local plane is related to that of the principal plane $\underline{D}_{1,2}$ by the equation:-

$$\underline{D}_{p,q} = \underline{H}^1\, \underline{D}_{1,2}\, \underline{H} \qquad (8.4)$$

The matrix $\underline{H}$ can be calculated from Mohr's circle to be:-

$$\begin{bmatrix} C^2 & S^2 & SC \\ S^2 & C^2 & -SC \\ -2SC & -SC & C^2-S^2 \end{bmatrix}$$

where C is the cosine and S the sine of the angle B.

By multiplying out equation (8.4) the elements of the elasticity matrix $\underline{D}_{p,q}$ are calculated as:-

$$\alpha^1_{11} = C^4\alpha_{11} + S^4\alpha_{22} + C^2S^2(2\alpha_{12} + \alpha_{33})$$

$$\alpha'_{12} = \alpha_{12}(s^4 + c^4) + s^2c^2(\alpha_{11} + \alpha_{22} - \alpha_{33})$$

$$\alpha'_{13} = c^3s(2\alpha_{12} + \alpha_{33} - 2\alpha_{11}) + s^3c(2\alpha_{22} - 2\alpha_{12} - \alpha_{33})$$

$$\alpha'_{22} = s^4\alpha_{11} + c^4\alpha_{22} + s^2c^2(2\alpha_{12} + \alpha_{33}) \qquad (8.5)$$

$$\alpha'_{23} = s^3c(2\alpha_{12} + \alpha_{33} - 2\alpha_{11}) + c^3s(2\alpha_{22} - 2\alpha_{12} - \alpha_{33})$$

$$\alpha'_{33} = \alpha_{33}(c^2 - s^2) + 4s^2c^2(\alpha_{11} + \alpha_{22} - 2\alpha_{12})$$

The primed constants now refer to the elements in the PQ directions whereas unprimed elements correspond to the principal directions as before.

An analysis can now be performed using these terms in the element stiffness matrices as described in the next section.

8.6 Computational Analysis

Before the two types of analysis could take place slight alterations were needed in the existing iterative program. The analysis using Octahedral stresses is first considered.

The graphs of stress against strain in the control tests which are given in table 8.1 were first replotted for the four loading cases L_1, L_2, L_3, L_4 and are shown in fig. 8.6. These graphs are now in the form to be used for the analysis of the wall at the loads of W = 8.8, 22, 52, 105 lbs. respectively. The first loading was applied instantaneously and only a very small amount of nonlinearity was measured and therefore a linear analysis of the wall was carried out for values of Young's Modulus and Poisson's ratio of 3.87×10^5 and .351 respectively.

For the second load case the graph L_2 was converted to a graph of Octahedral Shear Stress against Octahedral shear strain. For the simple uniaxial state of stress where $s_2 = s_3 = 0$, this is achieved by the equations:-

$$\tau_{oct} = \sqrt{2}/3.\ s_1$$

$$\gamma_{oct} = 2\sqrt{2}/3.\ (1+\nu).\ e_1 \qquad (8.6)$$

FIGURE 8.6. STRESS - STRAIN CURVES.

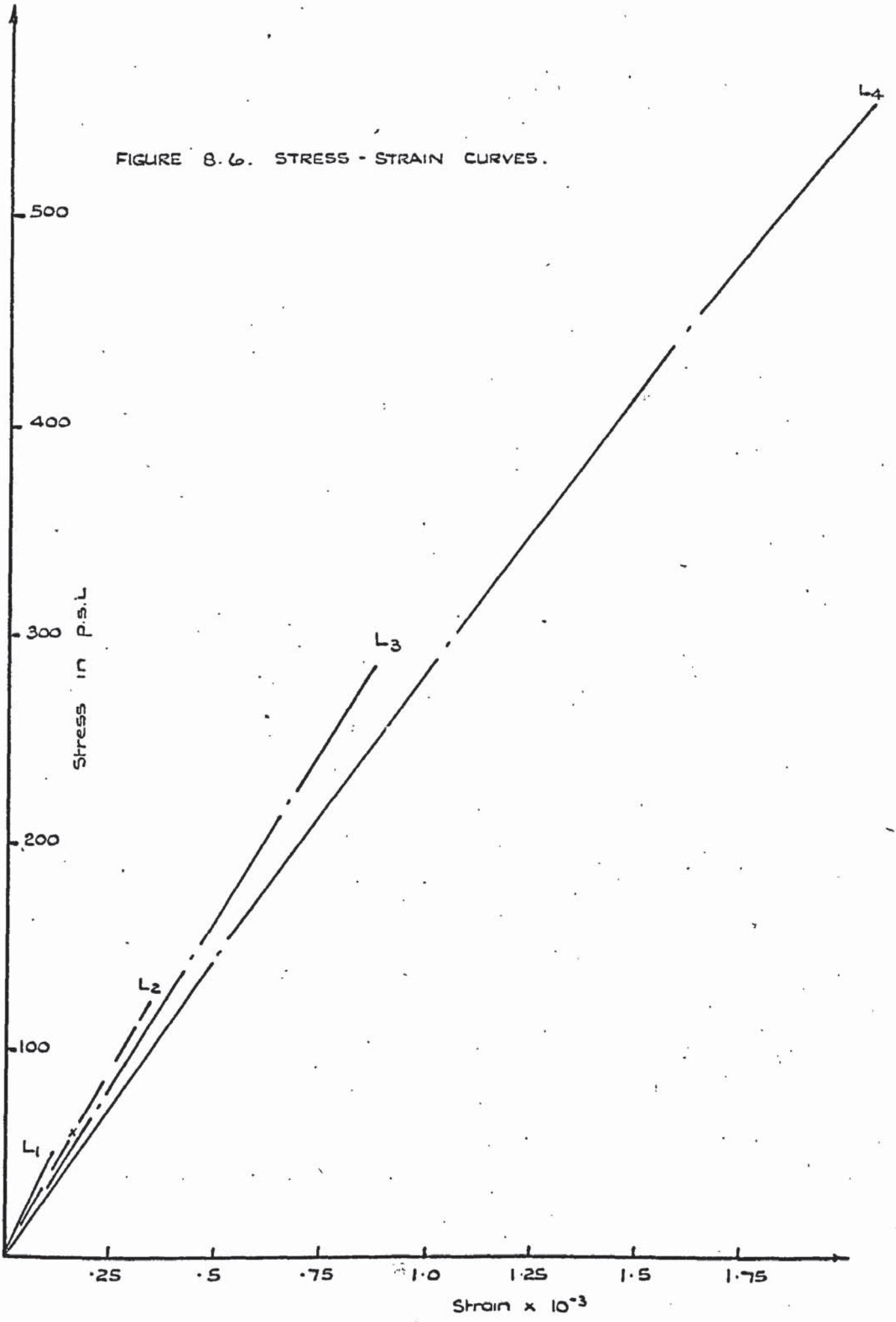

The resulting values are also given in table 8.1. The five points on this curve were fed in as data to the computer. As the elements were to be considered isotropic this was done twice corresponding to the P and Q directions. An initial value for Young's Modulus of 3.87×10^5 was assumed and hence the state of stress and strain in each element calculated. From this the Octahedral strain was evaluated and a value for the shear modulus was arrived at from the curve. Hence the new Young's modulus could be calculated and used in the next iteration.

A similar procedure was used in the analysis of the third and fourth load cases. No difficulty was encountered in the computation and usually three or, at the most, four iterations were sufficient for accurate convergence. This was due to the relatively small changes of Young's Modulus for each load case which were in the order of 8 per cent. The minimum tolerance value before the convergence of each element was taken as 0.005.

The stress-strain curves for the orthotropic analysis were taken from fig. 8.6. The rate of convergence was again very rapid and of the same order as the previous analyses. All these analyses took under 6 minutes on the Atlas computer. As previously mentioned, the elements of the elasticity matrix had been separately programmed to cater for the states of plane stress or plane strain and therefore the revised orthotropic elements given by equations 8.5 could be inserted into the iterative program with little difficulty. The five points on the stress-strain curve were fed in for both the principal directions and the initial value of Young's Modulus was calculated for a state of zero stress. The stresses were found in each element at the end of the first iteration and hence the principal strains and their angle of rotation B from the local axis was established.

From these strains the two values of Young's modulus E_1 and E_2 were found from the graphs and the next iteration initiated. The iterations were then repeated until the tolerence value in each element became .005.

8.7 Analysis of Results

Fig. 8.7 shows the graphs of load against deflection at points D_1, D_2 and D_3 on the shear wall. These are the positions of the dial gauges, as shown in fig. 8.5. The experimental load-deflection curves are shown as dotted lines while both the theoretical curves are shown as full lines. Both the octahedral (computation 1) and orthotropic (computation 2) methods appear to give results which are in good agreement with each other and with the experimental results.

The results show that when the shear wall is subject to heavy loads the octahedral method underestimates the deflections. On the other hand the orthotropic approach slightly overestimates these deflections. However the agreement between the theoretical and the experimental results appear to be reasonable. When the load W is 105.6 lbs., for instance, the maximum difference between the deflection given by the orthotropic approach and the experimental deflections do not exceed 8%. At this load the maximum difference between the experimental deflections and those obtained by the octahedral approach is only 10%.

In table 8.2 the values of the stresses s_x and s_y at strain gauge positions 1 to 4 are compared with each other under various loading stages. These two sets of results do not agree with one another very well. However on inspecting the results, it seems that, for the octahedral case, both stresses s_x and s_y increase linearly with the loads. This is remarkably so at all the points where stresses were calculated. This linear behaviour indicates that the material has, indeed, behaved in a

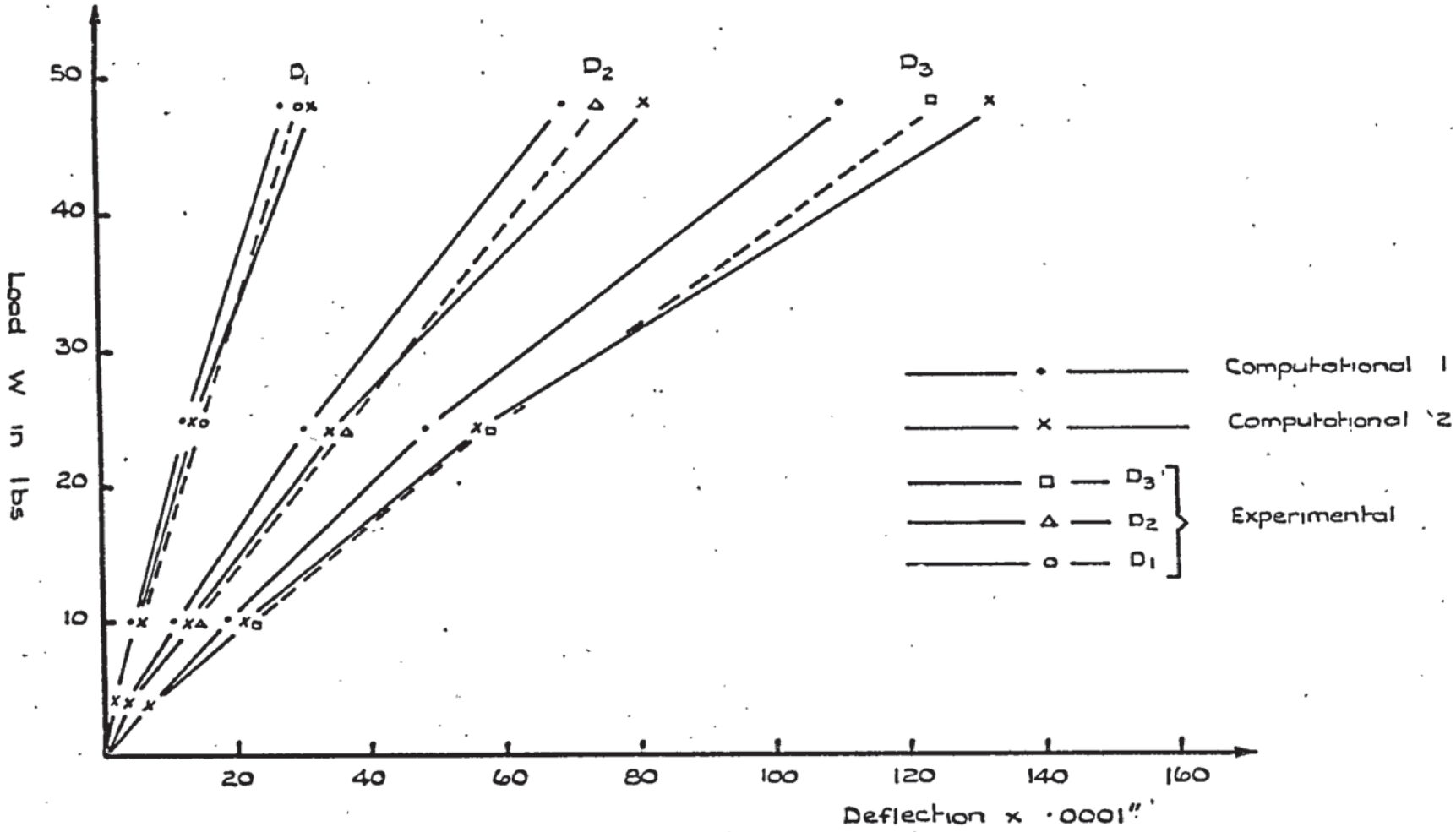

FIGURE 8.7 LOAD DEFLECTION GRAPHS FOR SHEAR WALL

	COMPUTATIONAL 1		COMPUTATIONAL 2		GAUGE NO.
W	s_x	s_y	s_x	s_y	
8.8	.583	20.09	.583	20.09	1
22	1.31	50.32	-3.77	72.40	
52.8	2.98	120.71	-8.66	173.72	
105.6	6.53	241.27	-16.45	348.56	
8.8	-.58	-20.49	-.58	-20.49	2
22	-1.29	-51.33	4.35	-71.48	
52.8	-2.89	-123.06	10.23	-171.24	
105.6	-6.43	-246.05	20.16	-341.45	
8.8	-7.079	-.43	-7.08	-.43	3
22	-17.73	-1.12	-24.99	.07	
52.8	-42.65	-2.73	-60.02	1.77	
105.6	-85.04	-5.335	-120.04	3.61	
8.8	6.63	4.59	6.63	4.59	4
22	16.6	11.52	20.55	7.79	
52.8	39.92	27.69	49.34	18.71	
105.6	79.66	55.23	98.73	37.44	

TABLE 8.2 COMPARISON OF COMPUTED STRESSES IN A SHEAR WALL

viscoelastic manner, that is the stresses have shown to be independent of time. For this reason these stresses can be considered to be reliably representing the actual stresses in the shear wall. The stresses obtained by the orthotropic approach (computation 2) often appear inconsistant and for this reason these stresses can not be relied upon.

The difficulties, stated earlier, concerning the measurements of strains experimentally, affected these results considerably. For this reason good agreement was not obtained between stresses calculated experimentally and those obtained by either method. The experimental results also showed a degree of inconsistancy, in spite of the fact that some of the tests were repeated. It was noticed that when strains were small or when the creep time was not sufficiently large, the results could be unreliable. The strain was changing fast while these measurements were being obtained. At small strains it was impossible to make use of fig. 8.6, since all the points on this graph, corresponding to measured strains, were very near the origin where various curves become indistinguishable. For these reasons, only selective results, obtained experimentally and theoretically, are compared in table 8.3.

These results do show that comparison between theoretical and experimental values can only make sense at high stresses. For instance values of s_y at gauge points 1 and 2 agree reasonably with the theoretical values, while the small stresses at these points do not agree with the theoretical results. There is also some agreement between values of s_y at gauge 4 with those obtained theoretically. However it is difficult to expect gauges 3 and 4 to give good results, since these gauges were deliberately positioned at points of stress concentration.

In spite of the above facts, the results given in this chapter and the other chapters indicate, that, while the finite element method gives

LOAD	COMPUTATIONAL		EXPERIMENTAL		GAUGE No.
W	s_x	s_y	s_x	s_y	
22	1.31	50.32	32	64	
52.8	2.98	120.71	50	140	1
105.6	6.53	241.27	120	241	
22	-1.29	-51.33		-75	
52.8	-2.89	-123.06	-27	-162	2
105.6	-6.43	-246.05	-39	-275	
22	-17.73	-1.12		-20	
52.8	-42.65	-2.75	-105	-30	3
105.6	-85.04	-5.34	-200	-60	
22	16.6	11.52	gauge	10	
52.8	39.92	27.69	did not	25	4
105.6	79.66	55.23	record	36	

TABLE 8.3 COMPARISON OF COMPUTED AND EXPERIMENTAL STRESSES IN A SHEAR WALL

good results for deflections, it does not appear to give favourable results for stresses. More detailed reasons for this will be given in the conclusions.

CHAPTER 9

GENERAL CONCLUSIONS

This thesis has investigated the suitability of matrix methods in analysing various structural problems in civil engineering. The main considerations which have been given attention in the linear use of this method have been:-

(i) Structural idealization

(ii) Computational problems

(iii) Finite element method

The most significant advantage of matrix methods for the analysis of complete structures is its ability to give a true representation of the structure. That is, a three dimensional structure consisting of prismatic members and plate components subject to 'in plane' and 'out of plane' forces. It was for this reason that the triangular element stiffness matrix which was described in chapter 2 was established. Emphasis was put on the analysis of complete structures and it has been shown that these problems can be idealized with little difficulty. It has been indicated in chapter 6 that the analysis of a structural part by assuming 'temporary' boundary conditions can be misleading. This is not to say though that the present methods could not be used for a reanalysis of a part of the structure using the forces which were determined in the first analysis as implied loads for the subsequent analysis. This type of 'method of sections' may well prove useful where highly irregular structures are concerned.

A major purpose of the present work was to produce computer algorithms capable of representing and analysing such complete structures which are also of complicated and irregular type. In order to make the programs versatile it became necessary to construct the overall stiffness matrix of the structure by triple multiplication of the displacement transformation matrices and the element stiffness matrices. This was so for three reasons.

Firstly, when constructing the displacement transformation matrix of an element, its general orientation in three dimensional space can be easily represented. Secondly, the degrees of freedom at the joints may be varied, at will, from joint to joint, in a manner that represents the actual condition at each joint exactly. These variations can be included with the joint data of each joint and thus used in the construction of the displacement transformation matrix. Finally, the construction of the element matrices individually enables the inclusion of various irregularities that often exist in real civil engineering structures. In the general programs available now, versatility was extended so far as to reduce the inclusion of many intricate factors to that of data preparation. These included the effect of existing gusset plates, haunches, and lumps; the effect of the centre lines of elements not meeting at joints to which they are connected, the Tee beam effect and the effect of offset of shear centres. It was these aspects of the program that made it possible to analyse such complicated structures as those given in chapter 6, where not only the shape of these structures were complicated and their joint connections irregular but also their degrees of freedom differed at many points and extended up to 2500 in number.

It is encouraging to notice that in spite of the number of equations involved and the irregularities encountered, the results were reasonable. There was no evidence to suggest that accumulative numerical errors, which occur in the inversion of such large matrices, had anything but secondary effect. Also it is unlikely that different techniques of inversion cause significantly different results providing they are reasonably sophisticated. In all cases the deflections obtained were exceptionally good. The stresses on the other hand did not always prove to be acceptable. Nevertheless these stresses in the case of the highly irregular bridge with about 2400 equations showed good agreement with other methods.

The fact that stresses do not agree with expected or experimental results is not solely due to the courseness of element subdivision. In the case of the table of chapter 5, subdivision of the elements did not always improve the results everywhere. The major reason for obtaining unexpected results for stresses is due to the fact that the element stiffness matrices were obtained using displacement, and not stress functions. It is therefore suggested that stress functions should be used to construct the element stiffness matrices. Only then can one expect reliable stress analysis of structures.

It has been generally accepted that a fine mesh size with a displacement conforming element will give good results but for the more practical applications of the finite element method neither requirement can be fully met. The 'bound' theorem, can no longer be theoretically justified for three dimensional structures unless the elements which meet at angles can be made to conform at least for displacement. This would involve the evaluation of a stiffness matrix in which 'in plane' and 'out of plane' action can be combined for neighbouring elements. The mixing of different types of elements also appears, at this stage, to lead to inaccuracies. and more research is needed to be done on evaluating stiffness matrices for differing shaped elements which are compatible.

The suitability of the method is largely dictated by the size and cost of the computer available. In using a tridiagonalisation scheme on a suitably shaped structure there is no upper limit in terms of numbers of elements and degrees of freedom although clearly inversion errors will start to become significant. Certainly for estimation of deflection the accuracy gained is sufficient.

The practical limitation of the structural size is governed by the stiffness matrix, or the part of the matrix which has to be stored in the computer while it is being inverted. An alternative method of storage to the sparse matrix technique would be to retain half the matrix, from the

leading diagonal outwards up to the most extreme element. In this case the storage requirement depends on the irregular band width of the matrix which in turn is governed by the greatest difference in joint numbering of the nodes defining any one element. It is also more usual to construct the overall stiffness matrix directly. On the other hand the sparse matrix technique does not depend on the maximum joint numbering difference but does store both sides of the symmetrical matrix. It is clear therefore that each is suited for different kinds of structures. In the case of the road bridge the joint numbering difference is quite small and hence a banded technique would be preferable. For the casing, which is a highly irregular structure, only the sparse matrix technique could be used.

The analysis of the deformation characteristics of the footing on the sand mass proved to give very promising results. There is clearly more room for research and improvement both on the theoretical and computational side.

Firstly, by introducing a three dimensional element a much larger scope of boundary conditions could be analysed and would allow the use of incompressible elements. As it stands, the program does not take into account the change in geometry of the medium as deformation becomes larger. This is very significant immediately around the footing. One method of improvement would be to use a quadrilateral or triangular element and recalculate its shape after every increment of load before evaluating the stiffness matrix. This would also allow for the redistribution of superimposed load which is exerted by the sand on either side of the footing.

The main improvements could be made on theoretically establishing the stress-strain relationship. This is, naturally, a problem which engineers have been investigating without absolute success for some time. It should be possible to make certain assumptions concerning the behaviour

of the soil for use in conjunction with the finite element method. The problem of tensile stresses occurring in the soil could be overcome by using an orthotropic element similar to that used in the last chapter and putting the value of Young's modulus to zero in the tensile direction. This may well involve using a nonlinear procedure which is a mixture of incremental and iterative types.

A definite advantage would be gained if the total strain in the soil could be separated into elastic and plastic components and more research is needed into this aspect.

In view of the assumptions which have been made concerning this problem, the results are very encouraging both in the comparison of deflection and strain distribution under the footing. It should be expected that the same, or even better, accuracy could be gained when using a similar method for clay type soils. In this case the medium acts continuously and effects of pore pressure can be included.

The incremental method of analysis would appear preferable to the iterative both in performance and convenience.

The chapter devoted to the nonlinear analysis of the shear wall does demonstrate the utility of an iterative technique. The method of analysis used here would provide a convenient approximate solution where suitable nonlinear theory is unavailable. Once again the two theoretical methods both gave good results as far as the deflections are concerned. The evaluation of the stresses was not satisfactory but here the suitability of using Perspex is also questionable. This was particularly the case here when strain gauge measurements were involved.

APPENDIX 1

A PROGRAM TO CONSTRUCT THE 'OUT OF PLANE' STIFFNESS MATRIX

FOR A TRIANGULAR ELEMENT

```
begin
real p,q,r,D,R,P,t,E,Q,d
integer i,n,j,m,u,v,s,g
array ki,ko(1:6,1:6),L(1:6),a,b,c,x,y(1:3),X,Y,Z(1:18),A,T(1:6,1:9)c
,T'(1:9,1:6),K(1:9,1:9)
 read(s)
cycle g=1,1,s
 read(R,t,E)
read array(x)
read array(y)


a(1)=x(2)*y(3)-x(3)*y(2)
a(2)=x(3)*y(1)-x(1)*y(3)
 a(3)=x(1)*y(2)-x(2)*y(1)
b(1)=y(2)-y(3)
b(2)=y(3)-y(1)
b(3)=y(1)-y(2)
c(1)=x(3)-x(2)
c(2)=x(1)-x(3)
c(3)=x(2)-x(1)

D=0.5(b(2)*c(3)-b(3)*c(2))
 Q=0.5(1-R)
P=(E*t*t*t)/(110592D*D*D*D*D*(1-R*R))

p=x(1)^+x(2)^+x(3)^+x(1)*x(2)+x(2)*x(3)+x(1)*x(3)
q=y(1)^+y(2)^+y(3)^+y(1)*y(2)+y(2)*y(3)+y(1)*y(3)
 r=2x(1)*y(1)+2x(2)*y(2)+2x(3)*y(3)+x(1)*y(2)+x(1)*y(3)+x(2)*y(1)+x(2)*y(3)c
+x(3)*y(1)+x(3)*y(2)

cycle j=1,1,3
L(j)=36a(j)^+6(b(j)^*p+c(j)^*q)+6b(j)*c(j)*r+24a(j)*(b(j)*(x(1)+x(2)+x(3))c
+c(j)*(y(1)+y(2)+y(3)))
repeat

L(4)=36a(1)*a(2)+12((a(2)*c(1)+a(1)*c(2))*(y(1)+y(2)+y(3))+(a(1)*b(2)+c
a(2)*b(1))*(x(1)+x(2)+x(3)))+6(b(1)*b(2)*p+c(1)*c(2)*q)+3(b(1)*c(2)+c(1)*b(2))*r

L(5)=36a(1)*a(3)+12((a(3)*b(1)+b(3)*a(1))*(x(1)+x(2)+x(3))+(a(1)*c(3)+a(3)c
*c(1))*(y(1)+y(2)+y(3)))+6(b(1)*b(3)*p+c(1)*c(3)*q)+3(b(1)*c(3)+c(1)*b(3))*r

L(6)=36a(2)*a(3)+12((a(3)*b(2)+b(3)*a(2))*(x(1)+x(2)+x(3))+(a(2)*c(3)+a(3)c
 *c(2))*(y(1)+y(2)+y(3)))+6(b(2)*b(3)*p+c(2)*c(3)*q)+3(b(2)*c(3)+c(2)*b(3))*r
```

```
X(1)=2b(3)*b(3)*b(2)-2b(2)*b(2)*b(3)
X(2)=8c(3)*b(1)*b(2)+2c(3)*b(3)*b(2)-8c(2)*b(1)*b(3)-2c(2)*b(2)*b(3)
X(3)=2b(1)*b(2)*b(3)-4b(3)*b(2)*b(2)-2b(3)*b(3)*b(\\2)
X(4)=2c(1)*b(2)*b(3)-4c(3)*b(2)*b(2)-2c(3)*b(3)*b(2)
 X(5)=4b(2)*b(3)*b(3)+2b(2)*b(2)*b(3)-2b(1)*b(2)*b(3)
X(6)=4c(2)*b(3)*b(3)+2c(2)*b(3)*b(2)-2c(1)*b(3)*b(2)
X(7)=8b(3)*c(2)*c(1)+2b(3)*c(3)*c(2)-8b(2)*c(3)*c(1)-2b(2)*c(3)*c(2)
X(8)=2c(2)*c(3)*c(3)-2c(2)*c(2)*c(3)
X(9)=2b(1)*c(3)*c(2)-4b(3)*c(2)*c(2)-2b(3)*c(3)*c(2)
X(10)=2c(1)*c(2)*c(3)-4c(3)*c(2)*c(2)-2c(3)*c(3)*c(2)
X(11)=2b(2)*c(3)*c(2)-2b(1)*c(3)*c(2)+4b(2)*c(3)*c(3)
X(12)=4c(2)*c(3)*c(3)+2c(2)*c(2)*c(3)-2c(1)*c(2)*c(3)
 X(13)=-2(4b(3)*b(1)*c(2)+b(3)*b(3)*c(2)+b(3)*b(2)*c(3)-4b(1)*b(2)*c(3)c
-b(2)*b(3)*c(2)-b(2)*b(2)*c(3))
X(14)=-1(8c(3)*c(1)*b(2)+2c(3)*c(3)*b(2)+2c(3)*c(2)*b(3)-8c(1)*c(2)*b(3)c
-2c(2)*c(3)*b(2)-2c(2)*c(2)*b(3))
X(15)=-1(2b(1)*b(3)*c(2)+2b(1)*b(2)*c(3)-8b(2)*b(3)*c(2)-2b(3)*b(3)*c(2)c
-2b(2)*b(3)*c(3))
X(16)=-1(2c(1)*c(3)*b(\\\\2)+2c(1)*c(2)*b(3)-8c(2)*c(3)*b(2)-2c(3)*c(3)*b(2)c
-2c(2)*c(3)*b(3))
 X(17)=-1(8b(2)*b(3)*c(3)+2b(2)*b(2)*c(3)+2b(2)*b(3)*c(2)-2b(1)*b(2)*c(3)c
-2b(3)*b(1)*c(2))
X(18)=-1(8c(2)*c(3)*b(3)+2c(2)*c(2)*b(3)+2c(2)*c(3)*b(2)-2c(1)*c(2)*b(3)c
 -2c(3)*c(1)*b(2))


Y(1)=4b(3)*b(1)^-2b(\\1)*b(2)*b(3)+2b(3)^*b(1)
Y(2)=4c(3)*b(1)^+2c(3)*b(3)*b(1)-2c(2)*b(1)*b(3)
Y(3)=2b(1)^*b(3)-2b(3)^*b(1)
Y(4)=8c(1)*b(3)*b(2)+2c(1)*b(1)*b(3)-8c(3)*b(1)*b(2)-2b(3)*b(1)*c(3)
Y(5)=2b(1)*b(2)*b(3)-4b(1)*b(3)^-2b(1)^*b(3)
Y(6)=2c(2)*b(1)*b(3)-4c(1)*b(3)^-2c(1)*b(3)*b(1)
Y(7)=2b(3)*c(1)*c(3)-2b(2)*c(1)*c(3)+4b(3)*c(1)^
Y(8)=2c(1)*c(3)^-2c(1)*c(2)*c(3)+4c(3)*c(1)^
Y(9)=8b(1)*c(3)*c(2)+2b(1)*c(1)*c(3)-8b(3)*c(1)*c(2)-2b(3)*c(1)*c(3)
Y(10)=2c(1)^*c(3)-2c(3)^*c(1)
Y(11)=2b(2)*c(1)*c(3)-4b(1)*c(3)^-2b(1)*c(1)*c(3)
Y(12)=2c(1)*c(2)*c(3)-4c(1)*c(3)^-2c(1)^*c(3)
Y(13)=-1(8b(3)*b(1)*c(1)+2b(3)^*c(1)+2b(3)*b(1)*c(3)-2b(2)*b(3)*c(1)c
-2b(1)*b(2)*c(3))
Y(14)=-1(8c(3)*c(1)*b(1)+2c(3)^*b(1)+2c(3)*c(1)*b(3)-2c(2)*c(3)*b(1)c
-2c(1)*c(2)*b(3))
Y(15)=-1(8b(1)*b(2)*c(3)+2b(1)^*c(3)+2b(1)*b(3)*c(1)-8b(2)*b(3)*c(1)c
-2b(3)*b(1)*c(3)-2b(3)^*c(1))
Y(16)=-1(8c(1)*c(2)*b(3)+2c(1)^*b(3)+2c(1)*c(3)*b(1)-8c(2)*c(3)*b(1)c
-2c(3)*c(1)*b(3)-2c(3)^*b(1)\\)
Y(17)=-1(2b(2)*b(1)*c(3)+2b(2)*b(3)*c(1)-8b(3)*b(1)*c(3)-2b(1)^*c(3)c
-2b(3)*b(1)*c(1))
Y(18)=-1(2c(2)*c(1)*b(3)+2c(2)*c(3)*b(1)-8c(3)*c(1)*b(3)-2c(1)^*b(3)c
-2c(3)*c(1)*b(1))


Z(1)=2b(3)*b(1)*b(2)-4b(1)^*b(2)-2b(2)^*b(1)
Z(2)=2c(3)*b(1)*b(2)-4c(2)*b(1)^-2c(2)*b(2)*b(1)
Z(3)=4b(1)*b(2)^+2b(1)^*b(2)-2b(3)*b(1)*b(2)
```

```
Z(4)=2b(1)*b(2)*c(1)+4c(1)*b(2)^-2c(3)*b(2)*b(1)
Z(5)=2b(2)^*b(1)-2b(1)^*b(2)
Z(6)=8c(2)*b(1)*b(3)-8c(1)*b(2)*b(3)+2c(2)*b(1)*b(2)-2c(1)*b(1)*b(2)
Z(7)=2b(3)*c(2)*c(1)-4b(2)*c(1)^-2b(2)*c(2)*c(1)
Z(8)=2c(1)*c(2)*c(3)-4c(2)*c(1)^-2c(2)^*c(1)
Z(9)=2b(1)*c(2)*c(1)-2b(3)*c(2)*c(1)+4b(1)*c(2)^
Z(10)=4c(1)*c(2)^+2c(1)^*c(2)-2c(3)*c(1)*c(2)
Z(11)=8b(2)*c(1)*c(3)+2b(2)*c(2)*c(1)-8b(1)*c(2)*c(3)-2b(1)*c(2)*c(1)
Z(12)=2c(2)^*c(1)-2c(1)^*c(2)
Z(13)=-1(2b(3)*b(2)*c(1)+2b(3)*b(1)*c(2)-8b(1)*b(2)*c(1)-2b(2)^*c(1)c
-2b(1)*b(2)*c(2))
Z(14)=-1(2c(3)*c(2)*b(1)+2c(3)*c(1)*b(2)-8c(1)*c(2)*b(1)-2c(2)^*b(1)c
-2c(1)*c(2)*b(2))
Z(15)=-1(8b(1)*b(2)*c(2)+2b(1)^*c(2)+2b(1)*b(2)*c(1)-2b(3)*b(1)*c(2)c
-2b(2)*b(3)*c(1))
Z(16)=-1(8c(1)*c(2)*b(2)+2c(1)^*b(2)+2c(1)*c(2)*b(1)-2c(3)*c(1)*b(2)c
-2c(2)*c(3)*b(1))
Z(17)=-1(8b(2)*b(3)*c(1)+2b(2)^*c(1)+2b(2)*b(1)*c(2)-8b(3)*b(1)*c(2)c
-2b(1)*b(2)*c(1)-2b(1)^*c(2))
Z(18)=-1(8c(2)*c(3)*b(1)+2c(2)^*b(1)+2c(2)*c(1)*b(2)-8c(3)*c(1)*b(2)c
-2c(1)*c(2)*b(1)-2c(1)^*b(2))

cycle i=1,1,6
ko(i,i)=L(1)*(X(i)^+2R*X(i)*X(i+6)+X(i+6)^+Q*X(i+12)^)+L(2)*(Y(i)c
^+2R*Y(i)*Y(i+6)+Y(i+6)^+Q*Y(i+12)^)+L(3)*(Z(i)^+2R*Z(i)*Z(i+6)+Zc
(i+6)^+Q*Z(i+12)^)+L(4)*(2X(i)*Y(i)+2R*X(i)*Y(i+6)+2R*Y(i)*X(i+6)+2c
X(i+6)*Y(i+6)+2Q*X(i+12)*Y(i+12))+L(5)*(2X(i)*Z(i)+X(i)*Z(i+6)*2R+2Rc
*Z(i)*X(i+6)+2X(i+6)*Z(i+6)+2Q*X(i+12)*Z(i+12))+L(6)*(2Y(i)*Z(i)+2R*c
 Y(i)*Z(i+6)+2R*Z(i)*Y(i+6)+2Y(i+6)*Z(i+6)+2Q*Y(i+12)*Z(i+12))

if i=6 then->101

cycle n=(i+1),1,6
ko(i,n)=L(1)*(X(i)*X(n)+R*X(i+6)*X(n)+R*X(i)*X(n+6)+X(i+6)*X(n+6)+Q*Xc
(i+12)*X(n+12))+L(2)*(Y(i)*Y(n)+R*Y(i+6)*Y(n)+R*Y(i)*Y(n+6)+Y(i+6)*c
Y(n+6)+Q*Y(i+12)*Y(n+12))+L(3)*(Z(i)*Z(n)+R*Z(i+6)*Z(n)+R*Z(i)*Z(n+6)c
+Z(i+6)*Z(n+6)+Q*Z(i+12)*Z(n+12))+L(4)*(X(i)*Y(n)+X(n)*Y(i)+R*X(i+6)*c
Y(n)+R*X(n)*Y(i+6)+R*X(i)*Y(n+6)+R*X(n+6)*Y(i)+X(i+6)*Y(n+6)+X(n+6)*Yc
(i+6)+Q*X(i+12)*Y(n+12)+Q*X(n+12)*Y(i+12))+L(5)*(X(i)*Z(n)+X(n)*Z(i)+Rc
*X(i+6)*Z(n)+R*X(n)*Z(i+6)+R*X(i)*Z(n+6)+R*X(n+6)*Z(i)+X(i+6)*Z(n+6)c
+X(n+6)*Z(i+6)+Q*X(i+12)*Z(n+12)+Q*X(n+12)*Z(i+12))+L(6)*(Y(i)*Z(n)c
+Y(n)*Z(i)+R*Y(i+6)*Z(n)+R*Y(n)*Z(i+6)+R*Y(i)*Z(n+6)+R*Y(n+6)*Z(i)+Y(c
i+6)*Z(n+6)+Y(n+6)*Z(i+6)+Q*Y(i+12)*Z(n+12)+Q*Y(n+12)*Z(i+12))

ko(n,i)=ko(i,n)
repeat
repeat
101:newline

print array(ko,10,0)
cycle u=1,1,6
cycle v=1,1,6
ki(u,v)=P*ko(u,v)
repeat
repeat
```

```
null(T)
d=1/(2D)
T(1,1)=c(1)*d
T(1,2)=1
T(1,4)=c(2)*d
T(1,7)=c(3)*d
T(2,1)=-b(1)*d
T(2,3)=1
T(2,4)=-b(2)*d
T(2,7)=-b(3)*d
T(3,1)=c(1)*d
T(3,4)=c(2)*d
T(3,5)=1
T(3,7)=c(3)*d
T(4,1)=-b(1)*d
T(4,4)=-b(2)*d
T(4,6)=1
T(4,7)=-b(3)*d
T(5,1)=c(1)*d
T(5,4)=c(2)*d
T(5,7)=c(3)*d
T(5,8)=1
T(6,1)=-b(1)*d
T(6,4)=-b(2)*d
T(6,7)=-b(3)*d
T(6,9)=1

matrix trans(T',T)
print array(T',1,3)
matrix mult(A,ki,T)
matrix mult(K,T',A)

print array(K,3,3)
 repeat


end of program
```

GENERAL DATA

1.number of elements
2.poisson's ratio,
3.thickness,
4.Young's modulus of element
5.'p' coordinates at corners 1,2 and 3 respectively
6.'q' coordinates at corners 1,2 and 3 respectively
Repeat items 2-6 for next element

APPENDIX 2

THE TERMS OF THE STRAIN MATRIX B*

The terms shown here are for an element orientated as in fig. 2.4. The full terms in a randomly orientated element are given by the program of appendix 1.

The terms generally take the form:-

$$X.(q_3^i.\ p_2^j.\ p_3^{3-j-i})\ L_m$$

where i, j and m take values between 1 and 3. For convenience this is written as:-

X(i,j)m where X is a scalar constant.

B* (1,1) = - (3,0)3

B* (1,2) = -4 (2,1)1 + 2(2,1)2 + (2,0)3 - (2,1)3

B* (1,3) = -(3,0)3

B* (1,4) = -2(2,1)1 + 4(2,1)2 + (2,0)3

B* (1,5) = -2(3,0)3

B* (1,6) = 2(2,0)3 - (2,1)3

B* (2,1) = -3(1,1)1 + 4(1,2)1 - (1,1)2 + (1,2)2 -11(1,0)3
-2(1,2)3 + 3(1,1)3

B* (2,2) = -(0,2)1 - (0,1)1 + 3(0,1)2 + (0,3)2 - 4(0,2)2 - 3(0,2)3
-(0,0)3 + 4(0,1)3

B* (2,3) = (1,1)1 + 3(1,1)2 + (1,2)2 - (1,0)3 -(1,1)3

B* (2,4) = -3(0,1)1 + 2(0,2)1 + 2(0,3)2 + (0,1)2 -33(0,2)2
(0,0)3 - 2(0,2)3 + (0,1)3

B* (2,5) = 2(1,2)1 - 2(1,1)1 + 2(1,1)2 + 2(1,1)3 - 2(1,0)3
-2(1,2)3

B* (2,6) = -3(0,2)1 + 2(0,1)1 - 2(0,1)2 + (0,3)2 + (0,2)2
+ (0,2)3 + 2(0,0)3 - 3(0,1)3

$B^*(3,1) = -3(2,1)1 - (2,1)2 - 2(22,0)3 + 3(2,1)3$

$B^*(3,2) = 3(1,2)1 - 5(1,1)1 - 3(1,2)2 + 5(1,1)2 + (1,2)3$
$+ 2(1,0)3 - 5(1,1)3$

$B^*(3,3) = (2,1)1 + 3(2,1)2 - 2(2,0)3 - (2,1)3$

$B^*(3,4) = 2(1,2)1 - 5(1,1)1 - 2(1,2)2 + 5(1,1)2 - 2(1,2)3$
$+ 2(1,0)3 + (1,1)3$

$B^*(3,5) = -2(2,1)1 + 2(2,1)2 - 4(2,0)3 + 2(2,1)3$

$B^*(3,6) = 2(1,1) - (1,2)1 + (1,2)2 - 2(1,1)2 + 4(1,0)3$
$- 3(1,2)3 - 4(1,1)3$

THE TERMS OF THE STIFFNESS MATRIX k*

The element is geometrically defined by the coordinates:- p_2, q_3, p_3.

The individual terms take the form:-

$$(p_2)^i \cdot (p_3)^j \cdot (q_3)^{6-i-j}$$

Hence the powers i and j can be used to define the term. These are given in brackets after the quantity. For instance,

$$18p_3p_2^3q_3^2 = 18(3,1)$$

where the term is multiplied by Poisson's ratio, it is primed hence,

$$4\nu p_3^4q_3^2 = 4(0,4)^1$$

All the following elements of $\underline{k}^*$ have to be multiplied by,

$$Et^3/(144(3,0)(1-\nu^2)).$$

$k^*(1,1) = 9(2,2) - 22(3,1) + 15(4,0) - 2(1,3) + (0,4) + (0,0)$
$+ 5(2,0) + 2(0,2) - 2(1,1) - 12(2,0)^1$

$k^*(1,2) = 4(1,1) - 5(2,3) + 9(3,2) - 11(4,1) + 2(1,0) - (0,1)$
$+ 2(5,0) - (0,5) - (3,0) - (2,1) - 2(0,3) + 6(1,2) - 10(3,0)^1 + 6(2,1)^1$

$k^*(1,3) = 8(3,1) - 7(2,2) - 2(1,3) + 2(4,0) + (0,4) + (0,0) - 3(2,0)$
$-2(1,1) + 2(0,2) + 2(2,0)^1$

$k^*(1,4) = 9(2,3) - 2(4,1) - 12(3,2) + 4(5,0) - (0,5) - (1,0) - (0,1)$
$+(1,4) - 2(3,0) + 5(2,1) - 2(0,3) - 2(2,1)^1 + 2(3,0)^1$

$k^*(1,5) = 5(4,0) + 6(2,2) - 10(3,1) - 4(1,3) + 2(0,0) + 2(2,0)$
$+4(0,2) - 4(1,1)$

$k^*(1,6) = 7(3,2) - 9(4,1) + 2(5,0) - 4(2,3) + 5(1,4) - 2(0,5)$
$-2(1,0) + (1,0) - (3,0) + 6(1,2) - 4(0,3)$

$k^*(2,2) = (6,0) - 6(5,1) + 16(4,2) - 18(3,3) + 16(2,4) - 6(1,5) + (0,6)$
$+15(2,0) - 4(1,1) + (0,2) + 5(4,0) + 27(2,2) - 20(3,1) + 2(0,4)$
$-10(1,3) - 6(4,0)^1 + 20(3,1)^1 - 6(2,2)^1$

$$k^*(2,3) = 3(2,3) - 11(3,2) + (5,0) - (0,1) + 2(1,0) + 4(1,4) - (0,1) - (3,0) - (2,1) - 2(0,3) + 6(1,2) - 2(2,1)^1$$

$$k^*(2,4) = 5(2,0) + 6(4,0) + 5(3,3) + 2(6,0) - 9(5,1) + (0,2) - (1,1) + (0,6) - 3(1,5) + 2(4,0) + 9(2,2) - 7(3,1) + 2(0,4) - 4(1,3) + 4(2,2)^1 - 4(3,1)^1$$

$$k^*(2,5) = 6(3,2) - (5,0) - 3(4,1) - 6(2,3) + 8(1,4) - 2(0,5) - 2(0,1) + 4(1,0) - 2(3,0) - 4(0,3) - 2(2,1) + 12(1,2) + 2(3,0)^1$$

$$k^*(2,6) = (6,0) - 3(5,1) + 5(3,3) + 6(2,4) - 9(1,5) + 2(0,6) + 2(2,0) + 2(0,2) - 15(1,1) - 3(4,0) + 4(2,2) + 11(3,1) - 14(1,3) + 4(0,4) + 4(4,0)^1 - 4(3,1)^1$$

$$k^*(3,3) = (4,0) + 6(3,1) + 9(2,2) - 2(1,3) + (0,4) + (0,0) + 5(2,0) + 2(0,2) - 2(1,1) - 6(2,0)^1$$

$$k^*(3,4) = 3(4,1) - 8(3,2) + (1,4) - (0,5) + 2(5,0) - (0,1) - (1,0) - 2(3,0) + 5(2,0) - 2(0,3) + (2,3) + 4(3,0)^1 + 6(2,1)^1$$

$$k^*(3,5) = 2(3,1) + 6(2,2) - (4,0) - 4(1,3) + 20(0,4) + 2(0,0) + 2(2,0) + 4(0,2) - 4(1,1)$$

$$k^*(3,6) = 3(4,1) - 3(3,2) - 8(2,3) + 3(1,4) + (5,0) + 2(0,5) + (0,1) - 2(0,1) - (3,0) - 4(0,3) + 6(1,2)$$

$$k^*(4,4) = 12(2,0) + (0,2) + 2(1,1) + 13(4,2) - 6(3,3) + 6(2,4) - 12(5,1) + (0,6) + 4(6,0) + 4(4,0) + 9(2,2) - 12(3,1) + 2(0,4) + 2(1,3) + 8(4,0)^1 - 6(2,2)^1 - 8(3,1)^1$$

$$k^*(4,5) = 13(4,1) - 2(5,0) - 16(3,2) + 6(2,3) + 4(1,4) - 2(0,5) - 2(0,1) - 2(1,0) - 4(3,0) + 10(2,1) - 4(0,3) - 4(3,0)^1$$

$$k^*(4,6) = 2(6,0) - 3(5,1) - 9(4,2) + 21(3,3) - 9(2,4) - 3(1,5) + 2(0,6) - (2,0) + 2(0,2) + (1,1) + 2(4,0) - 14(2,2) + 7(3,1) + 4(0,4) - 2(1,3) + 2(3,1)^1$$

$$k^*(5,5) = 12(4,0) + 20(2,2) - 16(3,1) - 8(1,3) + 4(0,0) + 4(0,4) + 4(2,0) - 8(1,1) + 8(0,2) + 8(2,0)^1$$

$$k^*(5,6) = 14(3,2) - (5,0) - 2(4,1) - 16(2,3) + 10(1,4) - 4(0,5)$$
$$- 4(0,1) + 2(1,0) - 2(3,0) - 8(0,3) + 12(1,2) + 4(3,0)^1 - 8(2,1)$$
$$k^*(6,6) = (4,2) + 13(2,4) - 6(3,3) - 12(1,5) + 4(0,6) + (6,0) + 4(0,2)$$
$$+ (2,0) - 4(1,1) - 2(2,2) + 5(4,0) + 10(3,1) + 8(0,4) - 16(1,3)$$
$$+ 8(2,2)^1 - 6(4,0)^1 - 8(3,1)^1$$

THE TERMS OF THE STRESS MATRIX S*

For convenience, the terms are defined in a similar fashion to that used previously. These take the form:-

$$X.(q_3).^{i}(p_2)^{j}.(p_3)^{3-i-j}$$

and can be written as:-

$$X(i,j)$$

This is primed when multiplied by Poisson's Ratio and doubly primed when multiplied by $.5(1-\nu)$

$S^*(1,1) = (3,0) - (1,2)^1 + (1,1)^1 + (1,0)$

$S^*(1,2) = -(2,0) + 3(2,1) + 2(0,2)^1 + 2(0,1)^1 - (0,0)^1 - (0,2)^1$

$S^*(1,3) = (3,0) - 3(1,1)^1 - (1,2)^1 + (1,0)^1$

$S^*(1,4) = -2(2,1) - (2,0) + (0,1)^1 + 3(0,2)^1 - 2(0,3)^1 - (0,0)^1$

$S^*(1,5) = 2(3,0) + 2(1,2)^1 + 2(1,0)^1 - 2(1,1)^1$

$S^*(1,6) = (2,1) - 2(2,0) + (0,2)^1 + 3(0,1)^1 - 2(0,0)^1 - (0,3)^1$

$S^*(2,1) = (1,0) + (1,1) + 3(1,2) + (3,0)^1$

$S^*(2,2) = 2(0,2) + 2(0,1) - (0,3) - (0,0) - (2,0)^1 + 3(2,1)^1$

$S^*(2,3) = -3(1,1) - (1,2) + (1,0) + (3,0)^1$

$S^*(2,4) = (0,1) + 3(0,2) - 2(0,3) - (0,0) - 2(2,1)^1 - (2,0)^1$

$S^*(2,5) = 2(1,2) + 2(1,0) - 2(1,1) + 2(3,0)^1$

$S^*(2,6) = (0,2) + 3(0,1) - 2(0,0) - (0,3) + (2,1)^1 - (2,0)^1$

$S^*(3,1) = (2,1)^{11} + 2(2,0)^{11}$

$S^*(3,2) = (1,2)^{11} + 2(1,0)^{11} - 5(1,1)^{11}$

$S^*(3,3) = 2(2,0)^{11} - 3(2,1)^{11}$

$S^*(3,4) = 2(1,2)^{11} - 2(1,0)^{11} - (1,1)^{11}$

$S^*(3,5) = 2(2,0)^{11} - (2,1)^{11}$

$S^*(3,6) = 3(1,2)^{11} - 4(1,0)^{11} + 4(1,1)^{11}$

All the above terms are multiplied by:-

$$\frac{\alpha_0}{4A^2}$$

APPENDIX 3

SPECIFICATION FOR THE USE OF THE ELASTIC ANALYSIS AND STRESS PROGRAMS

The joints of the structure to be analysed are split up into groups which are of as equal size as possible. For a three dimensional structure the maximum size of group varies with the total size of structure. Generally about 15 joints per group is satisfactory.

The joints and elements in each group are labelled in the following manner:-

Joints:

All joints including supports are numbered from 1 upwards so that each joint has a distinct number.

Joints within a group are numbered consecutively. Only after the joints in group 1 are all numbered can those of group 2 be numbered. These are then followed by the joints of group 3 and so on.

Apart from natural joints it is necessary to specify joints at the following places.

i) At every load point.

ii) At every change in cross section.

The joints within a group may be numbered in any order, but the analysis is likely to be faster if the joints are numbered so that joints with small and large numbers are not interconnected directly.

When possible the supports should be included within the last group.

Members:

Numbers from 1 upwards are given to all the members. It should be checked that all the members are uniform and unloaded between joints.

An arrow must be allocated to each member. The joint at the tail of the arrow being designated end 1 of the member. That at the head of the arrow is end 2.

Members within a group are numbered consecutively, the members of group 1 being numbered first. These are followed by members in group 2 and then 3 and so on. Members connecting joint group i to joint group i+1 are within the same member group i.

Rectangular plates:

These are numbered from 1 upwards. Each plate element must be rectangular. The number of rectangular elements into which a given plate must be divided varies from problem to problem. Each corner of the plate must be numbered 1 to 4, see fig. 1.2. All plates must be numbered using the same rules as those given above for members.

Triangular plates:

Similarly, these plates are numbered from 1 upwards. Each corner of the plate is numbered 1 to 3, see fig. 2.4. For best results, the plates must be divided into even patterns of approximately the same size.

Reference axes:

Using the right hand screw rule, sets of axes must be defined for the whole frame, each member, and each plate element. The member axes are defined with P being positive when it is from end 1 to end 2 of the member.

The P Q plane of the plate element is defined as the 'in plane' and the PR plane as the 'out of plane'. The P axis of the plate is positive when running from corner 1 to corner 2. The Q axis is positive when it is from corner 1 to corner 3.

Presentation of Joint, Member, and Plate Data

The data for joints, members and plates are presented group by group. These follow the general data whose specification is given below.

The order in which each group is fed in is given in a table shown overleaf. There follows a specification of the data required for the general data and joint and element data for each individual group.

General Data

1. Analysis number: An integer specifying the case number. This integer can be used as a code by the user.

2. Number of instructions to be computed before a restart is necessary. Usually equal to that in the job heading.

3. Run number. Usually unity.

4. Sparse matrix array size.

5. Starting block number on magnetic tape.

6. Total degrees of Freedom:

This is determined by counting the non-zero degrees of freedom in the joint data.

7. The number of groups into which the frame is divided.

8. The greatest number of prismatic members present in any joint group. This should be set to unity if no member is present.

9. The greatest number of joints present in any joint group.

10. The greatest number of rectangular plate elements present in any joint group. This is set to unity if there is no rectangular plate element in the structure.

11. The greatest number of triangular plate elements in any joint group. This is set to unity if there are no triangular plates in the structure.

12. A parameter specifying which of the five types of elements are present in the structure and require to be included in the analysis. This consists of five digits representing, the prismatic members, the rectangular plate elements under 'out of plane' forces, rectangular plate elements under 'in plane' forces, triangular plate elements under 'out of plane' forces, triangular plate elements under 'in plane' forces' respectively.

Order of Data Presentation for n Joint Groups

Structures having n joint groups that are numbered 1,2,3...i-1,i,i+1, ...n-1,n

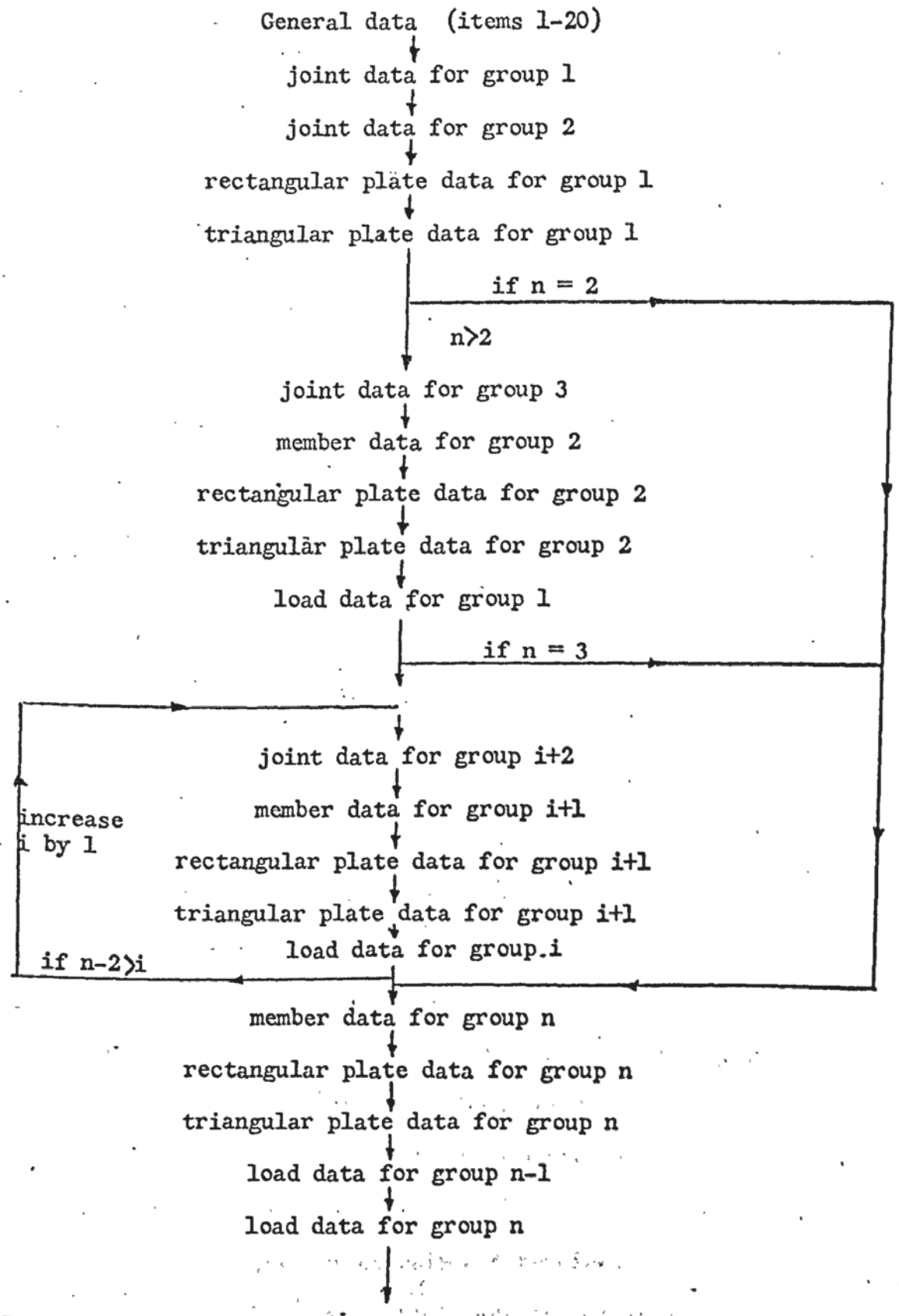

Return to item 1 of general data for next analysis or end data with -1 and ***Z.

The appropriate digit for the type of element takes the value of (1) if it is present in the structure and (0) if not. For example, if only members and 'in plane' triangular plates are present, then this would be set to 10001.

13. A parameter specifying what 'in plane' forces are required in the rectangular 'in plane' plate elements and having the following values:-

1.. if shear is required.

2. if tension and compression only are required

3. if shear, tension and compression are required

0. if no 'in plane' forces are considered

14. The number of loading cases that are acting on the structure to be analysed.

15. A parameter to specify the reactive forces at the restrained joints. This consists of six digits representing reactive forces that can act in X, Y, Z directions and moments in θ_X, θ_Y and θ_Z directions respectively. Suitable values of this parameter are:

For rigidly jointed plane frames	110001
pin jointed plane frames	110000
rigidly jointed space frames	111111
pin jointed space frames	111000

16. Printing parameter:

This is obtained by adding the following quantities:

10: if the stiffness matrices are required

1: if the reactions are required

The program always prints out joint displacements and member forces and moments. Since the stiffness matrices are of no use to the user, it is advisable to make the value of this parameter always equal (1) or (0).

17. Printing parameter:

0: if member forces only are required

1: if member and plate forces are required

18. The total number of prismatic members in the structure. Set to zero if no members present.

19. The total number of rectangular plate elements in the structure. Set to unity if no rectangular plates present.

20. The total number of triangular plate elements in the structure. Set to unity if no triangular plates present.

For each joint group the following data is required.

Joint Data for group i:

This consits of a list of the following five items for every joint.

1. Joint number
2. The X co-ordinate of the joint in the overall reference axes of the frame.
3. The Y co-ordinate of the joint
4. The Z co-ordinate of the joint
5. Degree of freedom parameter for the joint. This consists of six digits representing freedom in the X, Y, Z, θ_X, θ_Y and θ_Z directions respectively.

Examples of this parameter are:

110001 for a rigid joint in a plane frame that can move in X,Y and θ_Z directions while it has no freedom to move in Z, θ_X or θ_Y directions.

111000 for a pin joint in a space frame

111111 for a rigid joint in a space frame

1 for a hinged support of a rigid jointed plane frame allowing only rotation in θ_Z direction

As the computer program treats this parameter as an integer number, initial zeros are not written.

The joint data for a group must be terminated by zero.

Member data for group i:

For each member this consists of:

1. Member number
2. Joint number at end 1
3. Joint number at end 2
4. In plane joint number
5. Modulus of elasticity

6. Cross sectional area
7. Second moment of area about R axis, I_R
8. Second moment of area about Q axis, I_Q
9. Product moment of area about Q and R axes, (I_{QR})
10. Torsional stiffness, GJ, of the members
11. Offset, qc, measured from joint to centroid of the member in the Q direction*
12. Offset, r_c, measured from joint to centroid of the member in the R direction*
13. Offset, q_s, measured from centroid to shear centre of the beam in the Q direction*
14. Offset, r_s, measured from centroid to shear centre of the beam in the R direction*

* As defined by figures at the back of the appendix

If items 5-14 for a member are exactly the same as those of the previous member, then item 5 of the current member is set to -1 and items 6 to 14 are left out.

It is therefore advantageous to number members that have the same crosssectional properties consecutively so that items 5 to 14 are only prepared for one of these members. The following members will only have items 1 to 4 then a -1.

The 'in plane' joint of a member is a joint that lies in the PQ plane of the member but not on the P axis of the member. Usually this is another joint in the structure to which the member is not connected. Should no such joint exist then an artifical joint is created with zero degree of freedom. In all cases in the 'in plane' joint of a member must be chosen from those in joint group i or i+1.

Rectangular Plate data for group i:

For each plate this consists of:

1. Plate number

2. Joint number at corner 1

3. Joint number at corner 2

4. Joint number at corner 3

5. Joint number at corner 4

6. Modulus of elasticity

7. Poisson's ratio

8. Thickness of plate element

The plate data for a group must be terminated by a zero.

Items 6-8 can be repeated for the previous plate by inserting -1 in item 6.

If no rectangular plates are in the structure then zero is inserted for every rectangular plate group.

If there are rectangular plates in the structure but none in a particular group a dummy plate must be created, connected to appropriate joints and having zero modulus of elasticity.

Triangular plate data for a group i:

For each plate this consists of:

1. Plate number

2. Joint at corner 1

3. Joint at corner 2

4. Joint at corner 3

5. Modulus of elasticity

6. Poisson's ratio

7. Thickness of plate element

The plate data for a group must be terminated by a zero.

Items 5-7 can be repeated for the previous plate by inserting -1 in item 5.

As for rectangular plates, if there are no triangular plates in the structure a zero is inserted for every triangular plate group.

and a dummy plate is needed where there are no triangular plates in a group of a structure containing triangular plates.

Note:

It is of advantage to number members and plates of the same property consecutively.

Load Data for a joint Groupi:

For each joint group the load is presented as follows:-

1. -(i) where i is the loading case number. Thus the first set of independent loads are numbered -1.
2. Column number of first load.

The applied loads must be resolved into X, Y, Z, θ_x, θ_y and θ_z directions. The column number of a load is obtained by counting all the non-zero degrees of freedom in the joint group starting from the beginning of the joint data for that joint group up to and including the direction in which the load is acting.

3. Value of first load (with correct sign).
4. Repetition of items 2 and 3 for all the loads in the first load case.
5. Return to item 1 for next load case.
6. If no further load cases are required the load data is terminated by a zero.

Data specification for restarting elastic analysis program:

1. Analysis number.
2. Number of instructions to be completed before next restart.
3. Run number. Must be greater than 1.
4. Size of sparse matrix array.
5. Starting block number on magnetic tape. This is given by the print out of the previous run.
6. Items 18-20 in the general data.
7. Joint data for group i+3, where i is the number of times the reduction

loop has been completed and is given in the print out of the previous run.

8. Member and plate data following in the order previously given.

Data specification for use of stress program:

1. Analysis number.
2. Size of sparse matrix array.
3. Starting block number of magnetic tape. This is given on the print out of the elastic analysis program.
4. Printing parameter.

    -1: principal stresses only

    0: above plus, top and bottom surface, 'in plane' and 'bending' stresses

    1: above plus plate dimensions

    2: above plus stress and displacement matrices

5. Return to item 1 for next analysis number or end data with -1.
6. ***Z.

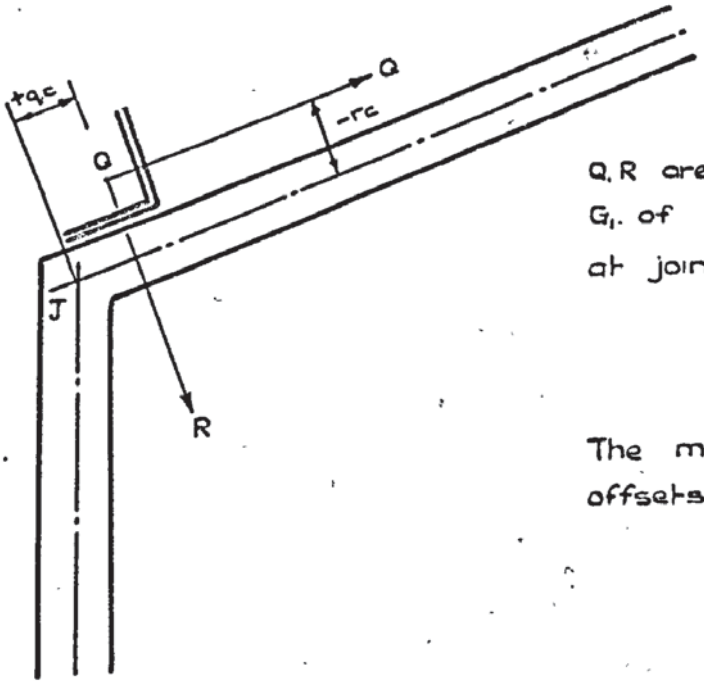

Q, R are local axes through the centroid G_1 of an angle beam having one end at joint J.

The magnitude and signs of the offsets are as shown.

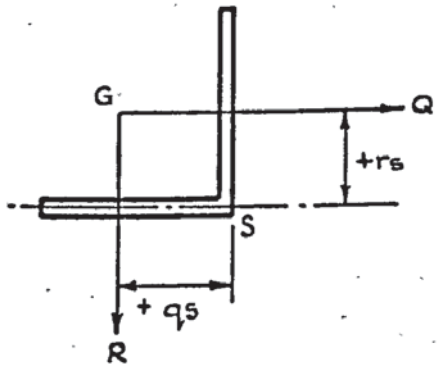

For the same angle, with shear centre at S, then the offsets qs and rs are as shown.

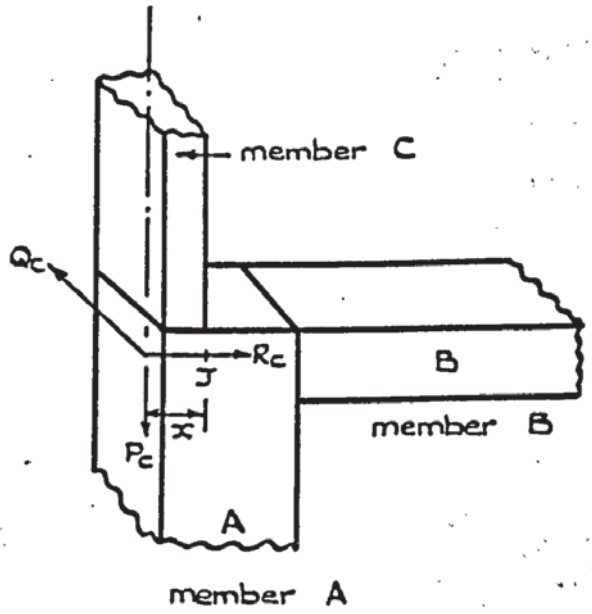

For example, qs, qc, rs, rc = 0 for members A and B as J, the joint, lies on the centroid of these beams. For member C, local axes Qc, Rc, Pc, then rc = -x and qc = 0

APPENDIX 4

DATA SPECIFICATION FOR NONLINEAR PROGRAMS

The joints of the structure are numbered concurrently from 1 upwards and include the supports. The member, rectangular and triangular plates are numbered from 1 upwards separately and their nodes numbered in the same manner as for the elastic analysis program. The order of each different block of data is as given below. The individual elements which make up each block of data are also given.

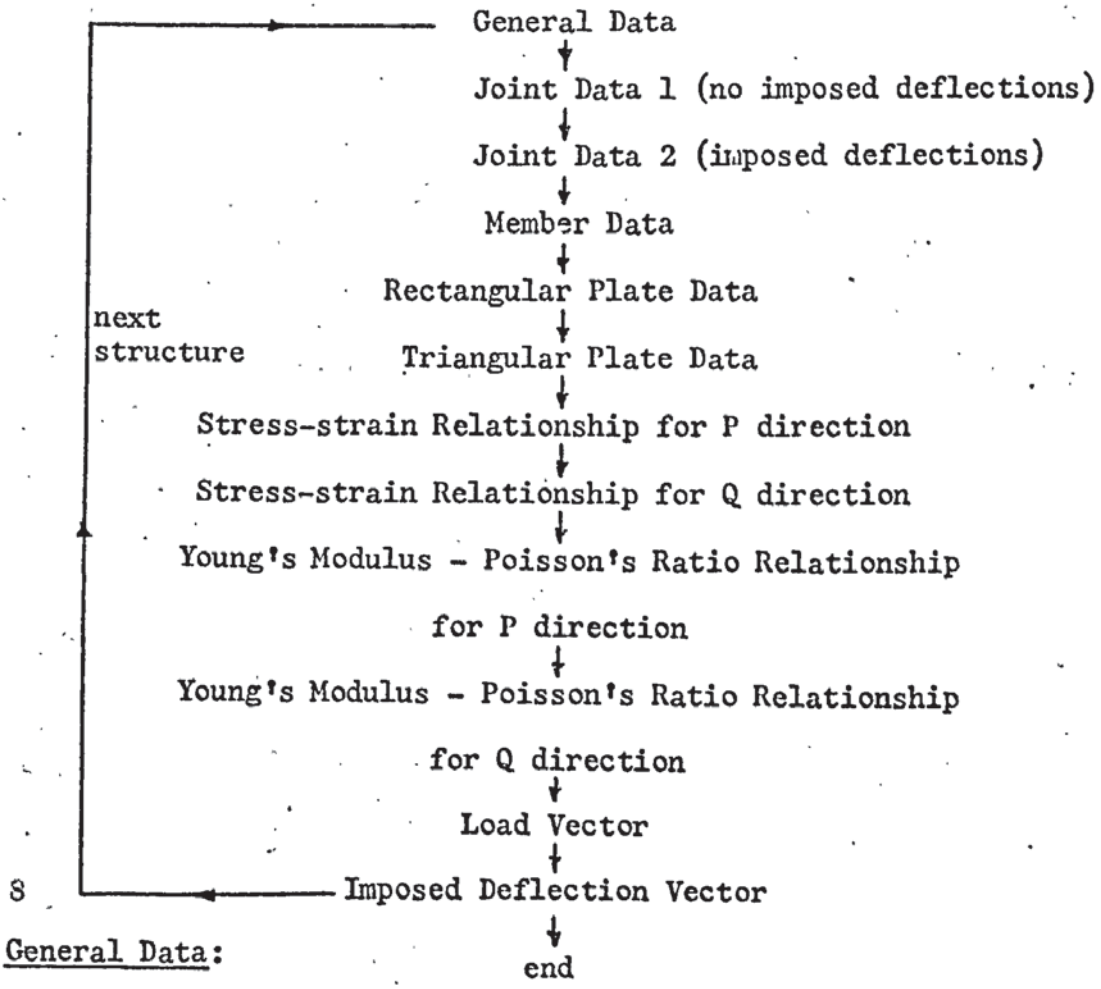

General Data:

1. Analysis number.
2. Number of instructions.
3. Run number.
4. Size of sparse matrix array.

5. Starting block number on magnetic tape.

Items 1-5 are similar in use and function to those used in the elastic analysis program.

6. Total number of joints in the structure.

7. Number of joints which have known deflections.

8. Number of members present.

9. Number of rectangular plates present.

10. Number of triangular plates present.

11. Parameter,

0: plane strain analysis

1: plane stress analysis

12. Number of points on the stress-strain curve, including the origin, in the P direction.

13. Number of points on the stress-strain curve, including the origin, in the Q direction.

14. Number of points on the E-δ curve in the P direction.

15. Number of points on the E-δ curve in the Q direction.

16. Tolerance: $\frac{(E_{new} - E_{old})}{E_{old}}$ under which 80% of the plates must fall before the iterations are terminated. If negative a linear analysis is carried out.

17. Tolerance (as above) above which none of the remaining 20% of the plates must lie.

18. Printing parameter:

-1: Deflections and stresses at the end of program, E and δ values.

0: Deflections and stresses, E and δ values for each iteration.

1: Prints out all displacement transformation, stiffness, overall striffness and stress matrices.

Joint Data 1:

This consists of a list of the following four items for every joint.

1. Joint number
2. The X - coordinate of the joint
3. The Y - coordinate of the joint
4. The degree of freedom parameter for the joint. This consists of a three digit number representing freedom in the X, Y, θ_z directions respectively. If this freedom exists the digit is 1, if it is restrained the digit is 0. All degrees of freedom having imposed deflections are considered to be restrained. The joint data is terminated with a zero.

Joint Data2:

(Omit if item 7 of general data is zero)

This consists of a list of the following two items for all joints having imposed deflections.

1. Joint number
2. Degree of freedom parameter

For this parameter the degree of freedom for the direction of the imposed deflection is considered free. All others are restrained.

Member Data:

For each member this consists of:

1. Member number
2. Joint number at first end
3. Joint number at second end
4. In plane joint number
5. Young's Modulus
6. Cross sectional area
7. Second moment of area I_R. Items 5-7 are repeated for a previous member by inserting a -1 for item 5. Member data is terminated with a zero.

Rectangular Plate Data:

For each plate this consists of:

1. Plate number
2. Joint number at corner 1
3. Joint number at corner 2
4. Joint number at corner 3
5. Joint number at corner 4
6. Modulus of elasticity
7. Poisson's ratio
8. Thickness of plate

Items 6-8 are repeated for a previous plate by inserting a -1 in item 6. Rectangular plate data is terminated by a zero.

Triangular Plate Data:

For each plate this consists of:

1. Plate number
2. Joint number at corner 1
3. Joint number at corner 2
4. Joint number at corner 3
5. Modulus of ealsticity
6. Poisson's ratio
7. Thickness of plate

Items 5-7 are repeated for a previous plate by inserting a -1 in item 5. Triangular plate data is terminated by a zero.

Stress-strain Relationship Data:

This consists of values of stress then strain for each point of change on the linearized curve starting with, and including the origin.

Young's Modulus - Poisson's Ratio Relationship Data:

This consists of values of Young's Modulus, then Poisson's ratio for each point on the curve starting with the lowest value for Poisson's ratio.

Load Data:

The load data is presented as follows:

1. -1
2. Column number of first load. This is obtained by counting all the non zero degrees of freedom in joint data 1 up to and including the direction in which the load is acting.
3. Value of first load
4. Repitition of items 2 and 3 for all the remaining loads.
5. If no further load is required the load data is terminated with zero.

Displacement Data:

The displacement data is presented as follows:

1. -1
2. Column number of first displacement. This is obtained by counting all the non zero degrees of freedom in joint data 2 up to and including the direction in which the deflection is imposed.
3. Value of first deflection.
4. Repitition of items 2 and 3 for all the remaining deflections.
5. If no further deflection is required the data is terminated with a zero.

Return to general data for next structure or terminate with:-

-1

***Z

REFERENCES

1. Timoshenko and S. Woinowsky-Krieger, "Theory of Plates and Shells", 2nd. ed. McGraw-Hill Book Co. 1959.

2. Zienkiewicz O.C. and Y.K. Cheung, "The Finite Element Method in Structural and Continuum Mechanics," McGraw-Hill Book Co. 1967.

3. Przemieniecki, J.S. "Theory of Matrix Structural Analysis, "McGraw-Hill Book Co. 1968.

4. Fraeijs De Veubeke, B.M. "Displacement and Equilibrium Models in the Finite Element Method", "Stress Analysis" Ed. O.C. Zienkiewicz, Wiley 1965.

5. Livesley, R.K. "Analysis of Rigid Frames by an Electronic Computer", Engineering, 176, 1953.

6. Livesley, R.K. "Matrix Methods of Structural Analysis", Pergamon Press, New York, 1964.

7. Argyris, J.H. " Energy Theorems and Structural Analysis", Butterworth Scientific Publications, London, 1960.

8. Turner, M.J., R.W. Clough, H.C. Martin and L.J. Topp, "Stiffness and Deflection Analysis of Complex Structures", J. Aero. Sci., 23, 1956.

9. Clough, R.W. "The Finite Element Method in Plane Stress Analysis, "Proc. 2nd. Conf. Elect. Computation, A.S.C.E., Kansas City, Mo, Nov. 1960.

10. Melosh, R.J. "A stiffness Matrix for the Analysis of Thin Plates in Bending," J. Aero. Sci., 28, 1961.

11. Gallagher, R.H. "Techniques for the Derivation of Element Stiffness Matrices", J.A.I.A.A., 1, 1963.

12. Fraeijs De Veubeke, B.M. "Upper and Lower Bounds in Matrix Structural Analysis", Matrix Methods of Structural Analysis, AGARDograph, 72, 1964.

13. Melosh, R.J. "Basis for Derivation for the Direct Stiffness Method," J.A.I.A.A., 1, 1963.

14. Zienkiewicz, O.C. and Y.K. Cheung, "The Finite Element Method for the Analysis of Elastic, Isotropic and Orthotropic Slabs", Proc. I.C.E., 28, 1964.

15. Pian, T.H.H. "Derivation of Element Stiffness Matrices," J.A.I.A.A., 2, 1964.

16. Pian, T.H.H. "Derivation of Element Stiffness Matrices by Assumed Stress Distributions", J.A.I.A.A., 2, 1964.

17. Bogner, F.K., R.L. Fox, L.A. Schmit, "The Generation of Interelement - Compatible Stiffness and Mass Matrices by the Use of Interpolation Formulas", Proc. Conf. Matrix Methods in Structural Mechanics, Air Force Inst. of Techn., Wright Patterson A.F. Base, Ohio, Oct. 1965.

18. Pian, T.H.H. "Element Stiffness Matrices for Boundary Compatibility and for Prescribed Boundary Stresses", as aobve.

19. Bazeley, G.P., Y.K. Cheung, B.M. Irons, O.C. Zienkiewicz, "Triangular Elements in Plate Bending, Conforming and Non-conforming Solutions", as above.

20. Fraeijs De Veubeke, B.M. "Bending and Stretching of Plates", as above.

21. Clough, R.W., J.K Tocher, "Finite Element Stiffness Matrices for Analysis of Plate Bending", as above.

22. Irons, B.M.R., Draper K.J. "Inadequacy of Nodal Connections in a Stiffness Solution for Plate Bending", J.A.I.A.A., Vol 3, 1965.

23. Melosh, R.J. "A flat Triangular Shell Element Stiffness Matrix", Proc. Conf. Matrix Methods in Structural Mechanics, Air Force Inst. of Techn., Wright Patterson A.F. Base, Ohio, Oct, 1965.

24. Severn, R.T. Taylor P.R. "The Finite Element Method for Flexure when Stress Distributions are assumed", Proc. I.C.E., June 1966.

25. Zienkiewicz, O.C., P. Mayer, Y.K. Cheung, "Solution of Anisotropic Seepage by Finite Elements," Proc. A.S.C.E. February 1966.

26. Hall, A.S. "Deformation and Stresses within the Joints of Plane Frames", UNICIV Report No. R-51, Aug. 1959.

27. Macleod, I. "Analysis of Shear Wall Structures", Ph.D. Thesis, Glasgow University, 1966.

28. Stagg and Zienkiewicz "Rock Mechanics in Engineering Practice", John Wiley and Sons Ltd., 1968.

29. Majid, K.I., A. Jennings "The Computer Analysis of Space Frames using Sparse Matrix Techniques," Paper C4, Int. Conf. Space Structures, University of Surrey, 1966.

30. Majid, K.I., M.A. Williamson, "Linear Analysis of Complete Structures by Computers", Proc. I.C.E., 38, 1967.

31. Williamson, M.A. "A Finite Element Approach to the Analysis of Complete Structures, "M.sc. Thesis, Manchester University.

32. Clough, R.W. "The Finite Element Method in Structural Mechanics, "Stress Analysis, Wiley 1965.

33. Argyris, J.H. "Continua and Discontinua", Proc. Conf. Matrix Methods in Structural Mechanics, Air Force Inst. of Techn., Wright Patterson A.F. Base Ohio, Oct. 1965.

34. Argyris, J.H. "Elasto Plastic Matrix Displacement Analysis of Three Dimensional Continua", J. Roy. A.Sc., 69, 1965.

35. Argyris, J.H. "Matrix Analysis of Three Dimensional Elastic Media. Small and Large Displacements, J.A.I.A.A., 3, 1965.

36. Pope, G.G., "A Discrete Element Method for the Analysis of Plane Elasto Plastic Stress Problems", R.A.F. Techn. Report No. 65028.

37. Marcal, P.V., I.P. King, "Elastic - Plastic Analysis of two Dimensional Stress Systems by the Finite Element Method", Int. J. Mech. Sci., 9, 1967.

38. Zienkiewicz, O.C., M. Watson, I.P. King, "A Numerical Method of Visco-Elastic Stress Analysis", Int. J. Mech. Sci., 10, 1968.

39. Zienkiewicz, O.C., Y.K. Cheung, "Plates and Tanks on Elastic Foundations. An Application of the Finite Element Method", Int. I. Solids Structures, 1, 1965.

40. Cheung, Y.K., D.K. Nag, "Plates and Beams on Elastic Foundations - Linear and Nonlinear Behaviour", Géotechnique, 18, 1968.

41. Clough R.W., R.J. Woodward, "Analysis of Embankment Stresses and Deformations", J. Soil Mech. A.S.C.E., 93, July 1967.

42. Girijavallabdan, C.V., L.C. Reese, "Finite Element Method for problems in Soil Mechanics", Proc. A.S.C.E., March 1968.

43. Christian, J.T. "Undrained Stress Distribution by Numerical Methods, "Proc. A.S.C.E. November 1968.

44. Herrmann, L.R. "Elasticity Equations for Incompressible and Nearly Incompressible Materials by a Variational Theorem", J.A.I.A.A., 3, No. 10.

45. Zienkiewicz, O.C., "Finite Element Procedures in the Solution of Plate and Shell Problems", Stress Analysis, John Wiley, 1965.

46. Timoshenko and J.N. Goodier, "Theory of Elasticity", 2nd. ed., McGraw-Hill Book Co., 1965.

47. Argyris, J.H., S. Kelsey, H. Kamel, "Recent Advances in Matrix Methods of Structural Analysis", AGARDograph, 72, 1964.

48. Turner, M.J.H., H.C. Martin, R.C. Weikel, "Further Developments and Applications of the Stiffness Method", as above.

49. Zienkiewicz, O.C., Y.K, Cheung, I.P. King, "Slab Bridges with Arbitrary Shape and Support Conditions", Report No. C/R/75/67 University of Wales, June 1967.

50. Harr M.E. "Foundations of Theoretical Soil Mechanics", McGraw-Hill, 1966.

51. Arthur, J.R.F., R.G. James, K.H. Roscoe, "The Determination of Stress Fields during Plane Strain Analysis of a Sand Mass", Géotechnique.

52. Bishop A.W., "The Strength of Soils as Engineering Materials", Géotechnique, 16, No. 2, June 1966.

53. Perspex, Acrylic Materials Properties", I.C.I Publication

54. Girijavallabdan, C.V. "Analysis of Shear Walls using Finite Element Techniques", A.S.C.E., 1969.

55. Bray, K.H.M. Ph.D., Thesis, University of Aston in Birmingham